CUMULATIVE DISSERTATION

Tracing the evolution of hillslope structure and hillslope hydrological response over ten millennia in two glacial forefields of different geology

by Anne Hartmann

A thesis presented for the degree of

Doctor of Natural Science (Dr. rer. nat.)

Submitted to the
Faculty of Science, Institute of Environmental Science and Geography
at the University of Potsdam, Germany

Prepared at the
Helmholtz Centre Potsdam GFZ
German Research Centre for Geosciences, Section Hydrology

Submitted: 19.09.2023
Defended: 23.02.2024

Supervisors:
Bruno Merz — University of Potsdam and GFZ, Germany
Theresa Blume — Helmholtz Centre Potsdam GFZ, Germany

Referees:
Referee 1: Bruno Merz — University of Potsdam and GFZ, Germany
Referee 2: Theresa Blume — Helmholtz Centre Potsdam GFZ, Germany
Referee 3: Daniel R. Hirmas — Texas Tech University, USA

Published online on the
Publication Server of the University of Potsdam:
https://doi.org/10.25932/publishup-62862
https://nbn-resolving.org/urn:nbn:de:kobv:517-opus4-628629

Summary

Assessing the impact of global change on hydrological systems is one of the greatest hydrological challenges of our time. Changes in land cover, land use, and climate have an impact on water quantity, quality, and temporal availability. There is a widespread consensus that, given the far-reaching effects of global change, hydrological systems can no longer be viewed as static in their structure; instead, they must be regarded as entire ecosystems, wherein hydrological processes interact and coevolve with biological, geomorphological, and pedological processes. To accurately predict the hydrological response under the impact of global change, it is essential to understand this complex coevolution. The knowledge of how hydrological processes, in particular the formation of subsurface (preferential) flow paths, evolve within this coevolution and how they feed back to the other processes is still very limited due to a lack of observational data.

At the hillslope scale, this intertwined system of interactions is known as the hillslope feedback cycle. This thesis aims to enhance our understanding of the hillslope feedback cycle by studying the coevolution of hillslope structure and hillslope hydrological response. Using chronosequences of moraines in two glacial forefields developed from siliceous and calcareous glacial till, the four studies shed light on the complex coevolution of hydrological, biological, and structural hillslope properties, as well as subsurface hydrological flow paths over an evolutionary period of 10 millennia in these two contrasting geologies.

The findings indicate that the contrasting properties of siliceous and calcareous parent materials lead to variations in soil structure, permeability, and water storage. As a result, different plant species and vegetation types are favored on siliceous versus calcareous parent material, leading to diverse ecosystems with distinct hydrological dynamics. The siliceous parent material was found to show a higher activity level in driving the coevolution. The soil pH resulting from parent material weathering emerges as a crucial factor, influencing vegetation development, soil formation, and consequently, hydrology. The acidic weathering of the siliceous parent material favored the accumulation of organic matter, increasing the soils' water storage capacity and attracting acid-loving shrubs, which further promoted organic matter accumulation and ultimately led to podsolization after 10 000 years. Tracer experiments revealed that the subsurface flow path evolution was influenced by soil and vegetation development, and vice versa. Subsurface flow paths changed from vertical, heterogeneous matrix flow to finger-like flow paths over a few hundred years, evolving into macropore flow, water storage, and lateral subsurface flow after several thousand years. The changes in flow paths among younger age classes were driven by weathering processes altering soil structure, as well as by vegetation development and root activity. In the older age class, the transition to more water storage and lateral flow was attributed to substantial organic matter accumulation and ongoing podsolization. The rapid vertical water transport in the finger-like flow paths, along with the conductive sandy material, contributed to podsolization and thus to the shift in the hillslope hydrological response.

In contrast, the calcareous site possesses a high pH buffering capacity, creating a neutral to basic environment with relatively low accumulation of dead organic matter, resulting in a lower water storage capacity and the establishment of predominantly grass vegetation. The coevolution was found to be less

dynamic over the millennia. Similar to the siliceous site, significant changes in subsurface flow paths occurred between the young age classes. However, unlike the siliceous site, the subsurface flow paths at the calcareous site only altered in shape and not in direction. Tracer experiments showed that flow paths changed from vertical, heterogeneous matrix flow to vertical, finger-like flow paths after a few hundred to thousands of years, which was driven by root activities and weathering processes. Despite having a finer soil texture, water storage at the calcareous site was significantly lower than at the siliceous site, and water transport remained primarily rapid and vertical, contributing to the flourishing of grass vegetation. The studies elucidated that changes in flow paths are predominantly shaped by the characteristics of the parent material and its weathering products, along with their complex interactions with initial water flow paths and vegetation development. Time, on the other hand, was not found to be a primary factor in describing the evolution of the hydrological response. This thesis makes a valuable contribution to closing the gap in the observations of the coevolution of hydrological processes within the hillslope feedback cycle, which is important to improve predictions of hydrological processes in changing landscapes. Furthermore, it emphasizes the importance of interdisciplinary studies in addressing the hydrological challenges arising from global change.

Zusammenfassung

Die Auswirkungen des globalen Wandels auf den Landschaftswasserhaushalt stellen eine der bedeutendsten Herausforderungen in der heutigen Hydrologie dar. Eine zuverlässige Prognose der zukünftigen Verfügbarkeit, Menge und Qualität des Wassers in Landschaften ist dabei von höchster Bedeutung. Es besteht weitgehender Konsens darüber, dass hydrologische Systeme aufgrund der weitreichenden Auswirkungen des globalen Wandels in ihrer Struktur nicht mehr als statisch betrachtet werden können. Vielmehr sind sie als ganzheitliche Ökosysteme zu betrachten, in denen hydrologische Prozesse mit biologischen, geomorphologischen und pedologischen Prozessen in Wechselwirkung stehen und sich gemeinsam entwickeln. Das Verständnis dieser komplexen Koevolution ist der Schlüssel für eine präzise Vorhersage der hydrologischen Entwicklung. Aufgrund mangelnder Beobachtungsdaten ist das Wissen über die Entwicklung und die Rückkopplung hydrologischer Prozesse, insbesondere in Bezug auf die Bildung unterirdischer (präferenzieller) Fließwege, innerhalb dieser Koevolution noch erheblich begrenzt. Das Ziel dieser Studie liegt in der Analyse der Wechselwirkungen zwischen Struktur und hydrologischer Reaktion auf der Hangskala, um ein besseres Verständnis über die Koevolution und möglicher Rückkopplungsprozesse zu erlangen.

Die vier in dieser Arbeit vorgestellten Studien befassen sich daher mit der Entwicklung hydrologischer, biologischer und physikalischer Struktureigenschaften sowie der Evolution hydrologischer Fließwege über einen Zeitraum von zehntausend Jahren in zwei gegensätzlichen Geologien. Mittels der Analyse von Moränen-Chronosequenzen in zwei Gletschervorfeldern, die jeweils aus silikatreichem bzw. kalkreichem Geschiebemergel entstanden sind, wird die komplexe Koevolution unter Berücksichtigung der Beschaffenheit des Ausgangsmaterials beleuchtet. Die Ergebnisse zeigen, dass die unterschiedlichen Eigenschaften von silikatreichem und kalkhaltigem Ausgangsmaterial unter den gegebenen Klimabedingungen zu Variationen in Bodenstruktur, Durchlässigkeit und Wasserspeicherung führen. Diese Unterschiede begünstigen im Vergleich verschiedene Vegetationstypen, was zu vielfältigen Ökosystemen mit unterschiedlichen hydrologischen Dynamiken führt.

Es wurde festgestellt, dass das silikatische Ausgangsmaterial die Koevolution stärker antreibt. Der Boden-pH-Wert, der sich aus der Verwitterung des Ausgangsmaterials ergibt, erweist sich als entscheidender Faktor, der die Entwicklung der Vegetation, die Bodenbildung und folglich die Hydrologie beeinflusst. Die saure Verwitterung des silikatischen Ausgangsmaterials begünstigt die Ansammlung von organischem Material, was die Wasserspeicherkapazität des Bodens erhöht und säureliebende Sträucher anzieht. Diese Sträucher wiederum profitieren von der hohen Wasserspeicherkapazität und fördern weiterhin die Anreicherung von organischem Material, was letztlich nach 10 000 Jahren zur Podsolierung führt. Tracer-Experimente zeigten, dass die Evolution der unterirdischen Fließwege durch die Entwicklung von Boden und Vegetation beeinflusst wurde, und umgekehrt. Die unterirdischen Fließwege änderten sich im Laufe einiger hundert Jahre von vertikalem, heterogenem Matrixfluss zu fingerartigen Fließwegen und entwickelten sich über mehrere tausend Jahre weiter zu Makroporenfluss, Wasserspeicherung und unterirdischen, lateralen Fließwegen. Die Veränderungen der Fließwege in jüngeren Altersklassen wurden durch Verwitterungsprozesse verursacht, welche die Bodenstruktur beeinflusseten, sowie von der Ent-

wicklung der Vegetation und deren Wurzelaktivitäten. In älteren Altersklassen führte die Anreicherung von organischem Material und die kontinuierliche Podsolierung zu einem Übergang zu erhöhter Wasserspeicherung und lateralen Fließwegen. Die schnelle, vertikale Wasserbewegung in den fingerartigen Fließwegen, kombiniert mit dem leitfähigen sandigen Material, trug zur Podsolierung und somit zur Änderung der hydrologischen Reaktion bei.
Im Gegensatz dazu zeigt der kalkhaltige Standort eine hohe pH-Pufferkapazität auf, was zu einer neutralen bis basischen Umgebung mit vergleichsweise geringer Ansammlung von abgestorbenem organischem Material führt. Dies bedingt eine geringere Wasserspeicherkapazität und begünstigt die Ansiedlung von Grasvegetation. Die Koevolution verläuft über die Jahrtausende vergleichsweise weniger dynamisch. Ähnlich dem silikatischen Standort treten markante Veränderungen zwischen den jüngeren Altersklassen auf. Im Gegensatz zum silikatischen Standort ändern sich die unterirdischen Fließwege nur in ihrer Form, nicht jedoch in ihrer Richtung. Tracer-Experimente zeigen, dass die Fließwege sich im Laufe einiger hundert bis tausend Jahre von vertikalem, heterogenem Matrixfluss zu fingerartigen Fließwegen verändern, was auf Wurzelaktivitäten und Verwitterungsprozesse zurückzuführen ist. Trotz der feineren Bodentextur ist die Wasserspeicherkapazität deutlich geringer als am silikatischen Standort, und der Wassertransport erfolgt überwiegend schnell und vertikal.
Die durchgeführten Studien verdeutlichen, dass die Veränderungen der Fließwege hauptsächlich von den Eigenschaften des Ausgangsgesteins und seinen Verwitterungsprodukten sowie von deren komplexen Interaktionen mit den ursprünglichen hydrologischen Gegebenheiten und der Vegetationsentwicklung geprägt waren. Im Gegensatz dazu spielt die Zeit keine entscheidende Rolle bei der Beschreibung der Entwicklung der hydrologischen Reaktion. Die Studie leistet einen wertvollen Beitrag zur Schließung der Lücke in den Beobachtungen der Koevolution von hydrologischen, biologischen, geomorphologischen und pedologischen Prozessen. Dies ist von großer Bedeutung, um Vorhersagen von hydrologischen Prozessen in sich wandelnden Landschaften zu verbessern. Gleichzeitig verdeutlicht diese Studie die Bedeutung interdisziplinärer Forschungsansätze zur Bewältigung kommender Herausforderungen in der Hydrologie im Angesicht des globalen Wandels.

Contents

List of Publications

Hartmann, A., Semenova, E., Weiler, M., and Blume, T.: Field observations of soil hydrological flow path evolution over 10 millennia, Hydrology and Earth System Sciences, 24, 3271–3288, https://doi.org/10.5194/hess-24-3271-2020, 2020

Author's contribution: Planning (jointly with Semenova, Weiler, and Blume) and conducting (jointly with Semenova) the field experiments, image preparation (with input from Semenova) and analysis; soil sampling and laboratory analysis, data validation and analysis, preparation and writing of the manuscript (with input from Blume and review and editing by Blume, Weiler and Semenova), corresponding author for publishing procedure.

Hartmann, A., Weiler, M., and Blume, T.: The impact of landscape evolution on soil physics: evolution of soil physical and hydraulic properties along two chronosequences of proglacial moraines, Earth System Science Data, 12, 3189–3204, https://doi.org/10.5194/essd-12-3189-2020, 2020

Author's contribution: Planning (jointly with Weiler and Blume) and conducting the soil sampling and laboratory experiments/analysis, data validation, data curation, preparation and writing of the manuscript (with review and editing by Blume and Weiler), corresponding author for publishing procedure.

Hartmann, A., Weiler, M., Greinwald, K., and Blume, T.: Subsurface flow paths in a chronosequence of calcareous soils: impactof soil age and rainfall intensities on preferential flow occurrence, Hydrology and Earth System Sciences, 26, 4953–4974, https://doi.org/10.5194/hess-26-4953-2022, 2022

Author's contribution: Planning (jointly with Weiler and Blume) and conducting the tracer experiments, image preparation and analysis; soil sampling and laboratory analysis, data validation, data processing and analysis, preparation and writing of the manuscript (with input from Blume and review and editing by Greinwald, Blume, and Weiler), corresponding author for publishing procedure.

Hartmann, A., Blume, T.: The evolution of hillslope hydrology: links between form, function and the underlying control of geology, submitted to Water Resources Research (in review), 2023

Author's contribution: Planning (jointly with Blume) and conducting field installations and the tracer experiments, soil sampling, laboratory analysis, data validation, data curation, data processing and analysis, preparation and writing of the manuscript (with, input, review and editing by Blume).

Supplementary co-author publications with minor contribution:

Maier, F., van Meerveld, I., Greinwald, K., Gebauer, T., Lustenberger, F., **Hartmann, A.**, and Musso, A.: Effects of soil and vegetation development on surface hydrological properties of moraines in the Swiss Alps, CATENA, 187, 104 353, https://doi.org/10.1016/j.catena.2019.104353, 2020

Greinwald, K., Dieckmann, L. A., Schipplick, C., **Hartmann, A.**, Scherer-Lorenzen, M., and Gebauer, T.: Vertical root distribution and biomass allocation along proglacial chronosequences in Central Switzerland, Arctic, Antarctic, and Alpine Research, 53, 20–34, https://doi.org/10.1080/15230430.2020.1859720, 2021

Musso, A., Tikhomirov, D., Plötze, M. L., Greinwald, K., **Hartmann, A.**, Geitner, C., Maier, F., Petibon, F., and Egli, M.: Soil Formation and Mass Redistribution during the Holocene Using Meteoric 10Be, Soil Chemistry and Mineralogy, Geosciences, 12, 99, https://doi.org/10.3390/geosciences12020099, 2022.

List of Figures

List of Tables

1 Introduction

1.1 Hydrology under the impact of global change

Global change represents one of the most pressing hydrological challenges of our time, where human activities exert a significant impact on the Earth's climate and ecosystems, with far-reaching consequences for the hydrological cycle (Abbott et al., 2019). Ensuring water availability is essential for human survival, and evaluating the consequences of global change on hydrological systems is indispensable for the well-being of forthcoming generations. Shortages, excessive water, or compromised water quality can potentially have life-threatening consequences (Mancosu et al., 2015). Changes in land cover and land use induced by human actions, including landscape degradation, along with anthropogenic climate change, play pivotal roles in driving alterations in water quantity, quality, and temporal availability (Bronstert et al., 2002; Jin et al., 2021).

Alterations in land use and land cover encompass diverse forms and stem from various causes. Some of these causes are indirectly man-made, as they are a consequence of anthropocentric climate change. A well-known example is the accelerated retreat of glaciers in the alpine mountainous regions (Marzeion et al., 2014; Roe et al., 2017) due to global warming. As a result of the shrinking ice masses, after a brief increase in runoff rates, a strong decrease in runoff is projected in the long term (Huss et al., 2008). Social consequences for energy production, economic consequences for the tourism sector, and ecological consequences for aquatic ecosystems are expected (Laurent et al., 2020). Moreover, the glacier retreat exposes new areas that will profoundly affect the landscape hydrology. The former glacial landscapes transform into completely new landscapes over a time span of centuries to millennia (Haeberli et al., 2019). The new land cover is projected to contain lakes, debris that will turn into young soils, and vegetation (Haeberli, 2017), all of which affect the local hydrology.

Another example of land cover change driven by global warming is the widespread epidemic outbreak of bark beetle populations across multiple continents (Williams and Liebhold, 2002). These conifer infesting beetles lead to the death of entire tree stands, bearing significant consequences for the local hydrology (Bearup et al., 2014). This profound shift in land cover is complex, impacting both storage and flow components (Goeking and Tarboton, 2020). Beyond the indirect human-induced shifts in land cover, there are also direct human interventions in land use that exert substantial influence on the landscape hydrology. Driven by the growing demand for food production, landscapes are progressively converted into agricultural areas. The world has lost 420 million hectares of forest for primarily agricultural purposes since 1990, with more than half of them being converted to cropland (FAO, 2020). These drastic changes in land use can have far-reaching effects on the local hydrology (Truong et al., 2022). Extreme man-made alterations of landscapes also result from surface mines. The global area of more than 57,000 km^2 is currently altered by surface mining (Maus et al., 2020). These mines significantly influence the local hydrology during their operational phase and present an entirely novel hydrological character during the restoration process post decommissioning (Ross et al., 2021). Faced with these rapid and far-reaching (global) changes, hydrologists are challenged to find ways to address the impact of these changes on

the (local) water cycle. Thus, it becomes imperative to explore the impact of global change (comprising climate change and land cover/use change) on hydrological processes. This investigation is vital to secure future water supply and to effectively plan the utilization and management of water resources (Lv et al., 2019).

The extreme interventions in hydrological systems will lead to future landscapes that deviate significantly from their past and present states. Under the impact of global change, hydrological systems may no longer be considered stationary systems (Ehret et al., 2014). For example, the exposure of areas previously covered by glaciers sets in motion vegetation development and soil formation, which takes place in coevolution with the given morphology and soil water movement. This complex process results in hydrological system alterations spanning from several centuries to millennia (Egli et al., 2006, 2008; D'Amico et al., 2014). A similar process occurs in reclaimed mining areas. The soil, biota, and water fluxes will coevolve dynamically over a long period of time on the previously degraded terrain (Clark and Zipper, 2016). The infestation of bark beetles often leads to tree clearance, followed by natural recovery or afforestation with young plants. These shifts in the system state trigger dynamic changes in the interactions among biota, soil, and water transport (Bearup et al., 2016; Šamonil et al., 2022). Consequently, for predicting the system dynamics under (global) change, the system-shaping feedback processes, which were previously not required to be incorporated into the representation of system dynamics, may now play a significant role (Ehret et al., 2014). To accurately predict how water flow in hydrological systems will evolve, it becomes essential to identify the system-shaping feedback processes during the coevolution of biota, soil, and water transport. Analyzing this coevolution offers the potential for a robust explanation of the underlying mechanisms (Fan et al., 2019).

An understanding of these coupled processes, even at the hillslope scale, is essential to assess the impact of global change. At the hillslope scale, the hydrological response is closely linked to the hillslope structure, including soil (hydraulic) properties and vegetation characteristics as they are a major control for water flow paths. In turn, soil (hydraulic) properties are modified by water and vegetation, as they are primary factors of soil development (Jenny, 1941) by influencing soil weathering (Hunt et al., 2021) and soil erosion. Furthermore, vegetation composition and coverage is highly dependent on water availability, but it also impacts water flow paths. Thus, the hydrology at the hillslope scale coevolves with pedological, biogeochemical, geomorphological, and ecological processes that interact with each other. In this context, the evolution of a subsurface flow network is of particular importance for the feedback processes and the overall hydrological system response.

Despite the significant role of subsurface hydrology in this hillslope feedback cycle, the evolution of subsurface water flow paths is challenging to observe. The lack of observations limits our understanding of the interdependence between changes in subsurface hydrology and changes in soil and biota. In order to improve our understanding of the hillslope feedback cycle, it is important to investigate the dynamics of subsurface hydrology during landscape evolution and its coevolution alongside the other landscape shaping processes.

1.2 Hillslopes as the key elements of landscapes

1.2.1 The hydrological function of hillslopes

Hillslopes serve as crucial landscape components that regulate water distribution across and beneath the Earth's surface. As the largest functional parts of catchments, hillslopes have a major impact on the overall hydrological catchment response (Dunne, 1978). Over 95% of the stream water has been transported through or over hillsides in the form of subsurface water or overland flow (Kirkby, 1988). Understanding and predicting the hillslope response is, among others, highly important in terms of flood prediction (Hallema et al., 2016), the evaluation of water availability for agricultural purposes (Marshall et al., 2009), or the assessment of slope stability (Biavati et al., 2006).
The essential role of hillslopes lies in their ability to partition, store, and release incoming water (Phillips, 2022). The individual functions are closely related and cannot be viewed separately from one another. Whether water that passed through the vegetation cover and reached the soil surface runs off as overland flow, infiltrates, runs off as subsurface storm flow, is stored in the soil matrix, or is transported to the saturated zone and released as base flow depends on the interplay of infiltration rates, soil moisture dynamics, and soil water drainage (Scherrer et al., 2007). Key factors such as soil texture, stratigraphy, and structure, including impeding layers and macropores, significantly define the hydraulic properties of the soil, thereby influencing the partitioning, storage, and release of water at the hillslope scale (Gnann et al., 2021).

1.2.2 The important role of subsurface hydrology

Subsurface hydrological processes are difficult to observe and therefore a major source for uncertainties in hydrological predictions (Beven, 2001). However, these processes are of great importance for the overall hydrological hillslope response. Soil largely controls the partitioning of water input into surface and subsurface water, the building of subsurface flow paths, subsurface water storage, and soil water residence times. The flow paths and rates at which water moves through the soil are decisive for plant water availability (Zhang et al., 2022), groundwater recharge (Tao et al., 2021), and stream discharge (Beiter et al., 2020). Understanding the storage structures and subsurface flow paths of the soil is important to understand the underlying mechanism of storage and release.
Water that infiltrates will either flow downwards (vertical flow) or laterally downslope. The latter occurs in the presence of a flow impeding layer, that is characterized by a lower hydraulic conductivity caused by, e.g., a change in soil texture (Hübner et al., 2017), impermeable bedrock (Janzen and McDonnell, 2015), compacted material (Janssen and Lennartz, 2007), or hard pan formed by displacement processes. The occurrence of subsurface lateral flow is a threshold process depending on the available storage capacity of the soil (Meerveld and McDonnell, 2006). Conditions for its formation are based on the antecedent soil moisture and the precipitation amount.
Subsurface flow (lateral or vertical) takes place both in the soil matrix and through preferential flow paths. Preferential flow is the phenomenon of water bypassing a substantial fraction of the porous media by moving rapidly along certain pathways (Hendrickx and Flury, 2001). Lateral preferential flow can significantly contribute to the hillslope subsurface stormflow response (Weiler and McDonnell, 2007).

The occurrence of (vertical/lateral) preferential flow can have effects on water storage (Rye and Smettem, 2017), the availability of water in the root zone, nutrient and contaminant transport (Jarvis, 2007) and consequently soil chemistry (Jin and Brantley, 2011; Bundt et al., 2000), as well as on groundwater quality (Khan et al., 2016) and recharge (Cheng et al., 2017). Based on their characteristics, three fundamental types of preferential flow are distinguished: macropore flow, funneled-flow caused by flow concentration due to flow-impeding features, and unstable flow concentrated in conductive fingers (finger flow) (Nimmo, 2009). Flow in macropores has been extensively studied (Beven and Germann, 2013) and is facilitated by cracks or large pores created by soil fauna and flora. Preferential flow in the form of finger(-like) flow is caused by certain circumstances of the subsurface, such as heterogeneity in the soil structure (e.g., a fine textured layer overlying a coarse textured layer) or hydrophobicity (Ritsema and Dekker, 1994). Surface microtopography, hydrophobicity, and vegetation cover can result in heterogeneous infiltration patterns that give rise to finger-like flow paths originating at the soil surface (van Schaik, 2009). Thus, the occurrence of preferential flow stems from various factors, indicating that beyond soil attributes, the interplay between soil and vegetation also plays a role in shaping subsurface flow paths. This interaction remains highly dynamic throughout landscape/hillslope development, being an essential component of the hillslope feedback cycle.

1.2.3 The hillslope feedback cycle

The hillslope feedback cycle refers to the intertwined system of interactions between soil, vegetation, water transport, and topography at the hillslope scale. A key component of this cycle is pedogenesis, the process through which soil is formed by the interplay between parent material (geology), climate, vegetation, and topography (Jenny, 1941). The type and composition of the parent material sets the initial conditions for pedogenesis, with its susceptibility to weathering and erosion defining the rate of soil development. The type and chemical composition of the parent material determines, in accordance with given climate conditions and topography, the weather-ability and the chemical composition of the soil. This subsequently affects the resulting soil physical properties (e.g., texture, bulk density, porosity, water holding capacity), hydrologic properties and processes (Lin, 2003), as well as soil fertility, consequently influencing vegetation cover (Hahm et al., 2014).
The resulting soil properties define water transport and thus the soil moisture, which in turn is a decisive factor directly and indirectly affecting soil formation. Water availability directly impacts soil formation by influencing chemical weathering and the transport of solutes and matter (Li et al., 2022), while its indirect effects manifest through its influence on vegetation cover. Water flow paths influence the distribution and availability of nutrients in concentration, which can either limit or enhance plant growth (Nimmo et al., 2009; Hahm et al., 2014). The vegetation itself influences weathering rates through the release of root exudates and acids, as well as below-ground plant activities. Biological activities of the vegetation also influence soil water flow paths (Wang and Zhang, 2017). Root activities can directly alter water flow paths by creating new channels for water movement. Indirect transformations may arise from organic matter enrichment, which affects soil hydraulic properties, or through an increase in soil hydrophobicity that alters infiltration patterns.
The topographic position, including relief, slope, and aspect (Egli et al., 2006) of the land surface play a

defining role in shaping microclimatic conditions. Consequently, these attributes influence weathering rates, material transport (erosion), and water transport (Jefferson et al., 2010; Fujimoto et al., 2008). Notably, landscape topography itself can undergo transformation through the impact of weathering and erosion processes, subsequently affecting both vegetation evolution and water transport patterns. The complexity of interactions and their evolution over time makes it particularly difficult to predict changes in the hillslope hydrologic response that stem from alterations in individual components of the hillslope feedback cycle.

1.3 Difficulties in predicting future hillslope hydrology

1.3.1 Disentangling the hillslope feedback cycle

To predict hillslope hydrology within the context of global change, it is essential to grasp the comprehensive interplay of feedback processes that shape the underlying system. By understanding the hillslope feedback cycle, we can identify critical processes influencing the hillslope hydrological response and establish connections between the past and future development of hillslopes under the impact of global change. The complexity arising from the web of intertwined connections, coupled with the overlap of long-term processes (soil pedogenesis) and short-term processes (soil function) that shape landscapes/hillslopes (Ma et al., 2017) during the coevolution of soil, vegetation, and hydrological response, presents a challenge in pinpointing the specific processes driving the hydrological response. To gain a fundamental understanding of how the hillslope hydrologic response changes during landscape evolution, including its coevolution with vegetation and soil, is the basis for the identification of relevant relationships and processes.
The approach of an integrative consideration of hydrology and soil science to improve the understanding and prediction of water transport in landscapes was already postulated by Lin et al. (2006). In the remarks on the basic principles of the newly defined research field 'hydropedology', Lin et al. (2006) elucidates that one of the initial steps to identify the interrelationships between hierarchical structures of soil and hydrologic systems involves observing the development of soil structure, which establishes both limitations and prerequisites for hydrological processes. Hence, the collection of field data is essential for improving our understanding of the principles governing the relationships between soil, vegetation, and hydrology. Numerous field studies have addressed the relationship between soil, vegetation and hydrology. The nature of the studies can be roughly classified into three distinct categories: comparative studies, space-for-time studies, and observatory-based studies. Comparative studies explore how soil, vegetation, and hydrological response interact at multiple sites, each of which exhibits variations in a specific characteristic (Bachmair and Weiler, 2012; Germer et al., 2010; Archer et al., 2013; Tian et al., 2017). As this method solely provides a snapshot of the relationship between two or more system characteristics, it is not feasible to gain a holistic understanding of the hillslope feedback cycle. Nevertheless, these studies offer initial insights into certain facets of the hillslope feedback cycle.
Space-for-time studies involve the comparison of sites that have experienced distinct time spans since a pivotal event, such as the abandonment of agricultural land (Hassler et al., 2011; Zimmermann et al., 2010; Hou et al., 2014), volcanic material deposition (Lohse and Dietrich, 2005; Yoshida and Troch, 2016), or glacier retreat (D'Amico et al., 2014). The limitation of these studies lies in their inability to continuously

observe the coevolution. The temporal resolution is often constrained by the local conditions, resulting in the consideration of only a few years to decades (Hou et al., 2014; Hassler et al., 2011; Zimmermann et al., 2010), or the consideration of only extreme end-members, such as a few decades and several million years (Lohse and Dietrich, 2005; Yoshida and Troch, 2016). Although the assumption that time is the only external factor influencing the studied sites is critical (Wojkowski et al., 2022), and the temporal resolution can be limited, this approach is promising to capture fundamental relationships between the components of the hillslope feedback cycle.
The most effective method for unraveling the hillslope feedback cycle is to conduct a controlled experiment under close-to-natural conditions, as has been done for more than ten years at the Biosphere 2 Landscape Evolution Observatory (Hopp and McDonnell, 2009). The Landscape Evolution Observatory is hosted by the University of Arizona and obtains three highly equipped, identical, artificial landscapes. Its primary aim is to measure and analyze the intricate relationships between various factors such as hydrologic partitioning, geochemical weathering, ecology, microbiology, atmospheric processes, and geomorphic transformations that occur during the early stages of landscape coevolution. An interdisciplinary team of scientists investigates the evolution from initially abiotic landscapes to increasingly complex ecosystems under controlled boundary conditions (Volkmann et al., 2018). This large-scale study project is an excellent opportunity to analyze and understand the processes of the hillslope feedback cycle, which requires not only sufficient financial resources but also, above all, time. Under the current pressure to assess the consequences of global change in a timely manner, a compromise between temporal resolution and the time required for knowledge acquisition becomes imperative. Thus, extensive and interdisciplinary space-for-time studies are a better choice to gain initial insights that can be further refined over time, drawing from real-time experimentation observations.

1.3.2 The uncertain role of preferential flow

Preferential flow is an important mechanism of subsurface water transport (Weiler and Naef, 2003), but due to its occurrence in different forms, also just as complex. The causes of preferential flow are manifold, encompassing factors like vegetation and soil properties (Zhang et al., 2015; Zehe and Flühler, 2001). They can also be susceptible to the impacts of global change (Zeng et al., 2013), or their evolution may be shaped by the preferential flow process itself (van der Heijden et al., 2013). While numerous studies have delved into the causes of preferential flow (Jarvis et al., 2009, 2016), observations concerning their dynamic progression remain scarce. As stated by Phillips (2022, p.12): " [...] the *why* of how these patterns form and persist [...]" is satisfactorily answered, but "[...] *how* these systems evolve is an open question [...]".
The lack of knowledge about this evolution leads to an insufficient consideration (Samouëlian et al., 2012) within modeling frameworks aimed at simulating the transformation of soil landscapes under changing conditions. Remarkably, even soil landscape evolution models, designed to model the complex evolution of soil landscapes by considering the dynamic exchange of water and sediments, currently omit the evolution of both vertical and horizontal subsurface flow paths, along with the occurrence of preferential flow (van der Meij et al., 2018). Neglecting these significant processes can result in inaccurately modeled transport and displacement processes (Sauer et al., 2012). The lack of knowledge stems from the challenge

of effectively observing the dynamic coevolution of water flow paths within the hillslope feedback cycle. There are several methods for observing the occurrence of preferential flow such as dye tracing, breakthrough curves, or scanning techniques (Allaire et al., 2009). Additionally, it is also possible to establish connections between soil/landscape attributes and the prevalence of preferential flow (Jarvis et al., 2009). However, observing the dynamic interaction between preferential flow and landscape attributes is difficult, as this feedback cycle can span numerous time scales (Ma et al., 2017).
Several studies have already investigated the evolution of the hydrological response by using a chronosequence approach (Lohse and Dietrich, 2005; Jefferson et al., 2010; Yoshida and Troch, 2016). With increasing age, these studies observed a transition from vertical to lateral flow paths. However, these chronosequence studies rely on a limited number of data points, and the age differences among classes are quite substantial (spanning several thousand to a million years). Furthermore, these studies do not directly focus on the coevolution of flow paths at the hillslope scale. Simultaneous observations of the evolution of subsurface flow paths, including preferential flow paths, and the evolution of soil (hydraulic) properties as well as other influencing variables, such as vegetation, remain insufficient. Nevertheless, such observations hold the potential to define or quantify links between the evolution of flow paths and the evolution of other components of the hillslope feedback cycle.

1.3.3 Hillslope structure as a hydrological response predictor

The concept of the 'form-and-function dualism' in hydrology (Fan et al., 2020) describes the connection between the structure of hydrological systems and its hydrological response. Similar to its use in biological science (Peterson, 2010), this dualism is based on the premise that form (analogous to the structure of the hydrological system) determines function (analogous to the response of the hydrological system). Characterizing both form and function is vital for describing hydrological systems (Angermann et al., 2017; Jackisch et al., 2017). Defining the link between function and form is crucial for extrapolating knowledge from gauged to ungauged systems (Sivapalan, 2006) and for modeling hydrological systems (under change).
The hydrological response and its description may differ based on the research question. A few studies have already examined the connection between structure and hydrological response, for instance, the effects of a macropore network on preferential flow paths (Fan et al., 2020), the link between catchment attributes and baseflow signatures (Gnann et al., 2021), or the connection between vegetation parameters and surface runoff generation (Chen et al., 2018). The identification of appropriate structure variables that influence the hydrologic response and the identification of appropriate signatures to describe the hydrological response is imperative for maximizing the benefits of linking structure to hydrological response (Gnann et al., 2021).
To employ the links between structure and hydrological response in a model-driven approach to forecast hydrological change, it is crucial to quantify the relationship between form and function. Using simple and frequently measured structure variables and response signatures that are easy to define would be a significant advantage in model applications. Considering the difficulty of disentangling the hillslope feedback cycle, studies that deal with the direct coevolution of structure and hydrological response and the derivation of links are rare.

1.4 Research aims and approach

1.4.1 Objectives and structure

Knowledge of the coevolution and interactions between hillslope structure and the hillslope hydrological response within the context of the hillslope feedback cycle remains limited. Particularly, the evolution of vertical preferential flow paths in relation to hillslope structure and the underlying parent material is mostly unexplored. The main objective of this thesis is to achieve a more comprehensive understanding of the hillslope feedback cycle by examining the coevolution of hillslope structure and hillslope hydrological response. To improve our understanding of the hillslope feedback cycle, the influence of the parent material on the hillslope feedback cycle is investigated, along with the formation of vertical preferential flow paths and the derivation of possible links between hillslope structure and hillslope hydrological response. The main questions addressed by this thesis are:

(i) How does the underlying parent material affect the coevolution of hillslope structure and hillslope hydrological response?

(ii) How do subsurface water flow paths, especially vertical preferential flow paths, evolve and affect subsurface water transport?

(iii) What possible connections can be established between the hillslope hydrological response and the hillslope structure?

This thesis comprises four studies, all aimed at addressing the aforementioned research questions. To investigate the coevolution of hillslope structure and hillslope hydrological response in relation to the parent material (i), the evolution of physical and hydraulic properties of soils developed from siliceous and calcareous parent material was investigated (Chapter 2). This investigation was supplemented with data regarding the development of vegetation characteristics (Chapter 5). The evolution of hillslope structure is then compared to information about the hillslope hydrological response, such as soil water response times, soil water storage, dominant flow path types, and the prevalence of preferential flow paths (Chapter 5). A detailed examination of vertical subsurface water flow paths (ii) was conducted through dye tracer experiments, shedding light on the genesis and progression of vertical preferential flow paths in soils originating from siliceous (Chapter 3) and calcareous parent materials (Chapter 4). The derivation of links between structure and hydrologic response (iii) enables drawing conclusions about the structural properties and their process interactions that need to be taken into account to project hydrological changes based on evolving characteristics of the hydrological system (Chapter 2 and Chapter 5).

1.4.2 Methodological approach

To study the coevolution of hillslope structure and hillslope hydrological response, a chronosequence approach was used. This approach is based on a space-for-time substitution, where a series of sites differ in age, but otherwise have similar characteristics such as tectonic history, topography, climate, and parent material. Thus, time is treated as the only variable. For this study, two chronosequences of glacial moraines situated in the Swiss Alps were selected as the study sites. Glacier forefields are particularly

well-suited for soil chronosequence studies due to the diverse landforms of varying ages that emerge as glaciers retreat. The retreat of glaciers gives rise to a succession of moraines representing different stages of deglaciation, ranging from recently deglaciated areas to those that have been ice-free for thousands of years. This natural chronosequence allows exploring the rapid soil development that occurs on glacial till, along with the evolution of vegetation and hydrological processes. Moreover, glacial forefields offer controlled settings with relatively consistent parent material and climate conditions, making it easier to isolate the effects of time on soil development and ecosystem dynamics. The ages of the moraines, representing the time since deglaciation, were determined using various methods including maps, aerial photos, the high-sensitivity beryllium-10 method, or the radiocarbon method as detailed by Musso et al. (2019). Both chronosequences encompass moraine ages ranging from 30 to 13 500 years. The first sequence consisted of moraines developed from siliceous parent material, while the second sequence developed from calcareous parent material. The two parent materials were selected as they are the two main types of subglacial bedrock in the Swiss Alps and show marked differences in the chemical and physical properties of their weathering products. These differences have significant implications for soil structure and nutrient availability, thereby influencing vegetation succession.

The first part of the thesis investigates the evolution of hillslope structure in terms of soil physical and soil hydraulic properties (Chapter 2). The second and third part investigate the evolution of vertical subsurface flow paths and analyze the occurrence of preferential flow in siliceous (Chapter 3) and calcareous soils (Chapter 4). The fifth part links the evolution of hillslope structure, including soil properties (Chapter 2) and further information on surface and vegetation characteristics to the hillslope hydrological response derived from soil moisture signals (Chapter 5) and to the occurrence of preferential flow. Chapter 2 shows in detail the depth-differentiated evolution of the hillslope structure in form of soil physical and soil hydraulic properties. The data is the outcome of extensive soil sampling and laboratory analysis. At the three plots per moraine and parent material, soil samples were collected using steel sampling rings at depths of 10, 30, and 50 cm. The soil samples were subsequently analyzed in the laboratory for information on porosity, bulk density, loss on ignition, organic matter content, retention curve, hydraulic conductivity curve, and grain size distribution. This study is the first to analyze the evolution of both soil hydraulic and physical properties in detail during the initial millennia of soil development. Chapters 3 and 4 comprise dye tracer irrigation experiments conducted with Brilliant Blue on three designated plots at each moraine. These irrigation plots were strategically situated in close proximity to the soil sampling sites as described in Chapter 2. Both studies employ a well-established digital image analysis technique on photographed stained flow paths. The observed dye patterns were systematically categorized into distinct flow type classes. Chapter 3 focuses on the evolution of water flow paths along with soil-forming processes in siliceous soil and the impact of the irrigation amount on the building of preferential flow paths. Chapter 4 investigates the evolution of subsurface flow paths across the soil chronosequence of calcareous soils and the impact of different irrigation intensities on the building of preferential flow paths and the maximum infiltration depth. The two studies are the first to investigate in detail the development of vertical subsurface hydrological flow paths in coevolution with soil (hydraulic) properties.

In Chapter 5, sprinkling experiments on three plots per moraine, chosen to align with the sites used for soil sampling (Chapter 2), were used to draw conclusions about characteristic hillslope hydrologic responses based on soil moisture signatures. The sprinkling plots were in close proximity to the locations of the blue

dye tracer experiments detailed in Chapters 3 and 4. The water used in the sprinkling experiments was labeled with deuterium (δ^2H) and the subsequent analysis of δ^2H in the soil water profiles was used to derive dominant water flow components (e.g., surface runoff, lateral subsurface flow, vertical percolation including preferential flow). Completed by the preferential flow occurrence derived from the results in Chapter 3 and 4, the evolution of the hillslope hydrological response was analyzed. Information on the hillslope structure was extended by information on the available water capacity derived from the retention curves (Chapter 2), information on the vegetation and root characteristics compiled from Greinwald et al. (2021b) and Greinwald et al. (2021a), information on surface characteristics as hydrophobicity, microtopography and saturated hydraulic conductivity compiled from Maier et al. (2020), Maier and van Meerveld (2021a), and Maier et al. (2021), and information on the soil pH provided by Musso et al. (2019). The ensemble of hillslope structural variables was used to investigate specific relationships between hillslope structure and hillslope hydrological response. This study represents the first comprehensive investigation into the coevolution of hillslope hydrological response alongside hillslope form over the initial ten millennia of landscape development.

The combination of Chapter 2 and Chapter 5 provides a holistic overview of how hillslope structure and hillslope response coevolve in landscapes developed from siliceous and calcareous parent material. Chapters 3 and 4 provide insight into the evolution of vertical subsurface preferential flow paths and their impact on subsurface water transport. In Chapter 5, the analysis of relationships between hillslope structure and hillslope response provides essential insights into potential links between these factors. These insights can help in predicting hydrological changes that arise from structural modifications.

2 The evolution of hillslope structure in siliceous and calcareous parent material

This chapter has been published as:

The impact of landscape evolution on soil physics: evolution of soil physical and hydraulic properties along two chronosequences of proglacial moraines

Anne Hartmann, Markus Weiler, and Theresa Blume

Originally published in:
Earth System Sciences Data, 12, 3189-3204, 2020, https://doi.org/10.5194/essd-12-3189-2020

Abstract

Soil physical properties highly influence soil hydraulic properties, which define the soil hydraulic behavior. Thus, changes within these properties affect water flow paths and the soil water and matter balance. Most often these soil physical properties are assumed to be constant in time, and little is known about their natural evolution. Therefore, we studied the evolution of physical and hydraulic soil properties along two soil chronosequences in proglacial forefields in the Central Alps, Switzerland: one soil chronosequence developed on silicate and the other on calcareous parent material. Each soil chronosequence consisted of four moraines with the ages of 30, 160, 3000, and 10 000 years at the silicate forefield and 110, 160, 4900, and 13 500 years at the calcareous forefield. We investigated bulk density, porosity, loss on ignition, and hydraulic properties in the form of retention curves and hydraulic conductivity curves as well as the content of clay, silt, sand, and gravel. Samples were taken at three depths (10, 30, 50 cm) at six sampling sites at each moraine. Soil physical and hydraulic properties changed considerably over the chronosequence. Particle size distribution showed a pronounced reduction in sand content and an increase in silt and clay content over time at both sites. Bulk density decreased, and porosity increased during the first 10 millennia of soil development. The trend was equally present at both parent materials, but the reduction in sand and increase in silt content were more pronounced at the calcareous site. The organic matter content increased, which was especially pronounced in the topsoil at the silicate site. With the change in physical soil properties and organic matter content, the hydraulic soil properties changed from fast-draining coarse-textured soils to slow-draining soils with high water-holding capacity, which was also more pronounced in the topsoil at the silicate site. The data set presented in this paper is available at the online repository of the German Research Center for Geosciences (GFZ; Hartmann et al. (2020c)). The data set can be accessed via the DOI https://doi.org/10.5880/GFZ.4.4.2020.004.

2.1 Introduction

Today's landscapes are affected by changes, e.g., in the form of climate conditions or land use. Insights into the complex and dynamic interplay between soil development and hydrological, geomorphological, and ecological processes in the context of landscape evolution provide important process understanding, which is important for predicting how landscapes will adapt to changes. Soil has a crucial role in landscape evolution since it influences and is also in turn influenced by vegetation, water, sediment, and solute transport. The soil properties are state variables that play an important role within this feedback cycle (van der Meij et al., 2018). The soil physical properties such as bulk density, porosity, and grain size distribution highly influence water flow (flow rates and flow direction), water storage, capacity, and drainage (Hu et al., 2008; Lohse and Dietrich, 2005; Reynolds et al., 2002) as well as root water availability (Hupet et al., 2002). In the course of soil development, these properties change and are influenced by (but in turn also influence) flora, fauna, and water availability. Over time, this interaction also leads to a change in soil water and material transport and their balance (Lohse and Dietrich, 2005). Knowledge of the development of physical and hydraulic soil properties, as well as their codependency, can provide important insights into the changes in hydraulic water balance and water availability during landscape evolution.

Several studies have focused on the alteration of soil biological, chemical and physical properties during soil development by studying soil chronosequences (Crocker and Major, 1955; Egli et al., 2010; Dümig et al., 2011; Vilmundardóttir et al., 2014; D'Amico et al., 2014; Hudek et al., 2017; Musso et al., 2019). Especially glacial forefields were proven suitable for this 'space for time approach' as soil develops rapidly on glacial till (e.g., Crocker and Major, 1955; Douglass and Bockheim, 2006; He and Tang, 2008; Dümig et al., 2011; Vilmundardóttir et al., 2014; D'Amico et al., 2014). The most commonly studied soil properties are pH value, organic carbon, total nitrogen, calcium carbonate, bulk density, and particle size distribution. It was found that in the very first 100 years of soil development, the pH value decreases fast, and that total nitrogen and soil organic carbon increase with the onset of vegetation (Crocker and Major, 1955; Vilmundardóttir et al., 2014; Egli et al., 2010). The young and poorly sorted soils with no depth-dependent property distribution (Crocker and Major, 1955) eventually develop into a layered soil system with vertical gradients in soil properties such as organic matter, color, bulk density, or particle size distribution. In these geological rather short observation periods (<200 years) soils show a high variability in particle size distribution within single age classes, without a specific trend in grain size distribution (Dümig et al., 2011). An extension of the observation period to several thousand years of soil development revealed an accumulation of clay-sized particles with increasing age (Douglass and Bockheim, 2006; Dümig et al., 2011). Another common finding is also a decrease in bulk density (Crocker and Major, 1955; Crocker and Dickson, 1957; He and Tang, 2008; Vilmundardóttir et al., 2014). The decrease in bulk density is often linked to ongoing vegetation succession, which causes an accumulation of organic matter and the development of a root system. Soil organic matter is also known to have an impact on soil hydrology since it influences soil structure as it contributes to aggregate formation and increases water-holding capacity. An increase in organic matter content was also found in a number of soil chronosequence studies (Burga et al., 2010; Douglass and Bockheim, 2006; Deuchars et al., 1999; Alexander and Burt, 1996). Especially in former glacial areas of cool and humid climate, the formation

of soils with a highly organic top layer is favored (Carey et al., 2007). The hydraulic behavior of these organic soils is less intensively studied than the mineral soils. Organic soils for example have a high total porosity (up to 90%) and a low bulk density (Carey et al., 2007). The listed soil chronosequence studies are not meant to be comprehensive but were selected as they are most comparable to the study presented here. A full literature review of chronosequence studies is beyond the scope of our data presentation. These studies showed that soil texture and soil structure change over time due not only to physical and chemical processes, but also to the influence of vegetation (Morales et al., 2010; Hudek et al., 2017). A change in soil structure and texture leads to a change in the soil's behavior which has a direct impact on the surface and subsurface water transport.

However, the focus of previous studies was primarily on the estimation of development rates of mainly chemical soil properties and the interaction between soil development and vegetation succession. Only a few studies have looked at how changing physical soil properties and organic matter content affect soil water transport (Lohse and Dietrich, 2005; Yoshida and Troch, 2016; Hartmann et al., 2020a), or have focused directly on the development of soil hydraulic properties in form of retention curves and hydraulic conductivity curves (Crocker and Dickson, 1957; Deuchars et al., 1999; Lohse and Dietrich, 2005). Both curves describe the soil hydraulic behavior and are highly soil-specific, since they depend strongly on soil physical properties. The retention curve is the relationship between volumetric soil water content and soil matric potential. The unsaturated hydraulic conductivity curve describes the relationship between unsaturated soil hydraulic conductivity and soil matric potential (or soil water content). While the hydraulic conductivity function gives information on how much water per unit of time can be transported through the partially filled pore system of the soil matrix at a certain matric potential, the retention curve gives information on how much water is available at a certain matric potential and how much the matric potential will change when a certain amount of water is removed from the soil. Based on these two relationships, the specific soil hydraulic behavior with characteristics such as storage capacity, drainability and the amount of plant-available water can be derived. Additionally, both non-linear relationships are important for the parameterization of physically based soil hydraulic models (Schwen et al., 2014; Bourgeois et al., 2016).

Previous investigations of the soil hydraulic properties development are only based on a few data points, and time periods that are either very long (comparing a 200 and a 4.1 million year old soil) or short (studying soils ranging from less than 50 to 200 years in age) and a small vertical and horizontal spatial resolution. Crocker and Dickson (1957) for example, determined the field capacity of soil samples on the basis of water content measurements after oven-drying at 110 °C and after centrifuging in a standard moisture equivalent centrifuge. Here, an increase in field capacity over the first 200 years of soil development was shown for two glacier forefields in southeastern Alaska, where the soils developed on glacial till mainly composed of quartz diorite. Lohse and Dietrich (2005) compared in situ field measurements of water content and matric potential, as well as experimentally derived in situ unsaturated hydraulic conductivities in the field at two depths of a 300 and a 4.1 million year old site on the Hawaiian islands. From 300 to 4.1 million years age, the hydraulic characteristics changed significantly with a shift from rather homogeneous to a layered system with strong differences in the hydraulic characteristics between the soil horizons, which developed from volcanic deposits (Lohse and Dietrich, 2005).

The development of soil hydraulic properties during the first few millennia of soil development has so far

not been investigated. We therefore focused on the co-evolution of soil hydraulic properties, soil physical properties, and organic matter content during the first 10 millennia of landscape evolution by using soil chronosequences at two glacier forefields. We chose forefields developed from silicate (Stone glacier forefield) and calcareous rocks (Griessfirn forefield). The study is expected to provide information on how strong the evolution of soil physical properties affects the development of soil hydraulic properties and to give insights about the changes to be expected in non-stationary landscape systems. The comparison of two sites is expected to highlight how the parent material influences the development. A detailed investigation of hydrologic flow path evolution on these same moraines can be found in Hartmann et al. (2020a).

The data set can be useful to improve predictions on hydrological processes during landscape development using soil and landscape evolution models (SLEMs). The incorporation of measured soil hydraulic properties from chronosequence studies in the calibration of SLEMs was proposed by van der Meij et al. (2018), for example, to account for the long-term evolution of soil hydraulic properties. This is important to improve the feedback modeling between soil structure and soil hydrologic processes as well as for an improved process reflection of the interaction of pedogenic, geomorphic, and hydrologic processes. Our data set is also suitable for the derivation or verification of pedotransfer functions for alpine soils. Pedotransfer functions are a less time-consuming and cost-effective method for determining the soil hydraulic properties (Vereecken et al., 2010) and are also used in SLEMs (van der Meij et al., 2018). They are designed to translate easy-to-measure soil properties such as organic carbon content, bulk density, grain size distribution, or porosity (Wang et al., 2009; Schaap et al., 2001) into soil hydraulic properties. The data set makes it possible to derive and test pedotransfer functions for both study sites in order to find out whether site properties such as parent material have an additional influence on the validity of the pedotransfer function. Further soil physical and hydraulic properties from chronosequence studies can be helpful to derive information of water and nutrient availability, which can be important for other chronosequence studies related to abundance, diversity and function of microbial life in initial soils as well as for studies of vegetation succession.

2.2 Material and methods

2.2.1 Study sites

We investigated how soil structure and soil hydraulic behavior change through time by using a soil chronosequence at two glacier forefields. The two study sites differ in their parent material. The selected proglacial moraines at the Stone Glacier forefield developed from silicate parent material (S-PM) and the moraines at the Griessfirn forefield from calcareous rocks (C-PM). The parent material is one of the five main factors of soil formation (next to climate, biota, topography, and time). The comparison of the two parent materials is expected to provide information on how under assumed equal climate conditions this site characteristic influences the development of structure and soil hydraulic behavior. It is already known that soils developed on calcareous material are richer in organic carbon and clay particles (Jenny, 1941), but little is known how strong these differences are throughout the course of soil development and how much they influence the soil hydraulic behavior.

2.2.1.1 Silicate parent material

The study area of the proglacial forefield developed on silicate parent material was formed by the retreat of the Stone Glacier and is located in the Central Swiss Alps, south of the Sustenpass in the Urner Alps (approx. 47° 43'N, 8° 25'E). Its elevation ranges from 1900-2100 m a.s.l. The area lies in the polymetamorphic "Erstfelder" gneiss zone, which is part of the Aar massif (Blass et al., 2003). The geology is defined by metamorphosed pre-Mesozoic, metagranitoids, gneisses, and amphibolites (Heikkinen and Fogelberg, 1980; Schimmelpfennig et al., 2014); thus the material is mainly acidic and rich in silicate.
The closest official weather station is located 18 km away at Grimsel Hospiz (46° 34'N, 8° 19'E) at an elevation of 1980 m a.s.l. The recorded annual mean temperature is 1.9 °C and the annual precipitation is 1856 mm (1981-2010) (MeteoSwiss, 2020a). The moraines of the Stone Glacier were exposed due to its retreat to the south. Four moraines were selected for this study (see Fig. 2.1). Schimmelpfennig et al. (2014) conducted a detailed dating study of the Stone Glacier moraines, based on high-sensitivity beryllium-10 moraine dating and found that the ages of the four moraines range between 160 and 10 000 years. The age of the youngest moraine was dated as 30 years based on maps and aerial photos. Table 2.1 provides an overview of the main characteristics of the four moraines including elevation, slope, dominant vegetation, vegetation cover, and soil type compiled from Maier et al. (2020) and Musso et al. (2020). The soil at the two youngest moraines was classified as a Hyperskeletic Leptosol. At the 3000-year-old moraine a Skelectic Cambisol and at the oldest moraine an Entic Podzol was found. Illustrations of the soil layers at each moraine can be found in Maier et al. (2020).
The vegetation cover differs significantly among the four age classes and was mapped in summer 2017 (Maier et al., 2020). The moraines are occasionally grazed by cows and sheep during the summer months, which we prevented during our study by the installation of fences. Whereas the vegetation cover at the oldest moraine is dominated by a variety of prostrate shrubs, small trees and several grasses, the 3000-year-old moraine has mainly a grassland cover with fern, mosses, sedges and forbs. The 160-year-old moraine is dominated by grasses, lichen, forbs, and shrubs. The vegetation cover of the youngest moraine is sparse with mainly grass, moss, forbs, and a few shrubs.

2.2.1.2 Calcareous parent material

The study area of the proglacial forefield developed on calcareous parent material was formed by the retreat of the Griessfirn and is located between 2030-2200 m a.s.l. in the Central Swiss Alps (approx. 46° 85'N, 8° 82'E). The geology is defined by limestone (Frey, 1965), thus the material is mainly calcareous. A more detailed description of the geological composition is provided by Musso et al. (2019). The closest official weather station located at a similar elevation (2106 m a.s.l.) is 48 km away at Mount Pilatus (46° 98'N, 8° 25'E). The recorded annual mean temperature is 1.8 °C, and the annual precipitation is 1752 mm (1981-2010) (MeteoSwiss, 2020a).
The four selected moraines were dated by Musso et al. (2019) based on historical maps and the radiocarbon method. The youngest moraine is 110 years old and is located at 2200 m a.s.l. The three other moraines are 160, 4900, and 13 500 years old and located at an elevation of roughly 2030 m a.s.l. (see Fig. 2.1). An overview of the main characteristics of the four moraines including elevation, slope, dominant vegetation, vegetation cover, and soil type compiled from Maier et al. (2020), Musso et al. (2019), and Musso et al.

(2020) is provided in Table 2.1. The soil at the two youngest moraines was classified as a Hyperskeletic Leptosol and at the two oldest moraines as a Calcaric Skeletic Cambisol (Musso et al., 2019). The two oldest moraines are densely covered with grass, dwarf shrubs, and sedge. The vegetation coverage of the two younger moraines is sparse with patches of grass and forbs at the 160-year-old moraine and patches of mostly mosses and lichens at the 110-year-old moraine.

Table 2.1: Overview of the main characteristics of the four moraines at the silicate and calcareous parent material. This information was compiled from the publications Maier et al. (2020), Musso et al. (2019), and Musso et al. (2020).

	Moraine age [years]	Complexity level	Elevation [m.a.s.l.]	Slope [°]	Aspect	Dominant vegetation	Vegetation Cover [%]	Soil type
Silicate parent material								
	30	low	1952	21	NE	Salix hastata	50	Hyperskeletic Leptosol
	30	medium	1959	34	NE	Epilobium fleischeri, Poa alpina	30	Hyperskeletic Leptosol
	30	high	1955	23	NE	Salix retusa,Trifolium pallescens	45	Hyperskeletic Leptosol
	160	low	1989	25	NE	Anthoxanthum alpinum,Salix retusa	80	Hyperskeletic Leptosol
	160	medium	1981	31	NE	Campanula scheuchzeri,Trifolium pallescens	80	Hyperskeletic Leptosol
	160	high	1989	26	NE	Salix glaucosericea,Anthoxanthum alpinum	95	Hyperskeletic Leptosol
	3000	low	1914	32	S	Carlina acaulis,Achillea moschata	60	Skeletic Cambisol
	3000	medium	1910	32	S	Vaccinium vitis-idaea,Carlina acaulis	85	Skeletic Cambisol
	3000	high	1888	25	SE	Thymus polytrichus,Trifolium nivale	70	Skeletic Cambisol
	10 000	low	1882	24	NE	Rhododendron ferrugineum, Vaccinium myrtillus	100	Dystric Cambisol
	10 000	medium	1882	29	N	Rhododendron ferrugineum,Vaccinium uliginosum	90	Dystric Cambisol
	10 000	high	1873	18	NE	Rhododendron ferrugineum, Calluna vulgaris	90	Dystric Cambisol
Calcareous parent material								
	110	low	∼2200	-	WNW	Saxifraga aizoides, Poa alpina	50	Hyperskeletic Leptosol
	110	medium	∼2200	-	WNW	Saxifraga aizoides, Poa alpina	52	Hyperskeletic Leptosol
	110	high	∼2200	-	WNW	axifraga aizoides, Poa alpina	63	Hyperskeletic Leptosol
	160	low	2038	35	E	Dryas octopetala, Saxifraga aizoides	70	Hyperskeletic Leptosol
	160	medium	2025	33	NE	Astragalus alpinus, Dryas octopetala	78	Hyperskeletic Leptosol
	160	high	2032	29	NW	Salix retusa, Festuca quadriflora	79	Hyperskeletic Leptosol
	4900	low	2019	28	SE	Anthyllis vulneraria, Lotus alpinus	100	Calcaric Skeletic Cambisol
	4900	medium	2016	33	NE	Luzula sylvatica ssp sieberi, Lotus alpinus	100	Calcaric Skeletic Cambisol
	4900	high	2018	34	W	Leontodon helveticus, Festuca rubra	100	Calcaric Skeletic Cambisol
	13 500	low	2001	35	NW	Alchemilla fissa, Ligusticum mutellina,	100	Calcaric Skeletic Cambisol
	13 500	medium	2012	38	NE	Anthoxanthum alpinum, Dryas octopetala	100	Calcaric Skeletic Cambisol
	13 500	high	2017	33	NE	Alchemilla conjuncta, Dryas octopetala	100	Calcaric Skeletic Cambisol

Figure 2.1: Glacier forefield and location of the four selected moraines of the silicate parent material (S-PM, left (© Google Maps, 2020a)) and the calcareous parent material (C-PM, right (© Google Maps, 2020b)).

2.2.2 Soil sampling and laboratory analysis

Soil sampling

Soils samples were taken during August and September of 2018 at the silicate site and during August and September 2019 at the calcareous site. Three sampling sites were chosen per moraine to capture three complexity levels (low, medium, high) of the vegetation coverage (Musso et al., 2019). Table 2.2 provides a detailed overview of the sampling scheme at each sampling site for both parent materials. At each sampling site, replicate samples were taken 3-4 m apart to account for spatial variability. The two sampling locations per sampling site are denoted as Location 1 and Location 2 in Table 2.2. For grain size analysis, at each sampling site two disturbed soil samples (one per sampling location) were taken at 10, 30, and 50 cm depth.

Table 2.2: Overview of the sampling scheme at each sampling site for both parent materials. The two sampling locations per sampling site are denoted as Location 1 and Location 2. Locations 1 and 2 were 3-4 m apart. The volume of the sample rings is given in the respective headers and the corresponding numbers of samples are provided for each soil depth.

	Silicate parent material						*Calcareous parent material*					
	Location 1			*Location* 2			*Location* 1			*Location* 2		
	100 cm^3	250 cm^3	*disturbed*	100 cm^3	250 cm^3	*disturbed*	100 cm^3	250 cm^3	*disturbed*	100 cm^3	250 cm^3	*disturbed*
Depth [*cm*]												
10	1	2	1	-	2	1	-	2	1	-	2	1
30	1	2	1	-	2	1	-	2	1	1	1	1
50	2	1	1	1	-	1	1	1	1	2	-	1

For the determination of porosity, bulk density, and loss on ignition as well as the derivation of the soil hydraulic properties, undisturbed soil samples were taken with steel sampling rings, which preserve the natural soil structure. At each sampling site and sampling location at the S-PM, two 250 cm^3 undisturbed soil samples were taken at a depth of 10 and 30 cm, and one 100 cm^3 sample was taken at a depth of 50 cm. Additionally at sampling Location 1, one undisturbed 100 cm^3 soil sample was taken at a depth of 10 and 30 cm, and one 250 cm^3 and two 100 cm^3 soil samples were taken at a depth of 50 cm. This sampling scheme provides 15 undisturbed soil samples at the depths of 10 and 30 cm and 12 samples at a depth of 50 cm per moraine. All 168 samples were used for the determination of porosity and bulk density. Due to the high stone content at the S-PM forefield, a few sampling rings were damaged and could not be used the following year. Therefore, the sampling scheme at the C-PM forefield had to be adapted to a reduced number of samples (see Table 2.2). At the C-PM forefield and Location 1 at each sampling site, two 250 cm^3 undisturbed soil samples were taken at a depth of 10 cm and 30 cm and one 250 cm^3 and one 100 cm^3 sample were taken at 50 cm. At Location 2, two 250 cm^3 samples were taken at 10 cm and one 250 cm^3 and one 100 cm^3 sample at 30 cm as well as two 100 cm^3 samples at 50 cm. This sampling scheme provides 12 undisturbed soil samples at the depths of 10, 30, and 50 cm per moraine. All 144 samples were used for the determination of porosity and bulk density.

Laboratory analysis

The laboratory analysis was carried out between October 2018 and June 2019 for the S-PM samples and between October 2019 and January 2020 for the C-PM samples. For the grain size analysis, we used a combination of dry sieving (particles > 0.063 mm) and sedimentation analysis (particles < 0.063 mm) with the hydrometer method. Particles between 2 mm and 0.063 mm were classified as sand, between 0.063 mm and 0.002 mm as silt and < 0.002 mm as clay. Particles larger than 0.063 mm were separated from the fine particles by wet sieving. They were then dried at 550 °C for combustion of organic matter prior to the dry sieving. Due to lab limitations, organic matter removal from the fine particles was only possible by floating off the lighter fractions prior to the sedimentation analysis. $Na_4P_2O_7$ was added 24 hours before sedimentation analysis as a dispersant to the sample solution to prevent coagulation of the particles. Particle size fractions were calculated as weight percentages of the fine earth (< 2 mm), thus excluding gravel and stones to prevent single larger stones from shifting or dominating the distribution. The gravel and stone fraction (particles > 2 mm) was calculated separately as a weight percentage of the entire soil sample. The porosity was determined by using the water saturation method and weighing the samples at saturation and after drying at 105 °C. The loss on ignition was determined by drying sub-samples (4-6 g) of 131 samples of the S-PM forefield and 144 samples of the C-PM forefield for at least 24 hours at 105 °C and then at 550 °C. The loss on ignition was then calculated by relating the weight loss after drying at 550 °C to the sample weight after drying at 105 °C.
A total of 15 undisturbed 250 cm^3 samples per moraine (six samples at both 10 and 30 cm depth and three at 50 cm depth) were used for the analysis of soil hydraulic properties in the form of retention curve and hydraulic conductivity curve. The soil hydraulic properties of the 120 soil samples were measured based on the experimental evaporation method (Schindler, 1980; Schindler and Müller, 2006). This laboratory-based method allows the simultaneous determination of retention curve and hydraulic conductivity curve. The water-saturated soil samples are dried evenly and slowly by evaporation. During this process, the weight of the soil sample and the matric potential at two heights in the soil core are measured. To conduct the experiment we used the ku-pF MP10 (Umwelt-Geräte-Technik GmbH, Germany). The device allows the experiment to be conduct simultaneously on 10 soil samples at a time, with each cycle taking 2 to 3 weeks. The device holds 10 soil samples on a rotating appliance and automatically measures the weight of each sample. The interval between individual sample measurements was set to 1 min, so that each sample was measured every 10 min. For the measurement of the matric potential, two tensiometers were installed at two different heights in the soil core. At each weight measurement, the device also records the tensiometer readings. The data analysis was carried out according to Peters and Durner (2008). Based on the weights the soil water content can be derived and is set in relation with the average measured matric potential to provide the retention curve. Based on the measured reduction in water content, a flow rate can be determined, and the hydraulic gradient can be derived based on the measured matric potentials. The combination of flow rate and gradient allows the determination of the unsaturated hydraulic conductivity for all measured water contents.

2.3 Data set of soil physical properties and their change through the millennia

2.3.1 Bulk density and porosity

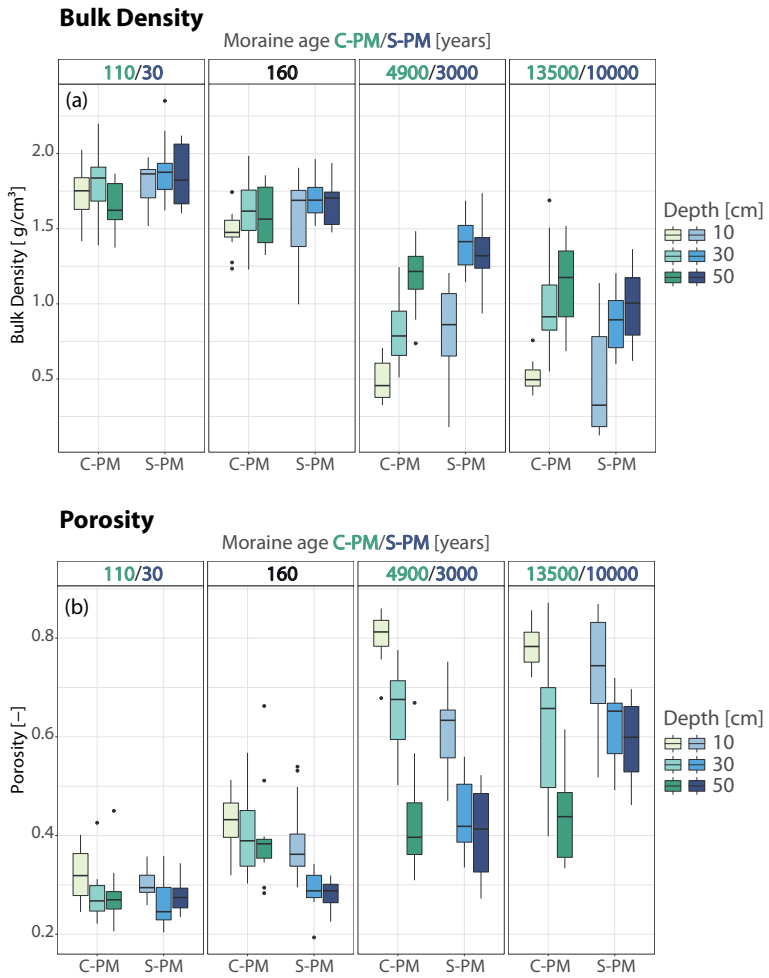

Figure 2.2: Development of bulk density and porosity at 10, 30, and 50 cm depth over 10 millennia on silicate (S-PM, shown in blue color scale) and calcareous (C-PM, shown in green color scale) parent material.

The obtained data sets of bulk density and porosity show a clear trend over the millennia in both properties at both soil chronosequences (see Fig. 2.2). At the C-PM forefield, the bulk density decreases along the chronosequence at all soil depths (see Fig. 2.2a). The decrease is most pronounced in the top layer and is weaker towards deeper soil depths. With increasing age an ongoing differentiation in bulk density along the soil profile is observed. At the youngest moraine of 110 years, the bulk density ranges mainly between median values of 1.6 g/cm^3 and 1.8 g/cm^3 with slightly higher values at 30 cm. At the 160-year-old moraine, the bulk density at all depths varies in median values between 1.5 and 1.6 g/cm^3. The 4900-year-old moraine has significantly lower bulk densities, with the lowest values in the top layer (median value in the top layer: 0.46 g/cm^3). The bulk density increases with depth and varies around 0.78 g/cm^3 at 30 cm and around 1.2 g/cm^3 at 50 cm. The oldest moraine of 13 500 years does not show major differences in

bulk density from the 4900-year-old moraine. The ranges of the values differ but the median values are quite similar.

At the youngest moraine at the S-PM forefield, the interquartile range (IQR) at all three depths overlaps; the bulk density values vary mainly between 1.7 and 1.9 g/cm^3. The bulk density at the 160-year-old moraine is lower and ranges mainly between 1.4 (lower end of IQR at 10 cm) and ∼1.75 g/cm^3 (upper end of IQR at all three depths). At this age class, the uppermost layer already shows the tendency to have a lower bulk density than the deeper soil. This is even more pronounced at the 3000-year-old moraine. The bulk density at 30 and 50 cm depth at this moraine ranges between median values of 1.3 (at 50 cm) and 1.4 g/cm^3 (at 30 cm), whereas the bulk density at 10 cm mainly ranges in IQR between 0.65 and 1.07 g/cm^3. At the 10 000-year-old moraine the bulk density is the lowest and varies in IQR between 0.2 and 0.78 in the uppermost layer. The IQR at 30 and 50 cm overlaps strongly. Here, the bulk density varies between 0.7 (lower end of IQR at 30 cm) and 1.17 (upper end of IQR at 50 cm).

A comparison of the 160-year-old moraine at both locations shows that the bulk density across the soil profiles is similar at both locations, but is in general lower at the C-PM. At the second-oldest moraines the bulk density at C-PM is also lower at all three depths compared to S-PM. However, this relation is reversed at the oldest moraine. The bulk density at 10 and 50 cm depth at S-PM is significantly lower even though the moraine is younger than the corresponding moraine at C-PM.

The porosity shows an increase along the age groups and an ongoing differentiation across the soil profile at both chronosequences (Fig. 2.2b). At C-PM the porosity at the youngest moraine is in a similar range along the soil profile, except for the top layer, which shows higher porosity values with a median at 0.32 (30-50 cm median value: ∼0.27). At the 160-year-old moraine, the values are already slightly higher and vary around median values of 0.38 and 0.43. The 4900-year-old moraine shows a strong increase in porosity and a clear differentiation between the individual depths. The porosity in the topsoil is highest with a median value slightly above 0.81. In the layers below, on the other hand, the porosity is lower (values vary around median values of 0.67 and 0.39 at 30 and 50 cm depth, respectively). Analogous to the development of bulk density, there is no striking difference between the two oldest moraines, the porosity values have a similar range.

At the S-PM forefield the porosity evolution shows similar tendencies. At the 30-year-old moraine the porosity at 30 to 50 cm depth ranges between 0.24 and 0.29. The porosity at 10 cm is slightly higher, with values in an IQR from 0.28 to 0.32. A differentiation between the soil depths is, however, already visible at the 160-year-old moraine, where the IQR of porosity values in the uppermost layer ranges from 0.34 to 0.4. The porosity at 30 and 50 cm depth, however, is not noticeably different from the same depths at the youngest moraine. Compared to the two youngest moraines the porosity in the uppermost layer at the 3000-year-old moraine is distinctly higher, with values of the IQR mainly ranging between 0.55 and 0.65. The porosity at 30 and 50 cm is also higher and varies over a broader range compared to the younger moraines. The IQRs of the two depths are overlapping. The porosity values range mainly between 0.33 and 0.5, with a median value at 0.41 at both depths. After 10 000 years of soil development the porosity reached its highest values ranging in an IQR from 0.67 to 0.83 in the uppermost soil layer and again in an overlapping IQR at 30 and 50 cm depth from mainly 0.5 to 0.66. In contrast to the 3000-year-old moraine the median values differ at 30 and 50 cm depth (0.65 at 30 cm and 0.6 at 50 cm).

A comparison of the two 160-year-old moraines at the two sites shows that the porosity at the C-PM is

higher at all three soil depths. However, while there is a strong change in porosity at all depths at S-PM between 3000 and 10 000 years of soil development, there is no clear difference between the two oldest age groups at C-PM.
The evolution of bulk density and porosity does not only reveal a constant decrease in bulk density and increase in porosity, but also shows a progressive differentiation of these values between the soil layers. Additionally, an increase in the range of values is also noticeable. Thus, with increasing age not only the vertical, but also the lateral variability in bulk density and porosity increases.

2.3.2 Soil texture

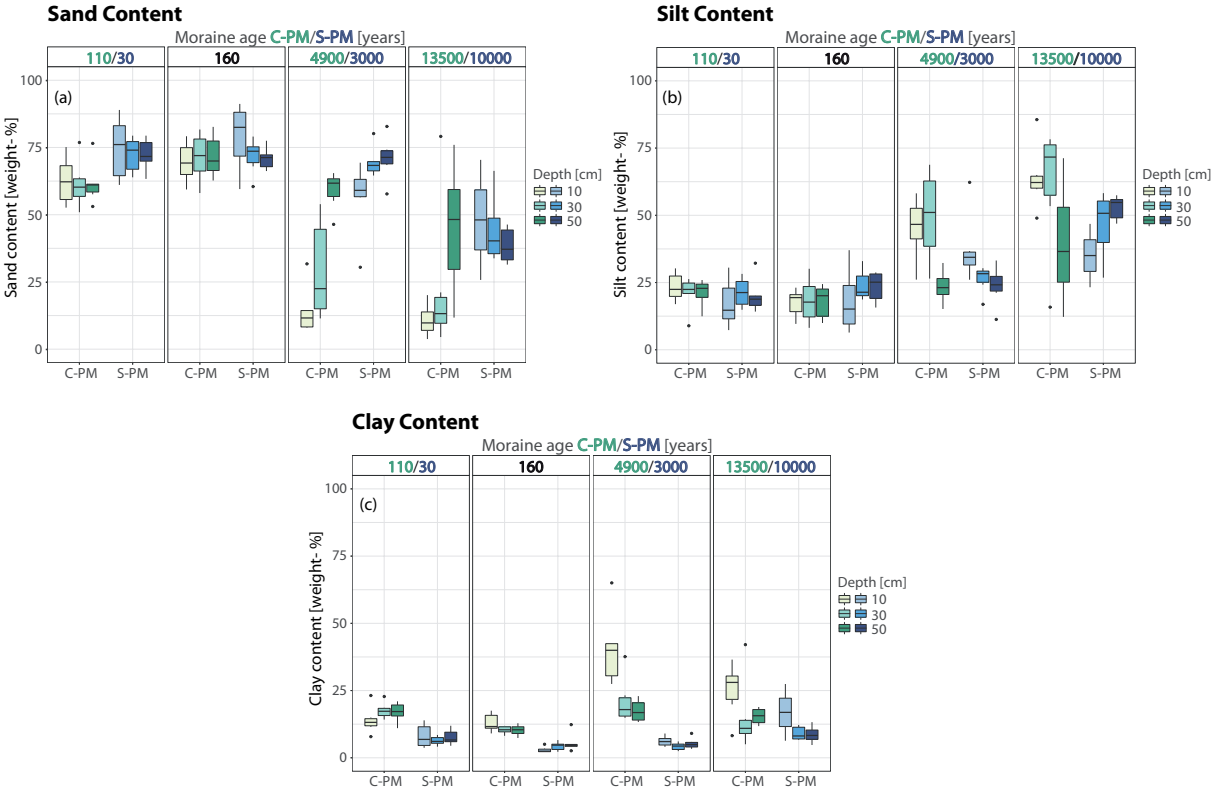

Figure 2.3: Development of sand, silt, and clay content at 10, 30, and 50 cm over 10 millennia on silicate (S-PM, shown in blue color scale) and calcareous (C-PM, shown in green color scale) parent material.

The development of the grain size distribution over the millennia shows a distinct reduction in the sand fraction at all three depths at both chronosequences (Fig. 2.3a). At C-PM, the fraction of sand at the youngest moraine with over 50 weight-%, accounts for the largest share of all grain sizes and is also relatively homogeneous with depth. The fraction of sand at the 160-year-old moraine is slightly larger compared to the youngest moraine. With increasing age, there is a significant reduction in the fraction of sand, especially in the upper layers. The sand content at the surface is reduced to $\sim$10 weight-% at the two oldest moraines, whereas the sand content at 50 cm is less affected. However, at 30 cm at the 4900-year-old moraine and at 50 cm at the 13 500-old-moraine the sand fraction varies over a broad range (15-45 weight-% and 30-60 weight-%, respectively).

At S-PM, the fraction of sand at the youngest moraine is relatively homogeneous across the soil profile. At the 160-year-old moraine, the fraction at the topsoil is slightly higher than at the youngest moraine. However, a differentiation with depth can already been seen with lower values in deeper layers. The reduction in sand content continues with increasing age, whereas at the 3000 year-old moraine the distribution with depth is reversed with the topsoil having a lower sand fraction than the deeper layers. At the 10 000 year-old-moraine, the profile distribution reverses again with the topsoil having now the highest values. In general, the fraction of sand at the individual depths and age classes is higher at the S-PM chronosequence compared to the C-PM chronosequence.
It has to be taken into account that the particle size analysis of the samples at a depth of 10 cm in the 10 000-year-old moraine at S-PM could only be carried out on two samples since the organic matter content of the other samples was too high. Since a complete removal of the organic matter content cannot be guaranteed, the two samples are subject to strong uncertainties. These uncertainties also apply to the other samples from the oldest moraines at both chronosequences that have a high organic matter content.
For the silt fraction, an increase at all depths over the chronosequence can be seen at both forefields. This is more pronounced at C-PM than at S-PM (Fig. 2.3b). At C-PM, the silt fraction at the 110- and 160-year-old moraines is mostly lower than 25 weight-% and homogeneous across the profile, but with slightly higher values at the youngest moraine. With increasing age, the silt fraction increases strongly, especially at 10 and 30 cm. After 13 500 years the silt fraction is at its highest at 30 cm (median: $\sim$ 72 weight-%), even higher than in the topsoil (median: 62 weight-%) and the lowest at 50 cm (median: 37 weight-%).
At S-PM, the silt fraction in the topsoil at the youngest moraine (median: <20 weight-%) is slightly lower than in the deeper soil (median $\sim$20 weight-%). The difference can be seen more clearly at the 160-year-old moraine, where the silt fraction at all depths is still mainly below 25 weight-%. After 3000 years of soil development the silt content at 10 and 30 cm is higher compared to the 160-year-old moraine, but the distribution reverses revealing a decrease in silt content with depth. The silt fraction at 50 cm is in the same range as at the 160-year-old moraine (median: $\sim$25 weight-%), whereas in the top layers the silt content increased to values ranging in the IQR from 31-35 weight-%. After 10 000 years the depth distribution is reversed again. Compared to the 3000-years old moraine the silt fraction in the topsoil is still in the same range, whereas the fraction at 30 and 50 cm increased to median values equal to and higher than 50 weight-%. Among S-PM and C-PM, the depth distribution of the silt content at the oldest moraine differs significantly. Whereas at S-PM the silt content increases with depth, the silt content at C-PM is highest at 30 cm (median value at 72 weight-%) and lowest at 50 cm (median: $\sim$30 weight-%).
The clay content increases with age at both chronosequences (see Fig. 2.3c). At the youngest moraine of both chronosequences the clay fraction is fairly homogeneous across the soil profile. At C-PM the topsoil has a slightly lower clay fraction (median: $\sim$13 weight-%) than the deeper layers (median $\sim$17 weight-%), but the values are in general slightly higher than at S-PM (median at all depths < 10 weight-%). At the 160-year-old-moraine, the clay fraction at both chronosequences is comparatively lower than at the youngest age class, but relatively homogeneous throughout the soil profile. The clay fractions at C-PM (median at all depths: $\sim$11 weight-%) are higher than at S-PM (median at all depths: < 10 weight-%). At the second-oldest moraine of the C-PM chronosequence the clay content increases at all depths, which is most pronounced in the top layer (median value around 40 weight-%). The oldest moraine, however,

shows lower values at 10 and 50 cm compared to the second-oldest moraine. The clay fraction in the topsoil at 13 500 years (∼28 weight-%) is still higher than at 50 cm, where at 30 cm the clay fraction is the lowest (median ∼10 weight-%). At S-PM only the topsoil shows a slight increase in clay fraction from 160 to 3000 years of soil development, while at the oldest moraine clay fraction increases at all depths, with the topsoil having the highest fraction (median value ∼17 weight-%). In comparison, the clay content at all age classes is higher at C-PM than at S-PM. A first investigation of the effect of the soil texture at the S-PM forefield on near-surface hydrology can be found in Maier et al. (2020).

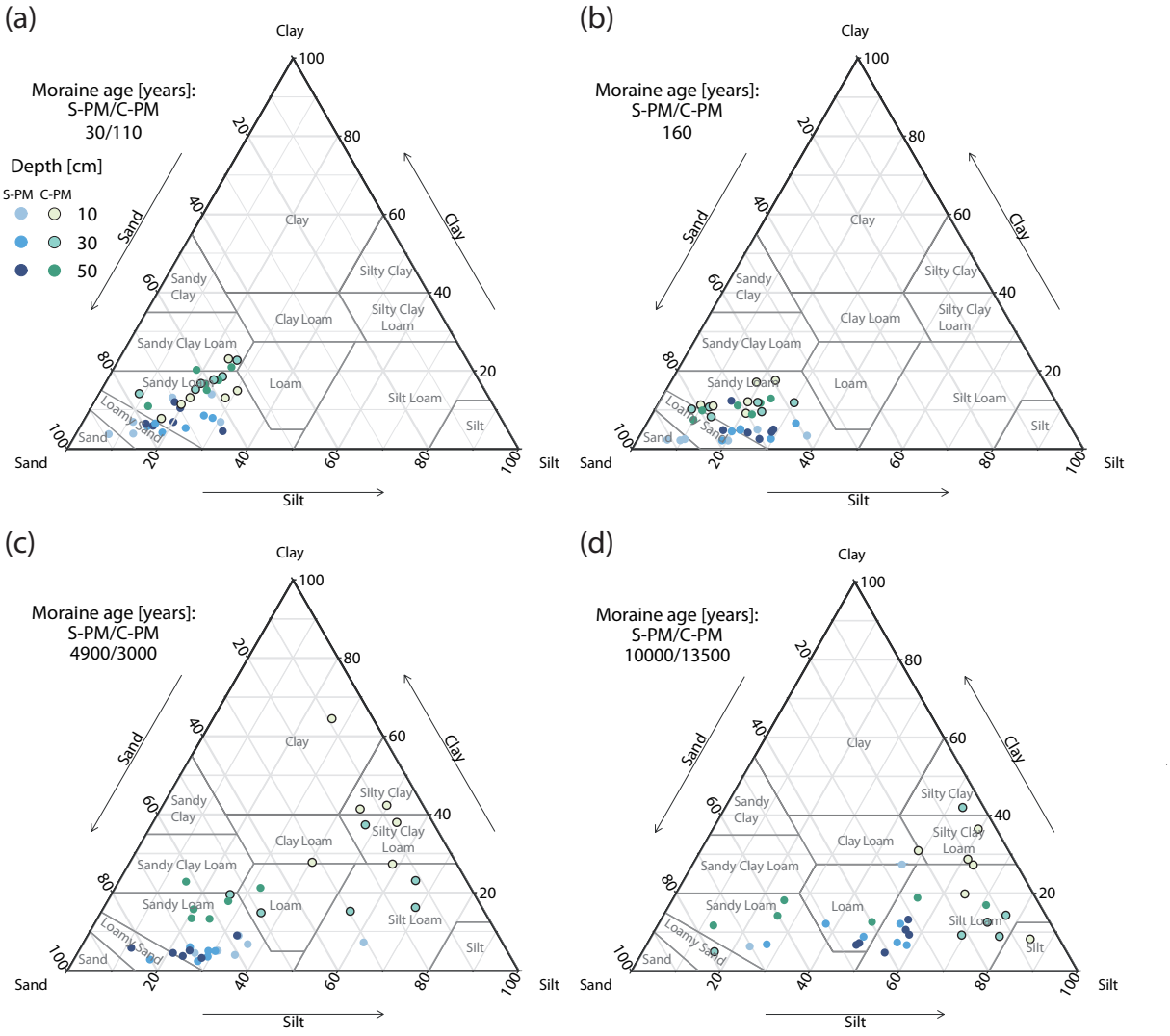

Figure 2.4: Ternary diagram for soil type classification using the USDA Textural Soil Classification. Each plot shows a single age class and compares the grain size distributions of both parent materials and all three depths.

Incorporated into a ternary diagram (Fig. 2.4) for soil type classification using the USDA Textural Soil Classification (Hamilton and Ferry, 2018), the grain size evolution reveals a clear shift in soil types at both chronosequences throughout the millennia. The soil types at the two youngest moraines at both chronosequences mainly vary between loamy sand and sandy loam. Soil types at the 3000- (S-PM) and 4900-year-old (C-PM) moraines differ from each other (Fig. 2.4c). Whereas at S-PM sandy loam is still

the prevailing soil type, the soil types at C-PM shifted to silty clay and silty clay loam in the topsoil and mainly loam and silt loam at 30 cm. At 50 cm sandy loam is still the main soil type. At the oldest moraine the soil types at S-PM also shift to loam and silt loam (Fig. 2.4d). At C-PM the topsoil at the oldest moraine is still mainly a combination of silt, clay, and loam. At 30 and 50 cm depth, however, next to loam and silt dominated soil also sandy loam is frequently present.

The gravel and stone fraction (see Fig. 2.5) here included only stones with a diameter between 2 and ∼100 mm. At both parent materials the gravel and stone fraction decreases with soil age. The decrease is most pronounced in the topsoil and at the oldest moraine in the C-PM forefield .

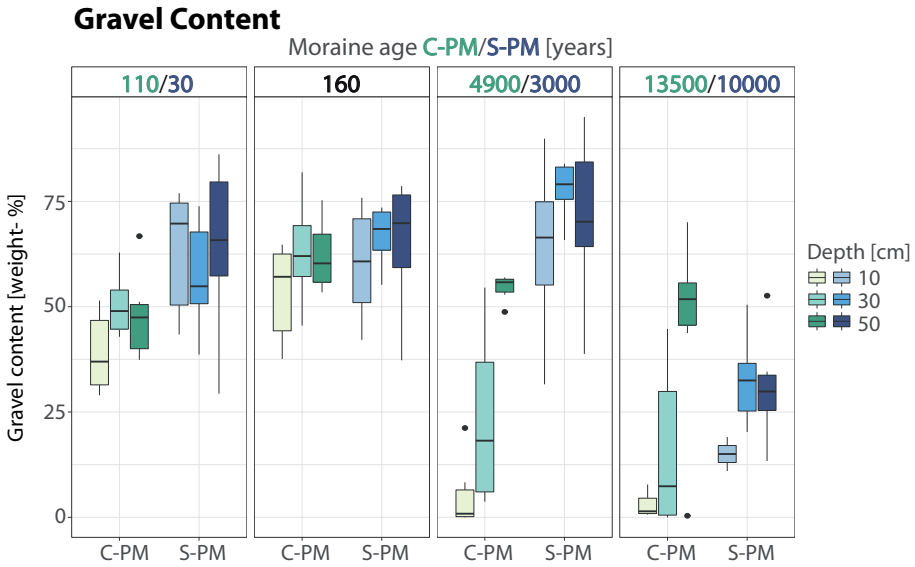

Figure 2.5: Development of gravel/stone content at 10, 30, and 50 cm over 10 millennia on silicate (S-PM, shown in blue color scale) and calcareous (C-PM, shown in green color scale) parent material.

Hartmann et al. (2020a) provides additional information on the evolution of stone content with depth for the S-PM forefield derived by image analysis of soil profile walls with a vertical extent up to 1 m.

2.3.3 Loss on ignition

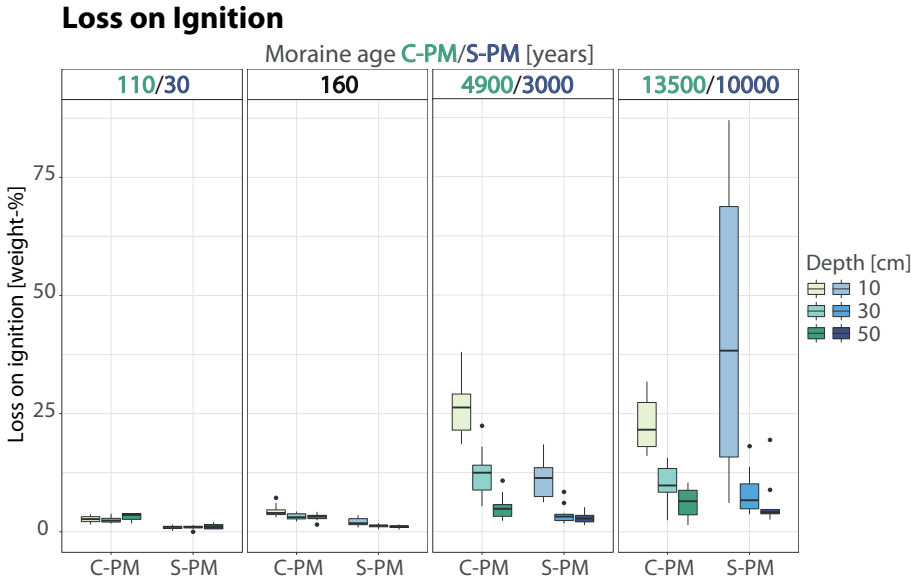

Figure 2.6: Development of loss on ignition at 10, 30, and 50 cm over 10 millennia on silicate (S-PM, shown in blue color scale) and calcareous (C-PM, shown in green color scale) parent material.

The loss on ignition is a measure of the organic substance in the soil and describes the proportion of the organic substance that was oxidized during annealing for 24 hours at 550 °C. The organic substance is a heterogeneous mixture of faunal and floral substances.

Both chronosequences show a significant increase in organic matter throughout the first 10 millennia of soil development, which is most pronounced in the upper soil layer (see Fig. 2.6). For both chronosequences at the two youngest moraines the organic matter content is still very low, with C-PM showing slightly higher values (< 2 weight-% at S-PM and 2-4 weight-% at C-PM). At these two age classes the organic matter content is homogeneously distributed over the profile, with a slight tendency to higher values in the topsoil at the 160-year-old moraine. At the medium-age moraines of both chronosequences (3000 and 4900 years) a significant increase in the organic matter content in the surface layer can be observed (median: 11 weight-% at S-PM and up to 26 weight-% at C-PM). There is also an increase at greater depths, which is more pronounced at C-PM. At the oldest moraine at S-PM the trend of increasing organic matter continues at all three depths. Here, the organic content in the topsoil makes up to two-thirds of the soil material. However, the organic matter content varies strongly, with a minimum of 6 and a maximum 87 weight-%. At greater depths, the organic matter content also increases compared to the 3000-year-old soil, but remains below 20 weight-%. The organic matter content decreases with increasing soil depth. At C-PM the organic matter content at the top layer of the oldest moraine is slightly lower compared to the second-oldest moraine. In general the organic matter content at all three soil depths does not differ considerably between the two age classes.

2.4 Data set of soil hydraulic properties and their change through the millennia

2.4.1 Retention curves

The retention curve, the relationship between volumetric soil water content and matric potential, is an important individual characteristic of soils, and depends strongly on soil physical and biological soil properties. The retention curves show a clear change over the millennia at both forefields (Fig. 2.7).

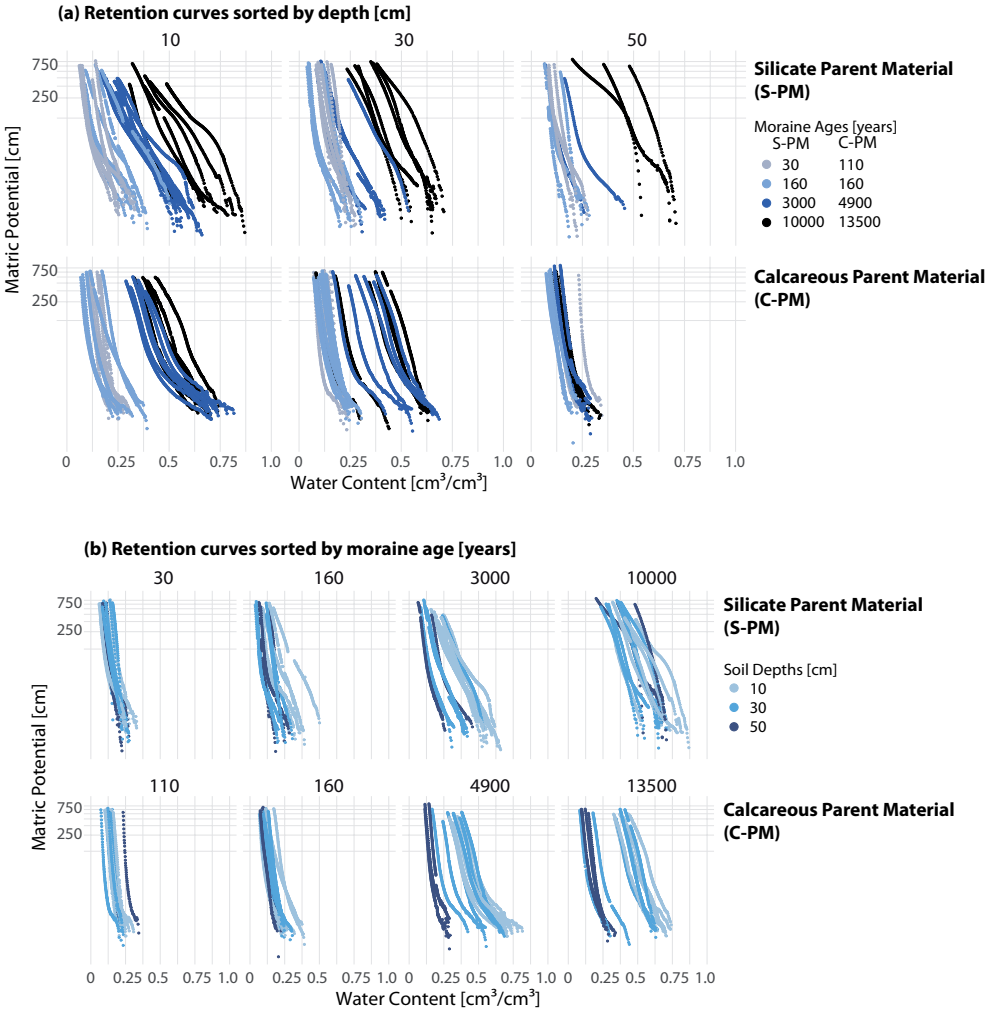

Figure 2.7: Development of retention curves at 10, 30, and 50 cm over 10 millennia on silicate (S-PM) and calcareous (C-PM) parent material sorted by depth (a) and moraine age (b).

At both chronosequences the lower end of the retention curves (nearly saturated conditions) show a clear shift to higher water contents with increasing moraine age, which is strongly coupled to the increase in porosity (equal to saturated water content) (see Fig. 2.7a). This trend is most pronounced in the top layer and decreases with soil depth. The air entry value, indicated by the first change in slope close to saturated conditions, shifts to higher matric potential, which is particularly pronounced in the organic layer at S-PM. At C-PM, however, this shift is not very pronounced, and especially at 50 cm depth, the retention curves

are all similar. However, at both chronosequences the slope of the curve above the air entry value shows the tendency to decline with increasing age. The variability in retention curves with depth also increases with age at both chronosequences (see Fig. 2.7b). After 3000 years at S-PM and 4900 years at C-PM, the retention curves of the three depths show clear differences, while at the youngest moraines of both chronosequences the retention curves of the three depths are similar indicating a homogeneous soil profile. For the older moraines, the increase in saturated water content and air entry value, as well as the decrease in slope, are most pronounced in the uppermost layer, this becomes less pronounced with increasing depth.

2.4.2 Hydraulic conductivity curves

The unsaturated hydraulic conductivity curve is another important flow-defining soil characteristic. It describes the relation between the unsaturated soil hydraulic conductivity and soil matrix potential (or soil water content, respectively). The hydraulic conductivity curves also change over the millennia (Fig. 2.8a).

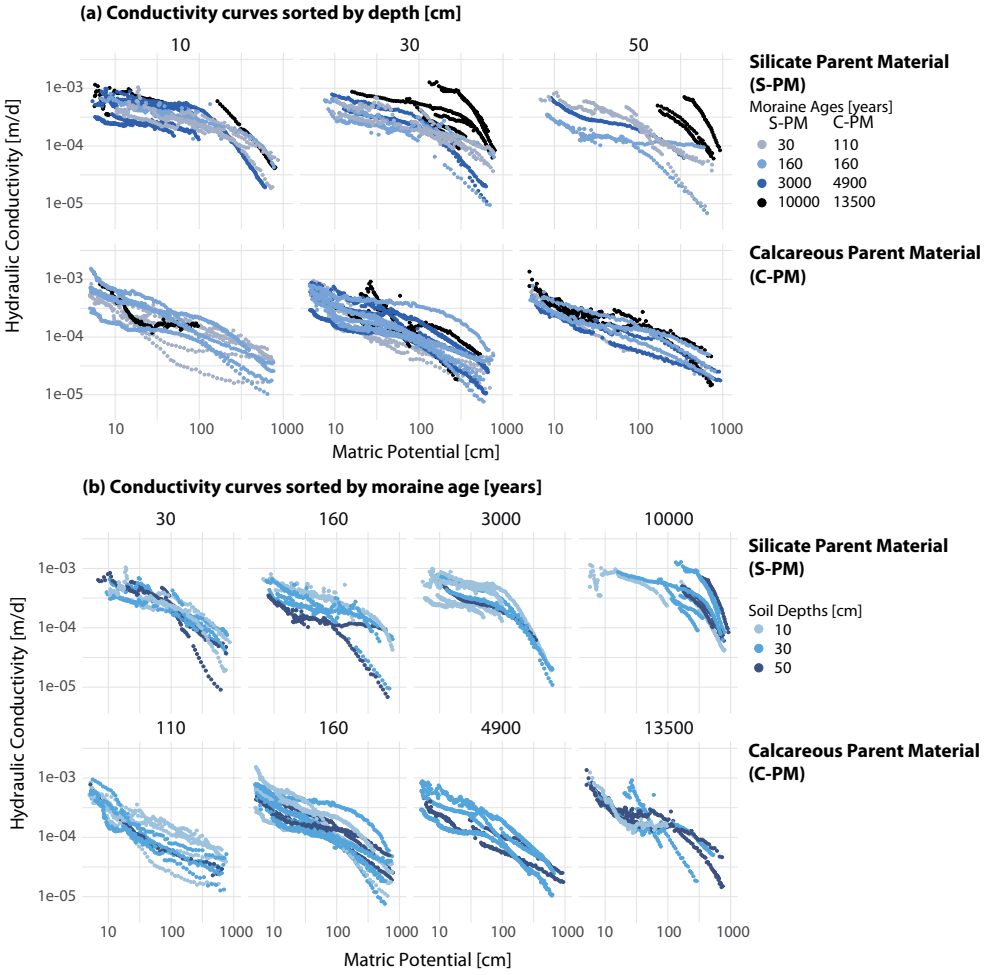

Figure 2.8: Development of hydraulic conductivity curves at 10, 30, and 50 cm over 10 millennia on silicate (S-PM) and calcareous (C-PM) parent material sorted by depth (a) and moraine age (b).

Out of the 60 soil samples taken at each moraine and analyzed by the method according to Schindler (1980), only 32 at S-PM and 41 at C-PM could be analyzed for the hydraulic conductivity curve according

to the method by Peters and Durner (2008). Seven of the excluded soil samples at S-PM and two at C-PM could not be used because the installation of the second tensiometer into the sample was prevented by stones. The other samples had to be excluded as the upper part of the sample dried out much faster than the lower part during the evaporation experiment. An approximately linear profile of the soil matric potential within the sample could thus no longer be assumed. This is typical for soils with large pore sizes, such as sandy soils. The excluded samples belonged to all age classes, but most of them belonged to the topsoil of the oldest moraines, where the organic matter content is very high (Fig. 2.6).
Despite the thin data basis, a trend is visible at both chronosequences that the heterogeneity in the conductivity curves increases with increasing moraine age (Fig. 2.8). At the S-PM forefield the conductivity curves at 10 cm show a sharp drop in conductivity, except for the young moraine. Here, the reduction in the conductivity reduces only slowly to a certain point at which the decrease continues faster. The conductivity curves of C-PM at 10 cm cannot be evaluated in this context, since the curves of the topsoil at the two oldest moraines could not be evaluated. However, the curves of the youngest moraine show a similar modest decrease in conductivity at higher matric potentials as at the young moraines at the S-PM forefield. The curves of the 160-year-old moraine at C-PM already show a sharper decrease in conductivity.
At 30 cm depth at S-PM, almost all curves show a slight reduction in conductivity. The curves of the 3000-year-old moraine are an exception here and show steeper curves. The curves at 30 cm at C-PM are very heterogeneous. The curves of the young moraines still show a rather slow decrease in conductivity, whereas the curves at the older moraines show a faster reduction. At 50 cm depth, the database at both chronosequences is not so extensive. While the conductivity curves at the S-PM forefield are very heterogeneous, the curves at the C-PM forefield are very close to each other with only a few single curves from the two oldest moraines showing a steeper slope towards increasing soil matric potential. At the S-PM forefield, the curves show a strong reduction in conductivities at higher matric potential, but this appears to occur at even higher matric potentials at the oldest moraine.

2.5 Data quality and uncertainties

The space-for-time substitution approach assumes that a sequence of sites (e.g., moraines) with similar site characteristics such as topography, climate, and parent material can be treated as a chronosequence. It is well known that the application of this chronosequence concept has some limitations. The assumption that time is the only factor affecting soil development in a spatial sequence of soils is rarely valid but the only option for a detailed historical tracking of landscape development at a particular location (Phillips, 2015). We therefore have to assume that differences in topography and elevation among the selected moraines only lead to moderate differences in soil hydrologic conditions. However, we made sure that slopes of the three selected plots per moraine were in a similar range. The plots at the silicate parent material range in slope from 18 to 34° with the majority of plots between 20 and 30°. The maximum elevation difference between the lowest and the highest plot is 116 m. At the calcareous site the slopes range from 29 to 38°, also with the majority of plots ranging between 33 and 35°. Here, three out of four moraines are at almost the same elevation. The elevation difference to the youngest moraine is 200 m.
While sampling, transport and analyses of the samples were handled with the uttermost care, we cannot

entirely exclude the possible occurrence of different adverse effects which would negatively impact our measurement uncertainty. A quantification of these uncertainties is difficult to achieve; however, we briefly discuss them below and give some indication for which of the sample uncertainties might be higher than for others.

All data shown were obtained on the basis of soil samples taken in the field. Soil samples are subject to various types of uncertainties. Due to the high spatial variability in vegetation cover and soil properties, it is difficult to represent a complete moraine by taking individual soil samples. In order to counteract this situation, we used the variability in vegetation cover as a proxy to bracket this variability. Thus, samples were taken at several locations with different vegetation complexity (low, medium, high) and by taking at least two replicates.

Undisturbed sampling with sample rings that are hammered into the ground is difficult to guarantee and requires great care. In alpine locations, the high stone content of the soil leads to an increased level of difficulty. This was particularly the case at the young moraines. Sampling was particularly difficult here and required repeated attempts to obtain a sample (which is likely biased towards less or smaller stones). Furthermore, the samples must be transported with as little disturbance as possible. Despite adequate precautions, it cannot be ruled out that vibrations occurred during the transport of the samples, which could have affected the structure of the soil samples. This applies particularly to the C-PM site, where the samples had to be transported part of the way by helicopter due to the difficult access to the site.

Even when processing the samples in the laboratory, handling of the samples can affect the structure. Also, the integrity of the samples can be influenced by laboratory methods. The complete saturation of the soil samples, which is necessary for many analyses but is rarely found under natural conditions, can lead to the displacement of fine particles in the sample. This could have affected the results of the soil hydraulic properties analysis. However, the resulting uncertainty cannot be quantified. Additionally, the particle size analysis of the samples at a depth of 10 cm in the 10 000-year-old moraine could only be carried out on two samples at the S-PM site since the organic matter content of the other samples was too high. The results of the two samples are subject to strong uncertainties since it could not be ensured that the entire organic matter could be removed. This also accounts for the other soil samples with a high organic matter content. The incomplete removal of the organic matter can lead to an overestimation of the silt and clay content.

Uncertainties in the analysis of the soil hydraulic properties result, on the one hand, from the already mentioned possible particle displacement during saturation or from the measuring device used. The installation of the tensiometers can lead to a compaction of the soil material around the tensiometer tips, which is more likely in the samples of the old moraines with strongly developed soil material. In the samples of the young moraines, on the other hand, the installation can shift stones and soil material, which affects the structure. When evaluating the evaporation experiment, the validity of the assumptions about the matric potential distribution must also be considered. Since a drifting apart of the matric potential in the upper and lower tensiometer excludes an approximately constant linear profile of the matric potential in the center of the sample, an evaluation of the conductivity curve is no longer justifiable. When evaluating the retention curves, this was not considered to be critical, since the averaged measured matric potential is related to the bulk water content, determined via the weight measurement.

2.6 Summary

The evolution of soil physical and hydraulic properties over ten millennia was investigated by analyzing soil samples of soil chronosequences in two glacier forefields; one glacier forefield developed on silicate and the other on calcareous parent material. The chosen soil chronosequences consisted of four age classes ranging in age from less than 100 years to more than 10 000 years. Spatial variability in soil properties was taken into account by selecting three sampling sites per moraine along a gradient of vegetation complexity (low, medium, high) and by taking replicate samples. Uncertainties due to sampling techniques, transportation or sample handling during laboratory analyses cannot be excluded, but were minimized as much as possible through careful handling. Soil physical properties in the form of bulk density, porosity, and organic matter content, as well as gravel, sand, silt, and clay fraction were analyzed at 10, 30, and 50 cm soil depth.

At both chronosequences a decrease in bulk density and an increase in porosity was observed at all depths. The trend was equally present at both chronosequences, but absolute values and depth profiles differ among the two parent materials at both sites. The grain size distribution shows a pronounced reduction in sand fraction and an increase in silt and clay fraction over time. The sand fraction at the calcareous site was initially lower than at the silicate site. This difference became stronger at the two oldest age classes, since the reduction in sand fraction was more pronounced at the calcareous site. The silt fraction, however, was almost equal at the youngest age classes at both sites, but increased strongly in the topsoil of the calcareous site. The smallest changes occurred in the clay fraction, which was higher at the calcareous site at all age classes.

The organic matter content also increased with increasing age at both sites. Whereas the organic matter content in the topsoil was higher at the calcareous site at the intermediate age classes, the silicate site showed a strong increase and a high variation at the oldest age class. With the change in physical soil properties and organic matter content, a pronounced change in hydraulic soil properties in the form of retention curve and hydraulic conductivity curve was also observed. The changes reveal an evolution from fast-draining coarse-textured soils to slow-draining soils with high water-holding capacity. With the increase in water-holding capacity being more pronounced in the topsoil at the silicate site. This also affected the evolution of hydrologic flow paths at these sites, as shown in Hartmann et al. (2020a).

The obtained data set provides important insights into the development and dynamics of soil structure and soil hydraulic properties for two different parent materials and thus can be useful for the understanding of interactions of pedogenic, biotic, geomorphic and hydrologic processes during landscape evolution.

3 The evolution of subsurface hydrological flow paths in siliceous parent material

This chapter has been published as:

Field observations of soil hydrological flow path evolution over 10 millennia

Anne Hartmann, Ekaterina Semenova, Markus Weiler, and Theresa Blume

Originally published in:
Hydrology and Earth System Sciences, 24, 3271-3288, 2020, https://doi.org/10.5194/hess-24-3271-2020

Abstract

Preferential flow strongly controls water flow and transport in soils. It is ubiquitous, but difficult to characterize and predict. This study addresses the occurrence and the evolution of preferential flow during the evolution of landscapes, and here specifically during the evolution of hillslopes. We targeted a chronosequence of glacial moraines in the Swiss Alps to investigate how water flow paths evolve along with the soil-forming processes. Dye tracer irrigation experiments with a Brilliant Blue FCF solution (4 g l^{-1}) were conducted on four moraines of different ages (30, 160, 3000, and 10 000 years). At each moraine, three dye tracer experiments were conducted on plots of 1.5 m x 1.0 m. The three plots at each moraine were characterized by different vegetation complexities (low, medium, high). Each plot was further divided into three equal subplots for the application of three different irrigation amounts (20, 40, and 60 mm) with an average irrigation intensity of 20 mm h^{-1}. The day after the experiment five vertical soil sections were excavated, and the stained flow paths were photographed. Digital image analysis was used to derive average infiltration depths and flow path characteristics such as the volume and surface density of the dye patterns. Based on the volume density, the observed dye patterns were assigned to specific flow type categories. The results show a significant change in the type of preferential flow paths along the chronosequence. The flow types change from a rather homogeneous matrix flow in coarse material with high conductivities and a sparse vegetation cover at the youngest moraine to a heterogeneous infiltration pattern at the medium-age moraines. Heterogeneous matrix and finger flow are dominant at these intermediate age classes. At the oldest moraine only macropore flow via root channels was observed in deeper parts of the soil, in combination with a very high water storage capacity of the organic top layer and low hydraulic conductivity of the deeper soil. In general, we found an increase in water storage with increasing age of the moraines, based on our observations of the reduction in infiltration depth as well as laboratory measurements of porosity. Preferential flow is, however, not only caused by macropores, but especially for the medium-age moraine seems to be mainly initiated by soil surface characteristics (vegetation patches and microtopography).

3.1 Introduction

The ability of soil to store and to transport water is essential for its ecosystem services such as nutrient cycling or water and gas balances (Clothier et al., 2008; Amundson et al., 2015; Hatfield et al., 2017; Shang et al., 2018). Thus, the interaction of water and soil is an elementary foundation for the existence and functioning of terrestrial ecosystems. This interaction is part of a large network of interactions of various ecosystem components (flora, fauna, material and energy fluxes, geomorphological conditions, and climate), which are also necessary for the existence and functioning of ecosystems. Soil filters the percolating water, redistributes it to groundwater or stream water or holds it against gravity and makes it available for plants.

The soil functions are influenced and controlled by soil properties, which can vary spatially on the small (Hu et al., 2008) and large scales (vertically along the profile and horizontally across landscapes; (Bevington et al., 2016)), as well as temporally. These properties include soil texture and structure, i.e., the pore- and grain size distributions, which in turn control the storage and transport capacity of the soil. Additional factors influencing soil functions are climate, topography, and vegetation. In undisturbed natural systems these factors are usually assumed to be constant at the observational timescale and the inherent system dynamics only become apparent on long timescales.

Preferential flow, which is defined according to Hendrickx and Flury (2001) as a phenomenon 'where water and solutes move along certain pathways, while bypassing a fraction of the porous matrix', has impacts on water storage (Rye and Smettem, 2017) and thus plant water availability. It furthermore affects the transport of nutrients and contaminants (Jarvis, 2007) throughout the vadose zone and consequently also soil chemistry (Jin and Brantley, 2011; Bundt et al., 2000) and groundwater quality. Allaire et al. (2009) attribute rapid flow and mass transport to flow through earthworm burrows, cracks in soil, and flow paths resulting from soil layering and hydrophobicity. They defined four types of preferential flow: crack flow, burrow flow (created by soil fauna), finger flow, and lateral flow along layer interfaces, where flow in burrows and cracks is also often classified as macropore flow. We will in the following distinguish flow in macropores according to their origin as crack flow and biopore flow, where the latter includes channels by activities of roots and soil fauna. Preferential flow in the form of macropore flow occurs mostly in fine-textured soils whereas finger and funnel flow rather occurs in soils with a coarse texture (Hendrickx and Flury, 2001). General factors which can cause preferential flow paths are surface structure and properties such as vegetation cover, microtopography or hydrophobicity, as well as subsurface soil properties such as soil structure and soil type, subsurface heterogeneities, flow instabilities, and plant root activities (Weiler and Naef, 2003; Clothier et al., 2008; Bachmair et al., 2009; Jarvis, 2007; van Schaik, 2009; Wang et al., 2018). Soil water conditions were also found to have an influence on the preferential flow path characteristics (Gimbel et al., 2016; Hardie et al., 2011; Bogner et al., 2008).

Many preferential flow-influencing properties such as soil structure, soil texture, or vegetation cover change during landscape evolution (e.g., Vilmundardóttir et al., 2014; Egli et al., 2010; Dümig et al., 2011) and thus also lead to a change in the soil hydraulic behavior (Lohse and Dietrich, 2005), which in turn has a direct impact on the surface and subsurface water transport. We therefore assume that the age of the soil has an influence on the prevailing preferential flow paths and thus the type and also the depth extent of the preferential flow paths can change over time. Especially root activities can lead to

the generation of preferential flow paths in deeper layers, which was found by Cheng et al. (2014) based on a comparison of young and older forest plantations. On a large timescale of several million years, Lohse and Dietrich (2005) found a transition from mainly vertical water transport in younger volcanic soils in the Hawaiian Islands to lateral water transport along the boundary of a subsurface clay layer. The younger soil was coarse textured with high saturated hydraulic conductivities along the profile and a rather low field capacity, whereas the older soil revealed a higher field capacity and a distinct reduction in saturated hydraulic conductivity throughout the profile due to clay accumulation. Yoshida and Troch (2016) observed a major change in flow paths from deep groundwater flow to shallow subsurface flow in volcanic catchments of ages between 200 000 and $82x10^6$ years. While the change of major flow paths with time has already been studied at the timescale on the order of 100 000 to millions of years, little is known about how flow paths change during these first 10 000 years of landscape development.

Areas with receding glaciers have been shown to be suitable for soil development studies (Crocker and Dickson, 1957; Douglass and Bockheim, 2006; He and Tang, 2008; Egli et al., 2010; Dümig et al., 2011; Vilmundardóttir et al., 2014; D'Amico et al., 2014). In the cool and humid climate regions of former glacial areas, the soils develop from mineral soils to soils with a highly organic topsoil. These organic soil types are less intensively studied with regard to their soil hydraulic behavior compared to mineral soils (Carey et al., 2007). It is known that these soils differ in their soil hydraulic properties from mineral soils (high total porosity -up to 90%- and a low bulk density; Carey et al. (2007)) but little is known about how this development impacts water flow paths. Therefore, this study addresses the occurrence and the evolution of preferential flow during the first 10 000 years of landscape evolution in glacial moraines in the Swiss Alps. More specifically, we test the hypotheses that (1) vertical subsurface flow path types and vertical extent of flow paths change through the millennia as: (2) the proportion of macropore flow will increase due to the development of biopores, (3) the soil develops from a homogeneously mixed material into a depth-differentiated soil system, and (4) physical weathering leads to a reduction in particle size and an increase in porosity.

Dye tracer experiments, and an analysis of soil texture and soil physical properties were used to investigate how water flow paths evolve with hillslope age. The hydropedological approach (Lin, 2003) that links pedon (Quisenberry et al., 1993), landscape (Cammeraat and Kooijman, 2009), and hydrologic processes studies has already been applied to the preferential flow phenomenon (Jarvis et al., 2012). Dye tracer experiments combined with digital image processing have been applied successfully to study preferential infiltration in soils (Weiler, 2001; Bogner et al., 2008; Blume et al., 2008; Laine-Kaulio et al., 2015; Hardie et al., 2011; Cheng et al., 2014). In our study we use this method to identify how flow paths change during the coevolution of soil, vegetation, and topography. Understanding the changes in preferential flow paths as a result of the natural coevolution of landscape-forming factors can provide valuable knowledge on how these systems can also change as a result of human intervention (Richter and Mobley, 2009).

3.2 Material and methods

3.2.1 Study site

The study area is located in the foreland of the Stein glacier above the tree line in the central Swiss Alps, south of the Sustenpass in the Urner Alps (approximately. 47° 43'N, 8° 25'E). Elevations range from 1900 to 2100 m a.s.l. The area lies in the polymetamorphic Erstfeld gneiss-zone, which is part of the Aar massif (Blass et al., 2003). The geology is defined by metamorphosed pre-Mesozoic rocks, metagranitoids, gneisses, and amphibolites (Heikkinen and Fogelberg, 1980; Schimmelpfennig et al., 2014); thus the material is mainly acidic and rich in silicate. The closest official weather station is located 18 km away at Grimsel Hospiz (46° 34'N, 8° 19'E) at an elevation of 1980 m a.s.l. For the norm period from 1981 to 2010, the station recorded an annual mean temperature of 1.9 °C and an annual precipitation of 1856 mm. The precipitation distribution throughout the year is fairly uniform with a slight increase in the winter months (MeteoSwiss, 2020a). The glacier foreland consists of moraines with unconsolidated glacial till. The humid and cool climate together with the nutrient-poor substrate and a relative high water permeability of the glacial till favor the formation of podsolic soils and humus in this area (Heikkinen and Fogelberg, 1980).

The moraines of the Stein glacier were exposed due to its retreat to the south. Four moraines were selected for this study (see Fig. 3.1). Schimmelpfennig et al. (2014) conducted a detailed dating study of the Stein glacier moraines, based on high-sensitivity beryllium-10 moraine dating and found that the ages of three moraines range between 160 to 10 000 years. The age of a fourth moraine was dated to 30 years based on maps and aerial photos.

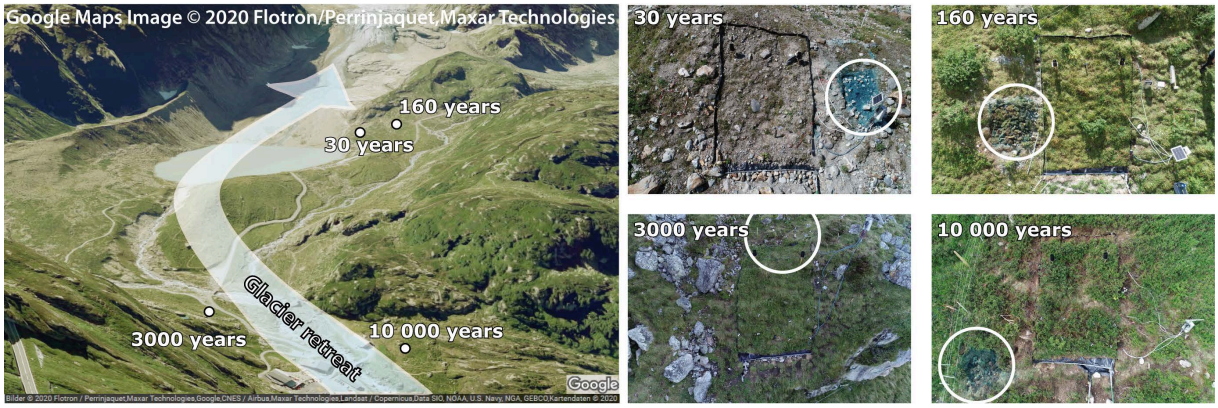

Figure 3.1: Location (left) and surface cover (right) of the four selected proglacial moraines of the Stein glacier. White circles show locations of one of the three Brilliant Blue experiment plots per age class. Photo of the location is provided by © Google Maps (2020a). Photos of the 30-, 160-, and 10 000-year-old moraines were taken after the Brilliant Blue experiment (photos taken by Florian Lustenberger).

The oldest moraine with an age of 10 000 years is facing northeast. The second oldest moraine with an age between 2000 and 3000 years is the only one facing south. The two youngest moraines were exposed in the years 1860 and 1980-1990, and thus have an age of 160 and 30 years, respectively. Both moraines are facing northeast and are located closer to the glacier tongue at a distance of approximately 1 km from the oldest moraines. Both moraines are south of the glacial lake Steinsee (1930 m a.s.l.), which is a proglacial

lake that was formed by the glacier retreat in 1924 (Blass et al., 2003).
The vegetation of the moraines was mapped in summer 2017 (Maier et al., 2020). Pronounced differences in vegetation coverage and species distributions were found among the four age classes. The vegetation of the oldest moraine was dominated by a variety of prostrate shrubs together with small trees and several grasses. On the 3000-year-old moraine, a grassland cover with fern, mosses, sedges, and forbs was found. The two youngest moraines however showed a lower degree of vegetation complexity. On the 160-year-old moraine, a combination of grasses, lichen, forbs, and shrubs was present. The youngest moraine still shows only a sparse vegetation cover with mainly grass, moss, forbs, and a few shrubs.

3.2.2 Field experiments

The dye tracer experiments were conducted between mid July and mid August 2018. We used Brilliant Blue FCF as dye tracer due to its good visibility, high mobility, and non-toxicity. We used a concentration of 4 g l^{-1}, at which the tracer shows good sorption and visibility (Weiler and Flühler, 2004). Three study plots were selected at each moraine, based on the degree of vegetation complexity (low, medium and high complexity). Vegetation complexity is characterized by vegetation coverage, the number of species, and the plant functional diversity. The functional diversity is calculated based on specific leaf area, nitrogen content, leaf dry matter content, Raunkiær's life form, seed mass, clonal growth organ, root type, and growth form. The collection of the required data and calculation of the vegetation complexity was done by the geobotany group of the University of Freiburg and is described in more detail in Maier et al. (2020).
The size of each study plot was 1.5 m x 1.0 m. The distances between the three study plots at each moraine ranged from 10 to 100 m. Each plot was further divided into three equal subplots of 0.5 x 1.0 m. Figure 3.2 shows the experimental design at each moraine and illustrates the irrigation procedure. The subplots were irrigated with three different amounts of dyed water (20 mm, 40 mm, and 60 mm) and an irrigation intensity of 20 mm h^{-1}. The irrigation intensity is relatively high with a return period of 2.8 years (Fukutome et al., 2017). In preparation of the tracer application, large vegetation in the form of shrubs and bushes was cut off to a height of a few centimeters to reduce interception. The tracer was applied with a hand-operated sprayer connected to a battery-powered pump which guaranteed a constant pressure for a uniform flow rate of 60 l h^{-1}. For a time-efficient irrigation of the three subplots with three irrigation amounts, the irrigation procedure was divided into three steps. In the first step all three subplots were irrigated simultaneously for 60 min in a sequence of 5 min of irrigation and a 5 min break. This provides an application of 20 mm to all three subplots. After finishing the first step the first subplot was covered to avoid any additional water input. In a second step, the other two subplots were simultaneously irrigated for an additional 60 min in a sequence of 5 min of irrigation and 10 min breaks. This provides an application of an additional 20 mm to each of the two remaining subplots. In the last step, only the third subplot was irrigated for 60 min in a sequence of 2 min of irrigation and 10 min breaks, while the other two plots remained covered providing an additional 20 mm to this subplot. After the end of tracer application, the entire plot was covered to avoid any disturbance by natural rainfall.
The next day each subplot was excavated in up to five profiles of 7 to 10 centimeters. After the profile cuts were made with pickaxes, spades, and hand shovels, the profile walls were cleaned. Hanging roots were cut off, and rocks were not removed but made visible. The profiles of each subplot were photographed

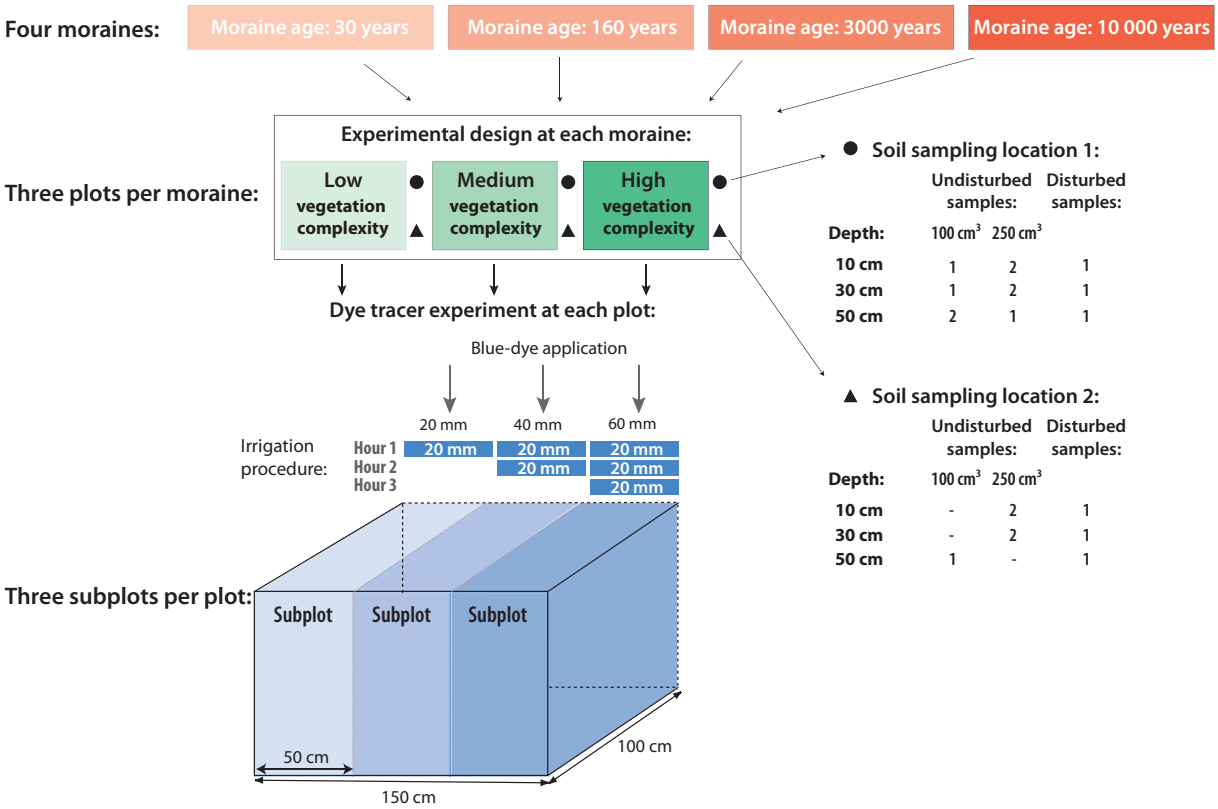

Figure 3.2: Illustration of the experimental design and soil sampling scheme at each moraine.

with a Panasonic Lumix DMC-FZ18 camera and at a resolution of 2248 pixels x 3264 pixels. A big umbrella was used to provide a uniform light distribution in the photographs and to avoid direct sunlight. A wooden frame for geometric correction and a grayscale (Kodak) attached to the frame (Fig. 3.3) for a later color adjustment were included in the photographs. Since dye tracer experiments only provide snapshots of flow patterns at 24 h after the irrigation, we cannot exclude the possibility that initial preferential flow paths were obliterated by a later downward movement of the infiltration front. However, as the probability of this special case is relatively low, we assume that these snapshots are a viable basis for the comparison of characteristic flow patterns along the moraine ages.

3.2.3 Image analysis

The image analysis procedure by Weiler (2001) was used to generate tricolor images of the photographs showing stained and unstained areas (Fig. 3.3). A detailed description of the method can be found in Weiler and Flühler (2004). Instead of using the original IDL (Interactive Data Language) software package, a similar Python version was used. Basically, geometric correction, background subtraction, and color adjustment were carried out to correct differences in image illumination and changes in the spectral composition of daylight. The delineation of rocks and plants was done manually. In the resulting tricolor image the horizontal and vertical length of a pixel correspond to 1 mm. Due to poor lighting conditions or a heterogeneous background color distribution in the soil caused by material transitions, small stones or organic matter, the image analysis software was not able to recognize all large dye stains as coherent

objects. Thus, a manual correction of the images using the photographs was necessary (see Fig. 3.3).

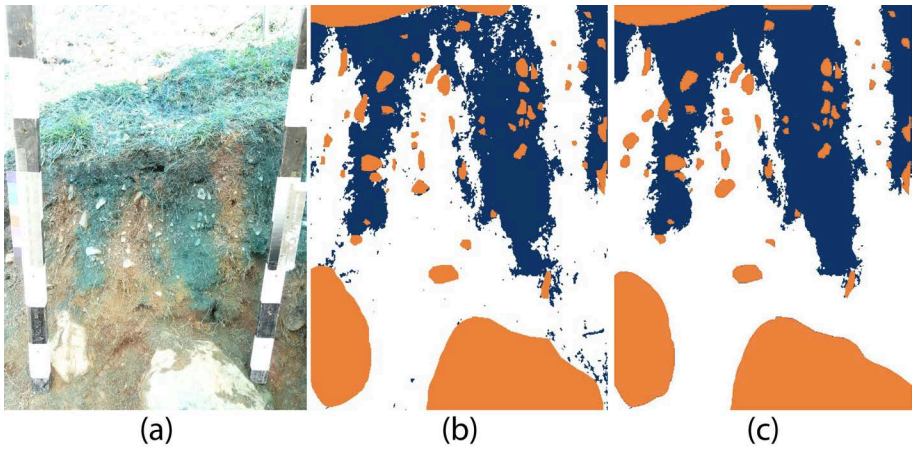

Figure 3.3: Exemplary image analysis procedure for the 40 mm irrigated subplot at the 3000-year-old moraine. (a) Photograph of the vertical soil profile with a wooden frame and an attached grayscale. (b) Software-generated tricolor image of the photograph. (c) Manually corrected tricolor image. Blue indicates stained soil; white indicates unstained soil; and orange indicates rocks.

For a quantitative comparison of the dye patterns the maximum infiltration depth, the volume density and surface area density, as well as the stained path width were calculated. These parameters are frequently used for an objective comparison and description of the dye patterns (Weiler and Flühler, 2004; Bachmair et al., 2009; Laine-Kaulio et al., 2015; Cheng et al., 2014; Gimbel et al., 2016; Laine-Kaulio et al., 2015; Mooney and Morris, 2008; Öhrström et al., 2002). Volume and surface area density are originally steorological parameters which are used to relate three-dimensional structures to measured two-dimensional parameters (Weibel, 1979). The volume density corresponds to the dye coverage and can be derived from one-dimensional information by calculating the fraction of stained pixels for each depth. The volume density profile is defined by the fraction of stained pixels per depth and is calculated as the average of all excavated profiles per plot. The surface area density in one dimension is calculated by using the intercept density, which describes the number of intercepts between stained and unstained pixels divided by the horizontal width of the soil profile. The profile of the surface area density describes the amount of intercepts per depth and is then also averaged over all photographed profiles per plot. Volume density provides no information about whether the stained area is the sum of many small fragments or a few large ones; thus the volume density alone should not be used to characterize flow patterns, and the surface area density should be used as a supplementary parameter. A high surface area density indicates a large number of small features.

Following the method described by Weiler (2001), the resulting dye patterns were next classified into flow type categories based on the proportions of three selected stained path width classes (stained path width <20 mm, 20 mm-200 mm, and >200 mm) relative to the volume density. The stained path width is equal to the horizontal extent of a stained flow path (Weiler, 2001). This classification method distinguishes between five flow types: (1) macropore flow with low interaction, (2) mixed macropore flow (low and high interaction), (3) macropore flow with high interaction, (4) heterogeneous matrix flow/finger flow, and (5) homogeneous matrix flow. Dye patterns which cannot be classified as one of these flow types are

categorized as undefined. The classification method based on proportions of the classes of stained path width is illustrated Figure 3.4.

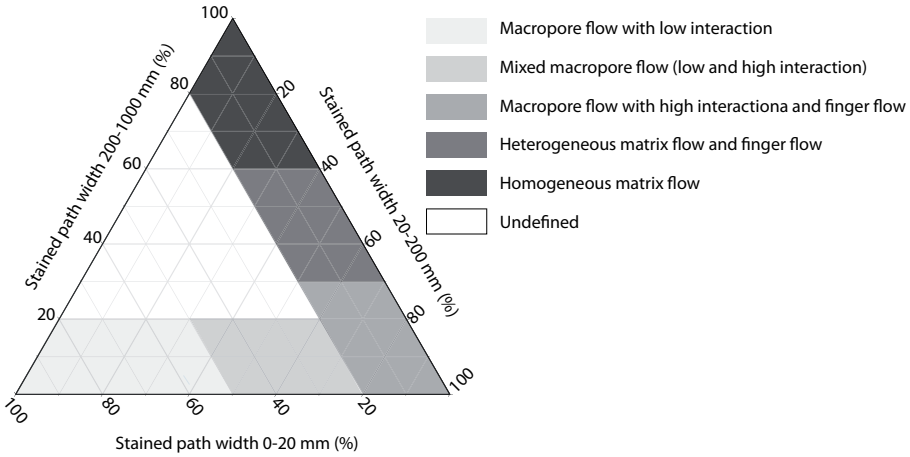

Figure 3.4: Flow type classification based on the proportion of the three stained path width classes: ternary diagram after Weiler (2001).

This method is based on the assumption that the dye patterns are mainly controlled by certain preferential flow processes and that each flow process creates a characteristic dye pattern that can be described by the extent and distribution of stained features.

This method was proven to be suitable for the investigation of Weiler (2001) and Weiler and Flühler (2004) and was also used in a variety of additional studies (Bachmair et al., 2009; Gimbel et al., 2016; Mooney and Morris, 2008). However, an extension of the flow type categorization was needed for our study site with soils of different ages, texture, and additionally a high stone content. In the extended classification, we avoid a clear differentiation between macropore flow and finger flow. The original classification assigns finger flow only when both classes of the medium-sized stained path width (20-200 mm) and the biggest stained path width (> 200 mm) account for approximately half of the dye coverage. This implies that finger flow is only prevalent when the dye pattern is characterized by a majority of broader stained path widths, ignoring the fact that the size of the finger-like flow paths can vary over a broad range (Wang et al., 2018). Thus, we argue that while finger flow and macropore flow are caused by different properties and flow mechanisms, they can lead to similar dye patterns and distributions of stained path width classes. This is especially the case for macropore flow with high interaction, which creates broader stained paths that could also be assigned to finger flow. Therefore, both flow types were considered in the extended classification for this class. Furthermore, it was observed that the presence of rocks within the image analysis interrupts homogeneous blue stained areas and thus leads to smaller stained path widths. Using the original classification scheme on a soil profile with high stone content suggests a heterogeneous flow pattern, which can be classified as heterogeneous matrix flow, finger flow, or macropore flow depending on the abundance of rocks. Therefore, an additional class has been introduced, which is used when homogeneous matrix flow between rocks takes place. The classification rule for the additional flow type class is based on the proportion of blue-dye coverage of the available permeable matrix space (profile width minus the sum of stone widths per row). If at least 95 % of the permeable space is stained by blue

dye, the flow type is classified as matrix flow between rocks.

3.2.4 Soil sampling and laboratory analysis

Soil samples were taken during August and September of 2018 close to each dye tracer plot. For grain size analysis, two disturbed bulk soil samples per depth were taken at 10, 30, and 50 cm depth at each plot. The total of 72 samples was analyzed in the laboratory between November 2018 and January 2019 by using a combination of dry sieving (grain sizes > 0.063 mm) and sedimentation analysis (grain sizes < 0.063 mm) with the hydrometer method (Casagrande, 1934). Organic matter removal was only possible by floating off the lighter fractions prior to grain size analysis. Since three plots were selected per moraine for the Brilliant Blue experiments, six samples per depth and age class (a total of 18 samples for each moraine) were available for the grain size analysis. Grain sizes between 2 and 0.063 mm were classified as sand, between 0.063 and 0.002 mm as silt and smaller than 0.002 mm as clay. Grain size fractions of particles < 2 mm were calculated as weight percentages of total weight of particles < 2 mm, thus excluding gravel and stones to avoid single larger stones shifting or dominating the distribution. The gravel and stone fraction was calculated separately as a weight percentage of the entire soil sample.
For the analysis of the structural parameters, soil samples were taken with sample rings to provide undisturbed cores which preserve the natural soil structure. At each plot two 250 cm^3 and one 100 cm^3 undisturbed soil samples were taken at a depth of 10 and 30 cm. Three samples of 100 cm^3 were taken at 50 cm depth. Thus, per age class, nine samples per depth were available for the determination of the structural parameters of porosity and bulk density. A detailed overview of the sampling scheme at each plot is given in Figure 3.2.
The porosity was determined in the lab using the water saturation method. For this method, sample weights were recorded at saturation and after drying at 105 °C. For saturation, the samples were placed in a small basin. The water level in the basin was increased stepwise by 1 cm per day. When the water level reached the top of the soil sample and the sample was fully saturated, the bottom of the sample was sealed and the weight at saturation was measured. Bulk density was determined by relating the dry mass after drying at 105 °C to the sample volume. The loss on ignition is a measure of the organic substance in the soil and describes the proportion of the organic substance that was oxidized during annealing for 24 hours at 550 °C. The loss on ignition was determined by drying subsamples (4-6 g) for at least 24 hours at 105 °C and then at 550 °C. The ignition loss is then calculated by relating the weight loss after drying at 550 °C to the sample weight after drying at 105 °C.

3.2.5 Statistical analysis

The nonparametric Kruskal-Wallis test was used to test the significance of the differences in the soil texture among the four moraines of differing age classes. It can be applied when the assumption of a normal distribution cannot be made and is also valid for small sample sizes. We applied the test to each grain size fraction across the four age classes. Average values were based on 18 samples per age class. The grain size distribution at 10 cm depth of the oldest moraine was excluded from consideration, since due to the high organic content not all organic matter could be removed and the results may therefore be erroneous.

3.3 Results

3.3.1 Soil texture and structural parameters

Comparing the depth-averaged soil texture over the millennia, we find that while the soil texture at the youngest moraine mainly consists of sand, the grain sizes decrease over the millennia with silt being the largest fraction after 10 000 years (Fig. 3.5). Clay content increased with age for the three older moraines, with the youngest moraine being the exception (having the second-highest clay content). The Kruskal-Wallis test with a 0.05 confidence level showed that differences in grain size fractions among the four age classes were statistically significant (p values < 0.05; sand of p=0.0013, silt of p=0.0006, and clay of p=0.0018).

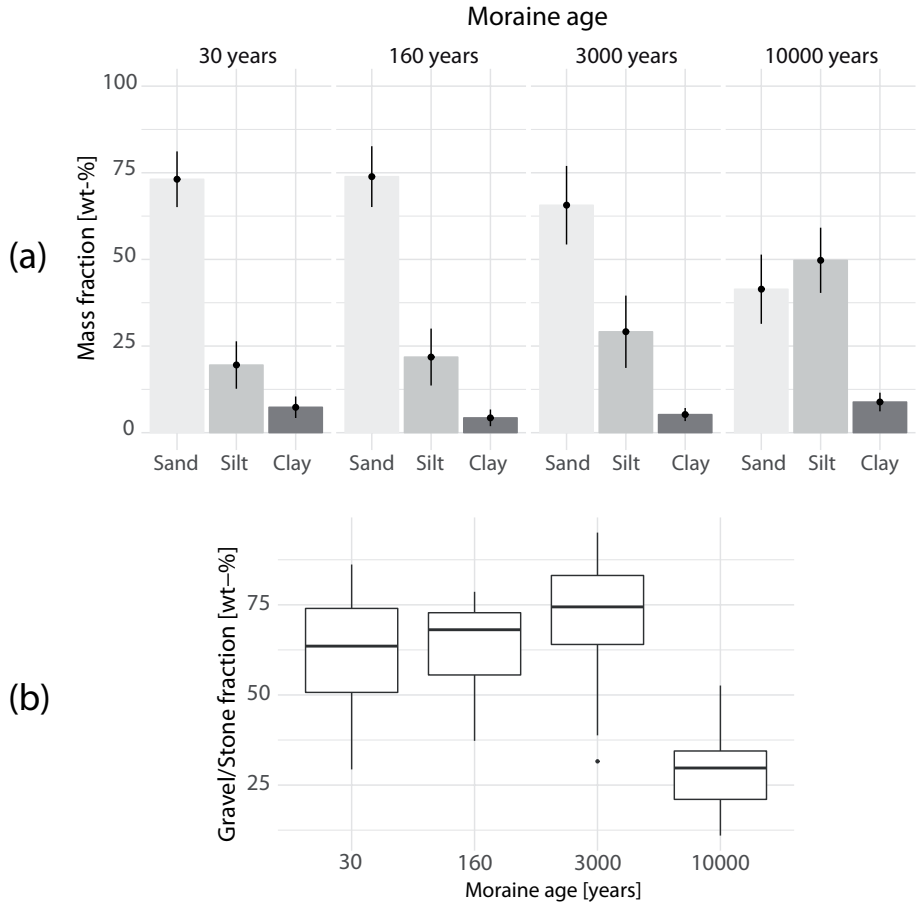

Figure 3.5: (a) Profile-averaged grain size fractions for the four moraines. Fractions are percentages of the fine earth fraction (<2 mm). (b) Profile-averaged gravel content (>2mm) calculated as the percentage of the entire sample weight. Each average is based on 18 samples.

A significant reduction in grain size over time was observed, which is most pronounced between 3000 and 10 000 years of soil development. The gravel and stone fraction is roughly the same at the three younger moraines and significantly lower at the oldest moraine (Fig. 3.5b). The structural parameters of porosity and bulk density also show a clear trend with age, with porosity increasing and bulk density decreasing (Fig. 3.6).

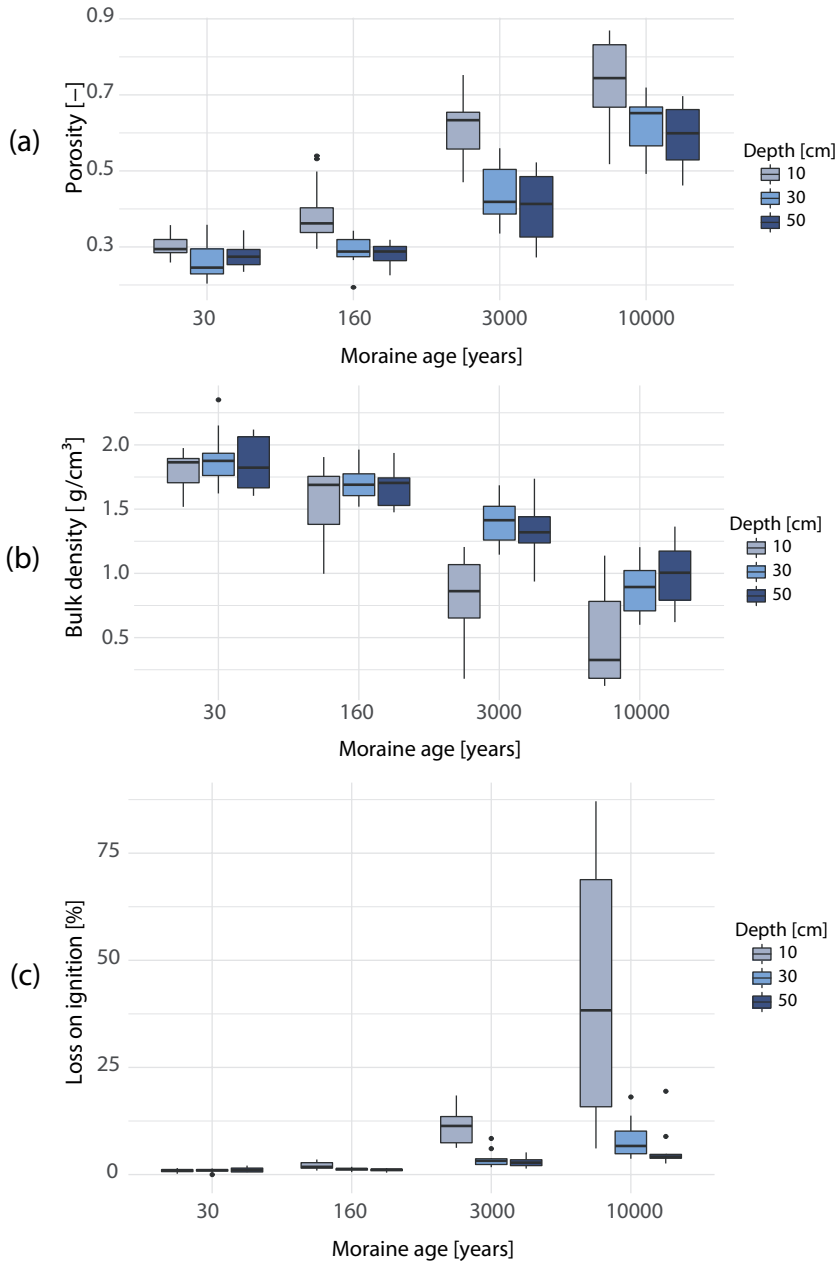

Figure 3.6: Evolution of soil porosity (a) bulk density (b), and loss on ignition (c) at 10, 30, and 50 cm depth.

The porosity observed at the youngest moraine ranges between 0.22 and 0.37, with no pronounced differences among the three soil depths. The 160-year-old moraine has a higher porosity in the upper 10 cm than the 30-year-old moraine. After 3000 years the increase in porosity continues but is now also visible at 30 and 50 cm, but with much higher values at 10 cm (Fig. 3.6a). After 10 000 years the porosity at 10 cm ranges from 0.6 to up to more than 0.8. The other two depths also experienced a further increase in porosity. The decrease in bulk density is also most pronounced in the top layer of the soil (Fig. 3.6b). While after 30 years the bulk density in the upper 10 cm ranges around 1.7 g cm^{-3}, the bulk density after 10 000 years is much smaller and ranges between 0.2 and 0.7 g cm^{-3}. After 3000 years the trend is also visible at 30 and 50 cm.

The loss on ignition, as a measure for the organic matter content, shows an increase throughout the first 10 millennia of soil development, which is most pronounced in the upper soil layer (see Fig. 3.6c). At the two youngest moraines, the organic matter content is still very low (< 2 weight-%, percentage by weight). At these two age classes, the organic matter content is homogeneously distributed over the profile, with a slight tendency to higher values in the topsoil at the 160-year-old moraine. The 3000-year-old moraine shows a strong increase in the organic matter content in the surface layer. At the oldest moraine, the trend of increasing organic matter continues in all three depths. Here, the organic matter content in the topsoil makes up to two thirds of the soil material. However, the organic matter content varies distinctly with a minimum of 6 weight-% and a maximum of 87 weight-%. In deeper depths, the organic content also increases compared to the 3000-year-old soil, but remains below 20 weight-%.
Even though the differences in soil physical characteristics between 30 and 160 years are comparatively small, the rates of change during this initial phase are highest (Table 3.1). Between 160 and 3000 years, the rates of change are significantly reduced and remain in a similar range between 3000 and 10 000 years.

Table 3.1: Linear rates of change in porosity, bulk density and grain size between adjacent age classes calculated based on median values Mass fraction: mf %.

	$Porosity\ [yr^{-1}]$			$Bulk\ density\ [g\ cm^{-3} yr^{-1}]$			$Grain\ size\ [mf\%\ yr^{-1}]$		
	10 cm	30 cm	50 cm	10 cm	30 cm	50 cm	*sand*	*silt*	*clay*
$Period\ [years]$									
$30 - 160$	5.1x10^{-4}	3.2x10^{-4}	1.1x10^{-4}	-1.3x10^{-3}	-1.4x10^{-3}	-9.1x10^{-4}	2.5x10^{-2}	1.5x10^{-2}	-2.0x10^{-2}
$160 - 3000$	9.5x10^{-5}	4.6x10^{-5}	4.4x10^{-5}	-2.9x10^{-4}	-9.7x10^{-5}	-1.4x10^{-4}	-3.2x10^{-3}	3.2x10^{-3}	3.1x10^{-4}
$3000 - 10\,000$	1.6x10^{-5}	3.3x10^{-5}	2.6x10^{-5}	-7.6x10^{-5}	-7.4x10^{-5}	-4.5x10^{-5}	-3.3x10^{-3}	2.4x10^{-3}	3.2x10^{-4}

3.3.2 Vertical-dye pattern analysis

Flow patterns traced with Brilliant Blue dye changed considerably with moraine age (Fig. 3.7). The volume density profile is a measure of the amount of blue dye per depth. The profile patterns of volume and surface area density show distinct differences among age groups, while differences between the vegetation complexity levels are not as clear (Fig. 3.7 and 3.8).

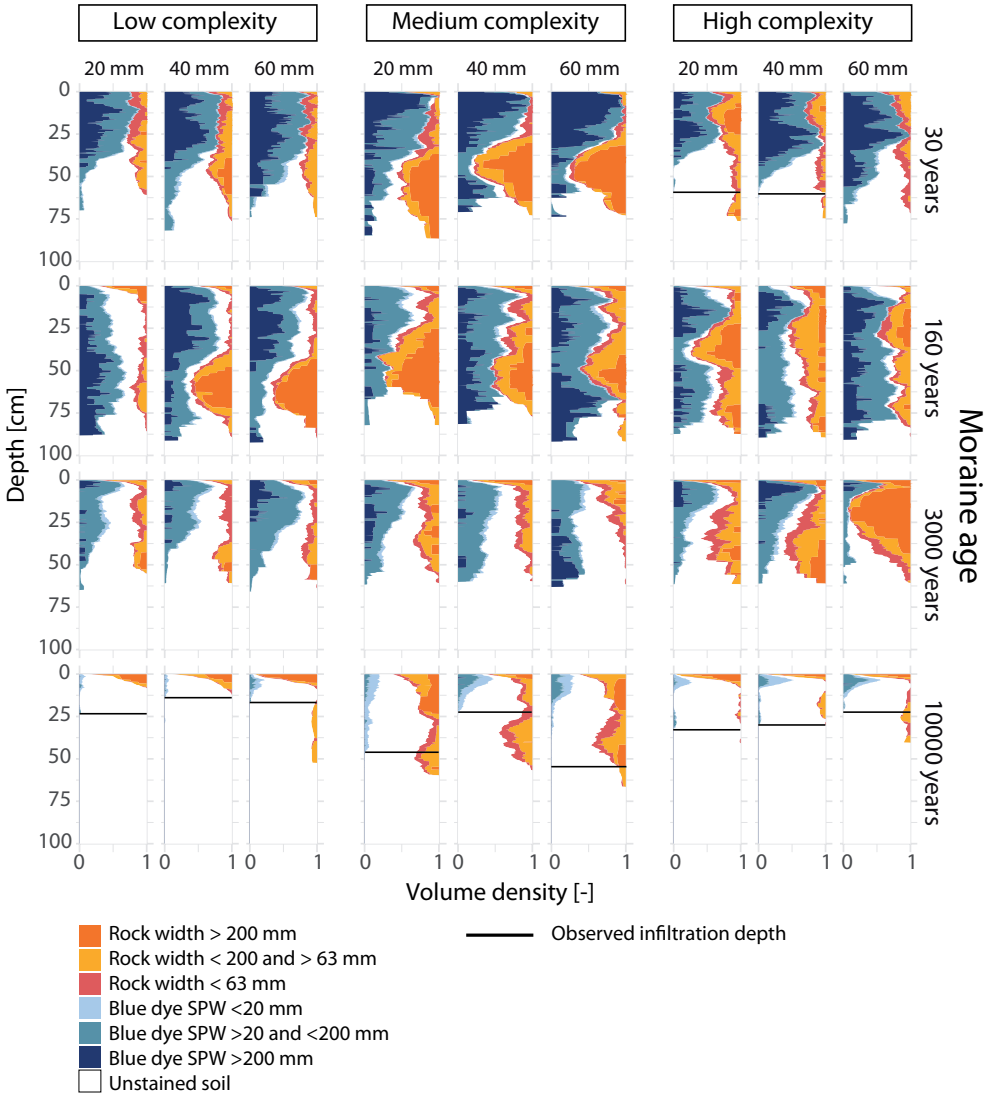

Figure 3.7: Volume density profiles per age class, vegetation complexity, and irrigation amount. The volume density is the fraction of stained pixels, here colored by flow path width (stained path width; SPW) and rock sizes.

The volume density of the blue dye was classified in three selected groups of stained path width (Weiler, 2001). Additionally, the volume density of rocks was also classified in three groups (Fig. 3.7).
An analysis of the average or maximum infiltration depth based on the dye profiles was not possible

because not all profiles could be excavated up to the maximum infiltration depth. In most cases large boulders prevented further excavation or the infiltration depth was more than 1 m. The latter was mostly the case at the youngest moraines. Only at the oldest moraine could a maximum infiltration depth be determined based on the dye profiles.

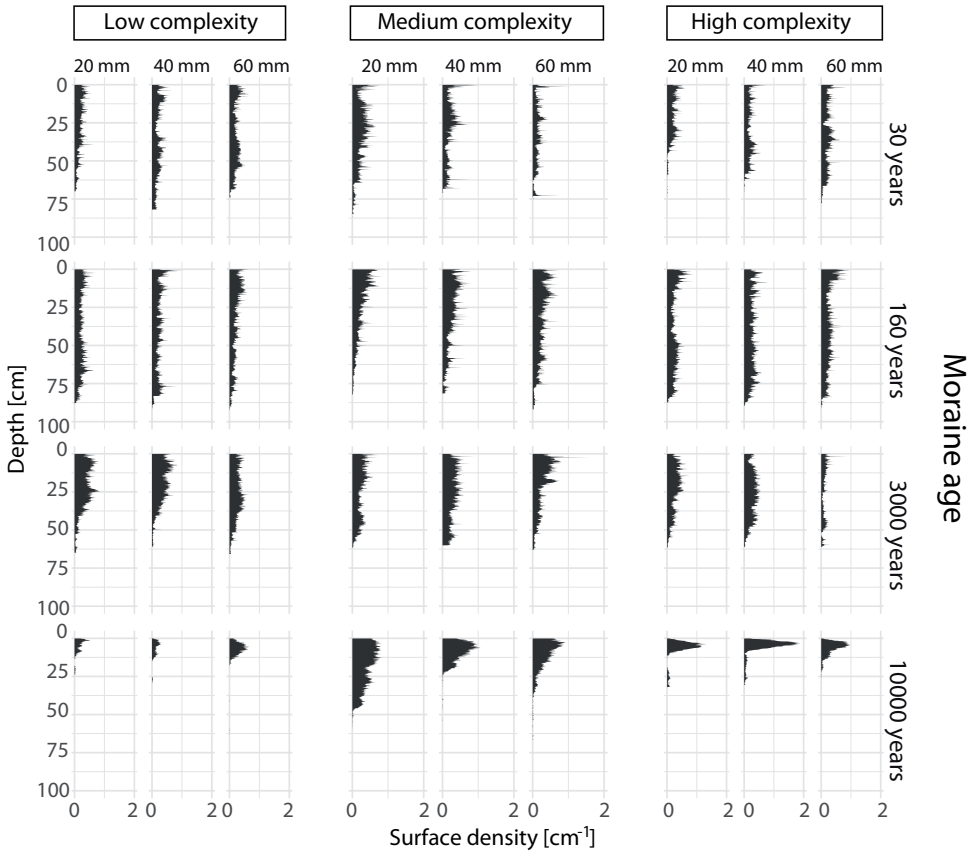

Figure 3.8: Surface area density profiles per age class, vegetation complexity, and irrigation amount (20, 40, and 60 mm). A high surface area density indicates a large number of small features.

Combining the volume density profiles with the surface area density profiles, it is possible to derive whether the stained area described by the volume density is made up of many small flow paths or few large ones. The shapes of the volume density profiles and the surface area density of the youngest moraine are all very similar across the vegetation complexity levels and irrigation amounts. The youngest moraine has a higher volume density of flow paths in the top half of the soil profile than all other moraines (Fig. 3.7). There are almost no unstained areas. Beginning from approximately 30 cm depth, the volume density declines. The surface area density profiles show an opposite pattern (Fig. 3.8). The surface area density is smaller in the upper half and increases in the lower half of the profile. The combination of both parameters indicate a homogeneous staining in the top half, where interruptions of stained areas are only caused

by rocks. In the lower part of the soil profiles the flow paths are subdivided, which is indicated by the increase in surface area density (apparent at the plots at 30 cm depth for low, 25 cm depth for medium, and 50 cm depth for high vegetation complexity). This combined with a decline in volume density indicates a narrowing of the flow paths. For the plots of low and high vegetation complexity, the change in flow paths coincides with a layer of higher clay and silt content. This layer does not exist at the plot of medium vegetation complexity. In this case, the narrowing and splitting up of flow paths is caused by large rocks. No clear differences are visible between the different irrigation amounts. The proportion of classes of the stained path width is controlled by the existence of rocks. The maximum infiltration depth is either controlled by the position of the clay layer or is deeper than the profile depth and therefore cannot be determined.

Comparing the 160-year-old moraine to the youngest moraine, we find that the volume density is lower and the surface density is higher in the upper part of the profile. Also unstained areas (colored white in Figure 3.7) are visible, which indicates that the higher surface density is not caused by the existence of rocks that split up a homogeneously stained area as was the case for the youngest moraine. In this case there is no total dye coverage of the permeable soil, and the preferential flow paths are initialized already near or at the soil surface. The surface density profiles show a decrease in the lower half of the soil profile, which either goes along with a decrease in the blue-dye coverage and an increase in the stone coverage or an increase in the blue-dye coverage without a significant change in stone coverage. Both indicate a reduction in the amount of separate flow paths and an increase in flow path widths, even if the permeable space is reduced due to an increase in rock content. Also the fraction of stained path width (SPW) bigger than 200 mm increases, which indicates that the dye plumes widens in deeper soil depths.

Compared to the two youngest moraines, the moraine of 3000 years shows in general a higher surface area density and a lower dye coverage combined with a higher fraction of an unstained permeable soil matrix. This indicates that similar to the 160 years old moraine water is transported in individual flow paths, but here there are more flow paths, and they have a smaller width. This can also be seen in the less frequent appearance of stained path width higher than 200 mm (Fig. 3.7). Similar to the 160-year-old moraine, preferential flow paths are already initialized at the top of the soil during infiltration (apparent from the white-colored areas across the profile in Figure 3.7).

The oldest moraine with an age of 10 000 years shows the highest surface area density and the lowest volume density combined with the lowest infiltration depths. The surface and volume density profiles show the same pattern: after a peak close to the soil surface, both density profiles show a decrease with soil depth. This means that the dyed water is only transported deeper into the soil via a few individual flow paths.

3.3.3 Flow type classification

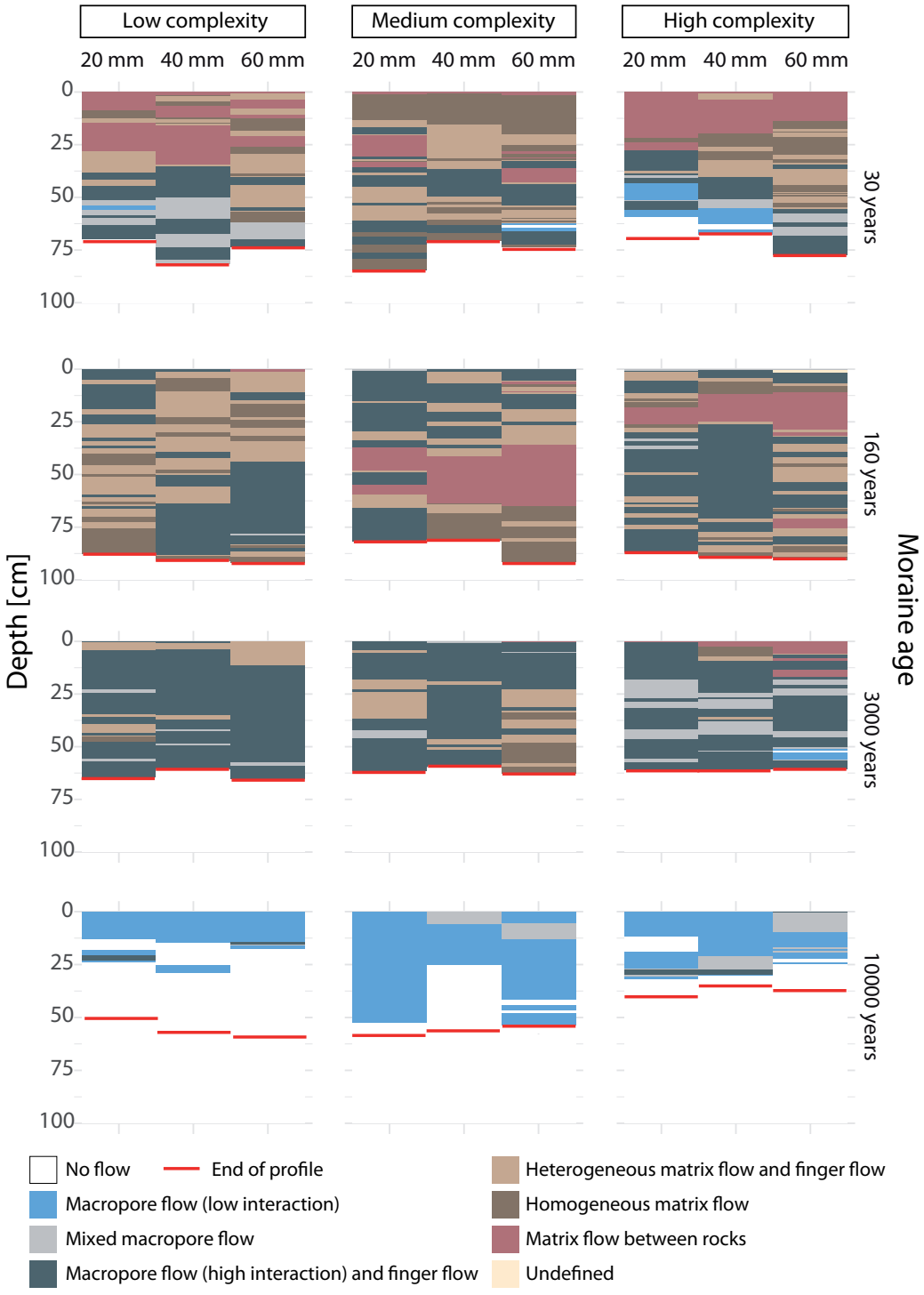

Figure 3.9: Profiles of flow types per age class, vegetation complexity, and irrigation amount.

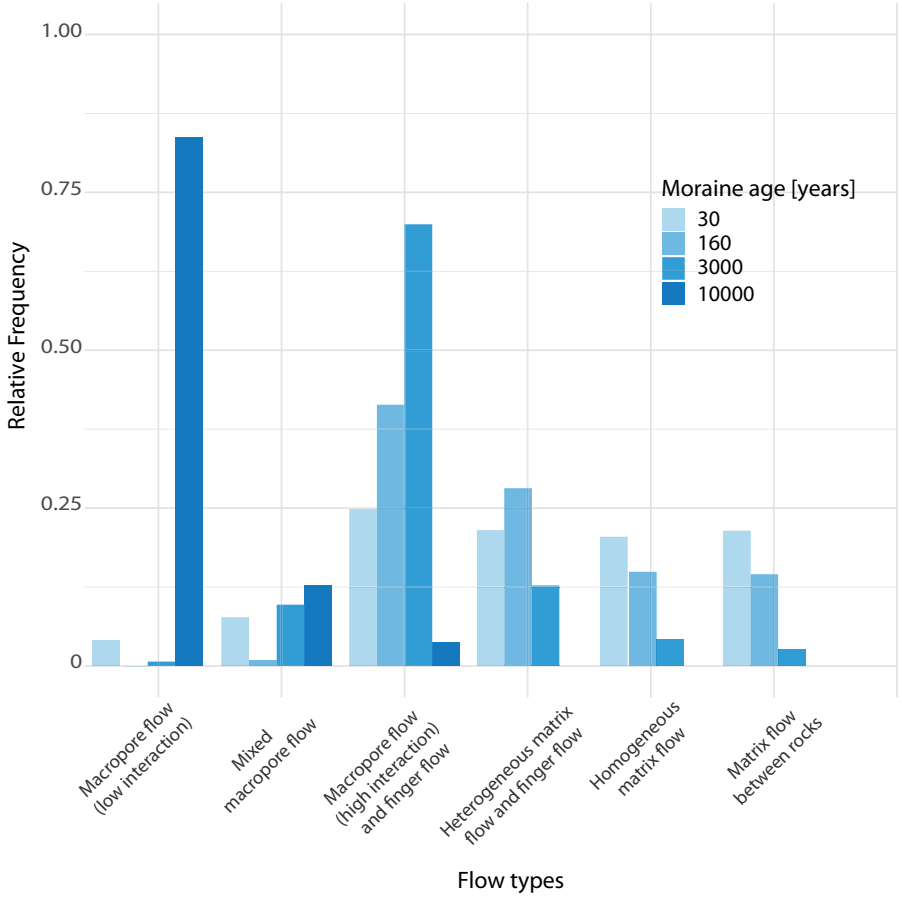

Figure 3.10: Relative frequency distribution of flow types of the four moraine age classes. Basically all observations fit into the six flow type categories. The fraction of observations categorized as "undefined flow type" is negligible.

Using the information in the volume density profiles and the stained path widths to characterize flow types (Weiler, 2001), we found a trend from a rather homogeneous flow pattern with matrix flow in fast draining coarse-textured soil at the youngest moraine to a more heterogeneous flow pattern with a mix of heterogeneous matrix flow and finger flow at both medium-age moraines (Fig. 3.9). While the flow characteristics of both the 160- and 3000-year-old moraine are dominated by finger flow with smaller stained path widths, this is much more pronounced in the 3000-year-old moraine. By contrast, the oldest moraine stands out clearly from the other age groups. Here, only macropore flow is predominant. For the deeper soil layers, this was confirmed during the field experiments, since the few macropore flow paths were clearly visible. For the topsoil, the result is less certain, as the blue areas were very difficult to identify during the image analysis due to the very dark color of the organic layer.

The relative frequency distribution of the flow types per moraine age class derived from the results in Figure 3.9 shows a clear shift in the flow type distribution along the age classes (Fig. 3.10). At the youngest moraine all types of finger flow and matrix flow are present, and the frequency distribution does not show a distinct peak at any flow type. With increasing age, macropore flow becomes more and more important, and the peaks in the frequency distribution become more and more pronounced (Fig. 3.10).

3.4 Discussion

3.4.1 Evolution of soil texture and structure

The early years: 30-160

The observation of bulk density, porosity and soil texture show significant differences between the age groups as well as some clear trends with age. The 30-year-old soil is characterized by coarse material, with a soil texture composed of almost three quarters of sand. The soil texture observed at the 160-year-old moraine does not differ strongly from the 30-year-old moraine, whereas slight changes are already evident in porosity and bulk density. These findings are similar to findings by Dümig et al. (2011), who found no specific trend in grain size distribution for soils in the range of 15 to 140 years at a soil chronosequence in the foreland of the retreating Damma glacier (Switzerland). They furthermore found a high variability in grain size distribution within the single age classes. However, in the same study a slight decrease in variability with increasing age and a noticeable higher clay content were found at the reference site with an age of more than 700 years. He and Tang (2008) also revealed a nonlinear increase in the maximum clay content for soils up to 180 years at a glacier foreland in a monsoon temperate region in southwestern China.

After 160 years of soil development, the porosity in the top layer increased, and bulk density decreased. In general, these changes could be linked to changes in grain sizes, as the breakdown of particles leads to an increase in total pore space (porosity) and thus to a reduction in bulk density (Arvidsson, 1998). However, since changes in grain sizes were only marginal, the vegetation development, which includes an increase in the root activities, litter accumulation, and biological activities in the root zone, is likely the main cause for changes in bulk density and porosity (Neris et al., 2012; Carey et al., 2007). The vegetation coverage of both moraines differs significantly (Maier et al., 2020). The youngest moraine still shows only low vegetation cover with only single plants (mainly grasses and forbs) and little root mass with an observed maximum rooting depth of 15 cm (occasionally up to 30 cm), whereas the 160-year-old moraine already has a relatively closed vegetation cover with a combination of shrubs and smaller plants like forbs and grasses forming a loose root network with roots up to a maximum diameter of 5-6 mm and a maximum depth of 35 cm (as observed during the excavation of the soil profiles).

Similar findings in bulk density evolution were also observed by Crocker and Major (1955), who found a decrease in the bulk density over the first 200 years of soil development from more than 1.4 g cm^{-3} to less than 0.8 g cm^{-3} for glacial till in southeastern Alaska. A less pronounced reduction was also found by Crocker and Dickson (1957). He and Tang (2008) found a reduction for the time span of 180 years from approximately 1.42 to 0.95 g cm^{-3} that was also more distinct in the upper horizon. Vilmundardóttir et al. (2014) revealed at a glacier foreland in southeastern Iceland under maritime climate conditions a reduction from 1.36 to 1.07 g cm^{-3} for a time span of 120 years . All studies mentioned above linked this decrease in bulk density to the vegetation development with time.

Intermediate stage: 3000 years

At 3000 years of soil development we observe a distinct increase in silt and a reduction in sand content and this development continues, as observed in the 10 000-year moraine, where the silt content now makes

up the largest share. These findings agree with findings by Douglass and Bockheim (2006), who studied several moraines in Buenos Aires with ages ranging from 16 000 years to 1 000 000 years and found an accumulation of clay-sized particles with increasing age, but with a decrease in the accumulation rate over the years. A high fraction of silt is very common for soils in mountain areas (Ellis, 1992). Physical weathering due to high fluctuations between day and night temperature and freezing cycles (Birse, 1980) leads to a reduction in grain size, without changing the particle mineralogy (Ellis, 1992).
The soil material at the 30-year-old moraine showed a relatively uniform porosity and bulk density throughout the profile. After 3000 years, porosity increases and bulk density decreased even further, and this development is now also visible in deeper soil depths. The continuous increase in porosity and reduction in bulk density can be attributed to the continuing change in soil texture on the one hand and on the other hand to the pronounced vegetation development. Especially the latter with the resulting accumulation of soil organic matter (see Fig. 3.6c) and the growth of an even denser root network that is now over 35 cm deep, is the main cause for the pronounced changes in the topsoil.

The late stage: 10 000 years

The oldest moraine shows a significantly higher silt content and porosity compared to the 3000-year-old moraine and a significantly lower bulk density. The change is visible at all soil depths, with the porosity in the uppermost depth being distinctly higher than the other depths. These differences in soil properties between the soil layers also indicate a progressive formation of distinct horizons in the soil.
The significantly higher porosity in the upper layer of the oldest moraine is caused by its thick organic layer (thickness up to 20 cm), which is characterized by porosity of up to 90 percent (this was also found by Nyberg (1995), in sandy-silty till on the western coast of Sweden and Carey et al. (2007), in organic soils in a permafrost region in northwestern Canada).
Musso et al. (2019) investigated the evolution of pore sizes in the top 5 cm at the same soil chronosequence and found an increase in the number of small soil pores and a decrease in the relative proportion of macropores (pore diameter > 0.05 mm) between 160 and 10 000 years. Thus the high porosity in the organic top layer at the oldest moraine is mainly composed of small pores. The top layer therefore has an increased water storage and water holding capacity. Due to the finer soil texture and higher porosity, the total storage water capacity of the oldest moraine is larger than that of the younger moraines.
An investigation of the saturated hydraulic conductivity evolution of the near surface (in 0-5, 5-20, and 20-40 cm) at the same chronosequence by Maier et al. (2020) found a decrease with increasing moraine age and soil depth. Saturated conductivity was found to be negatively correlated with the fraction of fine particles. The decrease in gravel content and the increase in silt seem to have an even a stronger effect on the saturated conductivity than the root network development (Maier et al., 2020).

Soil heterogeneity and vegetation complexity

It is well known that soil properties are spatially heterogeneous (Bevington et al., 2016; Hu et al., 2008). As it was not possible to account for this variability with a large sample size, i.e., with a large number of experiments, we decided to take a different approach: assuming that vegetation cover and subsurface flow paths are strongly linked, we took the variability in vegetation cover as a proxy and used it in an

attempt to bracket this variability: per moraine three locations that differ in their vegetation complexity (low, medium, and high) were chosen for soil sampling and the dye tracer experiments. The analysis of the structural soil properties shows that there is a slight increase in spatial heterogeneity with age, especially in the topsoil (increase in the interquartile ranges for all properties in the top layer in Fig. 3.6), but occasionally also individual depths show a higher heterogeneity, irrespective of age.
The flow path analysis differentiated according to the vegetation complexity showed no systematic influence of the complexity level on the results. Heterogeneities within the individual experimental subplots were taken into account by averaging the volume density and surface area density across the five vertical profiles per subplot instead of relying on individual profiles. We therefore assume that the results of the flow path analysis are sufficiently representative to investigate their evolution across the chronosequence.

3.4.2 Evolution of flow paths

The flow type classification by Weiler (2001) was used to classify the volume density patterns into flow type categories. A comparison between the observations made during the excavation and the derived flow types showed that in this case an adaptation of the flow type classification was necessary. On the one hand, this adaptation involved the treatment of rocks to prevent misclassification, and, on the other hand, we introduced the possibility of finger-like flow paths with smaller widths. After these adaptations the derived flow types correspond well with the observations made in the field.
The observed staining patterns and derived flow types show a significant difference between the age groups, whereas no significant difference was observed with respect to vegetation complexity and irrigation amount.

The early years: 30-160

At the 30-year-old moraine, the water infiltrates homogeneously into the soil, probably due to the very low vegetation coverage and the coarse material texture. The dye pattern showed a mainly homogeneous staining of the soil material; thus derived flow types are mainly matrix flow in the form of homogeneous and heterogeneous matrix flow as well as matrix flow between rocks. Also finger flow occurs at the boundary to the clay layer or is caused by large blocks of rock, which are surrounded by clay. The determined macropore flow takes place only within the clay layer at a depth below 50 cm. In the clay layer, no significant biopores were identifiable, which is why it is assumed that the water is transported in cracks or along material interfaces. The upper coarse soil material with large pores and a low water holding capacity causes the water to be transported quickly deeper into the soil.
After 160 years the derived predominant flow types shift to heterogeneous matrix flow and finger flow. The observed widening of the dye plumes in deeper soil depths might be caused by a change in material or a reduction of hydrophobicity with soil depth where the influence of plants and organic material decreases (Blume et al., 2009). The dye coverage images show unstained soil areas starting also at the top of the soil profile, which indicates that preferential flow paths are initialized already at the soil surface or in the near-surface layer. This was also observed during the irrigation where we saw that the irrigated water often mainly infiltrated in depressions. Grass patches also tend to inhibit infiltration. It was observed

that in the presence of dense grass patches, the water infiltrated only next to the patches, leaving the area below the patches unstained.

Intermediate stage: 3000 years

Similar observations were made at the 3000-year-old moraine. The image analysis revealed that preferential flow paths start at the soil surface and thus are initiated by vegetation and microtopography causing a heterogeneous infiltration pattern. Field observations also revealed that heterogeneous infiltration was not only created due to dense grass patches but also occured under relatively homogeneous grass cover. A laboratory test of the water drop penetration time (DeBano, 1981; Doerr et al., 2000) on a soil sample of the upper soil material showed that the organic layer is highly water repellent in dry conditions (air dried for 2 weeks; water drop penetration time > 10 minutes). An increase in the hydrophobicity index (Tillman et al., 1989) with increasing moraine age was also found by Maier et al. (2020). Thus, we conclude that the hydrophobicity of the organic top layer has a big impact on infiltration and the initiation of unstable flow. Unstable flow occurs when horizontal wetting fronts break into fingers or preferential flow paths during the downward movement (Hendrickx and Flury, 2001). Compared to the 160-year-old moraine the 3000-year-old moraine is characterized by a higher number of narrower preferential flow paths.
The derived dominant flow type class at the 3000-year-old moraine is macropore flow with high interaction/finger flow. Of both possible flow types, finger flow is the prevalent flow process causing the dye pattern. Several studies linked the formation of finger-like flow paths to hydrophobic properties of the soil (Wallach and Jortzick, 2008; Dekker and Ritsema, 2000; Ritsema and Dekker, 1994; Blume et al., 2008; Wang et al., 2018; Hardie et al., 2011). It is assumed that hydrophobic compounds that are released during the decay of litter (Reeder and Jurgensen, 1979) or by root activity (Doerr et al., 1998) coat soil particles or are deposited in the pore space and thus create a hydrophobic soil matrix (Doerr et al., 2000). The humid and cool climate of former glacial areas leads to a slow decomposition of vegetation and thus to an accumulation of hydrophobic compounds (Doerr et al., 2000).

The late stage: 10 000 years

At the oldest moraine, we saw a distinctly shallower infiltration depth (Fig. 3.7). During the experiment, no surface runoff was observed. Most of the water was stored in the organic top layer. The soil beneath the top layer was almost completely unstained, and water was transported only via a few macropores into deeper layers. A dense network of roots was only observed in the organic top layer, which included the thicker roots of the alpenrose (*Rhododendron ferrugineum*). The root network in the soil underneath was less dense with roots of smaller diameters but extended to a depth of more than 50 cm. Although the vegetation cover has been reduced to decrease interception, the interception storage capacity at the oldest moraine is still comparatively high. Thus, a reduction in the water available for infiltration cannot be ruled out.

Impact of rocks

The rock content at the 30-, 160-, and 3000-year-old moraines is relatively high, with especially large rocks (widths > 20 mm) in deeper parts of the soil (Figs. 3.5b and 3.7). The large rocks lead to a reduction of the permeable area and thus can cause funnel flow (Hendrickx and Flury, 2001). This type of preferential flow was especially observed at the youngest moraine, where large boulders (> 25 cm) located at deeper soil depths were surrounded by unstained fine-textured material. Smaller-sized rocks in the upper part seemed not to have an influence on water transport (apart from reducing the flow-through volume), since these rocks and the surrounding soil were completely stained.
A splitting of flow paths caused by rocks was also observed a few times at the 160- and 3000-year-old moraines. In this case, water flowing past the sides of medium-to-large-sized rocks creates a type of finger flow that is not caused by water repellency or air entrapment. The tendency of higher rock contents to increase the number of flow paths was also found by Bogner et al. (2014).

Flow path controls along the age gradient

Integrating all of our findings on soil structural parameters, texture, vegetation cover and flow path patterns provides an overview over their coevolution and highlights the derived major flow path controls (Fig. 3.11).

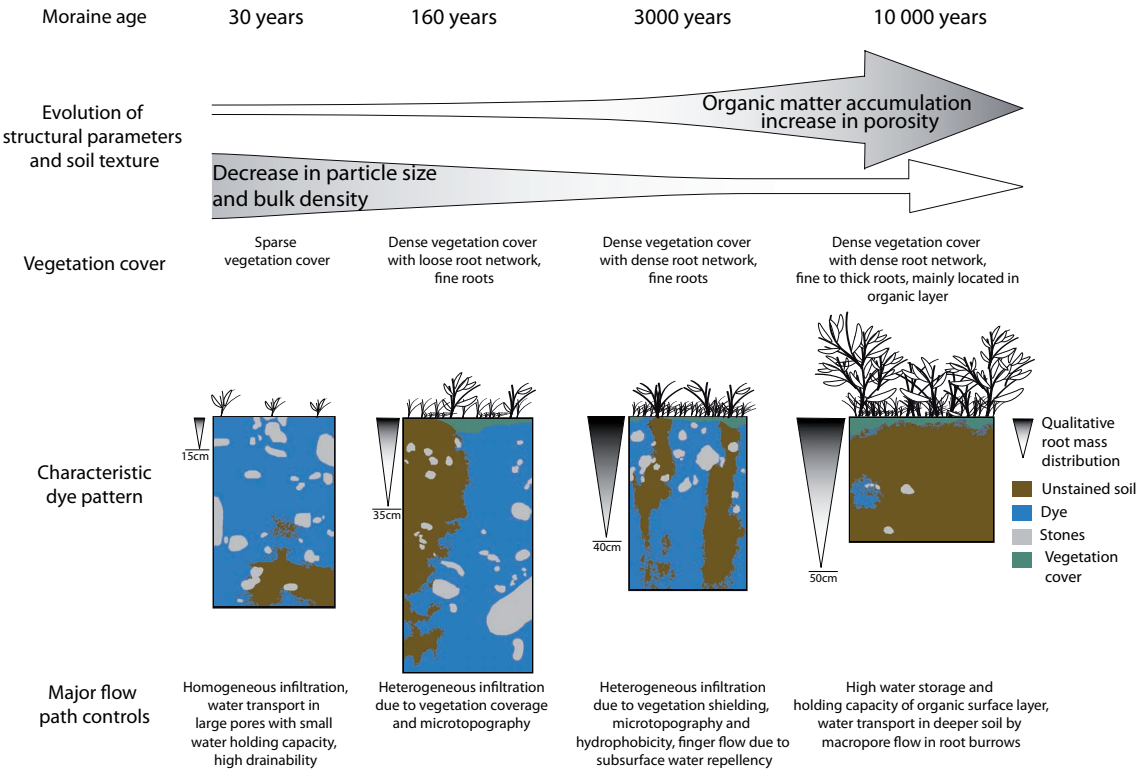

Figure 3.11: Sequence of observed characteristic dye patterns and derived flow path controls compared to the qualitative evolution of soil texture, structural parameters, and vegetation. The shade of the root mass distribution triangles is a measure for the vertical root mass distribution with a darker color indicating a higher root mass. The width of the triangles is a measure for the root mass comparison between the moraine ages, with broader triangles indicating a higher root mass.

Along the coevolution of soil and vegetation over 10 000 years the major controls of subsurface flow paths change. At the youngest moraine flow paths are only controlled by soil texture. The coarse material leads to the downward movement of the infiltration front. Preferential flow paths only occur at the interfaces between coarse and finer material.
At the medium-aged moraines flow paths are mainly controlled by vegetation shielding, microtopography, and hydrophobicity. The latter is assumed to have an increased impact at the 3000-year-old moraine. After 10 000 years of hillslope evolution, subsurface water transport is highly preferential and controlled by flow paths caused by root channels or boundaries of textural classes. Water storage in the organic layer which is also the main rooting horizon increases strongly.

3.5 Conclusions

Using Brilliant Blue dye experiments and soil sampling, we investigated the evolution of water transport paths along soil-forming processes. To our knowledge, this is the first study examining flow path evolution across the millennia in such detail. The evolution of the grain size distribution shows that grain size decreases with increasing age. The biggest changes are in the sand and silt fraction. Furthermore, water flow-defining structural parameters such as porosity and bulk density changes during soil development, resulting in an increasing water storage capacity with age. The depth-dependent evolution of these parameters supports our hypothesis that the soil material develops with increasing age from a homogeneously mixed material to a depth-differentiated soil system with vertical gradients in flow and storage defining soil properties. Changes in these flow-defining parameters are caused by the evolution of grain size distribution and vegetation.
The derived flow types also support our hypothesis that vertical subsurface flow path types and their vertical extent change through the millennia. Flow types change from homogeneous matrix flow in a fast-draining-coarse textured soil to a heterogeneous matrix and finger flow over the first 100-3000 years. At very young moraines, the water is homogeneously distributed within the soil matrix. However, the water storage capacity is relatively low due to the coarse material, and water is transported quickly deeper into the soil due to the high drainability. At the medium-age moraines, water is transported preferentially via finger-like flow paths deeper into the soil by leaving parts of the soil dry.
With increasing hillslope age, we expected macropores induced by root activities to become more important. After 10 000 years, where the amount of soil matrix macropores decreased significantly, macropore flow along roots plays an important role but is not very pronounced. Only a few roots reach beyond the organic top layer. However, this allows for a fast transport of water from the upper layer into deeper soil. The organic top layer has a pronounced influence on the soil water budget, by storing a significant amount of water. The increase in water storage with an increasing age of the moraines also caused a reduction in infiltration depth.
The proportion of preferential flow paths increases with soil age. Preferential flow is, however, not only caused by macropores, but especially for the medium-age moraines it seems more controlled by soil surface characteristics such as vegetation patches, microtopography and hydrophobicity. Thus, the evolution of flow paths is tightly linked to the complex interplay of soil-forming processes and vegetation

development over the millennia. A lot of changes in vegetation cover, soil (hydraulic) properties and flow paths occur within the first 160 years.
It was shown that the complex interaction of vegetation and soil development and its proven effect on flow path development also impacts the water balance, as the storage and conductivity properties of the soil change. However, the interplay between preferential flow paths and the soil hydraulic behavior not only influences the soil water budget but also runoff formation. These findings provide important insights into hydrological flow path evolution in transient systems.

4 The evolution of subsurface hydrological flow paths in calcareous parent material

This chapter has been published as:

Subsurface flow paths in a chronosequence of calcareous soils: impact of soil age and rainfall intensities on preferential flow occurrence

Anne Hartmann, Markus Weiler, Konrad Greinwald, and Theresa Blume

Originally published in:
Hydrology and Earth System Sciences, 26, 4953–4974, 2022, https://doi.org/10.5194/hess-26-4953-2022

Abstract

Soil hydrologic processes play an important role in the hydro-pedo-geomorphological feedback cycle of landscape evolution. Soil properties and subsurface flow paths both change over time, but due to a lack of observations subsurface water flow paths are often not properly represented in soil and landscape evolution models. We investigated the evolution of subsurface flow paths across a soil chronosequence in the calcareous glacier forefield at the Griessfirn glacier in the Swiss Alps. Young soils developed from calcareous parent material usually have a high pH value, which likely affects vegetation development and pedogenesis and thus the evolution of subsurface flow paths. We chose four glacial moraines of different ages (110, 160, 4900, and 13 500 years) and conducted sprinkling experiments with the dye tracer Brilliant Blue on three plots at each moraine. Each plot was divided into three equal subplots, and dyed water was applied with three different irrigation intensities (20, 40, and 60 mm h^{-1}) and an irrigation amount of 40 mm. Subsequent excavation of soil profiles enabled the tracing of subsurface flow paths. A change in flow types with increasing moraine age was observed from a rather homogeneous matrix flow at 110 and 160 years to heterogeneous matrix and finger-shaped flow at 4900 and 13 500 years. However, the proportion of preferential flow paths is not necessarily directly related to the moraine age but rather to soil properties such as texture, soil layering, organic matter content, and vegetation characteristics such as root length density and biomass. Irrigation intensity had an effect on the number of finger-shaped flow paths at the two old moraines. We also found that flow paths in this calcareous material evolved differently compared to a previous study in siliceous material, which emphasizes the importance of parent material for flow path evolution. Our study provides a rare systematic dataset and observations on the evolution of vertical subsurface flow paths in calcareous soils, which is useful to improve their representation in the context of landscape evolution modeling.

4.1 Introduction

Pedogenesis and its interaction with hydrological, geomorphological, and ecological processes plays an important and complex role in landscape evolution. Understanding the complex interaction between soil and water during landscape evolution is crucial for the understanding of natural history, but also for the application of modern landscape management practices such as landscape restoration. The parent material as the starting point for soil development has a strong impact on the resulting soil characteristics (Retzer, 1949). The mineral composition of the parent material determines the mineral composition of the soil and nutrients released during weathering, which can either be processed by flora and fauna or leached from the soil. The parent material influences weathering rates as well as the chemical and physical properties of the soil and thus soil formation (Sauer et al., 2015) and also vegetation composition (Michalet et al., 2002).
The role of water in pedogenesis is particularly multi-facetted (Lin, 2003) and often governed by feedback cycles: hydrology has a strong influence on the evolution of soil structure and texture, which in turn has an influence on soil hydrology. The hydraulic conditions influence geochemical and biological (weathering) processes (White and Blum, 1995). Soil water also serves as a transport medium and therefore influences the relocation of substances and particles within the soil matrix. Finally, soil water availability, which is also governed by the soil hydraulic conditions, influences vegetation composition and coverage.
Preferential flow (which is known to be ubiquitous) further complicates the investigation of these interactions, as it introduces additional spatial variability and leads to locally increased water availability, flow velocities, and deeper water transport - all of which will increase rates of weathering and transport in these locations. Preferential flow is, however, not only controlled by soil properties (Koestel and Jorda, 2014) but also by rainfall characteristics such as amount (Bachmair et al., 2009) and intensity (Wiekenkamp et al., 2016). Extreme rainfall events can exert a particularly strong influence on water partitioning and thus affect pedogenic (e.g., weathering, solute transport) and geomorphic (e.g., water erosion) processes (van der Meij et al., 2018).
Despite the importance of the hydrological processes in this context, their consideration within soil-landscape evolution models (SLEMs) is still insufficient (Samouëlian et al., 2012). Landscape evolution modeling is an important tool to better understand landscape formation but also to assess how landscapes are affected by global climate change (Montagne and Cornu, 2010) or anthropogenic interventions (Cui et al., 2021) such as land use change and hydrologic alterations (Newman et al., 2017). In particular, the evolution of vertical and horizontal subsurface flow paths – including the occurrence of preferential flow paths – are currently omitted in SLEMs (van der Meij et al., 2018), which can lead to incorrectly modeled transport and relocation processes (Sauer et al., 2012). One of the reasons for this neglect is the lack of knowledge of how soil hydraulic systems evolve over time. For a proper consideration of hydrologic processes in SLEMs, more field data on the evolution of soil hydraulic parameters and hydraulic function are needed (van der Meij et al., 2018).
While many studies have investigated soil development (e.g., Egli et al., 2010; He and Tang, 2008; Dümig et al., 2011; Vilmundardóttir et al., 2014; D'Amico et al., 2014), only a limited number of studies have investigated the evolution of soil hydraulic properties and subsurface flow paths. In previous field studies on the development of soil hydraulic properties, the main focus was on the saturated conductivity (K_{sat}), which was found to decrease with age and changes were mainly related to changes in soil properties such

as texture and bulk density (Brooks and Richards, 1993; Beerten et al., 2012; Maier et al., 2020). Beerten et al. (2012) found that hydraulic parameters describing the retention curves were harder to interpret and were affected by the organic carbon content. Lohse and Dietrich (2005) estimated points on the retention curves and hydraulic conductivity functions for a soil chronosequence from 300 to 4.1 million years of age developed from volcanic deposits. A shift to higher water retention and horizontal subsurface flow was observed alongside the development from a rather homogeneous to a layered system with increasing clay content. A similar change in hydrological pathways was found in volcanic catchments (ranging in age from 0.225 to 82.2 Ma), where pathways changed from deep percolation to shallow subsurface flow (Yoshida and Troch, 2016). These studies examined the development of flow paths on a rather large spatial and temporal scale and thus did not investigate vertical preferential flow paths. A detailed investigation of vertical subsurface hydrological flow paths in coevolution with soil (hydraulic) properties was so far only carried out for a chronosequence of 10 000 years on siliceous glacial till (Hartmann et al., 2020a), where an increase in preferential flow with increasing moraine age was found.

Previous studies showed conflicting results regarding the influence of rainfall intensity on preferential flow path occurrence. An increase in preferential flow with increasing rainfall intensity at the catchment scale was observed by evaluating the sequence of water content responses at different depths (Lin and Zhou, 2008; Wiekenkamp et al., 2016; Demand et al., 2019). Bromid tracer experiments in lysimeters with stony soils by Cichota et al. (2016) showed an increase in preferential flow with increasing irrigation intensity under soil moisture conditions near field capacity (comparing rainfall events of 5 mm h^{-1} and 20 mm h^{-1}). Wu et al. (2015) found, based on Brilliant Blue dye tracer experiments, a decrease in preferential flow at higher intensities (comparing rainfall events of 50 mm h^{-1}, 100 mm h^{-1}, and 150 mm h^{-1}), when the initial soil water content was high. However, as the relationship between flow paths and rainfall intensity can be influenced by various factors, cross-study comparisons are difficult and probably unlikely to identify the underlying controls. It is therefore crucial to investigate this relationship systematically and under controlled conditions.

Our study, carried out in the Swiss Alps, focuses on two main research gaps: (i) the evolution of vertical subsurface flow paths during soil formation in calcareous soils, and (ii) the impact of rainfall intensities on preferential flow occurrence as soils and hillslopes evolve over time. Calcareous soils are of special interest here, as they make up a third of the Earth's land surface area (Taalab et al., 2019). The high pH value of young calcareous soils determines plant nutrient availability (low P availability, high N loss (Hopkins and Ellsworth, 2005; Taalab et al., 2019)) and thus vegetation development (Michalet et al., 2002). Also, weathering rates and pedogenesis in calcareous soils differ strongly from other parent materials (Musso et al., 2022; Ehrlich et al., 1955). To investigate the temporal evolution of subsurface flow paths over the millennia, irrigation experiments were conducted on a set of four pro-glacial moraines with each moraine representing a different age class (chronosequence approach). We used Brilliant Blue dye to trace the occurrence of vertical subsurface flow paths across 13 500 years of landscape evolution recorded in our chronosequence and investigated a possible connection between the proportion of preferential flow paths to properties of the vegetation cover (e.g., coverage, root length density, biomass).

The chronosequence approach assumes that, for a sequence of sites (in this case, moraines) with similar characteristics such as topography, climate, and parent material on which the soil was formed, time can be treated as the only variable. It is well known that the application of this chronosequence concept has some

limitations, as landscape development is much more complex (Wojcik et al., 2021). The assumption that time is the only factor affecting soil development in a spatial sequence of soils is often the only option for the historical tracking of landscape development at a particular location and thus still a fundamental tool for representing temporal changes in the Earth's surface system (Phillips, 2015).
With our study we generated a rare systematic dataset and observations on the evolution of preferential flow paths in the context of landscape evolution, which will help to ensure proper handling of (subsurface) hydrologic processes and their role within the feedback cycle of the hydro-pedo-geomorphological system when it comes to soil and landscape evolution modeling.

4.2 Material and methods

4.2.1 Study site

The study area at the Griessfirn glacier forefield is located above the treeline between 2030-2200 m a.s.l. in the Central Swiss Alps (46° 85'N, 8° 82'E). The geology is dominated by schists, marl, and quartzites (Musso et al., 2019), but also includes limestone (Frey, 1965). The closest official weather station at a similar elevation (2106 m a.s.l.) is located at a distance of 48 km at Mount Pilatus (46° 98'N, 8° 25'E). The recorded annual mean temperature is 1.8 °C and the annual precipitation is 1752 mm (1981-2010) (MeteoSwiss, 2020a).
A chronosequence of four moraines was selected to investigate the effect of hillslope age on subsurface flow paths. The four selected moraines were dated by Musso et al. (2019) based on historical maps and additional radiocarbon dating. The youngest moraine is located at 2200 m a.s.l. and was dated to an age of 110 years (110a, a=years). The three other moraines are 160 (160a), 4900 (4.9ka, k=1000) , and 13 500 (13.5ka) years old and are located at an elevation of 2030 m a.s.l. (see Fig. 4.1). The choice of the 110a moraine as the youngest moraine is the result of the local conditions, as no adequate moraine younger than that could be identified that also ensured comparability in terms of elevation and microclimate (Musso et al., 2019). We therefore had to compromise and selected the moraine with an age of 110 years as our youngest moraine. At each moraine the vegetation was mapped (Greinwald et al., 2021b) and the soil physical characteristics were identified in 10, 30, and 50 cm depth (Hartmann et al., 2020b).
The vegetation coverage of the two young moraines is sparse with carpet-forming dwarf shrubs (e.g., *Dryas octopetala, Salix retusa*) stabilizing the slopes by their dense root stocks and facilitating the establishment of other plant species, such as patches of pioneer plants (e.g., *Saxifraga aizoides*) and mosses (e.g., *Tortella densa, Distichium capillaceum*) at the 110a moraine and *Anthyllis vulneraria, Saxifraga oppositifolia*, or *Silene acaulis* (pioneer plants) at the 160a moraine. The soil at the 110a and 160a moraines was classified as a Hyperskeletic Leptosol (Musso et al., 2019). At the 110a moraine the soil texture was identified as mainly sandy loam with tendencies to sandy clay loam, whereas the soil type at the 160a moraine was mainly identified as sandy loam and, in some occasions as loamy sand. The bulk density and porosity are homogeneous in the upper 50 cm at the 110a moraine and range between 1.6-1.9 g cm $^{-3}$ and around $\approx$ 0.3, respectively. The 160a moraine has a slightly lower bulk density ($\approx$ 1.55 g cm $^{-3}$) and higher porosity ($\approx$ 0.4), but both moraines have a similarly low organic matter content (<10 weight-%). The two older moraines (4.9ka and 13.5ka) are densely covered with grass (e.g.,

Festuca violacea agg.), dwarf shrubs (e.g., *Rhododendrum hirsutum, Vaccinium myrtillus, Vaccinium vitis-idaea*), and sedges (*Carex ferruginea, Carex sempervirens*). At both moraines, the soil was classified as a Calcaric Skeletic Cambisol (Musso et al., 2019). The soil texture varies over the top 50 cm. Silty clay and silty clay loam are dominant in the upper 10 cm, while loam and silty loam are predominant in 30 cm, and sandy loam in 50 cm. The soil at the 13.5ka moraine contains a little less clay in the top 50 cm but a little more silt than the soil at the 4.9ka moraine. The organic matter content in the top 10 cm at both old moraines is with ≈ 25 weight-% distinctly higher compared to the young moraines and declines with depth. Correspondingly, the porosity is with ≈0.8 distinctly higher and also rapidly declines with depth at both moraines, whereas the bulk density is low (≈ 0.5 g cm $^{-3}$) in the top soil and increases with depth, but still remains < 1.5 g cm^{-3} in 50 cm.

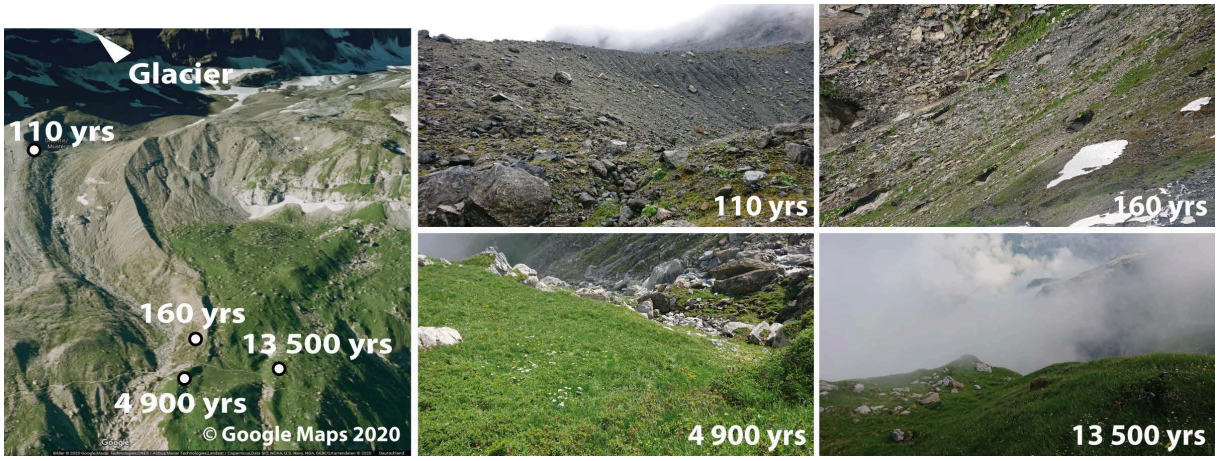

Figure 4.1: Location of the four selected moraines in the Griessfirn glacier forefield (left, photo by © Google Maps (2020b)) and the surface cover of each age class (right).

For the Brilliant Blue tracer experiments, three plots (1.0 x 1.5 m) were selected on each moraine. To capture the spatial heterogeneity of the vegetation cover, the plots at each moraine were chosen along a gradient in vegetation complexity (Greinwald et al., 2021b). At each plot, species richness, root length density (RLD), vegetation cover, above-ground biomass (BM), and the slope were measured or estimated by Greinwald et al. (2021a) (Table 4.1).

4.2.2 Dye tracer irrigation experiments

The dye tracer experiments were conducted between July 25th and September 14th, 2019. Each of the three 1.5 m x 1.0 m experimental plots per moraine was further divided into three equal subplots of 0.5 m x 1.0 m for individual irrigation with 40 mm of a 4 g l^{-1} Brilliant Blue FCF solution (Fig. 4.2). To reduce interception, large vegetation in the form of shrubs, bushes, and tall grass was cut to a height of a few centimeters before irrigation. The three subplots were irrigated with the same amount (40 mm) but different intensities (20, 40, and 60 mm h^{-1}). The irrigation intensities represent extreme events with return periods of 2.8, 60, and 100 years (Fukutome et al., 2017), respectively.
Each subplot was irrigated individually, while the other two were covered by a tarpaulin. A hand-operated sprayer and a battery-powered pump were used for tracer application. Since the irrigation system only

Table 4.1: Main plot characteristics and vegetation parameters at the tracer experiment plots (BM= above ground biomass, RLD= root length density, n.a.= analysis was not carried out).

Moraine age [years]	Plot #	Vegetation Cover [%]	Slope [°]	Species Richness	RLD [km m^{-3}]	BM [kg m^{-2}]
110	1	25	40	10	348.6	n.a.
110	2	15	21	10	315.1	n.a.
110	3	55	25	13	150.6	n.a.
160	1	50	42	11	293.2	4.7
160	2	20	35	11	201.4	5.7
160	3	75	23	13	165.9	3.9
4 900	1	90	23	21	939.8	5.5
4 900	2	90	27	21	822.9	9.6
4 900	3	100	25	33	1235.16	8.7
13 500	1	85	27	25	654.2	5.0
13 500	2	100	36	25	1197.2	3.6
13 500	3	80	37	27	608.7	4.6

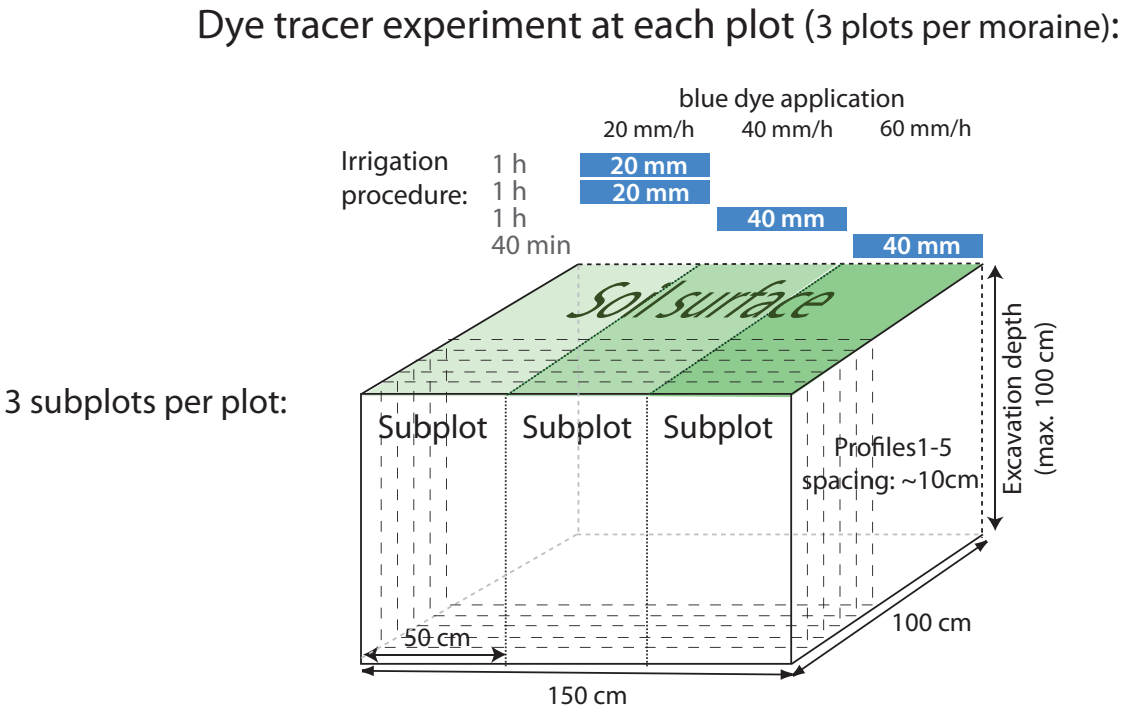

Figure 4.2: Illustration of the dye tracer experimental design at each moraine.

provided a flow rate of 1 l min^{-1} the different irrigation intensities were achieved by alternating intervals of irrigation and breaks. The first subplot was irrigated for 2 hours in a sequence of 1 minute irrigation and 5 minutes break to irrigate the subplot with 40 mm at an intensity of 20 mm h^{-1}. The intensity of 40 mm h^{-1} at the second subplot was achieved by a sequence of 1 minute irrigation and 2 minutes break for 60 minutes. The last plot was irrigated for 40 minutes in a sequence of 1 minute irrigation and 1 minute break to achieve an intensity of 60 mm h^{-1}. An overview of the experimental design and an illustration of the irrigation procedure is provided in Figure 4.2. After the experiment the whole plot was covered with a tarp to protect it from potential natural rainfall until the excavation on the following day.
A first vertical profile was excavated 10-15 cm downslope of the lower edge of the irrigated plot to check for subsurface lateral flow. The plots were then excavated in five vertical profiles in approximately 10 cm segments starting the first segment 10 cm upslope from the lower edge of the irrigated plot. Pickaxes, spades, and hand shovels were used to excavate the profiles. The profiles were cleaned carefully and protruding roots were cut off. Rocks and stones were not removed, but cleaned from soil. The soil profiles of the subplots were photographed with a Panasonic Lumix DMC-FZ18 camera and a resolution of 2248 pixels x 3264 pixels. To avoid direct sunlight and to provide a uniform light distribution, a large umbrella was used for shading. A Kodak gray-scale and a wooden frame were included in the photographs for a later geometric correction and color adjustment.

4.2.3 Image analysis and flow type classification

The photographs of the profiles were converted into tricolor images to differentiate between stained and unstained areas, as well as rocks by using the image analysis procedure by Weiler and Flühler (2004). To avoid possible interference from interactions around the inner and outer subplot boundaries, a buffer with a width of 6 cm between adjacent subplots and 5 cm to the outer plot boundary was excluded from the analysis. The analysis includes a geometric correction, a background subtraction, and a color adjustment to correct differences in image illumination and changes in the spectral composition of the daylight. A further correction of the tricolor images using the photographs was necessary, since – due to poor lighting conditions or a heterogeneous background color distribution in the soil caused by, for example, material transitions, small stones, or organic matter – the image analysis software was not able to recognize all large dye stains as coherent objects. Thus, the software detected interruptions within blue stains that did not correspond to the field observations and would have been identified as a large number of individual flow paths during the following analysis. The manual correction of the tricolor images using the original photographs eliminated these interruptions (Hartmann et al., 2020a). In the resulting tricolor images the horizontal and vertical lengths of a pixel correspond to 1 mm.
The volume density (VD) corresponds to the dye coverage and was calculated for each of the five profiles per subplot as the fraction of stained pixels in each pixel row, thus providing depth profiles of volume density. The surface area density (SAD) is an indicator for the number of individual flow paths and was calculated for each pixel row of the five profiles by using the intercept density, which describes the number of interfaces between stained and unstained pixels divided by the horizontal width of the soil profile. The combination of both profile parameters provides the information whether the stained area is the sum of many small fragments or a few large ones.

The dye patterns of each profile per subplot were then classified into flow type categories according to the approach proposed by Weiler and Flühler (2004). This classification is based on the proportions of three selected stained path width (SPW) classes (stained path width <20 mm, 20 mm-200 mm, >200 mm) on the volume density. The stained path width is equal to the horizontal extent of a stained flow path. This classification method distinguishes between five flow types: (1) macropore flow with low interaction, (2 mixed macropore flow (low and high interaction), (3) macropore flow with high interaction, (4) heterogeneous matrix flow/finger flow, and (5) homogeneous matrix flow. The five flow types differ in the spatial extent of the water transport and thus in the proportion of the involved soil matrix, which impacts flow velocities, water availability and solute transport. From (1) to (5) the preferentiality of the water transport decreases and the homogeneity and spatial water availability increases.

We define macropore flow as water transport via root channels, earthworm burrows, and flow along fissures largely bypassing the matrix. The characteristic dye patterns show narrow but long individual stains, which in some cases can be broader due to interactions with the surrounding soil matrix. The level of lateral interactions between the water transported via macropores and the surrounding soil matrix mainly depends on the soil matrix. In low-permeability or saturated soils the lateral interactions are usually minimal and the characteristic dye patterns show narrow but long individual stains. Permeable soils enable extensive lateral interactions between macropore water and the soil matrix. The dye patterns show broader individual stains.

Here, the term "finger flow" summarizes all flow types that cause finger-shaped flow patterns, which includes finger flow caused by flow instabilities in the wetting front (Nimmo, 2021), finger-shaped flow paths due to water repellency, air entrapment or textural layering (Hendrickx and Flury, 2001) and also funneled flow leading to vertical, elongated, finger-like flow paths. The latter is caused by the redirection and funneling of water by textural boundaries and large rocks (Hendrickx and Flury, 2001) or by the heterogeneity of soil hydraulic properties (Nimmo, 2021). The characteristic flow patterns of all these flow types are very similar and thus cannot be distinguished by the image analysis: they show broader, vertically elongated, coherent flow paths, which indicate a preferential vertical water transport, leaving large parts of the soil matrix dry.

Dye patterns that could not be classified as one of these flow types were categorized as undefined. We used a modified version (Hartmann et al., 2020a) of the Weiler and Flühler (2004) classification, which was more suitable for stony alpine soils. In the case of homogeneous matrix flow, the modified classification prevents a high stone content from leading to the detection of a heterogeneous flow pattern as a result of the coherent stained area being broken up into smaller pieces, which then could be falsely classified as heterogeneous matrix flow, finger-shaped flow, or macropore flow depending on the abundance of rocks. In this case the flow type is assigned to a new flow type class called (6) "homogeneous matrix flow between rocks".

The modified classification also avoids a clear differentiation between "macropore flow with high interaction" and "finger-shaped flow". As the original classification assigns finger-shaped flow paths only when the medium-sized stained path width (20–200 mm) and the biggest stained path width class (> 200 mm) account for approximately half of the dye coverage, fingers with smaller widths (not necessarily caused by macropores) were not detected as such and automatically counted as macropore flow with high interaction. Hartmann et al. (2020a) observed that finger-like flow paths with smaller widths were frequently present

in alpine soils. Their dye patterns and distributions of stained path width classes are similar to "macropore flow with high interaction". These classes cannot be distinguished from each other in the image analysis. Thus we renamed this class to (3) "macropore flow with high interaction/ finger-shaped flow".
The classification was done for each pixel row per profile. To quantify the proportion of preferential flow per profile, a preferential flow fraction index (PFF) was calculated as the proportion of all preferential flow type classes at each profile. As the flow type classification was done for each pixel row, the PFF is the number of pixel rows classified as a preferential flow type (flow types (1)-(4)) divided by the total number of pixel rows.
To determine a representative infiltration depth per subplot, we used the median value of the maximum staining depths per subplot. To obtain the distribution of maximum staining depths, we determined for each pixel column of the five profile images per subplot the location of the deepest blue-colored pixel. The median value was chosen to represent the infiltration depth, since this measure is less affected by outliers (e.g., single deep infiltration flow paths) than the mean value.

4.2.4 Statistical analysis

4.2.4.1 Statistical differences between profiles

A bootstrapped LOESS (local least-squares-based polynomial smoothing) regression (BLR) approach (Keith et al., 2016) was used to test differences between experiments in the observed VD profiles and SAD profiles with regard to moraine age and irrigation intensity. The BLR approach is a combination of bootstrapped data resampling with local least-squares-based polynomial smoothing (LOESS) regression and was proposed by Keith et al. (2016) for the comparison of any soil property profiles from datasets of two different characteristics. For the pair-wise test the two datasets containing several profile observations of the soil variable of interest are combined and resampled depth-wise n=1000 times by bootstrapping with replacement. Each resampled dataset is modeled using LOESS regression. Out of the 1000 LOESS regressions the 95 % confidence intervals are calculated and compared with the LOESS regression of the not-combined individual set of profile observations. When the modeled LOESS regression of the original dataset lies outside of the confidence interval, the null hypothesis that there is no difference between the two original datasets, is rejected. For the LOESS regression, we used all five profiles per subplot.

4.2.4.2 Statistical differences between median infiltration depths

To test for significant differences in observed infiltration depths among age classes and among irrigation intensities the non-parametric Mood's median test was used (Hervé, 2018). The significance level was set to $p < 0.05$. The Mood's median test compares median pairs of two or more groups. A p-value lower than 0.05 indicates that the median of at least one group is significantly different from the other groups. To identify which groups are statistically different, a pairwise Mood's median tests across groups was used as a post hoc test (Mangiafico, 2016). The test was also used to detect significant differences between the dye pattern characteristics among the age classes.
To investigate differences and similarities in the relationship between PFF and site or vegetation characteristics, a linear regression of PFF with site and vegetation characteristics was plotted by using the

ggplot2-package (Wickham, 2016). A 95 % confidence interval was chosen for the significance test of the linear relationship. All data analyses were carried out using R (R Core Team, 2017).

4.3 Results

4.3.1 Vertical dye pattern analysis

We consider the median maximum staining depth as the representative infiltration depth of the soil profile. The representative infiltration depths are less than 1 m, but vary strongly between the age classes and irrigation intensities (Fig. 4.3). Across the moraine ages the representative infiltration depths differ significantly (Fig. 4.3, top), but do not show an age trend. A significant relationship between irrigation intensity and representative infiltration depth is only found at the 13.5ka moraine, where the infiltration depth increases with irrigation intensity. Sorted by irrigation intensity, no distinct age trend in the infiltration depths is observed (Fig. 4.3, bottom).

The averaged volume density (VD) profiles (over the 5 profiles per subplot) of the three stained path width (SPW) classes per subplot are displayed in Figure 4.4. The sum of the VD profiles of the three SPW classes per subplot is equal to the VD profile of all stained areas (which is also equal to the dye coverage). At the two young moraines (110a and 160a) we observed clearer differences in the VD profiles between the experimental plots of the single age groups compared to between the irrigation intensities (Fig. 4.4). At both young moraines the VD of SPW>200 mm is high over the entire profile depth at the plots labeled plot 3. These are also the two plots with a distinctly higher vegetation cover (Table 4.1) at these otherwise sparsely vegetated young moraines. At the two other plots of the 110a and 160a moraines, the fractions of SPW>200 mm are high in the upper 10-20 cm, but distinctly decline with depth. At the 4.9ka and 13.5ka moraines the fraction of SPW>200 mm is lower in the upper 10-20 mm compared to the young moraines. Over the entire profile range, path widths of the category 20<SPW<200 mm most often have the largest share of the dye coverage. The proportion of SPW<20 mm is negligible at all age classes.

Most of the cross-section of plot 2 at the 4.9ka moraine and the subplot irrigated with 40 mm h^{-1} of plot 1 at the 160a moraine was occupied by a large boulder in the ground (see Fig. 4.14). Please note that due to the strong inhibition of the water transport, these subplots were excluded from further analysis. Further, it must be taken into account that the results of plot 1 at the 110a moraine are based on only two observations (= two profiles per subplot), as the excavation had to be interrupted due to an unforeseen change in weather conditions. Despite protection, the rest of the experimental plot collapsed due to a thunderstorm.

The depth integrals of the dye pattern characteristics were compared across all experiments using boxplots, where each box plot contained the information of 3 experiments à 5 soil profiles (Fig. 4.5). The dye coverage (= integral of the VD profile) corresponds to the area percentage of all blue-colored areas per profile (Fig. 4.5a). The proportions of the three SPW classes (Fig. 4.5b-d) are also given as the area percentage per profile. The dye coverage varies strongly (between the experimental plots) at the 110a and 160a moraines with the majority ranging between 10 and 60 $\%$ (Fig. 4.5a). The variation decreases with moraine age and the dye coverage at the oldest moraines mostly ranges between 20 and 50 $\%$. The proportion of SPW<20 mm increases slightly with age (Fig. 4.5b), but remains negligible with an average

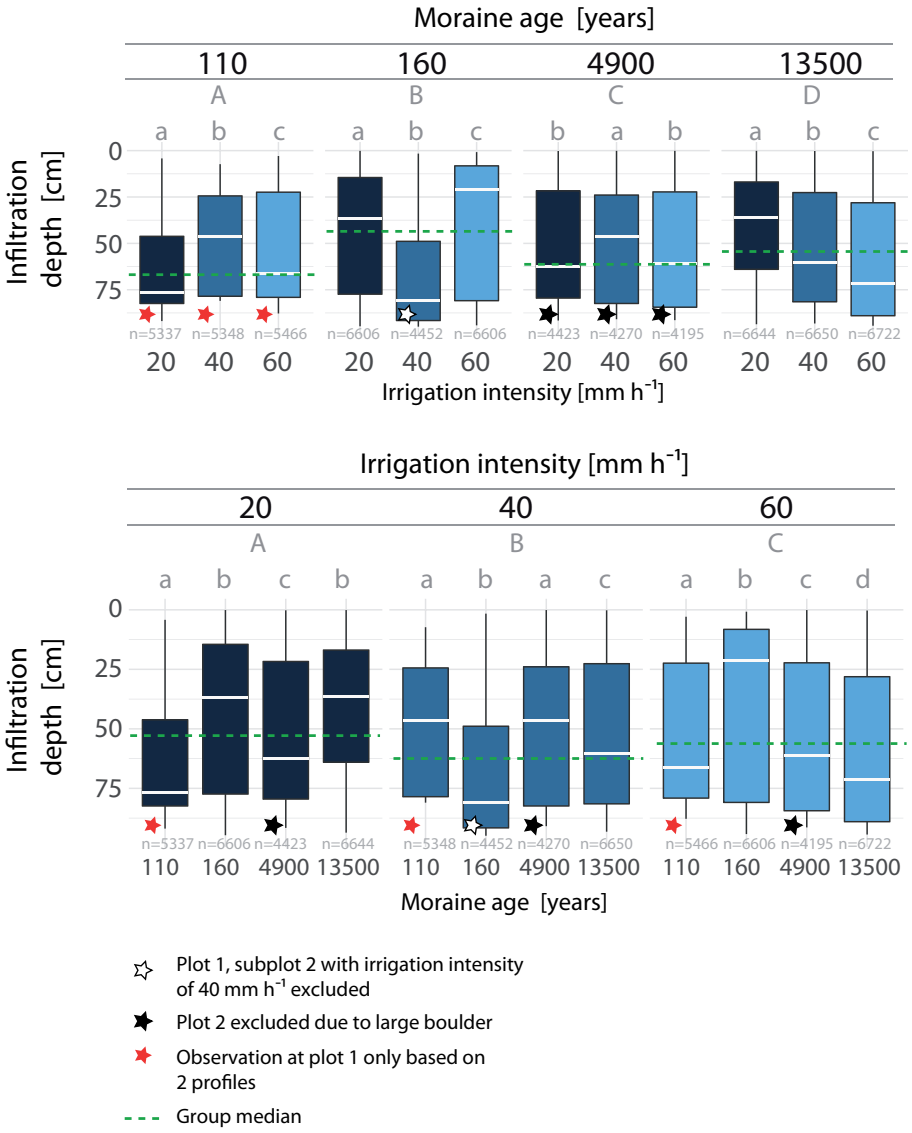

Figure 4.3: Maximum staining depth in each pixel column along the profile width at all excavated profiles at each age class (upper plot) and irrigation intensity (lower plot). Median values indicate the representative infiltration depth. Significant differences in median values are indicated by different letters. Upper case letters indicate the results of the Mood's median test in combination with a post hoc test among the age classes (upper plot) and irrigation intensities (lower plot). The dashed green line shows the group median used for the test. Different lower case letters denote the results among the irrigation intensity in each age class (upper plot) and the results among the age classes at each irrigation intensity (lower plot); n equals the number of pixel columns evaluated in each box plot.

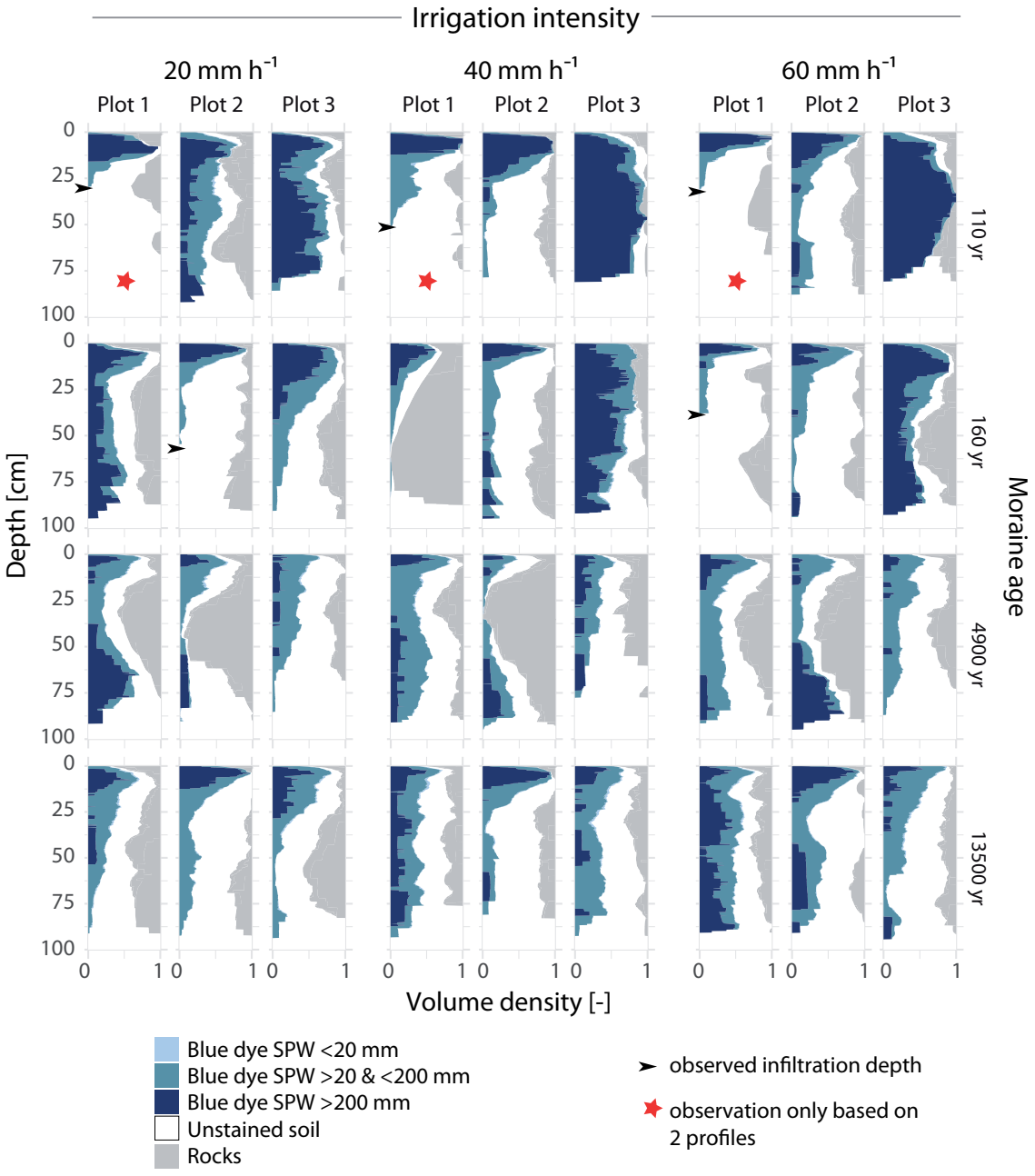

Figure 4.4: Mean volume density profiles per age class and irrigation intensity. The volume density is the fraction of stained pixels, color coded here by flow path width (stained path width, SPW) and rocks. Maximum infiltration depth was >1m in 31 of the 36 experiments. Arrows indicate the maximum infiltration depth < 1m at the remaining 5 plots.

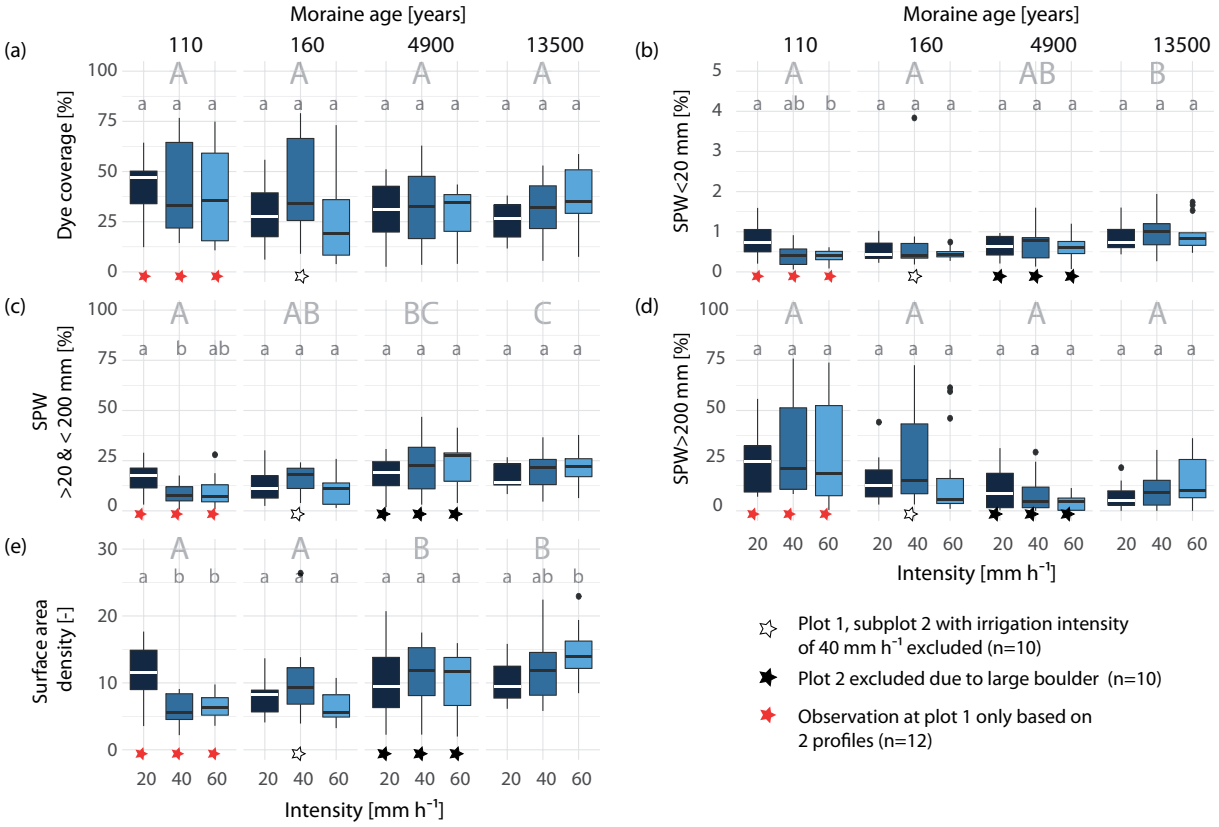

Figure 4.5: Box plots of dye staining characteristics compared across the three irrigation intensities and the four age classes (each box plot shows the data of 3 plots à 5 profiles, 15 profiles in total). (a) Dye coverage (volume density) in area percent of the entire soil profile, proportion of (b) stained path with (SPW) <20 mm, (c) 20 mm<SPW<200 mm, (d) and SPW>200 mm in area percent of the entire soil profile, and (e) integral of the surface area density (measure for the number of flow paths) per age class and irrigation intensity. Upper case letters indicate the results of the Mood's median test among the age classes. Different letters denote significantly different median values among the age classes (medians not shown). Lower case letters denote the results among the irrigation intensity in each age class.

area proportion of less than 2 % on the total profile area. An increase with age can be seen in the area proportion of 20<SPW<200 mm (Fig. 4.5c), with a corresponding decrease in the area proportion of the SPW>200 mm (Fig. 4.5d).

To clarify if the stained area described by VD (Fig. 4.5a-d and Fig. 4.4) is made up of many small flow paths or few large ones, VD has to be jointly interpreted with the surface area density (SAD) (Fig. 4.5e and Fig. 4.6), which is a measure for the number of individual flow paths. SAD increases along the chronosequence (Fig. 4.5e) with the exception of very high SAD values at the youngest moraine irrigated with 20 mm h^{-1}. A depth-differentiated display of SAD (for the increments of 0-20, 20-40, 40-60, and 60-100 cm) per age class and irrigation intensity is given in Figure 4.6. At the young moraines, the SAD in the upper 10-20 cm is comparable to that of the old moraines, but decreases more strongly with depth (Fig. 4.6). At 80 cm, SAD seems to be higher at the older moraines. The combination of SAD and VD reveals distinct differences in the staining patterns along the chronosequence. The young moraines are dominated by a high VD (in some cases restricted to the shallow depth only), a low SD, and a dominant fraction of SPW>200 mm. In contrast, the old moraines have a high fraction of 20<SPW<200mm combined with a high SAD, which indicates a higher number of smaller, narrow blue-colored areas and

thus more individual active flow paths at the older moraines and less individual flow paths but larger continuous areas used for water transport at the young moraines.

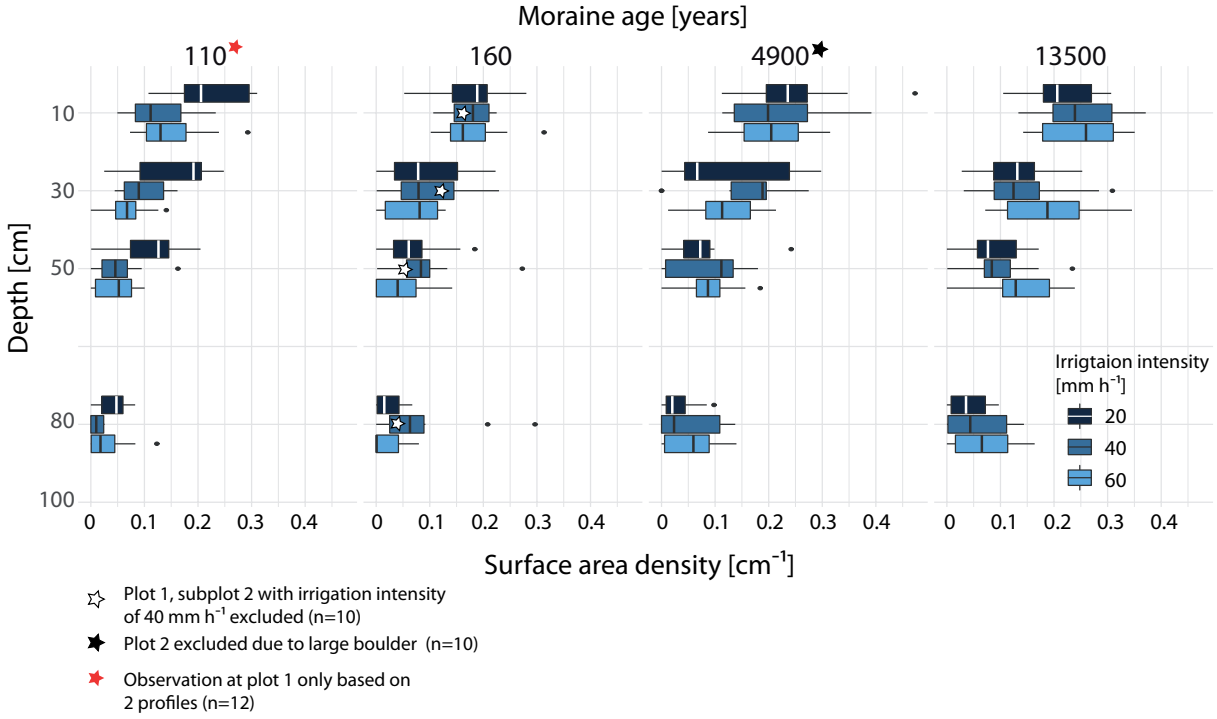

Figure 4.6: Surface area density (an indicator for the number of flow paths observed across the profile at a certain depth) for the depth increments of 0-20, 20-40, 40-60, and 60-100 cm per age class and irrigation intensity. Each box contains the information of the five profiles per subplot (n=15).

Different irrigation intensities mostly do not lead to significant differences between the resulting dye pattern characteristics (Fig. 4.5). Even though there are no statistically significant differences between the medians in dye coverage, the medians at the young moraines tend to decrease and at the old moraine to increase with increasing intensity (Fig. 4.5a). The respective fractions of the three SPW classes also seem to be affected by irrigation intensity, but changes are only significant for the two SPW classes <200 mm at the 110a moraine. At this age class a reduction in the median areal fraction with increasing intensity is observed for all three SPW classes. The interquartile range, however, increases for SPW> 200 mm. At the 4.9ka moraine, a tendency towards higher fractions of 20<SPW<200mm and a tendency towards lower fractions of SPW>200mm with increasing intensity are observed. On the ther hand, at the 13.5ka moraine a tendency towards higher proportions is found for both SPW classes. However, the differences between the intensity levels are not tested as statistically significant. A statistically significant increase of SAD with irrigation intensity can be seen at the 13.5ka moraine and a decrease at the 110a moraine (Fig. 4.5e). The SAD at the 160a moraine also tends to decrease with increasing intensity, but according to the Mood's median test the differences are not statistically significant. The depth distribution of SAD per irrigation intensity (Fig. 4.6) shows an increase in SAD with increasing irrigation intensity at all depths at the oldest moraine and a tendency to a higher SAD at the 4.9ka moraine starting at a depth of 20 cm. To quantitatively assess the impact of age and irrigation intensity on the dye pattern a statistical approach in the form of a bootstrapped LOESS regression (BLR) was used. The approach is designed

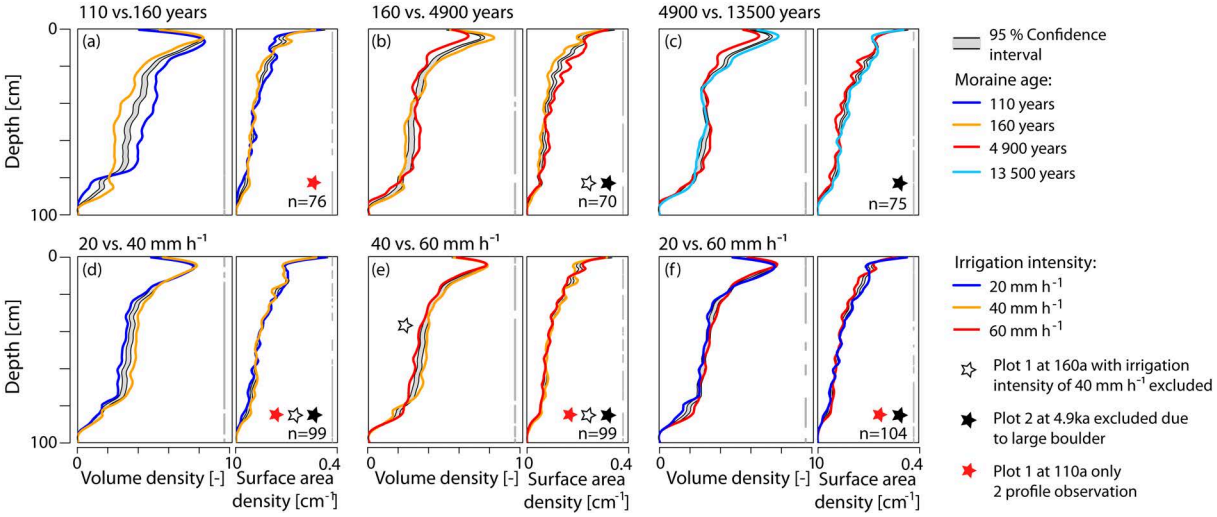

Figure 4.7: Differences in volume density and surface area density profiles with respect to (a-c) moraine age and (d-f) irrigation intensity. If the profile lines sit outside the gray-shaded confidence interval, the two profiles are considered to be significantly different. The parts of the depth profiles where this is the case are indicated by gray vertical bars on the right of each plot; n denotes the number of profiles used for the depth-wise re-sampling.

for a comparison of two datasets with profile observations (Keith et al., 2016). The results of the BLR approach for a pair-wise comparison of the averaged volume density and surface area density profiles are shown in Figure 4.7. Next to the 95 % confidence interval of the 1000 LOESS regressions (bootstrap resampled out of the combination of both compared datasets) the LOESS regression of both original datasets are shown. The differences between the two profiles are significant if the LOESS regression curves sit outside the confidence interval. It would actually be sufficient to plot only one LOESS regression of the original datasets (Keith et al., 2016), but we plotted both. Based on the moraine age as the test variable we compared the sets of all volume density and surface area profiles per moraine age along the chronosequence (Fig. 4.7 a-c). We find statistically significant differences in the volume density and surface area density profiles among the neighboring age classes. The gray vertical bar indicating where differences are significant is almost continuous and has only a few short interruptions.

When comparing the profiles with regard to the irrigation intensity irrespective of age, we see that significant differences are dominating, but the LOESS regression profiles are mostly located very close to the confidence interval (Fig. 4.7 d-f). The profile comparison between irrigation intensities, carried out individually for each age class, shows similar results (Fig. 4.8). At the 4.9ka moraine the gray bars indicating significant differences are often disrupted, with a slight tendency towards more significant differences in the upper half meter for VD. In contrast, at the 160a moraine and especially at the 13.5ka moraine, the regression lines are located far outside of the confidence interval, indicating significant differences across all irrigation intensities (except 20 vs. 60 mm h^{-1} at 160a).

To investigate the spatial variability within each age class we compared the profiles of the three plots per moraine (Fig. 4.9). In this case profiles across all irrigation intensities were used, revealing significant differences between the three plots for all age classes. The profiles at the 4.9ka and 13.5ka moraines show mainly significant differences, with no comparison within the age class being particularly striking. The LOESS regression profile lines comparing plot 1 and 2 with plot 3 at the two young moraines (110a and

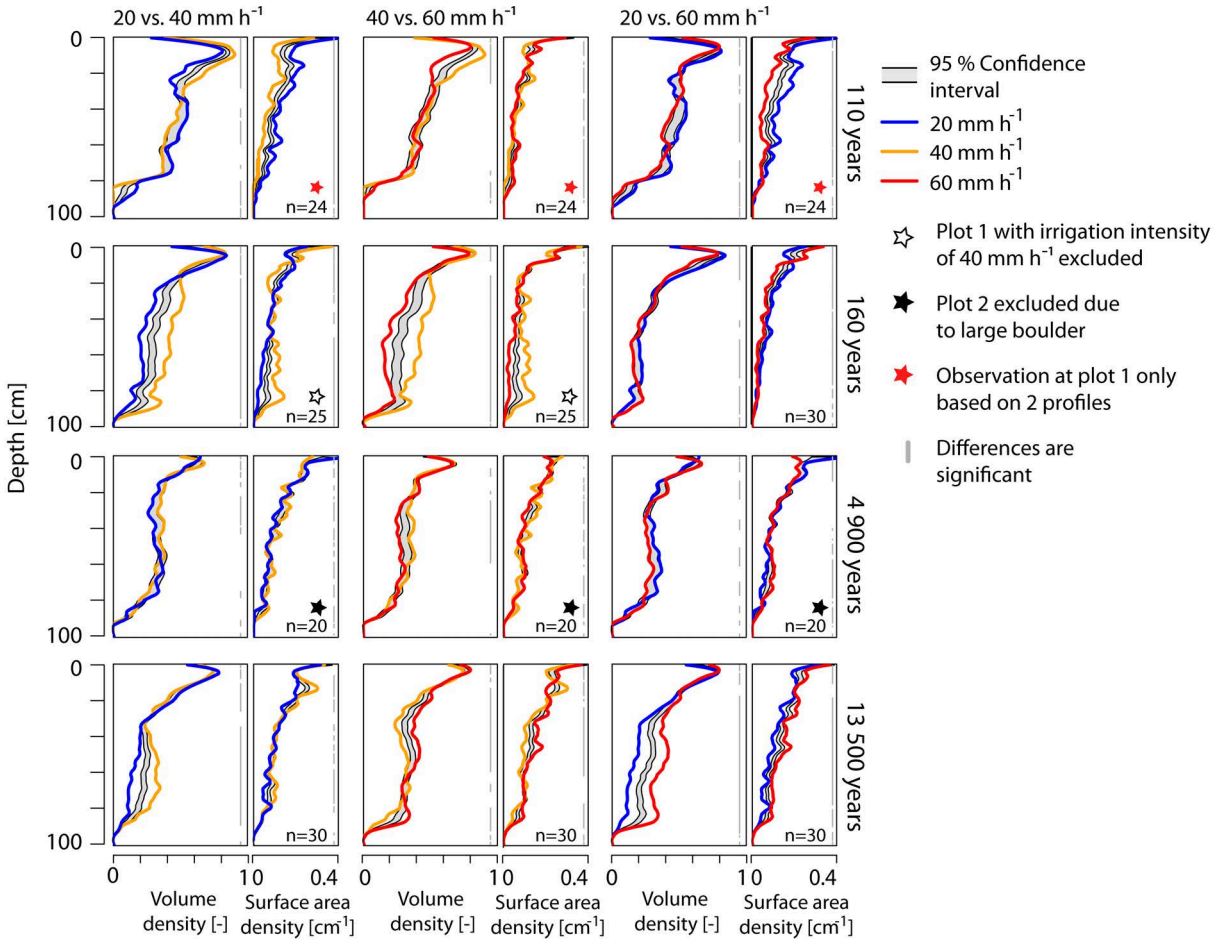

Figure 4.8: BLR test for differences in volume density profiles and surface area density profiles among the three irrigation intensities per age class. If the profile lines sit outside the gray-shaded confidence interval, the two profiles are considered to be significantly different. The parts of the depth profiles where this is the case are indicated by gray vertical bars on the right of each plot; n denotes the number of profiles used for the depth-wise re-sampling.

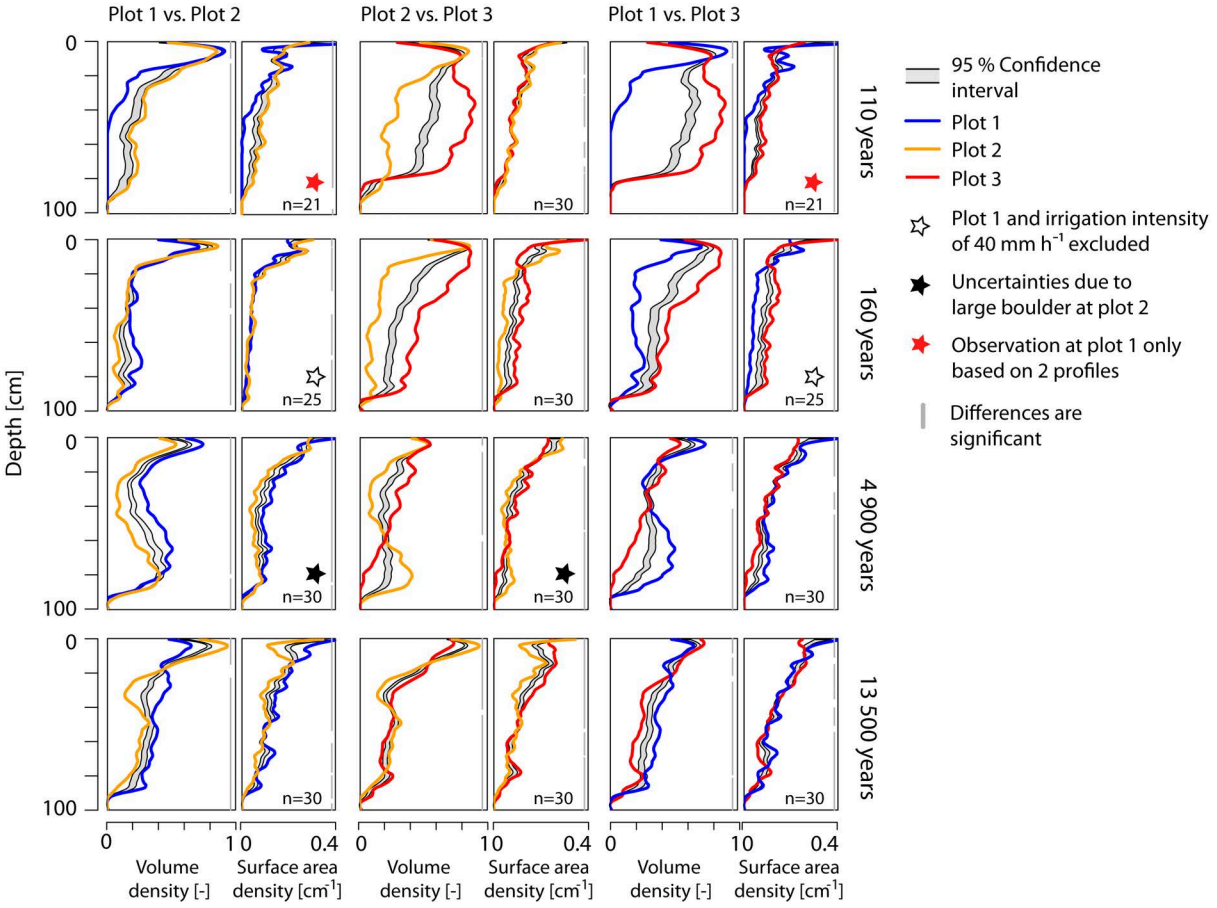

Figure 4.9: BLR test for differences in volume density profiles and surface area density profiles among the three experimental plots per age class. If the profile lines sit outside the gray-shaded confidence interval, the two profiles are considered to be significantly different. The parts of the depth profiles where this is the case are indicated by gray vertical bars on the right of each plot; n denotes the number of profiles used for the depth-wise re-sampling.

160a), however, lie far outside the confidence interval, which indicates strong differences between the profiles at plot 3 and the other two plots. This resembles the strong differences in the mean VD profiles (Fig. 4.4) at the two young moraines. Plot 3 at both moraines, clearly stands out from the other plots with a higher vegetation cover and a larger VD at greater depths.

4.3.2 Flow type classification

Using the VD profiles of the three SPW classes and their fraction of the total dye coverage to characterize flow types (Weiler, 2001), we found that, over the millennia, flow types transition from matrix flow to preferential flow in the form of finger-shaped flow (Fig. 4.10 a). At the youngest moraine, matrix flow is the predominant flow type (relative frequency > 0.6) followed by the flow type class "Macropore flow with high interaction/ finger-shaped flow". A reliable distinction between macropore flow with high interaction and finger-shaped flow could be made neither through the image analysis nor through on-site assessment. As narrow macropores were sometimes present (e.g., thin root channels), they certainly contribute to water transport, but it is also likely that this process is obscured by finger-shaped flow paths. Since the water transport patterns of both flow types cannot be distinguished and both show finger-shaped flow patterns, they are also referred to as finger-shaped flow in the following.
At the 160a moraine, the relative frequency of matrix flow already decreased to 0.5, and the frequency of finger-shaped flow increased. At the two oldest moraines, the dominant flow type is finger-shaped flow, and the relative frequency of matrix flow dropped below 0.3. Considering the entire profile depth of 1 m, the frequency of matrix flow decreases and the frequency of finger-shaped flow increases continuously with moraine age. A depth-differentiated view shows a higher proportion of finger-shaped flow at the 4.9ka moraine than at the 13.5ka moraine in the upper 20 cm (Fig. 4.10 a1). At the other depths (Fig. 4.10 a2 to a4), however, a continuous increase in finger-shaped flow frequency with moraine age was observed.
With regard to the irrigation intensity, no consistent impact on the flow type distribution across the millennia could be identified (Fig. 4.10 b). At the 110a and 160a moraines, the two dominant flow types (matrix flow and finger-shaped flow) show an almost-equal distribution across all irrigation intensities. A tendency towards less matrix flow is observed at the 4.9ka moraine, whereas at the 13.5ka moraine the frequency of matrix flow increases with increasing irrigation intensity. Differentiated by depth, we observed no systematic trend in flow type frequency distribution, with increasing irrigation intensity in the upper 20 cm for all age groups (Fig. 4.10 b1). Below a depth of 20 cm, the 4.9ka moraine and the 13.5ka moraine each show a trend-like behavior in the shift of the frequency distribution with irrigation intensity similar to what we see for the entire soil profile (Fig. 4.10 b2 to b4). Below a depth of 40 cm, the relative frequency of matrix flow also increases with increasing irrigation intensity at the 110a and 160a moraines (Fig. 4.10 b3-b4).

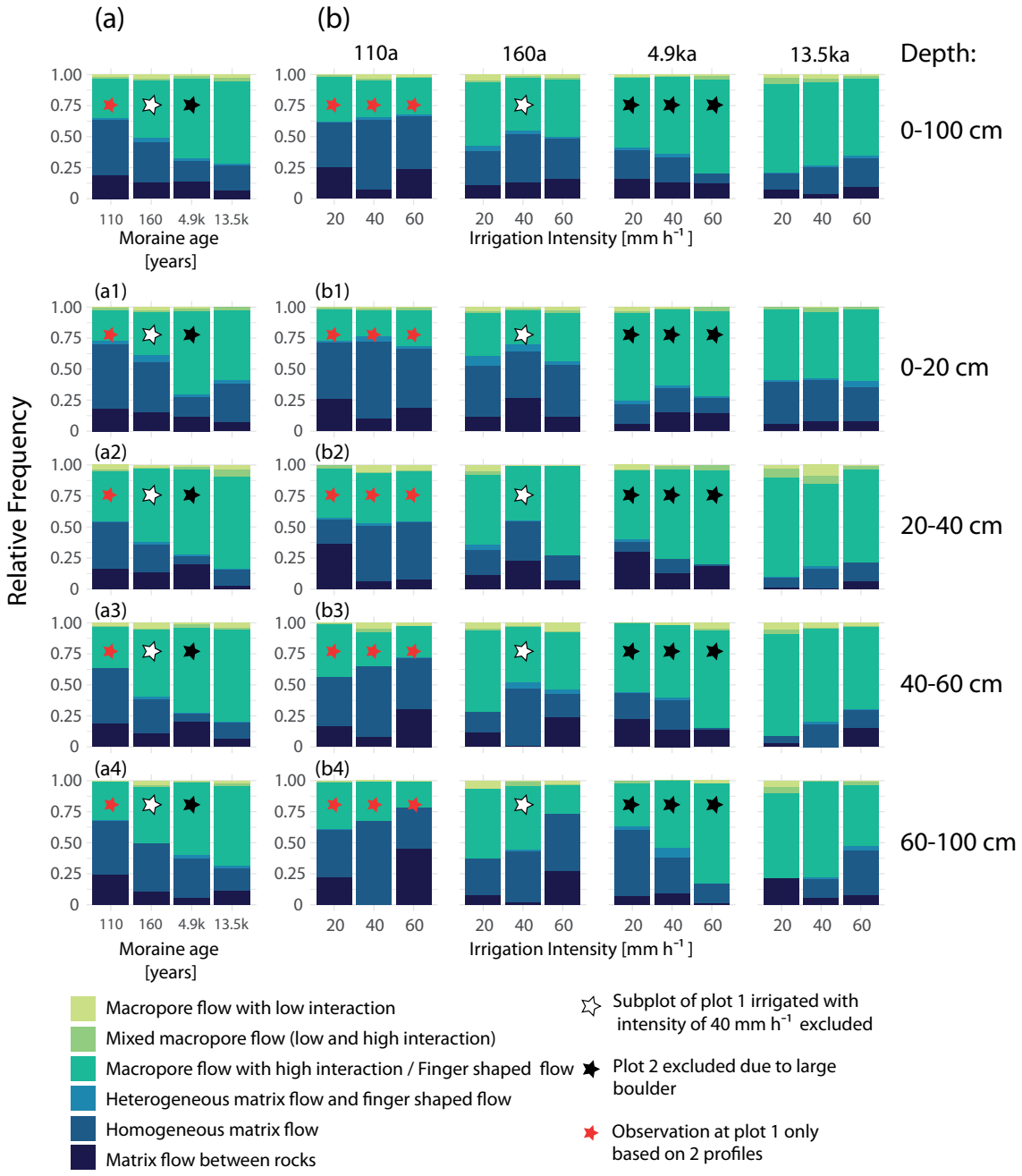

Figure 4.10: Relative frequency distribution of flow types (a) for the four moraine age classes, and (b) differentiated by irrigation intensity for each moraine age. The flow type frequency distribution is displayed once for the entire profile depth of 100 cm (a and b) and once differentiated by four depth segments (a1 to a4 and b1 to b4). Matrix flow types are displayed in a blue color scale and preferential flow types in a green color scale. A list of the relative frequencies of flow type occurrence can be found in Table 4.2 and Table 4.3 in the appendix.

4.3.3 Correlation of preferential flow frequency with site characteristics

Infiltration patterns and the formation of subsurface flow paths can be related to site characteristics. We tested the correlation between the preferential flow fraction (PFF) in the topsoil (0-20 cm) and the site characteristics listed in Table 4.1 by applying a simple linear model (Fig. 4.11). These site characteristics include age (which summarizes many physical and biotic characteristics), slope as a purely physical

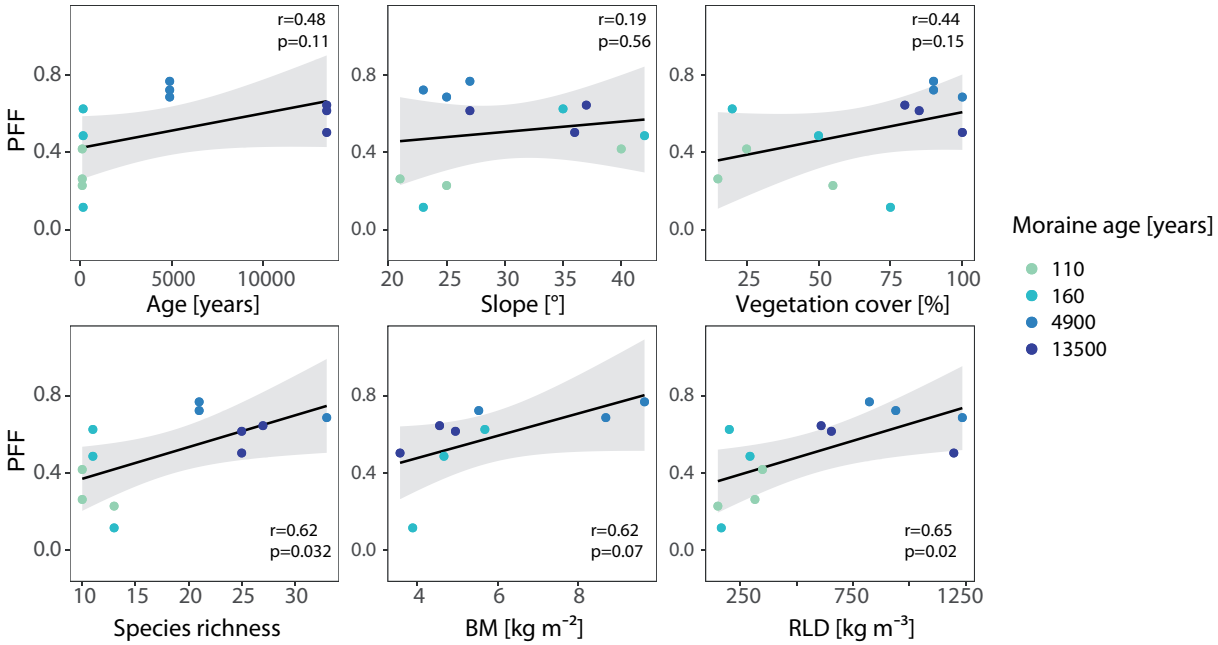

Figure 4.11: Frequency of preferential flow (PFF) in the upper 20 soil centimeters in relation to moraine age, slope, and vegetation characteristics (BM= above ground biomass, RLD= root length density).

descriptor and then several vegetation characteristics, such as vegetation cover, species richness, above ground biomass, and root length density. Although the sample size is quite small and the analysis cannot identify direct causalities and does not account for possible multi-collinearities, it nevertheless provides some insight into potential controls of preferential flow occurrence.

Between moraine age and PFF, we only observed a small and, at the 0.05-level, statistically not-significant ($p>0.05$ at $r<0.5$) correlation. A correlation between slope and preferential flow occurrence can also be ruled out ($r<0.2$). The vegetation cover shows the weakest correlation with PFF ($r<0.5$) out of the four tested vegetation parameters, whereas the species richness, BM, and RLD have a stronger correlation with PFF ($r>0.6$). The relationship ($r>0.6$) between PFF and BM is not statistically significant ($p=0.07$). However, since the p-value is affected by sample size, we have to point out that, due to missing data at the 110a moraine, the sample size for BM is reduced compared to the other vegetation properties (n=9 instead of n=12). This can negatively affect the comparability of the correlations. The relationships of PFF with species richness and RLD are both statistically significant ($p <0.05$), whereas the strongest linear relation exists between PFF and RLD ($r=0.65$).

4.4 Discussion

4.4.1 Evolution of flow paths

Across the chronosequence, we observed significant differences in the dye patterns (Fig. 4.7). Based on the flow type classification of the dye patterns we found that the frequency of matrix flow decreases with age, and the frequency of finger-shaped flow increases. The frequency of matrix flow is especially high (>0.6) in the top soil (0-20 cm) at the 110a and 160a moraines. However, at these two moraines, distinctly

more surface runoff was observed during the irrigation experiments than at the older moraines. At both young moraines, the high amounts of surface runoff (unfortunately unquantified) were mainly observed at plot 1 and 2. From purely visual observation, during irrigation, it seemed like the amount of surface runoff increased with irrigation intensity at the younger moraines. At these four plots the water infiltrated homogeneously in the top 10 cm, but there was hardly any staining in the soil below this depth (Fig. 4.4). Lateral subsurface flow, however, was not observed. In contrast, at plot 3 at both young moraines, deep infiltration and vertical homogeneous water transport were observed.

The surface of the young moraines is characterized by high-density stone deposits (Fig. 4.12), but since the stone cover was roughly similar at all three plots per age class we do not assume that the differences in surface runoff are related to the amount of stones at the surface. We observed that rocks at the surface mostly result in only very local, small-scale redistribution and preferential infiltration instead of surface runoff. We therefore link the differences in infiltration patterns and resulting staining patterns to the differences in vegetation cover. Whereas both plots labeled as plot 3 showed a high degree of vegetation coverage (> 50 %, Table 4.1), which was evenly distributed over the entire plot area (Fig. 4.12), plot 1 and 2 at both moraines had a low vegetation cover with only a few single vegetation patches between gravel and small stones. We hypothesize that structural sealing could be the cause for the reduced infiltration depths and higher amounts of surface runoff at plot 1 and 2 of the two young moraines, as surface runoff started only a few minutes after the start of the irrigation. At both moraines, the aggregate stability of the loamy to sandy soils with low organic matter content was found to be comparatively low (Greinwald et al., 2021c). Thus, high irrigation intensities are suspected to have caused the structural sealing of the soil surface, which induced overland flow on these otherwise coarse-textured soils with high saturated hydraulic conductivities (Maier et al., 2021) and a small water-holding capacity (Hartmann et al., 2020b). The disruption of the soil surface structure due to irrigation and the wash-in of released fine particles can lead to clogging of near-surface pores (Assouline, 2004), which results in a reduction in near-surface porosity and unsaturated hydraulic conductivity (Armenise et al., 2018). This phenomenon was also suggested by Maier and van Meerveld (2021a) during large-scale sprinkling experiments at the same moraines. The high vegetation cover at the other plots likely protected the soil surface from the impact of the irrigation, and a homogeneous and deep infiltration was observed (Fig. 4.4).

The pore space of coarse-textured, unsorted, sandy soil is mainly made out of large pores, which provide only a low water retention capacity and lead mostly to a fast downward transport of water (Hartmann et al., 2020b). The root system has a low density (Table 4.1, Greinwald et al. (2021a)) at the early stages of vegetation succession and does not impact the water transport. The sparse vegetation cover also does not inhibit infiltration and the water can infiltrate deep into the soil. Only larger stones and occasional clay lenses (the size of a few centimeters) or other material heterogeneities create heterogeneous matrix flow. At the two oldest moraines, the vegetation cover was dense and probably has a high interception storage capacity (albeit reduced by vegetation trimming). The fine textured soil with a higher porosity (and higher proportion of fine pores) and lower bulk density has a higher water retention capacity than the two young moraines. The soil is heterogeneous with a higher organic matter content in the upper layer and depth-gradients in porosity (decreasing) and bulk density (increasing) (Hartmann et al., 2020b). The root system is dense, with most of the root mass (> 90 %) located in the uppermost 30 cm (Greinwald et al., 2021a). At both moraines, deep infiltration, almost no surface runoff, and no subsurface lateral flow

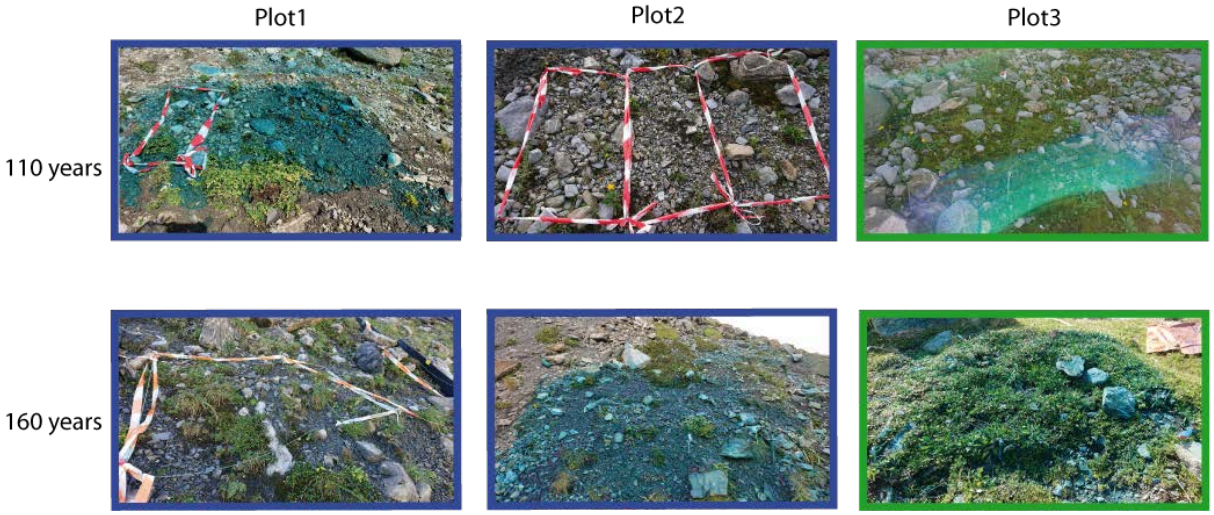

Figure 4.12: Surface of the plots at the 110- and 160-year-old moraine. Frame color indicates plots with a similar degree of vegetation coverage. Photograph of the high complexity plot at 110-year-old moraine is disrupted by lens flares due to backlighting.

were observed. The image analysis has shown that finger-shaped flow dominates (Fig. 4.10), with fingers already induced at the soil surface or within the upper 20 cm. Thus, water infiltrated heterogeneously, and/or the water transport pattern was affected by properties of the soil surface or of the upper soil layer. Heterogeneous infiltration patterns under grass cover causing finger-shaped flow with large parts of dry soil were also observed by de Jonge et al. (2009), who found water repellency to be the main cause for this flow pattern. The hydrophobicity index (HI) at each moraine was measured by Maier and van Meerveld (2021a). The mean HI at the youngest moraine is small (HI<2) and increases continuously with age (4.9ka: mean HI=5.05; 13.5ka: mean HI=9.36). The fraction of preferential flow paths in the top 20 cm, however, was highest at the 4.9ka moraine (Fig. 4.10). Inaccuracies in the comparison of HI with our results can arise from the dependency of soil hydrophobicity on soil moisture (de Jonge et al., 2009) and the fact, that HI was measured outside the experimental plots on different days than the irrigation experiments (likely different antecedent soil moisture). Water repellency is also positively correlated with the organic matter content (de Jonge et al., 2009; Mataix-Solera and Doerr, 2004) and is also higher when the organic matter is made up of complex compounds (Mainwaring et al., 2004).

Hartmann et al. (2020b) found a slightly higher organic matter content in the top 20 cm at the 4.9ka moraine compared to the 13.5ka moraine, which corresponds with the higher fraction of finger-shaped flow at the 4.9ka moraine. Hydrophobic organic compounds are also released by root activities (Doerr et al., 1998). We observed a significant correlation between the increase in preferential flow paths in the upper 20 cm and root length density and the above ground biomass. The connection of preferential flow paths and RLD is probably also attributed to the fact that roots form channels, which improve infiltration (Zhang et al., 2015). The strong correlation with above ground biomass, but less correlation with vegetation cover is more difficult to explain and likely depends on the vegetation species. The vegetation cover at the 13.5ka moraine was mainly composed of dense grass vegetation, while at the 4.9ka moraine, shrubs were also occasionally present, which, on the one hand, produces more biomass but also forms a root system

with a higher quantity of longer roots with larger diameters, which enhances infiltration locally.
Soil layering with layers of fine texture above coarse texture are known to facilitate the formation of finger-shaped flow (Morales et al., 2010). In such layered soils, homogeneous infiltration fronts become unstable and break into finger-shaped flow at the material boundaries (Starr et al., 1978; Hendrickx and Flury, 2001; Wang et al., 2018). At our sites, weathering and organic matter accumulation formed a surface layer with a finer grain size and higher water retention than the unweathered and coarser soil below, which is clearly pronounced at the 4.9ka and 13.5ka moraines (Hartmann et al., 2020b). Material heterogeneities such as gravel and sand patches, were also observed and likely facilitated the formation of finger-shaped flow paths.
Despite the almost 10 000 year age difference between the 13.5ka and the 4.9ka moraine, the 4.9ka moraine shows a higher proportion of preferential flow paths in the upper 20 cm, which is also associated with a higher proportion of BM, RLD, and vegetation cover. In addition, the clay content, organic matter, and porosity are also higher at the 4.9ka moraine (Hartmann et al., 2020b). This discontinuous trend raises concerns that the two moraines do not fall within the chronosequence approach assumptions that time is the only variable during landscape development. Thus it cannot be excluded that, for example, different initial site conditions, climate boundary conditions, or/and geomorphological disturbances could have led to different rates of change (Wojcik et al., 2021) in the topsoil.
Compared to the results described by Hartmann et al. (2020a) for soils developed from siliceous glacial till under similar climatic conditions, we found distinct differences in the flow path evolution at this calcareous forefield. While the flow path development was nearly identical in the first 5000 years in both geologies, it differs distinctly after 10 thousand years of landscape development. In both geologies, the flow paths developed from a more or less homogeneous to heterogeneous matrix flow at 160 years to finger-shaped flow after 5000 years. After more than 10 000 years of landscape development, subsurface hydrology at the calcareous geology is ruled by finger-shaped flow and deep infiltration, whereas at the siliceous geology, storage capacity in the top soil strongly increased, with a corresponding reduction in infiltration depths and a shift to macropore flow.

4.4.2 Impact of irrigation intensity

Studying the impact of irrigation intensities on subsurface flow paths is often hampered by the influence of different initial and boundary conditions (e.g., Wu et al., 2015; Cichota et al., 2016). Our study was specifically designed to minimize these effects by dividing the irrigation plots into three adjacent subplots. This allows for the assumption that the initial and boundary conditions (excluding the controlled irrigation intensity) of the subplots per plot were almost identical. From the end of July to the beginning of September 2019 we measured a precipitation amount of 360 mm at the glacier forefield. Matric potentials, measured by tensiometers in 10, 30, and 50 cm at the 160a, 4.9ka, and 13.5ka moraines, never dropped below field capacity. Thus, the initial soil moisture was consistently high across the irrigation experiments at all age classes.
The observed changes in dye patterns and flow paths with increasing irrigation intensity at the four age classes are schematically summarized in Figure 4.13. At the young moraines, we observed an increase in the frequency of matrix flow at greater depths with increasing irrigation intensity, which is evidenced by

an increase in the SPW>200 mm with a simultaneous decrease in the median dye coverage and a decrease in the number of flow paths (SAD) (Fig. 4.5e). The decrease in median dye coverage with increasing intensity is particularly pronounced at the four bare plots of these young moraines (data not shown). No clear trend can be seen at the two plots with a higher vegetation cover. However, the decrease in SAD and the increase in stained path widths indicates that water flow paths that reach greater depths tend to widen and to merge with increasing irrigation intensity. This process might be facilitated by higher water contents at greater depths or by a change in material properties.

At the 4.9ka moraine, however, we observed an increase in dye coverage (Fig. 4.5a) and an increase in the number of flow paths (Fig. 4.5e). The proportion of 20<SPW<200 mm increases (Fig. 4.5c) and the proportion of SPW>200 mm decreases (Fig. 4.5d), which then leads to an increase in the frequency of finger-shaped flow paths in the flow type classification (Fig. 4.10b2 to b4). At the 13.5ka moraine, we observed an increase in dye coverage (Fig. 4.5a), an increase in infiltration depth (Fig. 4.3), a broadening of the flow paths (Fig. 4.5c-d), and an increase in the number of flow paths (Fig. 4.5e and Fig. 4.6) with increasing irrigation intensity. Different from the 4.9ka moraine, the increase in the proportion of SPW>200 mm on the dye coverage leads to a transition to more matrix flow (Fig. 4.10) in the flow type classification.

The impact of irrigation intensity on water flow paths is slightly obscured by the process of flow type classification, as it is only based on the occurrence of the three SPW classes as fractions of the dye coverage (Weiler, 2001). The number of flow paths or the dye coverage itself are not taken into account. We observed at both age classes that, with increasing irrigation intensity, more fingers are generated, and more soil space is used for water transport (Fig. 4.5).

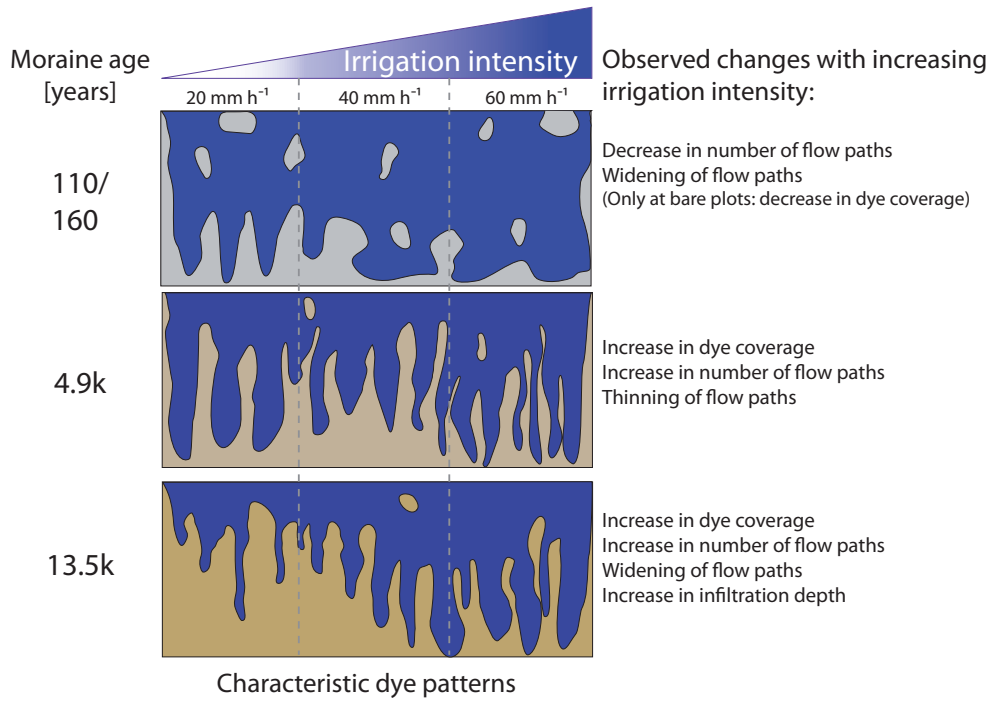

Figure 4.13: Characteristic dye patterns and observed changes with increasing irrigation intensity at the four age classes.

The formation of finger-shaped flow paths and their properties – such as number, flow velocity, or width – are also in a complex interplay with the surrounding soil moisture, flux, and soil properties (Nimmo, 2021). Studies focusing on the formation of finger-shaped flow paths found the finger width to be influenced not only by soil properties, and initial and boundary conditions (Glass et al., 1989), but also by the flow rate through the finger (Parlange and Hill, 1976; White et al., 1976), with higher flow rates leading to an increase in finger width. This was also observed by Ma et al. (2008), who also found a positive correlation between rainfall intensity, time of finger flow occurrence, and mean velocity. The increase in mean velocity of the fingers leads to a faster downward transport and thus deeper infiltration depths with higher irrigation intensities (Cremer et al., 2017). An increase in the number of fingers with higher fluxes was also observed (Sililo and Tellam, 2000). These findings by other studies are similar to our observations at the 13.5ka moraine. It is unclear what causes the different observations in the dominant flow path widths at the 4.9ka and 13.5ka moraines. We can only speculate whether the higher organic matter content, the higher root density, or soil properties such as the lower hydraulic conductivities and higher porosity play a role in producing narrower flow paths with increasing irrigation intensity at the 4.9ka moraine.

4.4.3 Uncertainties

Apart from the reduced sample size at plot 1 at the 110a moraine and the uncertainties due to large boulders at the 160a and 4.9ka moraines, some further uncertainties need to be mentioned. In general, the dark gray soil color at the 110a and 160a moraines made the color detection of the tracer difficult. In addition, at plot 3 of the 110a moraine, a setup of suitable lighting conditions was difficult due to stormy weather conditions. As a result, the lighting of the photographs was very unfavorable for the image analysis. Even during the profile excavation in the field, it was not possible to determine with great certainty whether the dark-colored, wet soil was stained or not. Thus, blue stains on larger stones along the profile depth were considered as an indicator for the validity of the observed dye tracer pattern, which shows an almost complete coloring of the soil (Fig. 4.4).
We further assume that the irrigation with the hand-operated sprayer, which had to be held close to the soil surface due to strong winds, sometimes led to a high force of application and promoted structural sealing at the bare plots of the 110a and 160a moraines. At both moraines, deep infiltration was often found at the boundaries of the bare plots. Since the plot boundaries were not irrigated, they were also not affected by structural sealing. Water running off to the sides infiltrated deep into the soil. This observation suggests that a more homogeneous and deep transport of the water can take place in this quite homogeneous and unsorted material (Hartmann et al., 2020b) if the surface is not influenced by particle displacement. Thus, it is assumed that the proportion of preferential flow paths at the young moraines is generally overestimated, and homogeneous to heterogeneous matrix flow with deep infiltration are probably the dominant flow types under natural rainfall conditions. As the plot boundaries (outer boundaries and boundaries of neighboring subplots) are excluded from the image analysis to avoid edge effects, the deep percolation observed here could not be accounted for in our quantitative analysis.

4.5 Conclusions

Based on Brilliant Blue dye experiments in a glacial chronosequence on calcareous parent material, we found that subsurface flow paths change with age: from homogeneous gravity-driven matrix flow in sandy, coarse-grained, loose soils with low root density at the young moraines to a heterogeneous matrix flow and finger-shaped flow paths in silty, layered soils with dense vegetation cover and high root density at the old moraines. The occurrence of preferential flow paths increases with soil age, but as it appears mainly in the form of finger-shaped flow paths, it is mainly controlled by soil surface characteristics (organic matter content, soil texture, soil layering) and vegetation characteristics (RLD, hydrophobicity, BM). We also found an increase in the number of preferential flow paths with increasing irrigation intensity at the two old moraines, which leads to an increase in soil space used for water transport and thus efficient infiltration preventing surface runoff, even at high intensities. When infiltration was not impaired by structural sealing, water percolated deep into the soil (> 1 m) at all four age classes. The observed finger-shaped flow paths and deep drainage, even after more than 10 000 years of landscape development, contrasts with the observed high storage capacity, reduced infiltration, and occasional macropore flow in a moraine on siliceous parent material of the same age (Hartmann et al., 2020a). The observed differences in flow path evolution in these two different geologies under nearly identical climate conditions emphasizes the important role of the parent material in landscape evolution.

Our findings deliver important insights on how landscape evolution affects hydrological processes in transient alpine landscapes, where glacial retreat is accelerating and thus more and more hillslopes are freed of ice and weathering, erosion, and plant succession are initiated. Our study made it clear that, due to the complexity of landscape development, time should not be regarded as the only primary evolutionary factor. The geology and the resulting landscape properties (e.g., soil structure and texture, vegetation, organic matter content) have a primary impact on the development of subsurface hydrological flow paths. The type of hydrological flow paths significantly influences the redistribution of solid and solutes and thus also affects landscape development. The feedback between soil hydraulic process and soil structure is an important aspect that needs to be included in SLEMs. Therefore, it is necessary to intensify studies on the main influencing factors (e.g., soil properties, vegetation characteristics) on preferential flow path formation. The data and observations provided here can thus help to improve the handling of hydrologic processes and their role within the feedback cycle of the hydro-pedo-geomorphological system when it comes to soil and landscape evolution modeling.

Appendix

Figure 4.14: Hidden boulders at the 160a (left) and 4.9ka (right) moraine. The boulder occupied most of the cross section of the subplot irrigated with 40 mm h^{-1} at plot 1 of the 160a and most of the cross section of plot 2 at the 4.9ka moraine. Due to this strong disturbance, the corresponding plot and subplot were neglected in the further analyses. The length of one black or white scale segment of the wooden frame equals 10 cm.

Table 4.2: Relative frequencies of flow type occurrence for the profile depth of 100 cm. Left: listed for each age class. Right: differentiated by irrigation intensity for each age class.

Depth: 0-100 cm																	
					110a			160a			4900a			13 500a			
					Differentiated by irrigation intensity [mm h^{-1}]												
Flow Type	110 a	160a	4900a	13 500a	20	40	60	20	40	60	20	40	60	20	40	60	
Macropore flow with low interaction	0.02	0.03	0.02	0.00	0.01	0.01	0.01	0.03	0.01	0.03	0.02	0.01	0.02	0.03	0.03	0.01	
Mixed macropore flow	0.01	0.01	0.01	0.03	0.02	0.01	0.02	0.02	0.01	0.02	0.01	0.01	0.02	0.04	0.03	0.02	
Macropore flow/Finger-shaped flow paths	0.32	0.47	0.65	0.56	0.29	0.21	0.29	0.34	0.28	0.39	0.56	0.62	0.75	0.71	0.67	0.62	
Heterogeneous matrix flow and finger-shaped flow paths	0.01	0.03	0.02	0.03	0.02	0.04	0.02	0.08	0.06	0.03	0.02	0.03	0.00	0.01	0.02	0.03	
Homogeneous matrix flow	0.45	0.33	0.17	0.32	0.48	0.62	0.48	0.41	0.37	0.41	0.23	0.20	0.08	0.13	0.21	0.23	
Matrix flow between rocks	0.19	0.13	0.13	0.07	0.19	0.10	0.19	0.11	0.27	0.12	0.15	0.13	0.12	0.07	0.03	0.09	

Table 4.3: Relative frequencies of flow type occurrence in the depth segments of 0-20, 20-40, 40-60, and 60-100 cm. Left: listed for each age class. Right: differentiated by irrigation intensity for each age class.

Depth: 0-20 cm

					110a			160a			4900a			13 500a		
					Differentiated by irrigation intensity [mm h^{-1}]											
Flow Type	110 a	160a	4900a	13 500a	20	40	60	20	40	60	20	40	60	20	40	60
Macropore flow with low interaction	0.01	0.03	0.02	0.00	0.01	0.01	0.01	0.03	0.01	0.03	0.04	0.01	0.00	0.00	0.00	0.00
Mixed macropore flow	0.02	0.02	0.02	0.03	0.02	0.01	0.02	0.02	0.01	0.02	0.01	0.01	0.04	0.02	0.04	0.02
Macropore flow/Finger-shaped flow paths	0.25	0.35	0.67	0.56	0.25	0.21	0.29	0.34	0.28	0.39	0.71	0.61	0.69	0.57	0.54	0.58
Heterogeneous matrix flow and finger-shaped flow paths	0.03	0.06	0.02	0.03	0.02	0.04	0.02	0.08	0.06	0.03	0.03	0.02	0.01	0.02	0.01	0.05
Homogeneous matrix flow	0.52	0.40	0.16	0.32	0.45	0.62	0.48	0.41	0.37	0.41	0.16	0.19	0.13	0.34	0.33	0.27
Matrix flow between rocks	0.18	0.15	0.12	0.07	0.26	0.10	0.19	0.11	0.27	0.12	0.06	0.15	0.14	0.05	0.08	0.08

					110a			160a			4900a			13 500a		
					Differentiated by irrigation intensity [mm h^{-1}]											
Flow Type	110 a	160a	4900a	13 500a	20	40	60	20	40	60	20	40	60	20	40	60
Macropore flow with low interaction	0.04	0.03	0.02	0.04	0.01	0.06	0.05	0.05	0.01	0.01	0.04	0.01	0.00	0.03	0.09	0.01
Mixed macropore flow	0.02	0.01	0.02	0.06	0.03	0.01	0.01	0.02	0.00	0.00	0.00	0.03	0.04	0.07	0.07	0.03
Macropore flow/Finger-shaped flow paths	0.40	0.58	0.68	0.74	0.40	0.41	0.40	0.57	0.44	0.72	0.55	0.72	0.76	0.80	0.66	0.75
Heterogeneous matrix flow and finger-shaped flow paths	0.01	0.02	0.01	0.01	0.01	0.02	0.01	0.05	0.01	0.00	0.03	0.00	0.00	0.00	0.02	0.00
Homogeneous matrix flow	0.37	0.23	0.07	0.13	0.20	0.45	0.47	0.20	0.31	0.20	0.08	0.11	0.02	0.08	0.16	0.15
Matrix flow between rocks	0.16	0.13	0.20	0.02	0.36	0.06	0.07	0.11	0.23	0.07	0.30	0.13	0.18	0.01	0.00	0.06

					110a			160a			4900a			13 500a		
					Differentiated by irrigation intensity [mm h^{-1}]											
Flow Type	110 a	160a	4900a	13 500a	20	40	60	20	40	60	20	40	60	20	40	60
Macropore flow with low interaction	0.02	0.05	0.05	0.04	0.00	0.05	0.03	0.05	0.03	0.07	0.00	0.02	0.05	0.06	0.04	0.03
Mixed macropore flow	0.01	0.01	0.05	0.01	0.01	0.03	0.00	0.02	0.01	0.01	0.00	0.00	0.01	0.03	0.00	0.00
Macropore flow/Finger-shaped flow paths	0.33	0.54	0.55	0.74	0.43	0.28	0.26	0.65	0.44	0.46	0.55	0.58	0.78	0.82	0.75	0.66
Heterogeneous matrix flow and finger-shaped flow paths	0.00	0.03	0.00	0.01	0.00	0.00	0.00	0.00	0.05	0.04	0.01	0.02	0.00	0.00	0.02	0.01
Homogeneous matrix flow	0.45	0.27	0.14	0.13	0.40	0.57	0.41	0.17	0.46	0.18	0.21	0.24	0.02	0.06	0.18	0.15
Matrix flow between rocks	0.18	0.11	0.23	0.06	0.16	0.08	0.30	0.11	0.00	0.24	0.22	0.14	0.13	0.03	0.00	0.15

					110a			160a			4900a			13 500a		
					Differentiated by irrigation intensity [mm h^{-1}]											
Flow Type	110 a	160a	4900a	13 500a	20	40	60	20	40	60	20	40	60	20	40	60
Macropore flow with low interaction	0.01	0.04	0.01	0.02	0.01	0.01	0.01	0.07	0.01	0.03	0.00	0.00	0.02	0.05	0.00	0.01
Mixed macropore flow	0.00	0.01	0.01	0.03	0.01	0.00	0.00	0.00	0.04	0.00	0.02	0.00	0.00	0.05	0.00	0.03
Macropore flow/Finger-shaped flow paths	0.31	0.45	0.58	0.64	0.38	0.32	0.22	0.56	0.51	0.24	0.35	0.54	0.81	0.68	0.78	0.49
Heterogeneous matrix flow and finger-shaped flow paths	0.00	0.01	0.03	0.02	0.00	0.00	0.00	0.00	0.02	0.00	0.03	0.08	0.00	0.00	0.01	0.04
Homogeneous matrix flow	0.43	0.38	0.31	0.18	0.38	0.67	0.33	0.29	0.41	0.46	0.53	0.29	0.16	0.00	0.15	0.36
Matrix flow between rocks	0.24	0.11	0.05	0.11	0.22	0.00	0.45	0.08	0.02	0.27	0.07	0.09	0.01	0.22	0.05	0.08

5 The relationship between structure evolution and the hydrological response

This chapter was submitted as:

The evolution of hillslope hydrology: links between form, function and the underlying control of geology

Anne Hartmann and Theresa Blume

This article is submitted to Water Resource Research (in review), 2023.

Abstract

Form and function are two main characteristics describing hydrological systems. While form summarizes the structure of the system, function represents the hydrological response. Little is known about how these characteristics evolve and how form relates to function in young hydrological systems. We investigated how form and function evolve during the first millennia of landscape evolution. We analyzed two hillslope chronosequences in glacial forelands, one developed from siliceous and one developed from calcareous parent material. Variables describing hillslope form included soil physical properties and vegetation characteristics. Variables describing hydrological function included soil water reaction times, soil water storage, drainage, and dominant subsurface flow types. We identified links between form and hydrological function via cluster analysis. Clusters identified based on form were compared in terms of their hydrological functioning. The comparison of the two different parent materials shows how strongly landscape evolution is controlled by the underlying geology. Soil pH appears to be a key variable influencing vegetation, soil formation and subsequently hydrology. At the calcareous site, the high buffering capacity of the soil leads to less soil formation and fast, vertical subsurface water transport dominates the water redistribution even after more than 10 000 years of landscape evolution. At the siliceous site, soil acidification results in accumulation of organic material, a high water storage capacity, and in podsolization. Under these conditions water redistribution changes from vertical subsurface water transport at the young age classes to water storage in the organic surface layer and lateral subsurface water transport after 10 000 years.

5.1 Introduction

Hillslopes as the largest functional parts of catchments have a major impact on the overall hydrological catchment response. More than 95% of the stream water has been transported through or over a hillside in form of subsurface or overland flow (Kirkby, 1988). Based on its function to store and to release water, soil plays a key role in the hillslope hydrological response and provides important ecosystem services (Clothier et al., 2008). For example, soil can store large amounts of water, which reduces flood risks and is valuable for agricultural purposes. Its ability to feed streams during dry seasons by slowly releasing water (Nippgen et al., 2016) is vital to both ecosystems and humans.

The hydrologic response of hillslopes is largely dependent on the soil water response to rainfall events. It is well known that the soil water response in form of soil water dynamics and subsurface flow paths is influenced by soil and surface characteristics of the hillslopes (Lohse and Dietrich, 2005; Blume et al., 2009; Wlostowski et al., 2021). Since the hillslope structure varies spatially (Nahar et al., 2004), the spatial variability of the hydrological response is also high. Hydrologic processes at the hillslope scale not only underlie spatial variations, but also develop and change over the years due to landscape evolution (i.e. weathering, soil development, vegetation succession) and the associated changes in the hillslope/soil structure. While the spatial variability in hydrological response already has been the focus of many studies (Maeda et al., 2006; Brocca et al., 2007; Singh et al., 2021), the temporal variability has been less studied, with the main focus often being on the seasonal variation (Wilson et al., 2004; Kim, 2009) or land use change effects (Sajikumar and Remya, 2015; Wojkowski et al., 2022; Truong et al., 2022).

To understand how the hydrological response coevolves with hillslope structure is crucial for the evaluation of how hydrological systems will adapt to changes in climate (Montagne and Cornu, 2010) or anthropogenic disturbances (Cui et al., 2021). Landscape evolution models are useful tools to investigate how landscapes will evolve in response to changes in driving forces, but due to missing field observations, these models still lack the consideration of important subsurface water transport processes (e.g., preferential flow, lateral flow) and the knowledge of how these processes coevolve with soil and vegetation characteristics (van der Meij et al., 2018). A few studies examined the hydrological response of soils of different ages in volcanic landscapes and linked the changes to significant changes in soil structure. Lohse and Dietrich (2005) for example, found differences in the catchment response of a 300-year-old Andisol and a 4.1 million year-old Oxisol. While the younger soil was coarse textured and drained freely via mainly vertical water transport, the old soil showed a decrease in permeability and mainly lateral flow due to the accumulation of secondary clay minerals. Comparing Holocene and Late Pleistocene lava landscapes, Jefferson et al. (2010) observed a reduction in base flow and an increase in lateral shallow underground flow and surface runoff. The same trend of lower base flow, more shallow subsurface flow, and more flashy runoff with catchment age was noted by Yoshida and Troch (2016), who compared 14 volcanic catchments ranging in age from 0.225 to 82.2 million years. They also relate the changes to the formation of impermeable layers as a result of progressive chemical weathering.

Comparable studies in other geologies are hard to find. Geology as a catchment (or landscape) forming factor (Troch et al., 2015) has a big impact on the coevolution of landscapes. Observations made in a specific geology cannot be simply transferred to other geologies. The physical and chemical properties of the parent material directly or indirectly affect the hydrological response. For a example, the bedrock

permeability directly impacts the hydrologic storage and release of catchments, as it was shown that a higher bedrock permeability leads to higher storage and base flow, but dampened peak flow (Pfister et al., 2017). The weatherability and chemical composition of the geology (parent material) indirectly affect the hydrologic response as they are primary controls for soil development (Jenny, 1941) and define the physical properties (e.g., texture, bulk density, porosity, water holding capacity) and consequently the hydrologic properties and processes (Lin, 2003) of the regolith and soil. However, in the evolution process, the soils also interact with other factors such as vegetation and water. The interplay between soil and water regulates the vegetation density and composition by providing nutrients in concentrations that can either limit or enhance plant growth (Hahm et al., 2014). Vegetation in turn also affects soil development and thus the hydrological response (Bonetti et al., 2021). For example, the development of organic layers can immensely increase water storage (Ramírez et al., 2017) and facilitate lateral subsurface flow (Yang et al., 2012). These complex feedback cycles make it hard to identify the specific links between structure and response, especially when several response-changing processes overlap.

In mountain regions, where the accelerated retreat of the glaciers exposes more and more young landscapes, structural changes during a time span of a few centuries to thousand years can be striking. However, little is known about the effects on the hydrological response. Especially the latter is of fundamental importance for decision makers and the future landscape management in these young landscapes. While the evolution of the hillslope form (in terms of soil structure/properties and vegetation characteristics) in proglacial moraines has been studied previously (Douglass and Bockheim, 2006; Egli et al., 2012; Vilmundardóttir et al., 2014), D'Amico et al. (2014)), the evolution of hillslope hydrological function related to the evolution of hillslope form during the first ten millennia of landscape evolution has so far not been investigated.

Our study aims at identifying how structure and the soil hydrological response coevolve in young proglacial hillslopes. In a second step, we attempt to identify which structural features are linked to the hydrological response. Identifiable links between the hydrological response and structural features would be useful also for the initial assessment of landscapes with little monitoring data, allowing to draw first conclusions about the hydrological response based on easily measured/observed landscape properties. The transfer of knowledge and process similarity is an essential step for the hydrological assessment of ungauged landscapes (Blöschl, 2016). Due to the importance of geology as a driving factor for catchment formation (Troch et al., 2015) we investigate and compare the evolution of hillslope structure and hillslope hydrological response in two contrasting geologies. More specifically, we investigated the questions: (i) Evolution of form: How does the evolution of soil structural features and vegetation characteristic differ between siliceous and calcareous parent material?, (ii) Evolution of function: How does the evolution of the hydrological response differ between the two parent materials?, and (iii) Which general links between structure and function can be identified (regardless of age and parent material)? We address these questions by studying two chronosequences of proglacial moraines. Each chronosequence consists of four moraines, which range in age from 30 to 13 500 years. One chronosequence developed from siliceous, the other from calcareous glacial till. For each chronosequence we measured soil physical properties (texture and structure) and included surface characteristics measured at the same sites by our collaborators (e.g., vegetation features (Greinwald et al., 2021a), hydrophobicity, micro topography (Maier et al., 2021; Maier and van Meerveld, 2021a)) to evaluate the evolution of hillslope structure.

We investigate the soil hydrologic response in form of soil water dynamics and subsurface flow paths by evaluating soil moisture signatures, soil water isotope profiles, and the occurrence of preferential flow from tracer irrigation experiments. We evaluate links between form and function by comparing the hydrologic responses (soil moisture signatures and preferential flow occurrence) of clusters derived from information on soil properties and surface/vegetation characteristics. With our study we expand the knowledge and data base on how hydrologic processes depend on landscape structure and coevolve within the feedback cycle of the hydro-pedogeomorphological system. Figure 5.1 provides a graphical overview of the approaches used to address the three research questions.

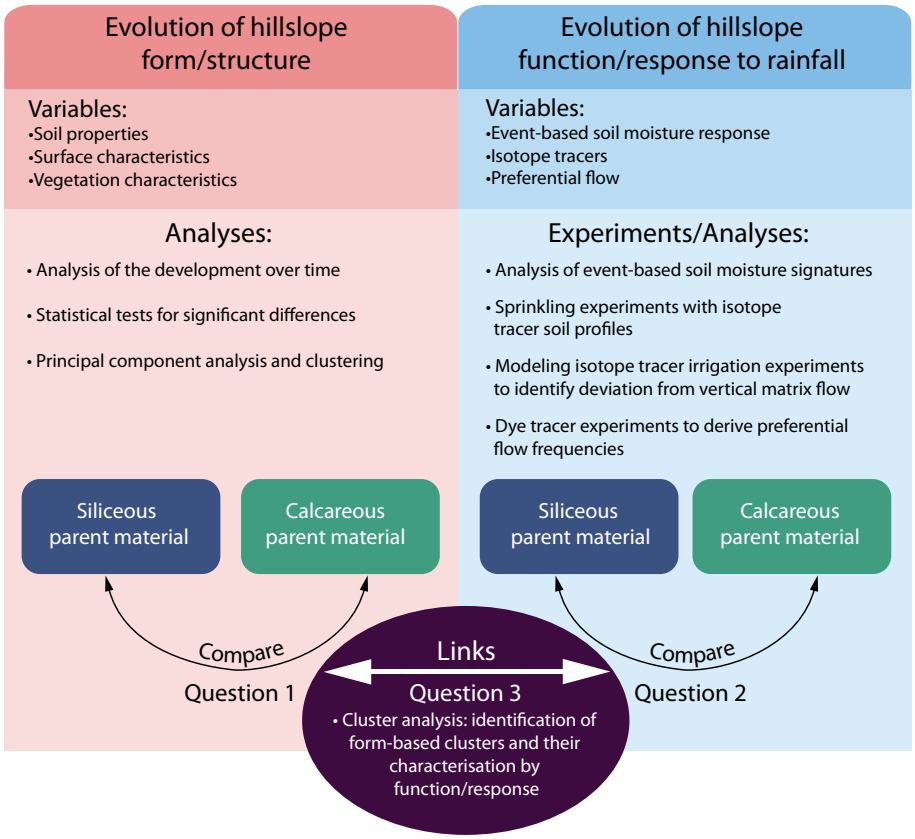

Figure 5.1: Overview of the approaches used for the three research questions of this study.

5.2 Material and methods

5.2.1 Study areas

We studied two chronosequences in two different glacier forefields in the Central Swiss Alps. Each chronosequence study was based on four moraines of different ages and included extensive sampling, surveying and irrigation experiments (Fig. 5.2). The first chronosequence is located in the glacier forefield of the Stein Glacier, south of the Sustenpass in the Urner Alps (47° 43'N, 8° 25'E) at an elevation of 1980 m.a.s.l. At this study area, the soils developed on siliceous glacial till. The second chronosequence is located in the glacier forefield of the Griessfirn, near the Klausenpass in the canton of Uri (appr. 46° 85'N,

8° 82'E). The study area is located at an elevation between 2030-2200 m a.s.l. Here, the soils developed on calcareous glacial till. The siliceous parent material (S-PM) consists mainly of metamorphosed pre-Mesozoic metagranitoids, gneisses, and amphibolites (Heikkinen and Fogelberg, 1980; Schimmelpfennig et al., 2014). The calcareous parent material (C-PM) is mainly limestone (Frey, 1965) deposited during the early Jurassic to Tertiary era (Musso et al., 2019). A detailed description of the parent material composition is provided by Musso et al. (2019) and Musso et al. (2020).

Figure 5.2: Glacier forefield and location of the four selected moraines of the silicate parent material (S-PM, left (© Google Maps, 2020a)) and the calcareous parent material (C-PM, right (© Google Maps, 2020b)). Figure adapted from Hartmann et al. (2020b).

The closest official weather station to the S-PM forefield (18 km) is Grimsel Hospiz (46° 34'N, 8° 19'E) at an elevation of 1980 m a.s.l. The recorded mean annual temperature is 1.9 °C and the mean annual precipitation is 1856 mm (1981-2010) (MeteoSwiss, 2020a). The closest official weather station to the C-PM forefield (48 km) is Pilatus Mountain (46° 98'N, 8° 25'E) at an elevation of 2106 m a.s.l. The recorded annual mean temperature is 1.8 °C and the annual precipitation is 1752 mm (1981-2010) (MeteoSwiss, 2020b).

At each glacier forefield, a moraine chronosequence of four different age classes was identified. Details on the dating of the moraine ages are provided by Musso et al. (2019). The four age classes at S-PM are 30 (30a; a=years), 160 (160a), 3000 (3ka; k=1000), and 10 000 (10ka) years and at C-PM 110 (110a), 160 (160a), 4 900 (4.9ka), and 13 500 (13.5ka) years. The choice of the 110 year old moraine at C-PM as the youngest moraine is the result of the local conditions, as no adequate moraine with an age of around 30 years could be identified that also ensured comparability in terms of elevation and micro climate. Choosing the 110 year moraine as our youngest moraine at C-PM was therefore the best compromise.

The soils were classified according to the World Reference Base for Soil Resources (IUSS Working Group WRB, 2014) (Musso et al. (2019), Musso et al. (2020), and Maier et al. (2020)). The soils at S-PM were classified as a Hyperskeletic Leptosol (30a,160a), a Skeletic Cambisol (3ka), and Dystric

Cambisol/Skeletic Cambisol/Entic Podzol (10ka). The soils at C-PM were classified as a Hperskeletic Leptosol (110a, 160a) and as a Calcaric Skeletic Cambisol (4.9ka, 13.5ka, Fig. 5.17).

The vegetation cover at both forefields differs among the four age classes. At S-PM, the vegetation cover at 30a consists mainly of sparsely distributed grass, moss, forbs, and a few shrubs. The 160a and 3ka moraines are occasionally grazed by cows and sheep, which was prevented for the duration of the experiments by fencing in the study areas. The dominant vegetation types at the 160a moraine are grasses, lichen, forbs, and shrubs. The 3ka is mainly covered by grasses with fern, mosses, sedges and forbs. The oldest moraine is dominantly covered by a variety of prostrate shrubs, small trees and several grasses. At the C-PM, the vegetation cover at 110a and 160a is sparsely distributed with patches of grass and forbs at the 160a and patches of mostly mosses and lichens at the 110a. The two oldest moraines (13.5ka and 4.9ka) are both densely covered with grass, dwarf shrubs and sedge. Until a few years ago both moraines were occasionally used for grazing. More information on the vegetation cover composition and an analysis of their functional community structure at both forefields is provided by Greinwald et al. (2021b).

Further information on vegetation and (soil) surface properties such as above ground biomass (BM), root length density (RLD), root density (RD), specific root length (SRL), surface coverage (SC) were determined by Greinwald et al. (2021a) and saturated hydraulic conductivity (KS), surface hydrophobicity (HP), and microtopography (MT) were determined by Maier et al. (2020), Maier et al. (2021), and Maier and van Meerveld (2021a). All of this information was recorded for each of three areas of the moraines (identified as plots 1-3) that comprise the experimental plots used for the tracer experiments described in section 5.2.2. Musso et al. (2019) measured soil-pH across the moraines in both forefields. The locations of the pH measurements differ slightly from the sampling locations of the other variables. The information is summarized in Table 5.1.

Table 5.1: Vegetation and (soil) surface characteristics of the four moraines at the siliceous and calcareous parent material.

	Moraine age [years]	Plot #	SC	RLD[a]	RD[a]	SRL[a]	BM[a]	Ksat (0-20cm)[b]	Ksat (20-40cm)[b]	HP[b]	MT[b]	pH range (mean)[c,d]
Siliceous parent material												
	30a	1	20	152.1	0.84	198.4	0.93	2510.5	74.2	1.6	0.52	6.1-6.7 (6.5)
		2	60	523.2	3.3	176.31	3.28	3831.5	83	1.25	0.36	
		3	50	250.9	1.5	152.1	5.1	2505.3	176.4	0.82	0.55	
	160a	1	100	1180.8	4.9	237.9	6.6	1925.7	296.5	2.55	0.29	4.7-5.5 (4.9)
		2	80	832.9	4.7	177.8	29.5	2219.0	99.3	1.4	0.36	
		3	60	798.7	5.1	188.6	3.2	1240.4	301.3	1.9	0.29	
	3ka	1	70	918.4	9.5	102.2	10.1	582	128.6	3.3	0.33	4.6-6.1 (5.2)
		2	80	825.6	6.3	131.3	11.4	744.9	120.8	2.04	0.58	
		3	90	861.7	10.0	88.4	8.1	1063.5	53.0	3.1	0.65	
	10ka	1	90	304.7	4.4	66.3	50.9	787.1	7.0	2.5	1.14	3.4-4.4 (4.0)
		2	80	463.6	3.7	122.1	23.9	219.8	16.7	9.1	0.64	
		3	100	424.2	4.2	98.8	18.9	263.3	29.3	4.2	1.08	
Calcareous parent material												
	110a	1	55	150.6	0.83	129.8	n.a.	n.a.	n.a.	n.a.	n.a.	7.6-7.8 (7.7)
		2	25	348.6	4.56	78.4	n.a.	n.a.	n.a.	n.a.	n.a.	
		3	15	315.13	1.36	222.4	n.a.	n.a.	n.a.	n.a.	n.a.	
	160a	1	20	201.4	1.27	172.3	5.7	4695.3	192.8	1.04	0.34	7.3-7.8 (7.6)
		2	50	293.18	2.75	104.3	4.7	472.9	72.7	2.46	0.36	
		3	75	165.9	2.97	58.1	3.9	1877.2	272.1	1.8	0.27	
	4.9ka	1	90	822.9	5.8	142.8	9.6	3206.0	38.8	5.5	0.63	4.5-7.8 (6.9)
		2	90	939.8	10.2	93.0	5.5	1670.9	31.6	2.96	0.29	
		3	100	1235.16	7.8	161.4	8.7	1124.5	40.9	6.73	0.26	
	13.5ka	1	85	654.2	9.5	68.34	4.9	799.4	23.9	7.72	0.3	5.9-7.8 (7.3)
		2	80	608.7	6.0	111.8	4.6	813.9	29.9	5.9	0.25	
		3	100	1197.3	10.4	121.3	3.6	890.1	6.8	14.5	0.28	

[a] This information was compiled from Greinwald et al. (2021a)
RLD=root length density [km m^{-3}], RD=root density [kg m^{-3}], SRL=specific root length [m g^{-1}], BM=above ground biomass [kg m^{-2}]
[b] This information was compiled from Maier and van Meerveld (2021b)
Ksat= saturated hydraulic conductivity [cm d^{-1}], HP=hdrophobicity [-], MT=microtopography [-]
[c] This information was compiled from Musso et al. (2022)
pH= pH-value [-] (range and mean)
[d] The locations of the pH measurements differ from the sampling locations of the other variables.

5.2.2 Tracer experiments

Two types of tracer experiments were conducted on each moraine to gain information on the hillslope responses. Dye tracer experiments were used to visualize vertical subsurface flow paths and to derive vertical subsurface flow types. Irrigation experiments on plots equipped with soil moisture sensors were used to draw conclusions about characteristic hillslope functions based on soil moisture signatures. The irrigated water was labeled with deuterium and the subsequent analysis of δ^2H in the soil water profiles were used to derive dominating water flow components (e.g., surface runoff, lateral subsurface flow, vertical percolation including preferential flow). Both experiments were conducted in direct vicinity to each other (Fig. 5.3).

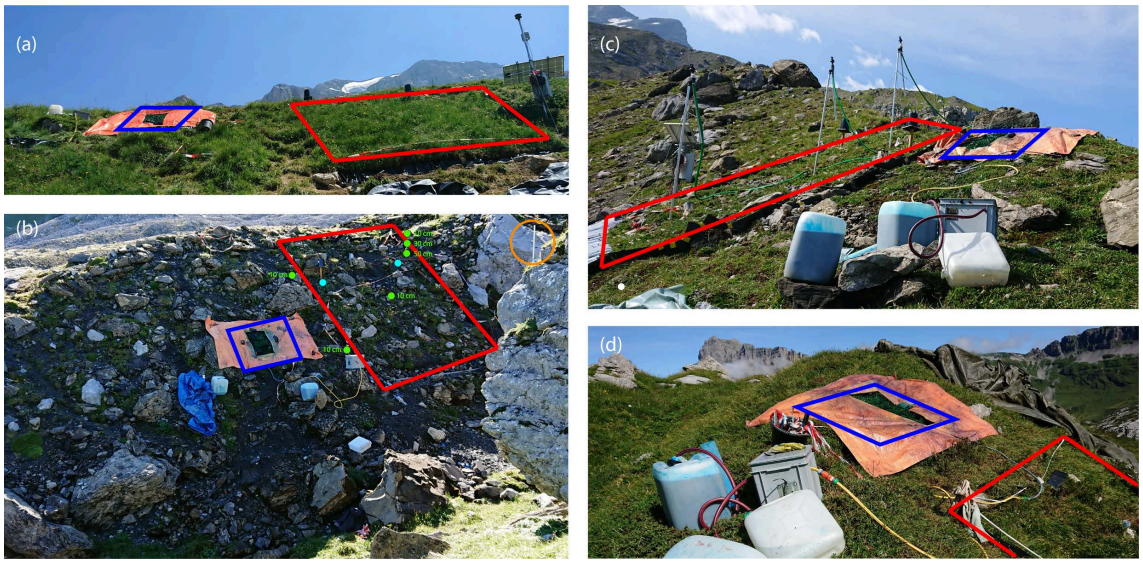

Figure 5.3: Examples for the positions of the dye tracer plots (blue rectangles) in relation to the isotope tracer plots (red rectangles) at three moraines at the C-PM forefield. Examples show experiments on the (a) 4.9ka, (b,c) 160a, and (d) 13.5ka moraine. b) The positions of the soil moisture sensors (green dots), tipping bucket (turquoise dots), and weather station (orange circle).

5.2.2.1 Dye tracer experiments

The dye tracer experiments at the S-PM chronosequence were conducted between mid-July and mid-August 2018 and at C-PM between August and mid September 2019. At each moraine, the experiments were carried out on three experimental plots (1 m x 1.5 m) differing in their vegetation complexity (Greinwald et al., 2021a). The experimental setup and detailed analysis of the dye tracer experiments are described in detail in Hartmann et al. (2020a) (S-PM) and Hartmann et al. (2022) (C-PM). Based on the resulting dye patterns a flow type frequency distribution was estimated using the classification method proposed by Weiler (2001) and modified by Hartmann et al. (2020a). Five flow types were distinguished: (1) macropore flow with low interaction, (2) mixed macropore flow (low and high interaction), (3) macropore flow with high interaction/finger-like flow, (4) heterogeneous matrix flow/finger-like flow, and (5) homogeneous matrix flow (incl. between rocks). Dye patterns, which could not be classified as one of these flow types were categorized as undefined. A preferential flow fraction index (PFF) was

calculated as the observed fraction of all preferential flow type classes (flow types 1–4) at each profile (Hartmann et al., 2022). The flow type classification was done for each depth segment of the soil profile, with the size of a segment being 1 mm. PFF is the number of segments classified as a preferential flow type divided by the total number of segments per soil profile.

5.2.2.2 Isotope tracer experiments

The δ^2H-irrigation experiments were conducted on three plots (4 m x 6 m) per moraine between mid July and September 2018 at S-PM and in August 2019 at the C-PM chronosequence. The 110a moraine at C-PM was excluded due to its difficult access. The irrigation plots were chosen along a vegetation complexity gradient (Greinwald et al., 2021a). Each plot was equipped with six soil moisture sensors (SMT100, TRUEBNER GmbH, Germany). A sensor profile with sensors in 10, 30, and 50 cm depth was installed at one side of the plot about one meter downslope the upper plot boundary. On the other side of the plot, two sensors were placed in 10 cm depth, one opposite to the sensor profile and the second sensor one meter upslope the lower plot boundary. The sixth sensor was placed at 10 cm depth in the center of the plot (Fig. 5.3). Two tipping bucket rain gauges per plot were installed for the monitoring of the irrigation experiments and natural rainfall events. Weather stations consisting of an extra tipping bucket, two solar radiation sensors (CS 305-ET, Campbell Scientific, Inc.) for measuring the incoming and reflected short wave radiation (300-1000 nm), a 2-D sonic wind sensor (WindSonic, Campbell Scientific, Inc.) for measuring wind speed and direction, as well as an air temperature and relative humidity sensor were installed at the 10ka, 3ka, and 30a moraine at the S-PM and at the 4.9ka and 13.5ka at the C-PM forefield. All data was recorded in a one minute resolution. Trenches were installed to record surface and subsurface flow. A detailed description of the surface runoff and subsurface flow measurements at the trenches and evaluation of the results is provided by Maier et al. (2021) and Maier and van Meerveld (2021a). The plots were irrigated on three consecutive days with three different irrigation intensities and δ^2H-concentrations. The irrigation intensity was increased step-wise every day while the isotope concentration was decreased. A detailed overview of the irrigation intensities and δ^2H-concentrations per plot, age class, and parent material is given in Table 5.2.

Soil profile samples for the isotope analysis were collected at each plot in 10 cm depth increments from a soil core of 8 cm diameter, excavated with a percussion drill a few days before the sprinkling experiments (Background samples), two days after the last irrigation experiment (Profile 1 samples), and 5-14 days after the last irrigation experiment (Profile 2 samples). The isotopic composition of the soil water was analyzed according to the equilibration method (Wassenaar et al., 2008). Soil samples were stored in airtight bags filled with dry air and sealed by welding. The samples were stored for 48 hours for equilibrium at a low temperature in the basement and then analyzed. In addition to the soil samples, three standard bags were prepared in the same manner containing 10 ml of water with a known δ^2H-concentration (-126.07, -67.27, -2.57 ‰), which were then handled the same as the soil samples. The isotopic composition in the headspace of the sample bags was measured with a wavelength-scanned cavity ring-down spectrometer (L2130-i, Picarro). The air was extracted from the bag into the spectrometer by inserting a needle into the bag via a previously attached silicone septum and connecting PVC tubing. A measurement was taken as the average over a 90 seconds period, when the standard deviation for H_2O was below 100 ppm, for δ^{18}O

Table 5.2: Irrigation amount, irrigation intensity and δ^2H-concentration of the irrigated water during the 3-day irrigation experiments at all three irrigation plots per age class at the S-PM and C-PM forefield.

Plot 1	*Irrigation day 1*			*Irrigation day 2*			*Irrigation day 3*		
	Amount [*mm*]	*Intensity* [*mm h*$^{-1}$]	δ^2H [‰]	*Amount* [*mm*]	*Intensity* [*mm h*$^{-1}$]	δ^2H [‰]	*Amount* [*mm*]	*Intensity* [*mm h*$^{-1}$]	δ^2H [‰]
Moraine									
Siliceous parent material									
30a	21	23	51.05	33	54	-11.30	36	61	-61.11
160a	23	22	76.72	52	56	10.13	63	90	-56.05
3ka	16	14	95.16	44	63	45.25	35	67	-61.66
10ka	12	13	242.41	27	26	26.57	19	33	-53.12
Calcareous parent material									
160a	27	26	205.90	60	61	130.25	70	79	71.29
4.9ka	26	24	230.37	45	49	128.86	41	77	81.20
13.5ka	25	22	240.42	31	32	143.09	51	56	79.76

Plot 2	*Irrigation day 1*			*Irrigation day 2*			*Irrigation day 3*		
	Amount [*mm*]	*Intensity* [*mm h*$^{-1}$]	δ^2H [‰]	*Amount* [*mm*]	*Intensity* [*mm h*$^{-1}$]	δ^2H [‰]	*Amount* [*mm*]	*Intensity* [*mm h*$^{-1}$]	δ^2H [‰]
Moraine									
Siliceous parent material									
30a	18	14	49.42	27	33	-11.02	27	46	-58.85
160a	20	23	85.69	32	40	5.17	54	62	-53.32
3ka	14	11	92.97	24	32	5.31	31	43	-54.10
10ka	12	13	242.48	22	24	12.19	24	43	-60.69
Calcareous parent material									
160a	26	24	233.04	47	50	124.61	42	63	72.18
4.9ka	22	23	209.28	37	45	152.44	46	79	99.81
13.5ka	25	23	257.99	35	35	118.66	48	72	72.57

Plot 3	*Irrigation day 1*			*Irrigation day 2*			*Irrigation day 3*		
	Amount [*mm*]	*Intensity* [*mm h*$^{-1}$]	δ^2H [‰]	*Amount* [*mm*]	*Intensity* [*mm h*$^{-1}$]	δ^2H [‰]	*Amount* [*mm*]	*Intensity* [*mm h*$^{-1}$]	δ^2H [‰]
Moraine									
Siliceous parent material									
30a	19	15	63.26	30	37	-3.62	32	48	-57.44
160a	23	20	73.77	25	43	6.53	57	81	-64.57
3ka	19	16	85.15	29	31	6.43	31	44	-54.25
10ka	10	11	236.79	17	23	18.51	18	32	-53.12
Calcareous parent material									
160a	22	24	264.48	53	58	123.37	53	70	73.91
4.9ka	25	23	232.14	38	44	121.92	51	61	74.53
13.5ka	26	24	244.28	45	59	96.41	52	78	69.56

below 0.6 ‰and for δ^2H below 1.2 ‰. The standard bags were measured before and after the soil samples to transform the measurements into the δ-notation relative to the Vienna Standard Mean Ocean Water (VSMOW) and to account for any temperature related drift. The data was corrected according to Gralher et al. (2016) to account for the potential risk of CO_2 formation during the equilibration caused by organic material and soil bacteria. Water samples of the irrigation water enriched with δ^2H were sampled from the storage basins directly before the experiment and were analyzed with a similar wavelength-scanned cavity ring-down spectrometer (L2130-i, Picarro, Inc.) in the Stable Isotope Lab at Freiburg University.

5.2.3 Soil physical and soil hydraulic properties estimation

To describe the hillslope form in terms of soil physical and hydraulic properties disturbed and undisturbed soil samples were taken in 10, 30, and 50 cm depth at the irrigation experiment plots next to the soil moisture sensor profile and 1 m upslope of the lower plot boundary. At the 110a moraine at C-PM, the samples were taken in the undisturbed parts of the dye tracer experiment plots. We determined soil texture (gravel, sand, silt, and clay content), porosity, bulk density, organic matter content, the retention curves and soil hydraulic conductivity curves. A detailed description of the methods and data differentiated by depth is provided in Hartmann et al. (2020b). The data sets are available at Hartmann et al. (2020c).
Based on the measured retention curves, the van-Genuchten parameters (Van Genuchten, 1980) required for soil water transport model parametrization were determined with the curve fitting function of the HYPROP-Fit software (Pertassek et al. (2015), METER Group, Inc. USA). Using the fitted curves, the available water capacity (AWC) was determined as the difference in water content between pF=1.8 (field capacity) and pF=4.2 (permanent wilting point) with pF =$\log_{10}$(|pressure head [cm]|).

5.2.4 Soil moisture response analysis

The hillslope hydrological functions such as generation of overland flow, vertical percolation, water storage, etc. are largely determined by the soil hydrological response. For an inter-comparison of the soil hydrological responses, we used soil moisture signatures describing the soil moisture reaction to each event of the δ^2H-irrigation experiments. Five soil moisture signatures (Fig. 5.4 and Table 5.3) were used to describe the soil water dynamics in terms of velocity, timing, and magnitude. The event response time (RT) reflects the velocity of the first soil water response and is thus a characteristic of the effective soil hydraulic conductivity. It is defined as the number of minutes between the start of irrigation and the first soil moisture response. This was defined as the point in time when the soil moisture increase was larger than 0.04 cm^3 cm^{-3}, thus increasing above the noise range of the sensors.
The relative peak timing (PT) provides information on the balance between infiltration and drainage. This signature is defined as the time between the end of irrigation and Θ_{peak}. Θ_{peak} is defined as the maximum water content during the event period, which is the period from the start of irrigation to three hours after the end of irrigation. Negative values indicate that Θ_{peak} was reached before the end of irrigation, which can be caused either by saturation or a balance between infiltration and drainage during irrigation (steady state). To differentiate if the cases of PT<0 are caused by saturation or by steady state soil moisture conditions during irrigation, we calculated the available remaining storage at peak soil moisture (PS, available peak storage) based on the difference between the saturated water content (Θ_{sat}) and Θ_{peak}. PS

values close to 0 indicate that the soil moisture peak was reached due to saturation. An available storage distinctly greater than 0 indicates the occurrence of steady state flow.

The magnitude of the soil water response can be derived based on the soil moisture peak amplitude. We calculated the relative maximum storage increase (SI) by relating the difference between the soil moisture Θ_{peak} and Θ_{init} (response amplitude, Branger and McMillan (2020)) to the irrigation amount in mm (I). To convert the moisture response amplitude from m^3/m^3 to mm, the response amplitude was multiplied by the depth increment represented by the sensor readings (20 cm). SI thus provides information on how much of the irrigation water filled up the short term storage in the soil (either directly or by displacing old water). To evaluate a post-event storage increase (ES), we related the difference between the water content three hours after the end of irrigation and Θ_{init} converted to mm to the irrigation amount. This parameter provides information on how much of the irrigated water (directly or by displacement) the soil can still hold three hours after the end of irrigation. The comparison of both signatures provides insights on the storage properties of the soil. The smaller the differences between SI and ES, the higher the water holding capacity of the soil. High SI-values, but low ES-values, on the other hand, indicate a low storage capacity and a fast subsurface water transport.

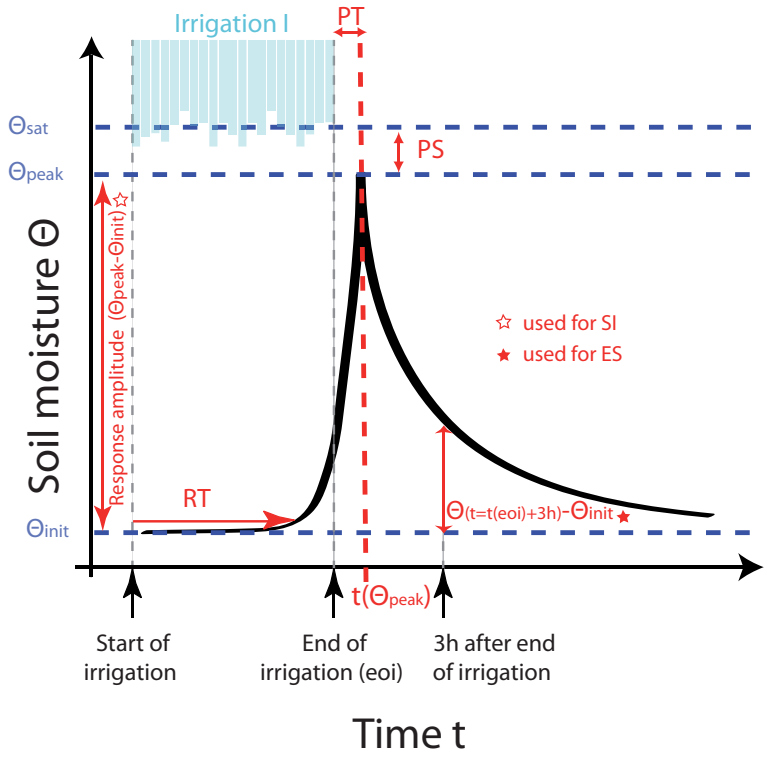

Figure 5.4: Visualization of the event-based soil moisture signatures listed in Table 5.3.

Table 5.3: Overview of the event-based soil moisture signatures and their calculation.

Soil moisture signature [unit]	Abbreviation	Calculation	Description
Event response time [min]	RT	$t(\Theta - \Theta_{init} > 0.04)$	Velocity of soil water response,
Relative peak timing [min]	PT	$t(end\ of\ irrigation) - t(\Theta_{peak})$	Balance between infiltration and drainage
Available peak storage [$\frac{cm^3}{cm^3}$]	PS	$\Theta_{sat} - \Theta_{peak}$	Balance between infiltration and drainage
Relative maximum storage increase [%]	SI	$\frac{(\Theta_{peak} - \Theta_{init}) * 200[mm]}{I[mm]} * 100\%$	Magnitude of soil water response, maximum storage change
Relative event storage increase [%]	ES	$\frac{(\Theta_{3h\ after\ end\ of\ irrigation} - \Theta_{init}) * 200[mm]}{I[mm]} * 100\%$	Magnitude of soil water response, Differences to SI: information on storage capacity

5.2.5 Modeling of soil water isotope profiles

To infer dominant water flow processes based on one-dimensional δ^2H-profile information, we used the approach proposed by Müller et al. (2014). The approach is based on the assumption that characteristic deviations between δ^2H-profiles modeled only by vertical matrix flow and measured δ^2H-profiles, provide conclusions about dominating flow components such as lateral subsurface flow and vertical percolation including preferential flow. The soil water isotope profiles were modeled by using the modified version (Stumpp et al., 2012) of the HYDRUS-1D software package (Šimůnek et al., 2016). This model calculates the transient water flow by numerically solving the Richards equation and the isotope transport with the advection–dispersion model. The model does not account for fractionation processes during evaporation that can lead to an isotopic enrichment of the soil.

Each irrigation experiment plot was modeled individually by parameterizing a 150 cm deep soil profile. The estimated van Genuchten parameters based on the measured water retention curves and measured saturated hydraulic conductivities (Maier et al., 2020) were used to parameterize the Richards equation. Since van Genuchten parameters were available in 10, 30, and 50 cm depth, the model domain was subdivided into three materials (material 1: 0-20, material 2: 20-40, and material 3: 40-150 cm). At depths with two measured retention curves, a parameter set describing the mean retention curve was used. This was done by averaging the parameters and double checking visually if the resulting retention function can be considered the mean of the functions.

The modeling period extends from the day the background δ^2H-profile was sampled to the day the second δ^2H-profile was taken after the last irrigation experiment. For the atmospheric boundary conditions we calculated the daily potential evapotranspiration using the FAO-Penman-Monteith method (Allen et al., 1998) based on the measured information on temperature, wind speed, humidity, and incoming and reflected shortwave radiation. The mean values from both rain gauges per plot were used as the precipitation input.

The depth dependent water extraction due to root water uptake was specified by measured root length density distributions down to a depth of 1 m provided by Greinwald et al. (2021a), which were measured in the same soil samples used for the soil water isotopic analysis. The initial pressure head conditions for the water transport were set to field capacity and the initial distribution of the δ^2H-concentration was specified by using the background profile information (sampled before irrigation). δ^2H-concentration of the natural rainfall was either specified by laboratory measurements of occasional rainfall events or by

monthly mean values from the GNIP station Grimsel (IAEA/WMO, 2021) which is located in a distance of 20 km to S-PM and 50 km to C-PM at an elevation of 1950 m.a.s.l. The δ^2H-notation describes the divergence of the isotopic composition of a sample in relation to the VSMOW. Natural waters contain mostly less heavy isotopes than the VSMOW, which leads to negative δ^2H values. Due to our step-wise enrichment of the irrigation water δ^2H-values range from negative to positive values. To calculate the δ^2H-transport with non negative values an offset of 120 was added to the input isotopic concentrations. The longitudinal dispersivity (D_L), a transport parameter in the advection–dispersion model, was unknown and had to be determined by manual calibration. For simplicity, D_L was assumed to be constant with depth. Each model was executed with seven different values for D_L (0.1, 0.5, 1, 1.5, 3, 5, 10, and 15 cm). The best fit D_L was identified visually by comparing model output isotope profiles to measured isotope profiles.

5.2.6 Statistical Analysis

The statistical analysis was carried out using R (R Core Team, 2017). The Mood's median test (Hervé, 2018) and the pairwise Mood's median post hoc test (Mangiafico, 2016) were used to test for significant differences in the observed soil-, surface-, and vegetation characteristics between the geologies and age classes. We tested for differences in the medians, as the median is less affected by outliers. The Mood's median test is a non-parametric test that compares median pairs of two or more groups. The significance level was set to $p < 0.05$.

A kmeans clustering and a principal component analysis using the prcomp-function was applied to the hillslope form/structure information consisting of the soil property data in the top 10 cm and vegetation/surface characteristics. The 110a moraine at C-PM was excluded from this analysis due to missing data. To test for significant differences in the preferential flow fractions (PFF) and soil moisture signatures describing the hillslope response among the four clusters identified by kmeans, the Tukey's HSD (Honestly Significant Difference) test was used. The significance level was set to $p < 0.05$. The used abbreviations and units of the soil-, surface-, and vegetation characteristics are listed in Table 5.4.

Table 5.4: Abbreviations and units of soil, vegetation and surface characteristics used in the principle component and cluster analysis.

Characteristic	Abbreviation	Unit
Sand content	Snd	weight-%
Silt content	Slt	weight-%
Clay content	Cly	weight-%
Porosity	PO	$cm^3\ cm^{-3}$
Bulk density	BD	$g\ cm^{-3}$
Available Water Capacity	AWC	vol-%
Sat. hydraulic conductivity	Ksat	$cm\ d^{-1}$
Above ground biomass	BM	$kg\ m^{-2}$
Organic matter content	OM	weight-%
Hydrophobicity	HP	[-]
Microtopography	MT	[-]
Surface coverage	SC	%
Root length density	RLD	$km\ m^{-3}$
Root density	RD	$kg\ m^{-3}$
Specific root length	SRL	$m\ g^{-1}$

5.3 Results

5.3.1 Evolution of hillslope form

5.3.1.1 Evolution of soil characteristics

The development of the soil properties in form of median values in 10-50, 10, 30, and 50 cm depth for the two geologies is shown in Figure 5.5. Figure 5.6 shows the results of the Mood's median test for differences in soil properties between the age classes per geology (a) and between the geologies per age class (b). For the particle sizes at a depth of 10 cm at the 10ka moraine, a visual assessment of the differences was necessary because the sample size is significantly smaller than for the other age classes and geology (n=2, instead of 6), which would produce misleading results in the Mood's median test.

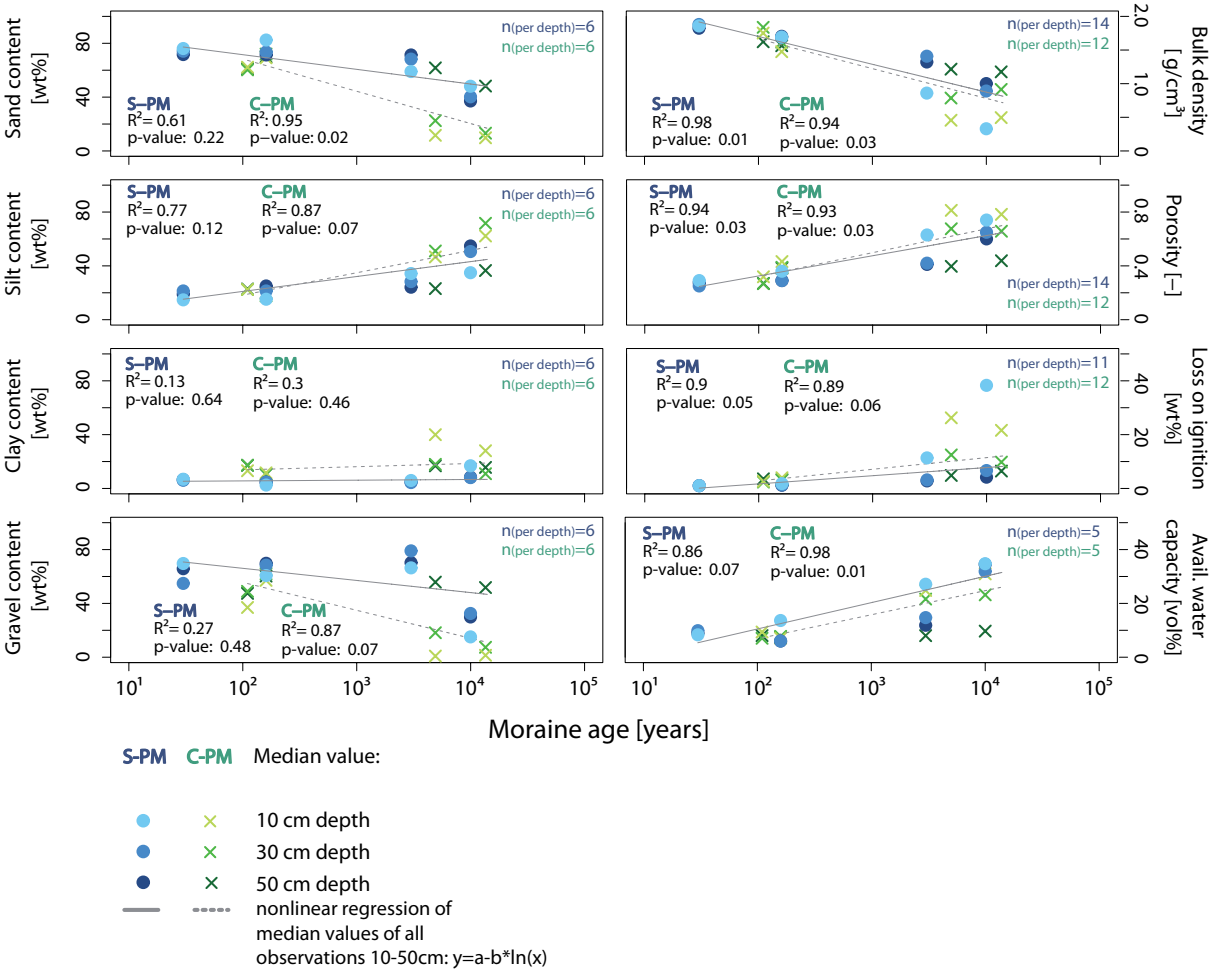

Figure 5.5: Evolution of median values of bulk density, porosity, loss on ignition, and sand, silt, and clay content at the siliceous (S-PM) and calcareous (C-PM) parent material for each age class in 10, 30, and 50 cm depth. The non-linear regression shows the age trend of the median of all values in 10 to 50 cm depth. n denotes the number of observations per depth and age class. Note that at the 10ka at S-PM at 10 cm depth n is only 2 for the observations of the sand, silt, clay, and gravel content.

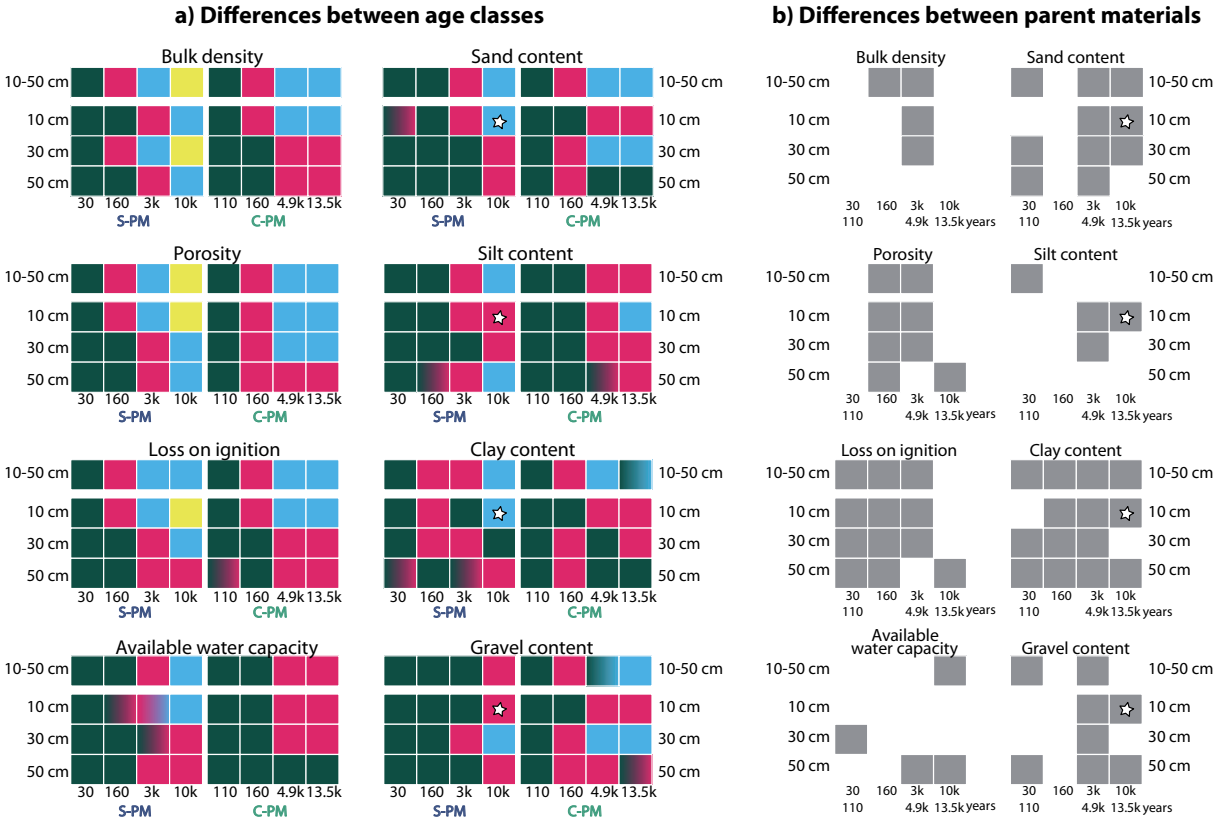

Figure 5.6: a) Mood's median test for significant differences between the age classes per parent material in the soil properties in 10-50, 10, 30, and 50 cm. Different colors denote significant differences between the age classes. Age classes with the same color are not significantly different by the Mood's median test at the 0.05 level of significance. b) Mood's median test for significant differences in the soil properties in 10-50, 10, 30, and 50 cm depth between the parent materials per age class and depth. Grey boxes indicate a significant difference between the parent materials. PO=porosity, BD=bulk density, AWC=available water capacity, Snd=sand content, Slt=silt content, Cly=clay content, Grvl=gravel content. White star: visual evaluation of the differences. A visual assessment of the differences was necessary due to significantly different sample sizes, which lead to misleading results in the Mood's median test.

The two geologies differ significantly in their soil structure (Fig. 5.6b). At both geologies, we observed a decrease in sand content over time (Fig. 5.5). At the young age classes, the sand content at both geologies is high and differences between the geologies are small (110/30a, Figure 5.5) or not significant (160a, Figure 5.6b). With increasing age, the sand content at the calcareous parent material decreases significantly (Fig. 5.5 and Fig. 5.6a). This is particularly pronounced at the depths of 10 and 30 cm. At the siliceous site, the sand content also decreases with age, but not as strongly. The silt content of both geologies shows no significant differences for the two young age classes (Fig. 5.6b). At the calcareous parent material, the silt content increases significantly with age (Fig. 5.6a), especially at the depths of 10 and 30 cm. The calcareous parent material has a significant higher clay content at all age classes compared to the siliceous parent material, but no clear age trend can be seen at either location.

Differences between the geologies in the development of bulk density and porosity are only significant at the medium age classes (160a and 3ka/4.9ka, Figure 5.6b). A distinct decrease in bulk density with an associated distinct increase in porosity is observed at both geologies. While at the siliceous parent material, the bulk density and porosity differ significantly at all four age classes, the differences between

the two oldest age classes at the calcareous parent material are not significant (Fig. 5.6a). Bulk density and porosity continuously develop in one direction (decrease in bulk density, increase in porosity) at the siliceous parent material, whereas at the calcareous parent material the differences between the oldest age classes are very small with the tendency to show a discontinuous development (extrema at 4.9ka instead of 13.5ka). The organic matter content increases with age at the siliceous parent material (Fig. 5.6b) and is particularly high in the upper 10 cm at the oldest moraine. At the calcareous parent material, the organic matter also increases with age (Fig. 5.5) and is significantly higher at the age classes from 110 to 4.9ka years compared to the siliceous parent material. At the oldest moraine of 10k years, the organic matter content of the siliceous parent material at 10 cm depth exceeds that of the calcareous parent material (Fig. 5.5). The available water capacity increases with age at both geologies (Fig. 5.5). At the siliceous parent material, this increase is particularly distinct in the upper 10 cm up to an age of 3000 years. At 10k years, the available water capacity in 30 and 50 cm depth varies in a similarly high range as in 10 cm depth. At the calcareous parent material, the available water capacity increases equally at 10 and 30 cm depth, with the highest values being reached at a depth of 10 cm. At a depth of 50 cm, on the other hand, the increase is only very slight, which leads to a large difference between the available water capacity in 10 and 50 cm depth.
Comparing both geologies, the most significant differences are found for the second oldest moraines (3k/4.9ka, Fig. 5.6b). In the calcareous parent material, we observed a discontinuity in the age trend along the chronosequence with higher values in porosity, clay content, organic matter content, and lower values in bulk density at this age class compared to the oldest age class.

5.3.1.2 Cluster analysis based on structural variables

To identify similarities and differences in form/structure across age classes and between the two parent materials, a cluster analysis was conducted. This cluster analysis was based on a prior principal component analysis of the set of form variables (soil surface properties, surface characteristics and vegetation characteristics). The data on pH could not be included in the analysis due to an incompatibility of sampling locations and sampling strategy. However, because of its great importance, the influence of pH will be included in the discussion later on. The principal component analysis of the combined set of form data at S-PM and C-PM comprising soil properties in 10 cm depth and surface/vegetation characteristics (Table 5.1) shows that 70% of the variation in the data across the plots can be explained by the first two principal components (Fig. 5.7). Soil properties such as porosity, bulk density, sand content, and available water capacity have the highest impact on the data distribution along the PC1 axis. Along the PC2 axis, microtopography and vegetation properties such as biomass, root length density and organic matter content have the highest impact.

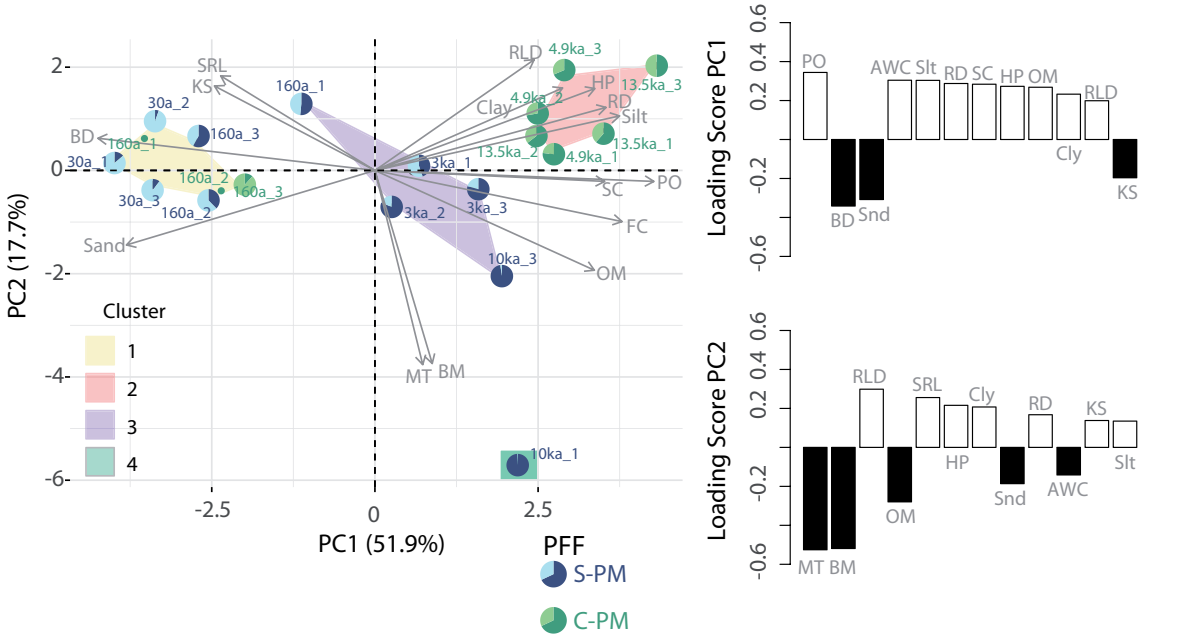

Figure 5.7: Left: Principal component analysis of data sets of S-PM and C-PM including soil properties at 10 cm depth and surface/vegetation characteristics data at each experiment plot per moraine with kmeans clustering. Pie charts show the corresponding preferential flow fraction (PFF) in the respective darker color. Right: The loading scores of the soil properties in 10 cm depth and surface/vegetation characteristics. Loading scores describe how much each variable contributes to PC1 and PC2. White indicates positive and black indicates negative loading scores. An explanation of the abbreviations is given in Table 5.4.

We used kmeans clustering to identify four groups of plots with similar soil properties and surface characteristics in the first two principal components. Three of the four clusters are arranged primarily along the PC1 axis. Cluster 1 on the far left side on PC1 (Fig. 5.7) consists exclusively of the young moraines of both parent materials (30a+160a S-PM and 160a C-PM). The location of the cluster is determined by a high sand content and high bulk density (and correspondingly low porosity). Cluster 2 is located in the top right quadrant (positive segment of PC1 and PC2) and consists exclusively of the old moraines of C-PM (4.9ka + 13.5ka). A low sand content (but high silt and clay content), as well as high root density, root length density, and hydrophobicity are mainly responsible for the location of the plots in this cluster. Cluster 3 is located close to the origin of the coordinate system and extends in the negative and in the positive direction along PC2. This cluster consists exclusively of moraines from S-PM with all three plots from the 3ka, one from the 10ka and one from the 160a. The plot from the young moraine (160a) is located in the positive PC2 segment with higher saturated hydraulic conductivity, specific root length and lower organic matter and above ground biomass. The plots from the old moraines (3ka and 10ka) are mostly located in the negative segment of PC2, which is marked by a higher content of organic matter and above ground biomass. The fourth cluster consists of a single plot of the 10ka moraine at S-PM and has its unique location mainly due to the high above ground biomass, organic matter and microtopography.

5.3.2 Evolution of hillslope function

5.3.2.1 Modeling isotope tracer irrigation experiments to identify deviations from vertical matrix flow

We use the deviations between measured soil water δ^2H-profiles and modeled δ^2H-profiles (modeled by purely assuming vertical matrix flow) to infer dominant water flow processes as proposed by Müller et al. (2014). Both the measured and the modeled profiles of the δ^2H-concentration in the soil water 2 days and 5-14 days after the 3rd irrigation are shown in Figure 5.8.

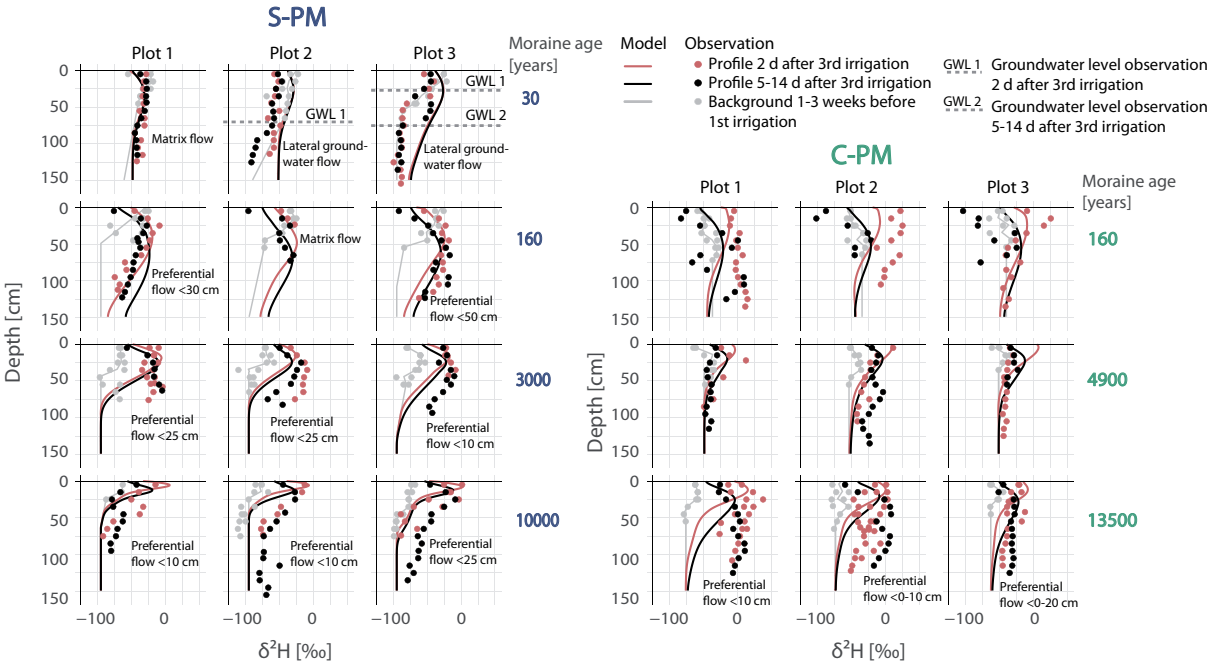

Figure 5.8: Measured and modeled δ^2H-isotope profiles after the irrigation experiments at both chronosequences, with the model assuming pure matrix flow.

For S-PM, the modeling results show a good reproduction of the profiles of plot 1 at the 30a moraine and in the upper 60 cm of the three plots at the 160a moraine. The other two plots at the 30a moraine are influenced by groundwater flow, which can be derived from the homogeneous isotopic concentrations in the lower part of the soil profile (Müller et al., 2014). Saturated conditions were also observed during soil sampling with the percussion drill, which allowed an approximation of the groundwater levels (GWL1 and GWL2 in Figure 5.8) for the days of sampling. The influence of groundwater was also confirmed by the observations of lateral runoff (Maier et al., 2021). Due to the proximity of the 30a moraine to the glacial lake and the position of the plots 1 and 2 relatively close to the foot of the slope, subsurface lateral water flow plays a big role in the subsurface water transport. The 30a moraine at S-PM was the only moraine where groundwater was observed.

At the 160a moraine, the deuterium concentration below 60 cm soil depth is overestimated by the model at plot 1 and underestimated at plot 3. The isotopic composition at the 3ka and 10ka moraines is also mainly underestimated below a soil depth of 30 cm. An underestimation of the isotope signal by the model can be an indicator for preferential water transport (Müller et al., 2014), as under preferential water

flow conditions, the isotopic signal can reach greater depths faster than under matrix flow conditions. The modeling results in plot 1 and 2 of the 160a moraine at C-PM show an underestimation of the modeled isotopic composition of the profiles taken 2 days after the third irrigation. At plot 3, differences occur only in the upper 70 cm. Below that, the deviations are rather small. The underestimation can again indicate preferential water transport. The deuterium concentration of the second profile is mainly overestimated at all plots. However, the second δ^2H-profile was obtained in the morning after a nocturnal snowfall event with an unknown δ^2H-concentration which strongly increases the uncertainty of the model results. At the three plots of the 13.5ka moraine and plot 2 at 4.9ka moraine, the model underestimates the δ^2H-concentration, which suggests the occurrence of preferential flow. At plot 1 and 3 of the 4.9ka moraine, the profiles have only little variation with depth, which is reproduced by simulating matrix flow. However, this low variability can also be caused by a high dispersivity and/ or fast vertical water transport, which leads to a fast disappearance of the isotopic signal.

5.3.2.2 Soil moisture signatures

The soil moisture signatures for each age class, parent material, and observation depth are displayed in Figure 5.9 and Figure 5.10.

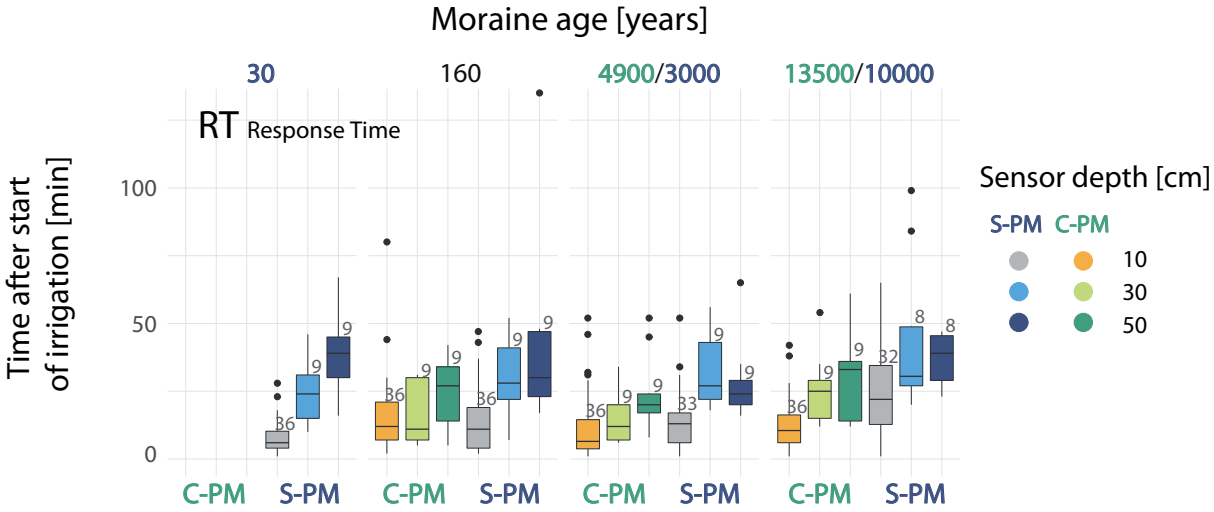

Figure 5.9: Soil moisture response time (RT) for age each class and sensor depth (10, 30, and 50 cm) for both geologies. Small numbers indicate the sample size of each box.

The five soil moisture signatures (Fig. 5.4 and Table 5.3) describe the soil water dynamics in terms of velocity, relative timing of the peak, and magnitude. The irrigation signal reaches the sensors at C-PM faster than at S-PM (Fig. 5.9). The response time (RT) increases slightly with age at both geologies. The time until the soil moisture peak is reached in relation to the end of irrigation (peak timing=PT, Fig. 5.10a) reveals that especially the C-PM moraines reach the maximum water content already during irrigation (PT<0). At S-PM this is mainly the case in the top soil at the 30a, 160a, and 3ka moraine. At the oldest S-PM moraine (10ka), the peak soil moisture is mostly reached after the end of irrigation (PT> 0). At the C-PM moraine, the available peak storage (PS, differences between the laboratory-based measured saturation water content and the peak soil moisture content) for the cases PT<0 is relatively high (> 20

Vol-%), which indicates that during the irrigation process the soil is not fully saturated and an equilibrium between infiltration and deep drainage is established. In contrast, PS values at S-PM are small, which indicates that saturation occurs before the end of irrigation. High PS values indicating steady state flow were only found in 10 cm depth at the 3ka moraine. However, small differences and negative values should be interpreted with caution due to the uncertainties in the laboratory-based determination of the saturated water content and the uncertainties in the transferability of laboratory data to field measurements.

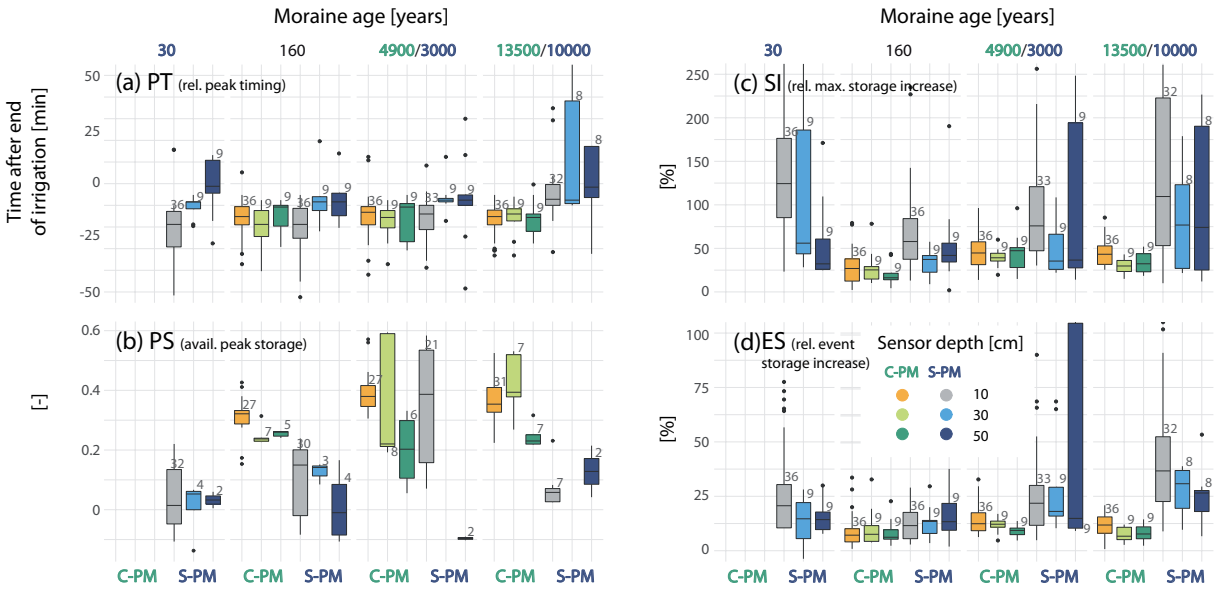

Figure 5.10: Timing of soil moisture peak relative to the end of irrigation (PT=relative peak timing) (a), difference between soil moisture peak and saturated water content (PS) for PT<0 (b), relative maximum storage increase (SI) (c), and relative event storage increase (ES) (d) for all irrigation events at each geology, age class and sensor depth (10, 30, and 50 cm). Small numbers indicate the sample size of each box.

The relative maximum storage increase (SI) at the S-PM moraines is higher compared to C-PM. Especially in the topsoil of the 30a moraine and in 10 and 50 cm depth of the 10ka moraine at S-PM, SI mostly exceeds the irrigation input several times over (Fig. 5.10c). A disproportionate increase in soil moisture could indicate lateral water input. At C-PM however, the relative maximum storage increase is consistently below the precipitation input.

The relative event storage increase (ES), which describes the storage increase 3 hours after the event as fraction of the irrigation amount and provides information on water holding capacity, increases at S-PM from the young moraines to the old moraines, with the 3ka occasionally showing very high ES values. Compared to the maximum storage increase the event storage increase in the topsoil at the 30a and in 10 and 50 cm depth at the 10ka moraine is distinctly smaller. The event storage increase at C-PM is small with values consistently below 50% of the precipitation input.

5.3.2.3 Dye tracer irrigation experiments

Detailed results of the dye tracer experiments can be found in Hartmann et al. (2020a) (S-PM) and Hartmann et al. (2022) (C-PM). Here we only give a brief summary of the observed flow types (Fig. 5.11), which were then used to calculate the preferential flow fraction per profile.

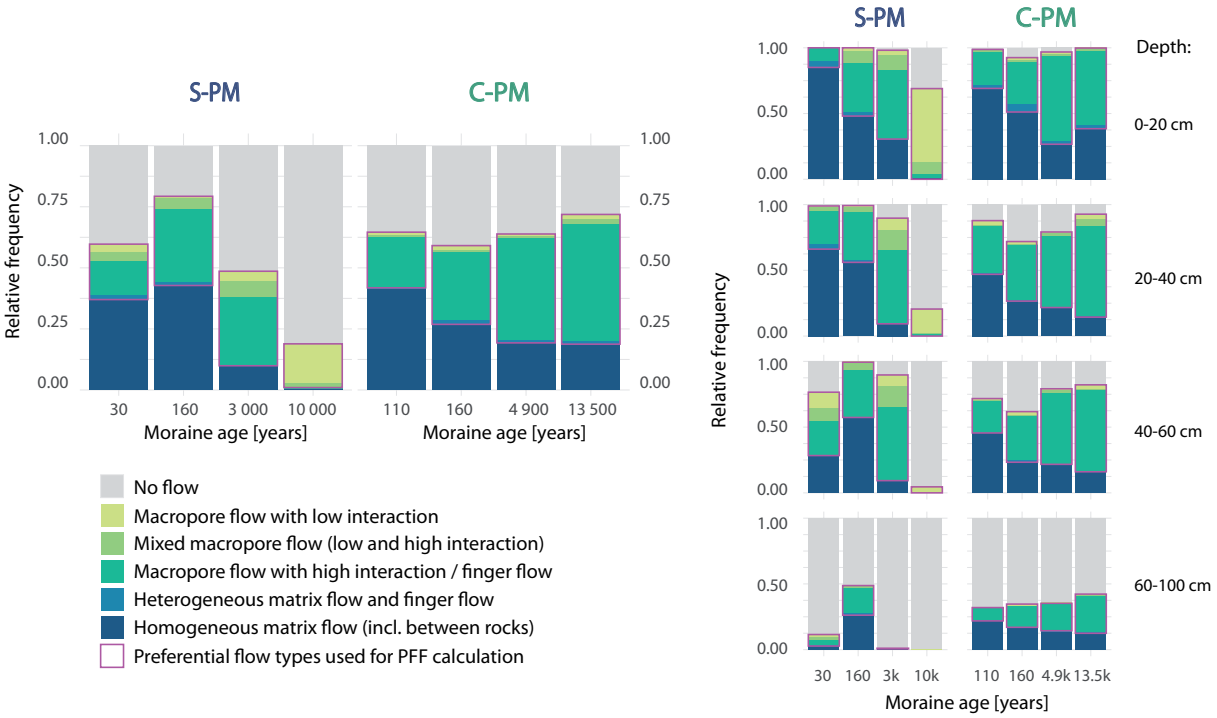

Figure 5.11: Evolution of flow type distribution at both chronosequences. Left: across the complete profile depth (Hartmann et al., 2020a, 2022). Right: differentiated by depth. Red frames outline the preferential flow types used for the PFF calculation.

The flow pattern classification into flow types shows a decrease in matrix flow with increasing age at both geologies. At the calcareous parent material, matrix flow is more dominant, especially at the youngest age class, whereas at the oldest moraines finger-like flow is dominant. The two young moraines at the siliceous parent material are dominated by matrix flow. Preferential flow in form of finger-like flow is also present, with a higher frequency at the 160a moraine. In the upper 20 cm the flow type frequency follows a clear age trend with an increase in preferential flow (finger-like flow and macropore flow) with increasing moraine age. At the 10ka moraine, the infiltration depth is distinctly lower compared to the younger age classes. This is the only moraine where macropore flow was observed, which is the dominating flow type at this age class. A significantly lower infiltration was also found below a depth of 60 cm at the 3ka and 30a moraine. The 30a moraine shows a high frequency of preferential flow at these depths. Preferential flow occurs here as funneling caused by large blocks of rock surrounded by clay and in form of macropore flow in cracks and finger like flow along material interfaces of a loam/clay horizon at 50 cm depth (Hartmann et al., 2020b).

We calculated the preferential flow fraction (PFF) as the occurrence of preferential flow observations (outlined in red in Figure 5.11) as fraction of all flow type observations (excluding no flow). PFF is displayed per geology, age class, and depth in Figure 5.12. No continuous age trend is observed for PFF in the top soil layer at the calcareous parent material, as the 4.9ka moraine shows the highest PFF. Only from a depth of 20 cm downwards do we observe a continuous increase in PFF with moraine age.

At the siliceous parent material, the fraction of preferential flow increases continuously with age in almost all three observation depths. An exception is the youngest moraine, where the proportion of preferential

flow in 50 cm depth is higher than at the 160 a moraine (median>0.8). The highest PFF of all age classes at both parent materials was found at the 10ka moraine (siliceous parent material). Here we observed either no flow or a few preferential flow paths (macropore flow), resulting in PFF = 1. The sample size is determined by the number of irrigation plots per age class (3), the number of subplots per plot (3), and the number of photographs taken per subplot (5). The maximum sample size is 45. If the number is lower, it indicates that there are no observations of infiltrated water at this depth, or the number of photos has been reduced due to local conditions (e.g., huge boulders).

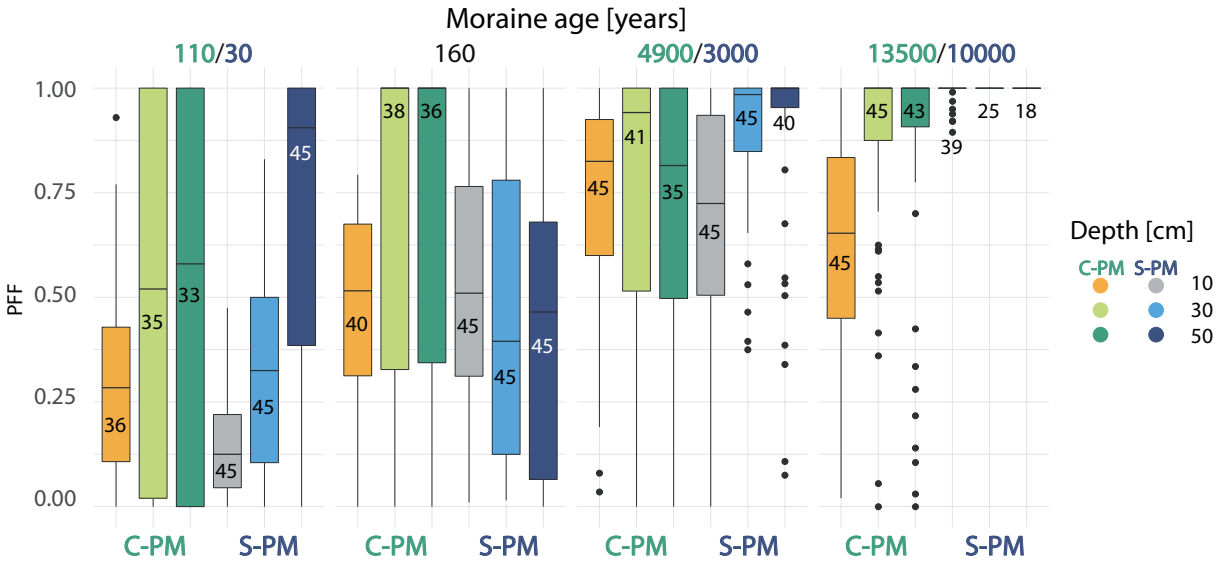

Figure 5.12: Preferential flow frequency as preferential flow fraction (PFF) at each age class of both geologies at 10, 30, and 50 cm depth. Numbers inside the boxes indicate the sample size. PFF=1 means that only preferential flow was observed. At the 10ka moraine at S-PM mostly no flow or preferential flow was observed, resulting in PFF=1 with almost no variability. Small numbers indicate the sample size of each box.

5.3.3 Links between hillslope form and hillslope function

To investigate if clusters based on form (soil properties at 10 cm depth and vegetation/surface characteristics) show different behavior/functioning we plotted for each cluster the observed hillslope responses (soil moisture signatures and PFF) and observations of surface- and subsurface flow volumes by Maier et al. (2021) and Maier and van Meerveld (2021a) (Fig. 5.13). The distribution of soil properties at 10 cm depth and vegetation/surface characteristics within each individual cluster is shown in Figure 5.18 in the appendix. In terms of form, the main difference between cluster 1 and cluster 2 lies in the soil texture and root system development. While cluster 1 represents the plots with a mainly coarse texture and low vegetation cover and thus only a weakly developed root system, cluster 2 is defined by finer material and a well-developed root system. Cluster 3 lies mainly in between these two clusters, but is defined by a higher above ground biomass and a pronounced microtopography. Cluster 4 is characterized by the highest organic matter content, highest above ground biomass, and highest available water holding capacity.

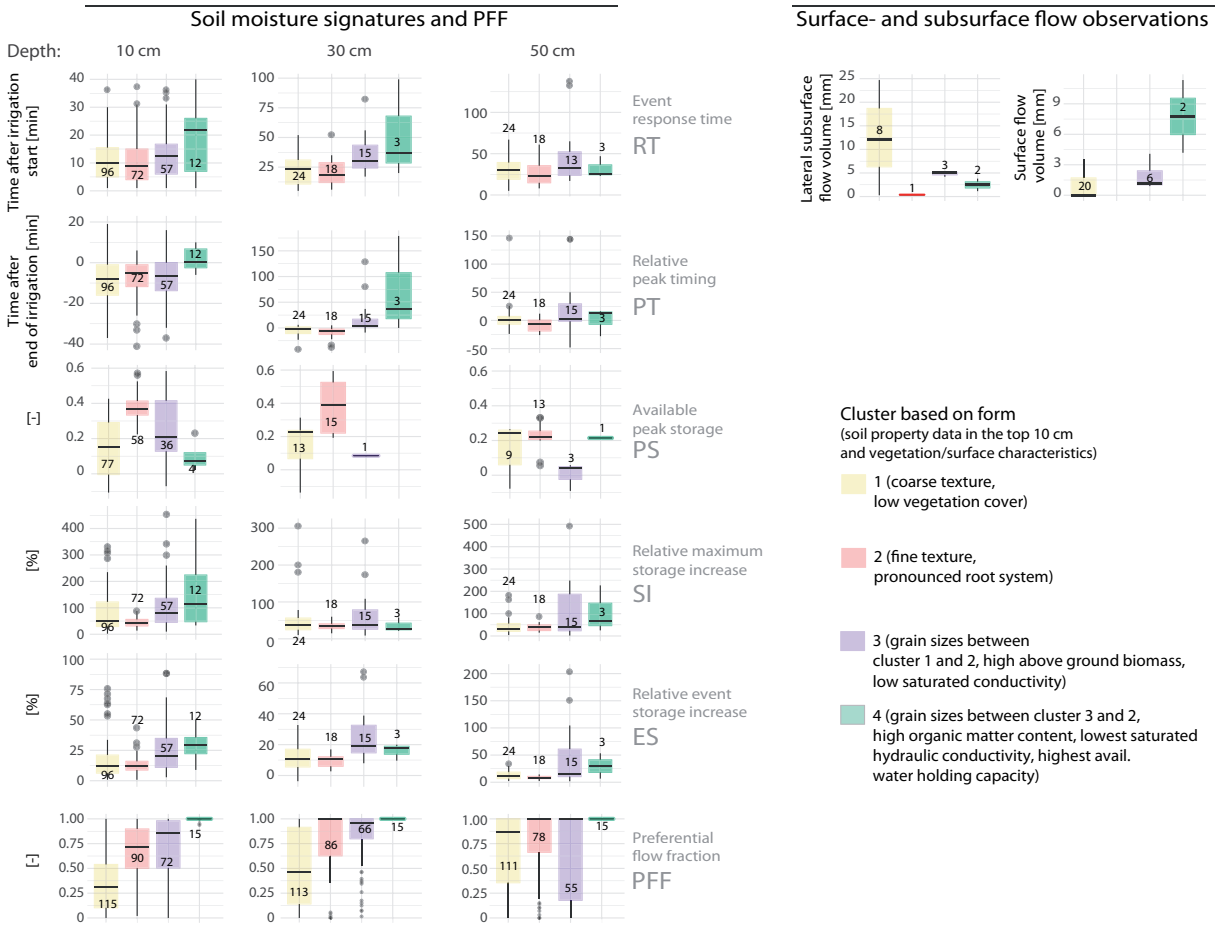

Figure 5.13: Left: Distribution of the soil moisture signature parameters and PFF in the four clusters based on form. Right: Surface- and subsurface flow observations by Maier et al. (2021) and Maier and van Meerveld (2021a) in the four clusters. Small numbers indicate the sample size of each box.

The soil moisture signatures in cluster 1 indicate cases of steady state transport conditions, soil saturation and subsurface lateral flow. At these sites surface and lateral subsurface flow was also observed (Maier et al., 2021; Maier and van Meerveld, 2021a). The median response time at 10 cm depth in cluster 1 is around 10 minutes and increases to approx. 24 to 28 minutes at 30 and 50 cm depth, respectively. The peak soil moisture at 10 cm depth is mostly reached before the end of irrigation (PT<0). At 30 cm depth, this is the case for only half of the observations and at 50 cm depth for less than 40% of observations. The available storage at peak soil moisture (PS) helps to identify in cases of PT<0, whether the peak soil moisture was reached due to saturation or due to an equilibrium between infiltration and deep drainage. At 10 cm depth, the PS values vary in a wide range from 0 to 0.35, indicating that in some cases saturation (PS close to 0) and in some cases steady state transport conditions (PS>0) were reached. At 30 and 50 cm depth PS is mostly higher than 0.1, which leads to the assumption that steady state transport occurs more frequently. A relative maximum storage increase SI of more than 100% of the irrigation input indicates an additional water input through lateral flow. At 10 cm depth, the median SI is at around 50%, but the interquartile range reaches from about 30 to 120% with a few outliers over 200%. The relative event storage increases after the end of irrigation (ES) at 10 cm depth is lower (median around 12%) and

the interquartile range smaller (7-20%) compared to SI. Only a few outliers show values of up to 75%. Cluster 1 has very high variations in preferential flow frequency (PFF) at 10, 30, and 50 cm depth. The median values increase with depth from 0.31 to 0.48, and 0.87, but are always the smallest compared to the other clusters.

Soil moisture signatures in cluster 2 indicate exclusively steady state transport conditions. Lateral subsurface flow was only observed at 1 out of 18 of the sites found in cluster 2 (Maier et al., 2021). The flow volume was less than 1% of the irrigation input. The response times are slightly smaller compared to cluster 1. In more than 80% of the observed sensor responses at 10 and 30 cm depth and more than 70% at 50 cm depth, the peak soil moisture was reached before the end of irrigation (PT<0). The available storage at peak soil moisture (PS) in these cases exceeds 0.2 at all three depths, indicating solely steady state water transport conditions. Cluster 2 shows the smallest variation range in the relative maximum storage increase and the relative event storage increase. The relative maximum storage increase at all three depths is mostly below 50% and the relative event storage increase is mostly below 20% of the irrigation input. The preferential flow frequency increases with depth. At 10 cm depth, the median PFF is around 0.7, and the interquartile range reaches from 0.5 to around 0.9. At 30 and 50 cm depth half of the observed PFF = 1.0. The lower end of the interquartile range also increases to more than 0.6 at 30 and 50 cm depth.

In cluster 3, cases of steady state water transport and subsurface lateral flow were indicated by the soil moisture signatures. Subsurface flow and surface flow was also observed at the sites found in this cluster by Maier et al. (2021) and Maier and van Meerveld (2021a). The response times of cluster 3 are longer at all three depths compared to cluster 1 and 2 (medians are 13, 31, and 35 minutes at 10, 30, 50 cm depth). At 10 cm depth, more than 60% of the soil moisture observations showed a peak already before the end of irrigation. In 30 and 50 cm depth, the proportion is only 6% and 20%, respectively. In most cases of PT<0 at 10 cm depth, the available peak storage is higher than 0.1, indicating that saturation was not reached and steady-state water transport was dominant. The median maximum storage increase is around 80% of the irrigation input at 10 cm depth, and below 50% at 30 and 50 cm depth. At 10 and 50 cm depth in more than 25% of the observations, the maximum storage increase was higher than the irrigation input, indicating additional water input from lateral flow. The preferential flow frequency in cluster 3 is higher at 10 cm depth compared to cluster 1 and 2 (median >0.8). At 30 cm depth the majority of PFF is higher than 0.75, whereas the lower quartile at 50 cm depth is at PFF=0.18 and the median, and upper quartile at PFF=1.0.

In cluster 4 the soil moisture signatures indicate high water storage capacities and subsurface lateral flow (also observed by Maier et al. (2021)). Cluster 4 consists of only one experimental plot and thus has only a small number of observations, which certainly affects the statistical significance of the observations. The response time in cluster 4 at 10 cm depth is the highest of all four clusters. The median time to the first sensor response is more than 20 minutes. Even at the depth of 30 cm, the median response time is highest in cluster 4 and the upper quartile clearly exceeds that of the other clusters. At 50 cm depth, on the other hand, there are no clear differences to the other clusters. At cluster 4, only 25% of the observations at 10 cm depth showed a soil moisture peak before the end of irrigation. At 30 and 50 cm depth, only one out of three observations showed PT<0. The maximum PT values are also distinctly higher for cluster 4 at 10 and 30 cm depth than for the other clusters. The upper quartile is at 10 cm depth about 6 minutes and at 30 cm depth even over 100 minutes after the end of irrigation. Only at 50 cm depth there is not much

difference to the other clusters. The very few cases of PT<0 showed an available peak storage between 0.05 and 0.2. The maximum storage increase at 10 cm depth is the highest compared to the other four clusters. It is also the only cluster with a median maximum storage increase higher than the irrigation input. The upper quartile is even higher than twice the irrigation input, which indicates a lot of lateral water transport. The median event storage increase is highest at 10 and 50 cm depth compared to the other clusters. The preferential flow fraction at cluster 4 is 1.0 at all three depths.

5.4 Discussion

5.4.1 Evolution of hillslope form

The clustering of the young moraines of both geologies into a single cluster and the clustering of the two older age classes into one cluster per geology (Fig. 5.7) shows that age and geology determine differences in hillslope structure, with age becoming less important and geology becoming more important as time progresses. The PCA reveals that differences in soil structural characteristics such as sand content and porosity as well as in surface and vegetation characteristics such as microtopography, above ground biomass and root characteristics separate the old moraines of both geologies into different clusters. We find that at both geologies physical, chemical, and biological weathering processes cause a decrease in the sand content in favor of the silt and clay content (Fig. 5.5). We assume that biological weathering processes (breakdown of particles by roots and root exudates) are constantly gaining in importance due to the advancing plant development over the millennia of landscape development. The constant biomass accumulation and the reduction in grain sizes with increasing age lead to an increase in porosity and a decrease in bulk density and thus to an increase in available water capacity.
However, there are some specific differences in the soil and landscape development between the parent materials that need to be discussed. In the calcareous glacier forefield, we found finer grain sizes at the oldest moraines (Fig. 5.5), despite higher chemical weathering rates at the siliceous parent material (Musso et al., 2022). Insolation weathering (Weiss et al., 2004) of the dark colored bare soil found at the young calcareous moraines may lead to a stronger breakdown of the particle sizes. At the chronosequence of calcareous moraines, we observed a discontinuous trend in some soil properties. Here, the clay content, organic matter content, and the porosity are higher at the 4.9ka compared to the 13.5ka moraine (plus correspondingly lower bulk density, Fig. 5.5). This discontinuous development does not fit into evolution of soil properties observed in undisturbed systems (Douglass and Bockheim, 2006; Dümig et al., 2011; Vilmundardóttir et al., 2014). Also weathering indices derived by Musso et al. (2022) indicated stronger weathering at the 4.9ka moraine compared to the oldest moraine of the same geology. We have to consider that in this case the assumption of the chronosequence approach, that all moraines developed under the same environmental conditions and disturbances and only differ by their age is not completely valid. Different initial site conditions or/and geomorphological disturbances (Wojcik et al., 2021) may have led to different rates of change at the calcareous moraines, which led to a slightly higher development stage at 4.9ka. There is evidence that the 13.ka moraine was deposited during the younger Dryas advance phases which were colder and dryer and thus might hampered the soil formation (Musso et al., 2020). However, this uncertainty has only a marginal effect on the observed differences in the development of the moraines

on the two different geologies.
At the chronosequence of siliceous moraines, the development of organic matter and available water capacity is continuous but shows a distinct increase between the two oldest moraines. The development of organic matter and the available water capacity is strongly related to the vegetation cover. The 3ka moraine is mainly covered with grass, whereas the 10ka moraine has a dense vegetation cover consisting mainly of *Rhododendron ferrugineum* and *Vaccinium myrtillus*, both acid-loving species of ericaceous shrubs. There is a pronounced accumulation of organic matter at the 10ka moraine where the organic top layer in part reaches a thickness of 30-50 cm. This organic layer consists to a high proportion of mor humus due to difficult to decompose substances such as lignin, cellulose and phenolic compounds in the litter produced by the ericaceous shrubs (D'Amico et al., 2014; Pornon and Doche, 1996). The high content of organic material has a positive effect on the available water capacity (Khaleel et al., 1981).
The available water capacity at both chronosequences increases with age and is relatively similar up to a moraine age of 160 years. At the older moraines the available water capacity at the siliceous parent material exceeds that of the calcareous parent material, despite the latter having more fine-grained material (higher silt and clay content, Fig. 5.5). The available water capacity was derived from the measured retention curves (Hartmann et al., 2020b). In contrast to the high sand content, the retention curves at the old siliceous moraines show a clay-like to loamy-silty curve progression. At the calcareous moraines, however, the curves show a silty curve progression analogous to the grain size distribution. In case of the 10ka moraine (S-PM), the high retention can be explained by the high proportion of dead organic material, which influences structural variables (bulk density and porosity) and increases the absorption capacity of the soil (Yang et al., 2014). Although the 3ka moraine (S-PM) has a coarser soil texture and lower organic matter content than the 4.9ka moraine (C-PM), the available water capacity of the 3ka moraine is higher. However, the derived organic matter content does not differentiate between living (e.g., roots) and dead (humus) organic matter. Greinwald et al. (2021a) reported a dense root network and a high root fraction (>99%) in the upper 30 cm at 4.9ka. We therefore assume that the main part of the organic substance is made up of living organic matter at the 4.9ka and humus at the 3ka moraine, with the latter having a higher impact on the water retention.
The soil formation and the vegetation characteristics at the old moraines show distinct differences between the parent materials. The 10ka moraine (S-PM) was densely covered with acid loving ericaceous shrubs. We assume that a positive feedback loop between the pH-level and ericaceous shrubs led to a strong increase in shrub vegetation. The low pH-values of the topsoil due to weathering of the siliceous parent material favor the settlement of ericaceous shrubs, which further lower the pH-value through litter production (Schaetzl, 2002) and root activities and in turn improve their own living conditions. Musso et al. (2019) reported at S-PM a steady decrease in pH from about 6.5 at the youngest moraine to about 4 at the 10ka moraine. The dense growth of ericaceous shrubs was possibly favored by the cessation of grazing. Under low-pressure grazing *Rhododendron ferrugineum* has a selection advantage, as this species is avoided by live-stock due to its toxicity and can then spread more rapidly (Ellenberg, 1988; Treter et al., 2002; D'Amico et al., 2014). Especially *Rhododendron ferrugineum* is known to dominate subalpine landscapes and to out-compete other species, which can lead to vegetation covers up to 90-100% (Pornon and Doche, 1996). The species is also known to prevail especially on degraded/overgrazed soils (Costantini and Dazzi, 2013). The recovery of previously grazed areas likely results in an increased

vegetation cover with the spreading of already existing shrubs (Scherrer and Pickering, 2005). Due to the proximity to the local farm it is very likely that the 10ka moraine was formerly grazed by sheep and goats. Musso et al. (2020) reported trails in the slope, which point to previous livestock farming. The high organic matter production and the low pH-value of the highly conductive, sandy soil at the 10ka moraine favor podsolization. Unlike Musso et al. (2019), who described the soil at the 10ka moraine as an entic podzol, we found a podzol with a clearly developed eluvial (albic) horizon overlying an iluvial horizon (Fig. 5.17 in the appendix). A lack of the albic horizon was also observed, which explains different classifications by Musso et al. (2019), Musso et al. (2020), and Maier et al. (2020). The formation of podzol is also favored by the humid and cool-temperate climate in this area (Heikkinen and Fogelberg, 1980; Egli et al., 2001) and can lead to the formation of hard pan, which was present here at an early stage as solidified soil. At the calcareous parent material, the 13.5ka moraine showed a similar vegetation cover as the 4.9ka moraine. Both moraines are mainly covered with grass. The soil pH at the calcareous chronosequence does not change much over the millennia (mostly between 7 and 8, Musso et al. (2019)), since the carbonate-rich soil material buffers the organic and carbonic acids. Compared to the soil at the young moraines, a color change to a more brownish hue can be seen in the upper 50 cm of the old moraines, but weathering and soil formation are less profound compared to the old moraines on siliceous parent material (Musso et al., 2022). The soil material at greater depths still very much resembles the material of the young moraines.

5.4.2 Evolution of hillslope function and links to form

The relevant observations on soil development, vegetation cover and dominant flow components are summarized in Figure 5.14 and supplemented with information on the occurrence of surface and subsurface runoff during the sprinkling experiments by Maier and van Meerveld (2021a) and Maier et al. (2021). At the siliceous parent material we found a distinct transition in water transport processes over the first millennia of landscape evolution (Fig. 5.8-Fig. 5.12). The coarse textured young soil at the 30a moraine has a low water retention and high drainability. The water transport is dominated by fast vertical water movement. Only the plots located down-slope in close proximity to the glacial lake showed subsurface flow caused by near surface groundwater and let to saturation runoff during the sprinkling experiments. At the intermediate age classes the soil water storage capacity increases due to the reduction in grain sizes and organic matter accumulation. The water transport is mainly vertical and increasingly preferential in form of finger-like flow (Fig. 5.11) caused by surface structure and hydrophobicity (Hartmann et al., 2020a). Saturation runoff and lateral flow was observed but rarely occurred. At the oldest moraine of 10k years, surface and lateral subsurface flow as well as water storage in the organic surface layer play the dominant role in water redistribution (Fig. 5.10). Vertical water transport beyond the organic top layer in form of macropore flow along root fissures was observed, but contributes little to the water redistribution. Only a few flow paths that went beyond the organic layer were observed during the dye tracer experiments (Fig. 5.17).

The results are similar to findings by Lohse and Dietrich (2005) who found a transition from mainly vertical to lateral water transport processes between a 300-year-old Andisol and a 4.1 million-year-old Oxisol. Also Yoshida and Troch (2016) reported a transition of the major flow pathways from deep

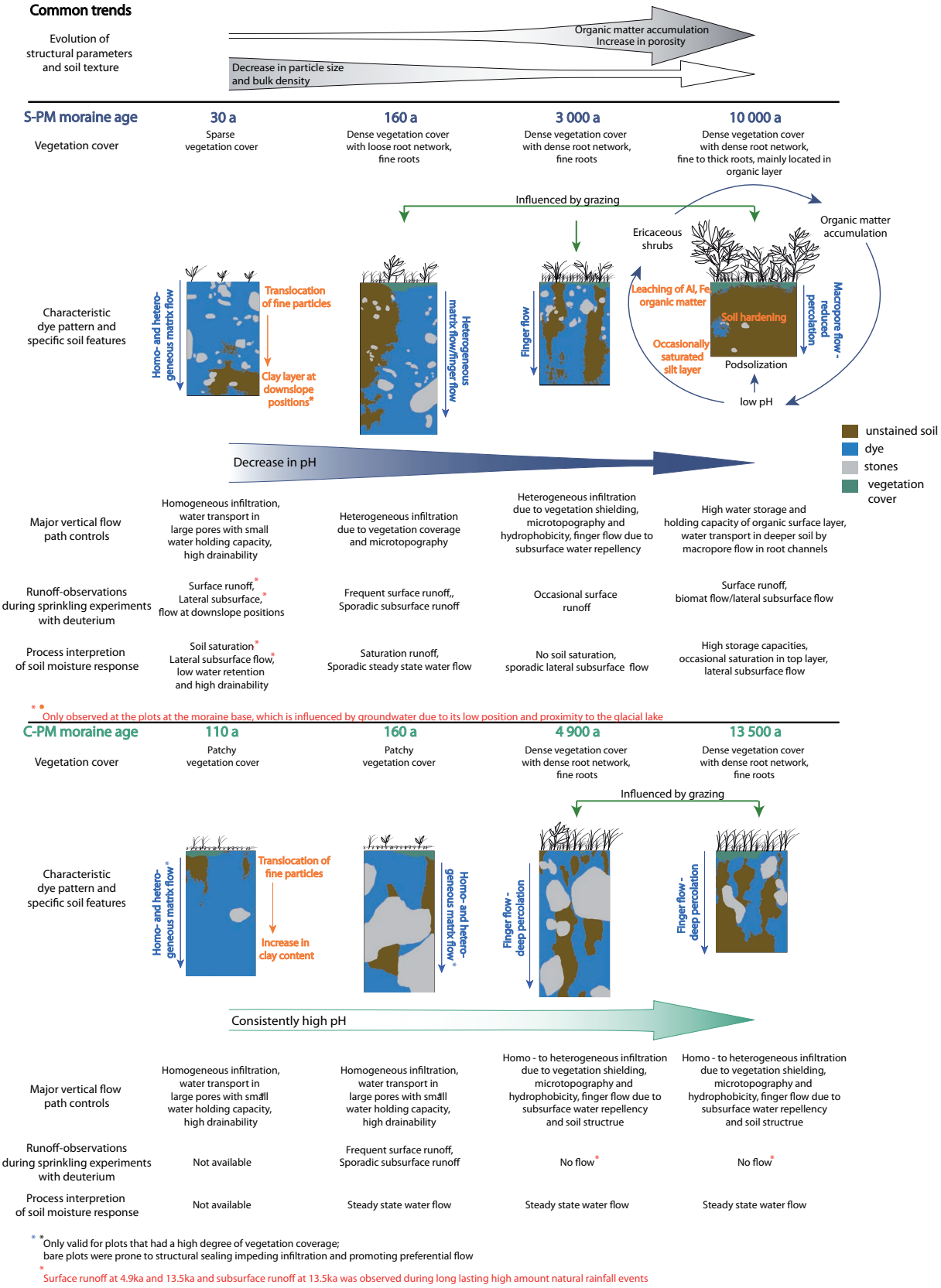

Figure 5.14: Sequence of observed vegetation characteristics, runoff observations, dye pattern characteristics and soil features (process and properties) along the chronosequences at S-PM and C-PM. Figure adapted from Hartmann et al. (2020b).

percolation to more shallow subsurface flow with increasing age of volcanic catchments. In contrast to the findings by Lohse and Dietrich (2005), the transition of major water flow paths from vertical to horizontal is not caused by the accumulation of clay particles. Lateral subsurface flow and biomat flow occurs due to the progressive accumulation of organic matter that initiates podsolization and the concomitant subsurface consolidation. Thus, at the 10ka moraine, the organic layer plays an important role in water redistribution. The high eco-hydrological significance of the organic horizon in alpine regions was also pointed out by Yang et al. (2014). The high water retention capacity of the organic layer captures large amounts of rainfall and prevents further percolation. This explains why surface runoff and lateral subsurface flow occurred only on the second or third day of irrigation (Table 5.5) together with deep percolation via preferential flow (Fig. 5.8). We assume that the first irrigation filled the storage of the organic layer to such an extent that the water input of the following days led to saturation runoff and to lateral subsurface runoff. As the hydraulic conductivity of organic soils is highly anisotropic with higher conductivities in the lateral than vertical direction (Beckwith et al., 2003; Chason and Siegel, 1986), lateral flow probably occurred in form of biomat flow within the organic layer and along the interface with the underlying less permeable soil material. The high water retention of the organic layer leads to a high water availability, which has a positive effect on the vegetation and thus in turn again on the organic matter content (Yang et al., 2009). This creates a positive feedback loop between soil moisture and organic matter content, which was primary set in motion by the low pH value and therefore delayed conversion of the raw humus in the siliceous material.

In contrast to the siliceous parent material, water transport processes did not change significantly in the first millennia of landscape development at the calcareous parent material. The water transport at all moraines is dominated by fast vertical water movement (Fig. 5.10). The water is transported mainly via matrix flow at the young moraines, which becomes more preferential in form of finger-like flow with increasing moraine age (Fig. 5.11). In the most cases, an equilibrium between infiltration and drainage was observed without saturation of the topsoil. Only at the 160a moraine, surface runoff was observed during the sprinkling experiments (the experiments were not conducted on the 110a moraine). Runoff at this moraine is probably caused by the dense stone cover but also structural sealing was observed, which partly led to a reduced infiltration capacity (Hartmann et al., 2022; Maier et al., 2021). The transport velocity decreased and the storage capacity increased from the young to the old moraines, which is caused by the decrease in particle sizes and increase in organic matter content. However, the development is not continuously with age. Storage properties are highest at the 4.9ka moraine followed by 13.5ka moraine and the lowest at the youngest moraine, which correlates with the organic matter content (Fig 5.6).

The distinct differences between the hydrologic response evolution in the two glacier forefields show that age alone cannot be used as a control variable to predict hydrological responses of ungauged landscapes as stated by Yoshida and Troch (2016). It is therefore advisable to consider the age of a catchment according to the concept of Troch et al. (2015), which defines the catchment age (here applied to hillslopes) as a function of the activity of the catchment forming factors (climate, geology and tectonics). Under nearly the same climate and tectonic history the activity of the calcareous geology, in driving the coevolution of vegetation, soil, and hydrologic response, seems to be lower compared to the siliceous parent material.

5.4.3 General links between hillslope form/structure and hillslope function

The identification of links between the hydrological response and structural features would allow for a first assessment of the hydrological response in ungauged landscapes using easily measured/observed variables. The "form-and-function dualism" in hydrology was previously discussed in e.g., Angermann et al. (2017), Fan et al. (2020), and Gnann et al. (2021). The success of a detailed assessment of the form and function relationship in heterogeneous environment depends on the observation scale (Angermann et al., 2017; Jackisch et al., 2017) as well as a proper selection of form variables and function signatures (Gnann et al., 2021). We tested whether the data set of our interdisciplinary study provides links between hillslope form and hillslope function. The form variables of our data sets are commonly used in environmental science studies (e.g., ecology, botany, geomorphology, geography). Although these variables are not necessarily related to a specific hillslope response, they can indirectly affect hillslope function and thus still serve as proxies for the hillslope response. For example the root variables (RD, RLD, SL) do not directly refer to the presence of a macropore network that can be activated (Fan et al., 2020), but the presence of roots can affect subsurface water transport and these variables are frequently measured by (geo-)ecologists and (geo-)botanists. Also above ground biomass is a frequently measured variable in environmental science, which does not directly relate to hydrological processes, but provides information about the presence of vegetation that for instance could influence the infiltration patterns. The saturated hydraulic conductivity, which is measured using soil samples or point measurements, is very heterogeneous and only integrated on a sub-scale and therefore not representative for larger scales (Jackisch et al., 2017). However, since it is often measured in hydrological studies, it is a proxie worth considering in this framework.

We derived general links by testing whether different clusters of hillslopes identified by these variables describing form or structure are also different in their hydrological response. To this end we carried out a cluster analysis of soil structure and vegetation/surface characteristics at each plot, independent of age and parent material. We found that a thick organic layer is linked to high storage properties and lateral subsurface flow. The comparatively high storage properties in cluster 4 (Fig. 5.13), which were identified by the longest reaction times, positive peak timings and largest storage increase, are linked to a high amount of organic matter content of various decomposition stages, which goes along with a high available water capacity. We confirmed the occurrence of lateral subsurface flow based on direct outflow measurements and local storage changes that go beyond the precipitation input. Similar findings were reported by Yang et al. (2014) who also found high storage capacities in the organic layer, together with lateral subsurface flow in alpine grassland.

In contrast, soil textural information alone is not found to be a good predictor of the hillslope hydrological response. The grain size distribution in cluster 4 is in a similar range as in cluster 1 (Fig. 5.18 in the appendix), but due to the high organic matter content in cluster 4 physical properties (porosity and bulk density) and the hydrological response are significantly different from cluster 1. The positive effect of organic matter on soil water retention is widely known (Rawls et al., 2003) and information on organic matter content is next to textural information already an essential feature within the hydrological characterization of soils (e.g., via pedotransferfunctions, Pachepsky and Van Genuchten (2011)). We also conclude that the type of organic matter is essential to predict its impact on the hydrologic response. Comparing cluster 2 and 3, the grain size distribution in cluster 3 is coarser (also lower porosity and higher

bulk density) and the organic matter content lower, but also the vertical saturated hydraulic conductivity is lower. Interestingly, the hydrologic response in cluster 3 shows more water storage and occasional lateral subsurface flow, whereas cluster 2 shows little water storage and mainly steady state vertical water transport. As already stated, in the derived organic matter content, we do not differentiate between living (e.g., roots) and dead (detritus or humus) organic matter. We assume based on observations in the field and the lower root density in cluster 3, that the main part of the organic substance in cluster 3 is made up of dead organic material. High proportion of dead organic material are known to have a decreasing effect on the saturated hydraulic conductivity (Demir and Doğan Demir, 2019; Jarvis et al., 2013), whereas the dense root network of the grassland vegetation in cluster 2 enhances infiltration by providing additional flow paths for water transport (Leimer et al., 2021).

General links between structural properties and the occurrence of lateral subsurface flow could not be identified. While the organic top layer is a good indicator for the occurrence of lateral subsurface flow in clusters 3 and 4, lateral subsurface flow observed in cluster 1 is driven by the hillslope position at the footslope. Lateral subsurface flow at the observation plots in this cluster was caused by a permanent shallow groundwater table. While we did measure lateral flow at the trenches of the irrigation plots we found that a relative maximum storage increase>100 % based on soil moisture measurements (Fig. 5.13) is a much more easily obtained indicator for lateral subsurface flow.

Our analysis also identifies a link between PFF and above ground biomass (Fig. 5.13) and at the same time we see that PFF increases with decreasing specific root length and saturated hydraulic conductivity (Fig. 5.18). The link between these variables might be related to our chronosequences design. To what extent these links also exist elsewhere requires further investigation. In our chronosequence study, we observed a transition from homogeneous unconsolidated coarse textured soil (cluster 1) to a layered soil system (cluster 2 to 4), which together with vegetation development leads to the formation of finger-like flow paths (cluster 2-3) and macropore flow (cluster 4). The above ground biomass, which decreases from cluster 1 to 4 is an indicator for the change in vegetation. The vegetation develops in clusters 1 to 3 from small pioneer plants to grassland (clusters 1 and 2) to herbaceous to shrub vegetation (cluster 3). Cluster 4 is dominated mostly by shrub vegetation. This development also influences the infiltration pattern, which becomes increasingly heterogeneous from cluster 1 to 4. With the type of vegetation cover, the root system also changes, which also has a major impact on PFF. The specific root length increases from cluster 1 to 4. High SRL values indicate root systems made up of long and thin roots, while smaller values indicate shorter, thicker roots. The pattern across the clusters matches the vegetation observation. The small pioneer plants in cluster 1 have very fine and long roots, which theoretically could form preferential flow paths (Ghestem et al., 2011), but their effect on water transport is small compared to abiotic factors (coarse textured soil). For the grass vegetation in clusters 2 and 3, the root network is already denser and the roots larger, which (among other factors) promotes the formation of finger-like flow paths. The shrub vegetation in cluster 4 primarily develops near-surface, woody roots. The high proportion of preferential flow is due to the small amount of water that preferentially infiltrates macropores beyond the organic layer. We conclude that in our chronosequence study the occurrence of preferential flow is closely linked to vegetation characteristics as above ground biomass and the architecture of the root system.

The saturated hydraulic conductivity is often used as an indicator in the context of land use/cover changes and the impact on hydrological flow paths such as overland flow and subsurface stormflow (Godsey and

Elsenbeer, 2002; Zimmermann et al., 2006; Archer et al., 2013; Tian et al., 2017). Higher saturated hydraulic conductivities are often related to the occurrence of water flow in macropores (Archer et al., 2013). In our study we observed an increase in PFF with decreasing saturated hydraulic conductivity. However, the magnitude of the hydraulic conductivity cannot be directly linked to PFF and is more of an indicator for the progression of weathering and soil formation processes that also lead to changes in the vertical subsurface flow paths. In clusters 1 to 3, finger flow is the dominant preferential flow type. The increase in the occurrence of finger-like flow paths from cluster 1 to cluster 3 is more related to the ongoing formation of defined soil layers through weathering processes and an increasing heterogeneous infiltration through the vegetation development. The only known relationship between saturated hydraulic conductivity and finger-like flow is the positive correlation between saturated hydraulic conductivity and finger width (Parlange and Hill, 1976), which is, however, irrelevant for PFF. Also, the saturated conductivity has not proven to be a reliable indicator for the occurrence of lateral subsurface and overland flow. There appears to be only a negative correlation between the amount of overland flow (if any) and the saturated conductivity. Similar to Jackisch et al. (2017) our analysis showed that for conclusively linking hillslope form and hillslope function both need to be evaluated in their own "context" and "spatial circumstances".

5.5 Conclusions

Our investigation of the evolution of hillslope form and function in two glacier forefields with different parent materials shows that chemical composition of the parent material affects the hydrological functioning. Soil pH seems to be the key variable that determines vegetation development, soil formation (hillslope form) and subsequently hydrology (hillslope function). The sites in our study are exposed to approximately the same weathering conditions. Although the calcareous material breaks down faster into finer-grained material, it is the acidic weathering of the siliceous material that results in a large accumulation of dead organic matter, which profoundly affects storage and transport properties by increasing the water storage capacity. Water redistribution is dominated by vertical subsurface water transport only at the two youngest age classes. Podsolization occurs at the siliceous parent material, sometime between 3000 and 10 000 years of landscape development. After 10 000 years of soil development water storage in the organic surface layer, lateral subsurface water transport and overland flow become the major components controlling water redistribution. At the calcareous site, the high pH-buffering capacity of the soil leads to less soil formation and fast, vertical subsurface water transport dominates the water redistribution even after more than 10 000 years of landscape evolution.

It is unclear whether the differences in hydrologic flow paths in turn impact the vegetation development. We assume that at the siliceous parent material, the increase in storage properties in the topsoil triggered a positive feedback cycle and that the increase in water and nutrient availability favored the settlement of ericaceous shrubs, which in turn have a positive effect on the storage capacity of the soil. At the calcareous parent material, on the other hand, important plant nutrients are likely to be leached and thus lost from the root zone. This limits the development of larger vegetation which could improve the storage capacity in the topsoil by organic matter production.

Our study showed that form and function develop differently on chemically different parent materials, making the parent material an important proxy for linking form and function. The partitioning into surface and subsurface lateral flows, but also the development of the subsurface vertical flow paths is clearly influenced by the material development, but also to a large extent by the accompanying vegetation development and soil formation, which significantly impacts the local water budget. We found that the interplay between geology, vegetation, and the occurrence of an organic surface layer are essential landscape features that are linked with the hydrological response and should be thoroughly considered when reading and interpreting the landscape to assess the hydrological functioning of ungauged areas.

The accelerated retreat of glaciers exposes more and more young alpine landscapes, which will undergo pronounced changes within a few decades and centuries. Our study will be helpful for decision makers to assess the hydrological development of these young landscapes. The benefit of our findings is, however, not only limited to the application in proglacial areas, but could also be used for the renaturation of degraded hillslopes. Incorporating our findings in landscape evolution models could improve the proper description of the hydrological response within these models. We would furthermore stress that we were only able to make these findings by collaborating closely across disciplines. We see this kind of interdisciplinary approach including joint data collection and interpretation as indispensable to assess developments of hydrological systems, especially in the context of climate change.

Appendix

Ratios of surface and subsurface runoff during the irrigation experiments

Table 5.5 shows the ratios of surface and subsurface runoff during the irrigation experiments with deuterium. Each plot at each moraine was irrigated for three days with three different irrigation intensities and deuterium-concentrations. The data shows that subsurface water transport processes dominate the transport processes at both forefields.

Table 5.5: Ratio of surface[a] and subsurface[a] runoff in % of the irrigation water for all three irrigation plots and intensity per age class at the S-PM and C-PM forefield. Data by (Maier and van Meerveld, 2021a) and (Maier et al., 2021).

	Plot 1					
	Irrigation day 1		*Irrigation day* 2		*Irrigation day* 3	
	Surface runoff ratio [%]	Subsurface runoff ratio [%]	Surface runoff ratio [%]	Subsurface runoff ratio [%]	Surface runoff ratio [%]	Subsurface runoff ratio
Moraine						
S-PM						
30a	0	0	0	0	4	0
160a	0	0	0	10	2	8
3ka	0	0	0	0	3	0
10ka	0	0	42	4	22	20
C-PM						
160a	3	0	7	0	11	0
4.9ka	0	0	0	0	0	0
13.5ka	0	0	0	0	0	0
	Plot 2					
	Irrigation day 1		*Irrigation day* 2		*Irrigation day* 3	
	Surface runoff ratio [%]	Subsurface runoff ratio [%]	Surface runoff ratio [%]	Subsurface runoff ratio [%]	Surface runoff ratio [%]	Subsurface runoff ratio
Moraine						
S-PM						
30a	11	44	11	81	6	92
160a	16	0	6	0	5	0
3ka	0	0	17	0	9	0
10ka	0	0	0	10	11	19
C-PM						
160a	0	0	10	0	5	3
4.9ka	0	0	0	0	0	0
13.5ka	0	0	0	0	0	0
	Plot 3					
	Irrigation day 1		*Irrigation day* 2		*Irrigation day* 3	
	Surface runoff ratio [%]	Subsurface runoff ratio [%]	Surface runoff ratio [%]	Subsurface runoff ratio [%]	Surface runoff ratio [%]	Subsurface runoff ratio
Moraine						
S-PM						
30a	8	78	11	32	11	55
160a	0	0	4	0	3	0
3ka	0	0	0	0	0	14
10ka	0	0	6	0	5	0
C-PM						
160a	6	0	4	0	5	1
4.9ka	0	0	0	0	0	1
13.5ka	0	0	0	0	0	0

[a] This data was compiled from and can be accessed via Maier and van Meerveld (2021b)

Calibration of the longitudinal dispersivity for one-dimensional water transport modeling

To model the water transport with HYDRUS-1D, the longitudinal dispersivity (D_L) was determined by manual calibration. For simplicity, D_L was assumed to be constant with depth. For the calibration, the model was executed with seven different values for D_L (0.1, 0.5, 1, 1.5, 3, 5, 10, and 15 cm). A visual comparison of the model output with the measured isotope profile (Fig. 5.15 and 5.16) was used to identify the best fit. The resulting longitudinal dispersivities are listed in Table 5.6. D_L decreases with increasing moraine age. Moraines at the siliceous parent material have lower dispersivities than at the calcareous parent material.

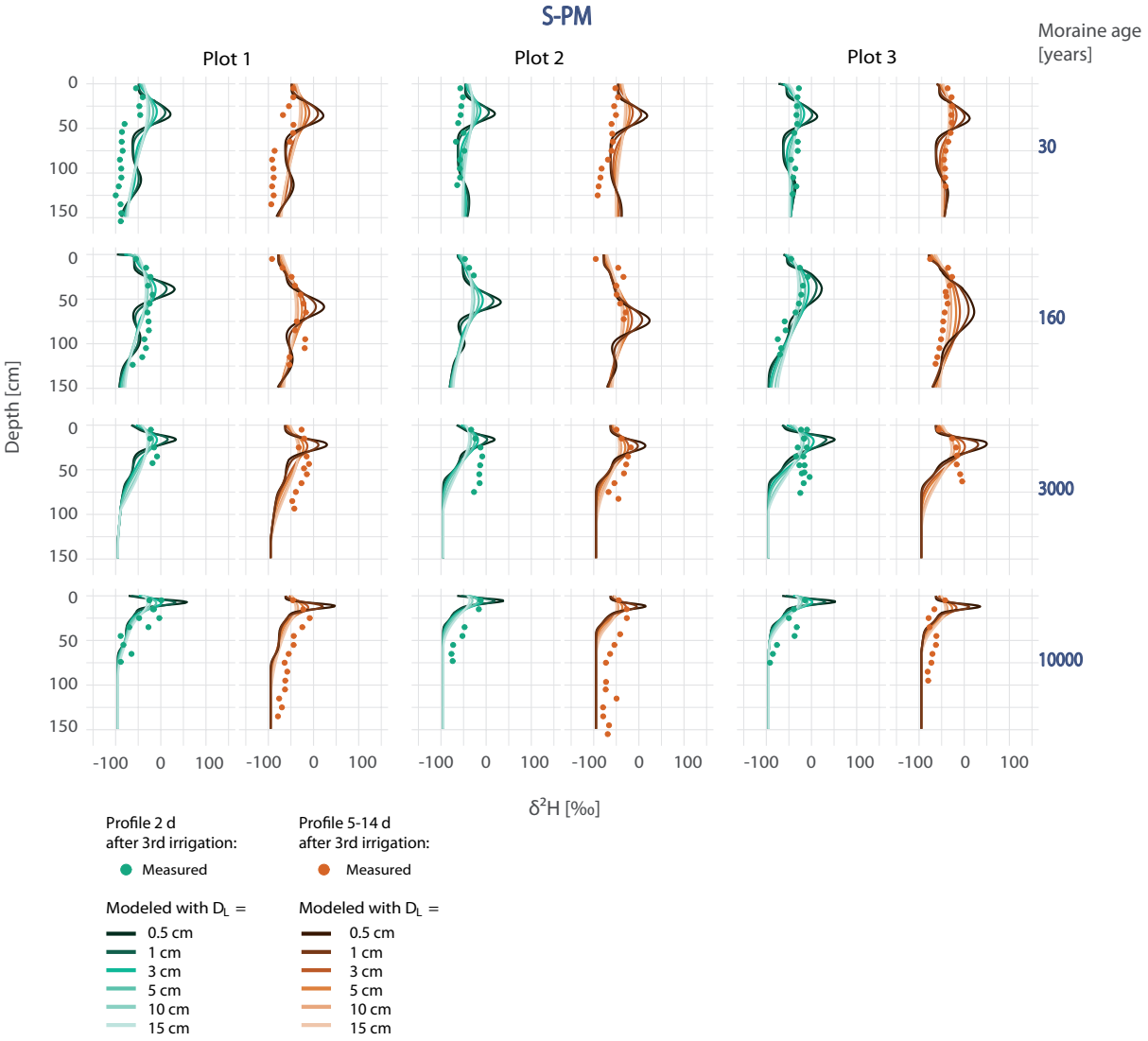

Figure 5.15: Manual calibration of the longitudinal dispersivity (D_L) for the siliceous parent material. Displayed are modeling results of the δ^2H-profiles with seven different values for D_L (0.1, 0.5, 1, 1.5, 3, 5, 10, and 15 cm) compared to the field observations. A visual validation was used to estimate which order of magnitude of D_L is most realistic for the δ^2H-transport. Modeling results and observations of the profiles taken two days after the third irrigation are displayed in green shades. Orange shades show the modeling results and observations of the profiles taken 5-14 days after the third irrigation.

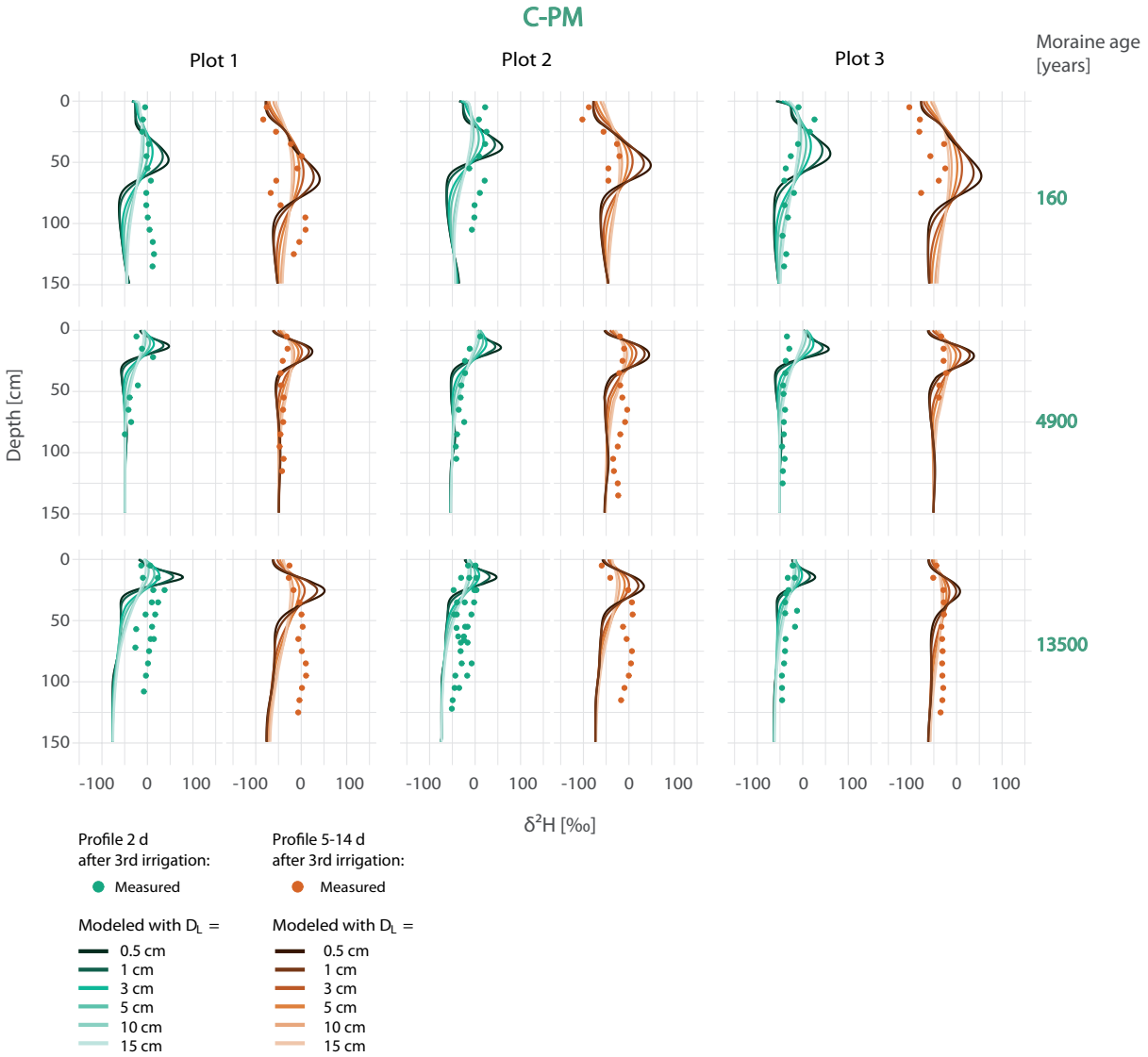

Figure 5.16: Manual calibration of the longitudinal dispersivity (D_L) for the calcareous parent material. Displayed are modeling results of the δ^2H-profiles with seven different values for D_L (0.1, 0.5, 1, 1.5, 3, 5, 10, and 15 cm) compared to the field observations. A visual validation was used to estimate which order of magnitude of D_L is most realistic for the δ^2H-transport. Modeling results and observations of the profiles taken two days after the third irrigation are displayed in green shades. Orange shades show the modeling results and observations of the profiles taken 5-14 days after the third irrigation.

Table 5.6: Dispersion coefficients at S-PM and C-PM estimated by visual calibration.

S-PM		C-PM	
Age	D_L [cm]	Age	D_L [cm]
$30a$	10		
$160a$	7	$160a$	15
$3ka$	5	$4.9ka$	10
$10ka$	3	$13.5ka$	5

Photographs of typical flow patterns at each age class

Figure 5.17 shows examples of the observed subsurface flow paths highlighted by blue dye at the four moraines at the siliceous (S-PM) and calcareous (C-PM) parent material. The soil classification according to the World Reference Base for Soil Resources (IUSS Working Group WRB, 2014) was done by Musso et al. (2019), Musso et al. (2020), and Maier et al. (2020) at the same moraines, but different soil pits. Unlike Musso et al. (2019), who described the soil at the 10-year-old moraine as an entic podzol, we found a podzol with a clearly developed eluvial (albic) horizon overlying an iluvial horizon. The soil below the eluvial horizon was solidified and only a few single roots and flow paths were observed in this depth during the dye tracer experiments.

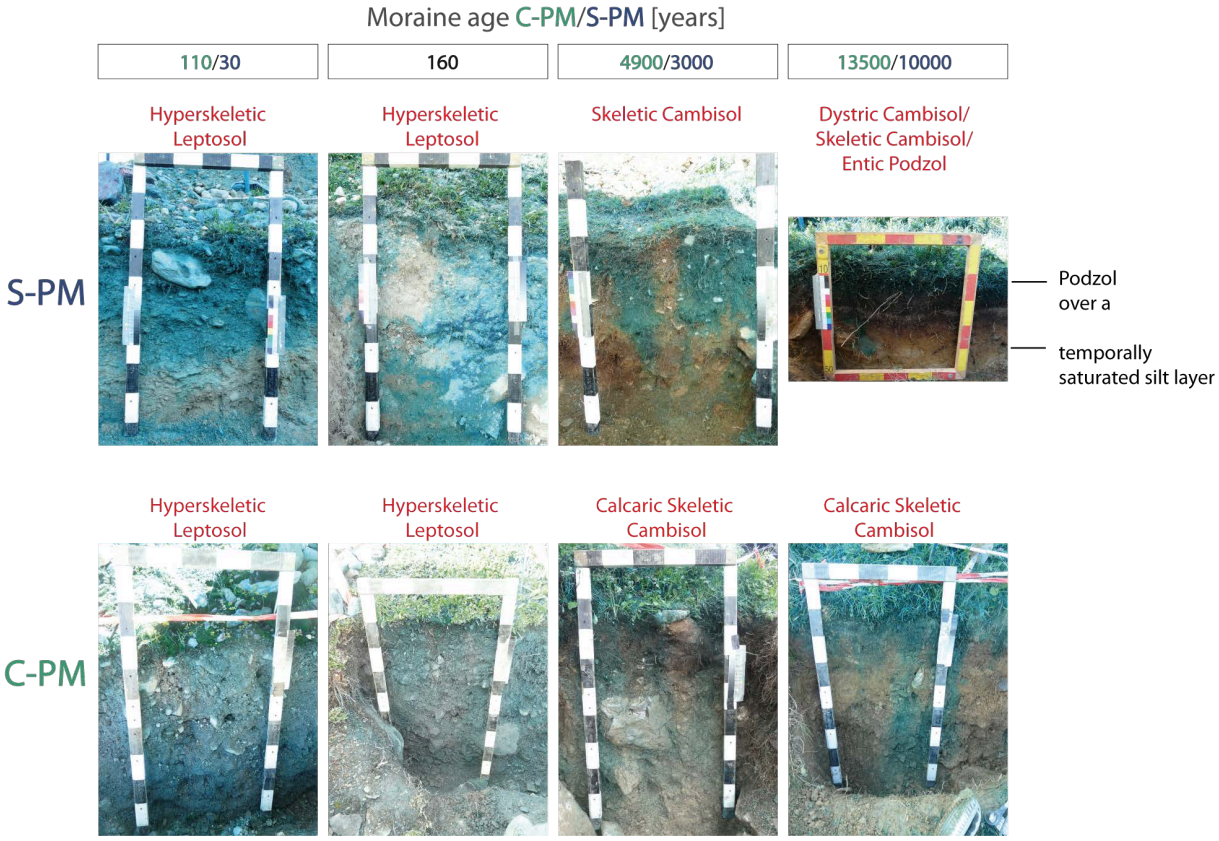

Figure 5.17: Examples of the observed subsurface flow paths highlighted by blue dye at the four moraines at S-PM and C-PM. In red: the WRB (IUSS Working Group WRB, 2014) soil classification (Musso et al., 2019, 2020; Maier et al., 2020). Black: Additional observations during the profile excavations. The length of each segment of the wooden frame equals 10 cm.

Distribution of soil properties and surface characteristics within each cluster

The clusters in section 3.1.2 were determined based on a prior principal component analysis of the set of form variables (soil surface properties, surface characteristics and vegetation characteristics). Figure 5.18 shows the distribution of each of these characteristics within each cluster. PFF (Fig. 5.13), above ground biomass (BM), specific root length (SRL), and saturated hydraulic conductivity (Ksat, Fig. 5.18) show a similar distribution pattern across the clusters (with SRL and Ksat showing an inverse distribution).

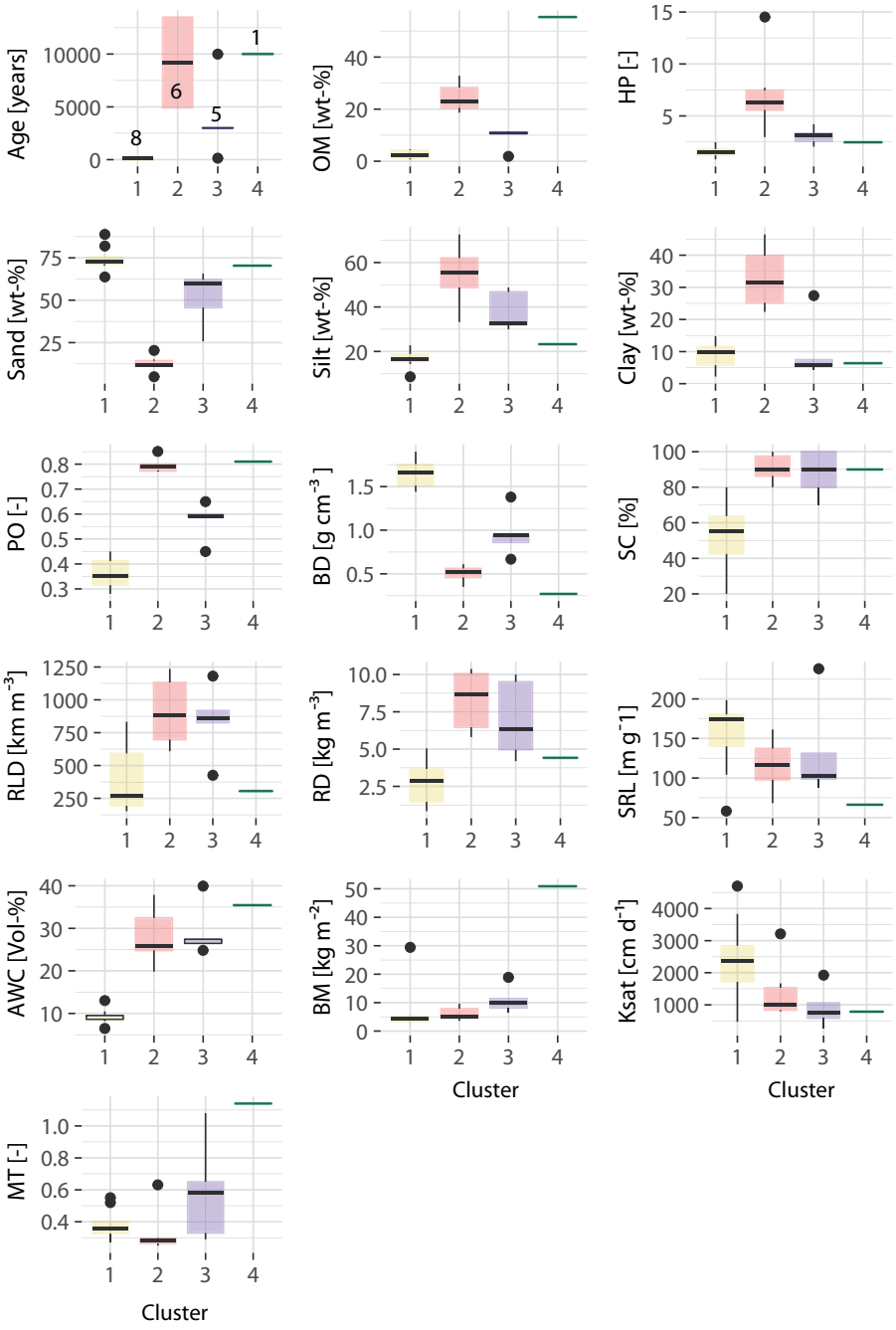

Figure 5.18: Boxplots showing the distribution of age, soil properties at 10 cm depth, and surface/vegetation characteristics within the four clusters. Clusters were derived based on a principal component analysis using the shown soil properties and surface/vegetation characteristics. An explanation of the abbreviations is given in Table 5.4.

6 Synthesis

The four studies significantly contribute to advancing our understanding of the processes within the hillslope feedback cycle. To demonstrate their contribution to the overall objective and address the main questions, the studies are discussed in terms of: i) the impact of geology on the evolution of hillslope structure and hydrological response, ii) the development of (preferential) subsurface flow paths within the hillslope feedback cycle, and iii) potential links between hillslope structure and hydrological response, which are particularly relevant for understanding and predicting future hillslope hydrology under the influence of global change.

6.1 Geology as a driving factor of the hillslope feedback cycle

Comparing the coevolution of hillslope structure and hillslope hydrological response in two very different geologies allows analyzing the general impact of the parent material on the hillslope feedback cycle. Climate and tectonics are also recognized as crucial external factors influencing catchment/hillslope evolution (Troch et al., 2015). To solely investigate the impact of geology, the other driving factors must be excluded. For this purpose, two chronosequences of glacial moraines in the Swiss Alps were selected and compared. These chronosequences were located in similar climatic regions with nearly identical tectonic histories over the past ten millennia but developed from two very different parent materials (siliceous versus calcareous). The comparison of both parent materials reveals distinct differences in hillslope structure, vegetation characteristics, soil properties, and hillslope hydrological response after an initial period of 10 000 years of landscape evolution.

6.1.1 Different susceptibility to weathering affects soil structure and hydraulic properties

The data presented in Chapter 2 offers a comprehensive understanding of the evolutionary changes in physical and hydraulic properties of soils derived from siliceous and calcareous glacial till over the initial ten millennia following the glacier's retreat, contributing valuable insights into landscape evolution. The trend in soil structure, including reductions in grain size and effects on porosity and bulk density within the first 100 years of soil development in both parent materials, aligns with observations in the literature (He and Tang, 2008; Dümig et al., 2011; Vilmundardóttir et al., 2014).

The data set reveals distinct differences in the evolution of soil structure between the two parent materials over the span of 160 to 10 000 years of landscape evolution. The calcareous material weathers into finer-grained material, whereas the siliceous material develops a stronger organic surface layer. An important discovery was that, despite the finer soil texture, water retention at the older age classes was lower in the calcareous soils compared to the siliceous soils. While the carbonate content of calcareous soil might reduce water retention by coating clay particles (Khlosi et al., 2013), the retention curves reveal unusually high water retention in the siliceous parent material. The retention curves for the oldest calcareous moraines match the measured grain size distributions of a silty soil, while the retention curves

for the oldest siliceous moraines indicate a clayey to loamy-silty soil, despite a high proportion of sand. The comparison of the retention curves with the data on organic matter leads to the conclusion that the siliceous soil's high water retention is attributed to a substantial proportion of dead organic material. It is widely recognized that highly organic soils exhibit distinct soil hydraulic properties, characterized by an increased water retention capacity compared to mineral soils (Carey et al., 2007).
The differences in soil structure and subsequently soil hydraulic properties between the two parent materials, found in Chapter 2, arise from differences in weathering processes and their products. The dark color of the calcareous material likely makes it more susceptible to insolation weathering. However, as limestone is more susceptible to chemical weathering by carbonic acid formed through the dissolution of carbon dioxide in rainwater, the main weathering process at the calcareous site is carbonate leaching. The calcium carbonate content provides the calcareous glacial till with a high buffer capacity against acids, leading to a modest decrease in soil pH over the millennia, while the soil formed from siliceous glacial till showed a strong decrease in pH (Musso et al., 2019). Acidification and weathering of primary minerals are the main processes at the siliceous site (Musso et al., 2022). Thus, soil pH appears to be a key variable indicative of differences in the coevolution of soil, biota, and water transport between the two parent materials.

6.1.2 Differences in soil pH indicate differences in the hydrological response over the long term

The findings presented in Chapter 5 reveal significant differences in the hillslope hydrological response between the two parent materials after a period of 10 000 years of landscape evolution, attributed to differences in the (chemical) weathering processes. These differences in weathering processes, indicated by differences in soil pH, affect vegetation development, soil formation, and subsequently water transport. The acidic weathering of the siliceous material (Musso et al., 2019) favors the settlement of acid-loving (ericaceous) shrubs, which produce litter with difficult-to-decompose substances like lignin, cellulose, and phenolic compounds (D'Amico et al., 2014; Pornon and Doche, 1996). The slower decomposition rate of shrub vegetation (Musielok et al., 2021) leads to a high proportion of mor humus in the organic top layer. Consequently, the organic carbon stock at the old siliceous moraine is more than twice as high compared to the old moraines at the calcareous site (Musso et al., 2022). However, it remains unclear whether the dense growth of ericaceous shrubs is solely attributable to the pH value or whether the gradual colonization of ericaceous shrubs, along with the associated increased accumulation of organic matter, has improved the living conditions of shrubs and facilitated their further settlement. The organic topsoil, with its special hydraulic properties, plays a significant role in water redistribution and is of great eco-hydrological importance in alpine regions (Yang et al., 2014). The accumulation of dead organic matter, as already mentioned, profoundly impacts storage properties by increasing soil water retention (Chapter 2) and, consequently, water storage capacity (Chapter 5). The enhanced water availability has a positive effect on vegetation, which in turn feeds back to the organic matter content (Yang et al., 2009). This interplay results in a positive feedback loop between soil moisture, vegetation, and organic matter content.
Interestingly in contrast to the retention curves, the hydraulic conductivity curves of the siliceous soils at

the oldest moraines resemble the progression of a sandy soil, displaying a high (vertical) conductivity near saturation and a sharp decline with increasing soil water tension (Chapter 2). These findings support the high water storage found in Chapter 5 by hinting that under unsaturated conditions infiltrating water is primarily stored in the large pore space of the organic layer and vertical downward percolation mainly occurs when nearly saturated conditions are reached. Organic soils are known for their anisotropic behavior, exhibiting higher conductivities in the lateral than vertical direction (Beckwith et al., 2003; Chason and Siegel, 1986). This might be one of the main causes of reduced infiltration depths and the occurrence of lateral flow observed at the oldest siliceous moraine (Chapter 5).
The combination of sandy material, high organic matter content, and acidic conditions at the siliceous moraines results in the formation of soluble organic acids and their transport deeper into the soil, where they form complexes with aluminum and iron, leading to podsolization and hardening of the soil in deeper layers between 3000 and 10 000 years of landscape development. The accumulation of organic matter and the ongoing podsolization process fundamentally affect the hydrological hillslope response (Chapter 5). At the oldest age class of the siliceous site, water redistribution is governed primarily by water storage in the organic surface layer, lateral subsurface water transport (biomat flow) (Maier et al., 2021), and overland flow (Maier et al., 2021). Conversely, at the younger age classes, vertical subsurface water transport dominates water redistribution. In contrast, at the calcareous site, soil formation is less extensive, with a predominantly grass-covered vegetation and fewer shrubs. Rapid vertical subsurface water transport continues to dominate water redistribution, even after more than 10 000 years of landscape evolution.
Although soil pH appears to be a significant factor driving differential landscape development between the two parent materials, other aspects affecting vegetation development may also play essential roles. This study ignores the important aspect of nutrient availability that results from weathering of the parent material. Nutrient availability is an important factor in vegetation development, which can also be influenced by soil pH. The nutrients and pH levels necessary for optimal vegetation growth also depend on the vegetation species. Regardless, the findings in Chapter 2 and 5 lead to the conclusion that the chemical composition of the parent material plays a major role in driving the hillslope feedback cycle in alpine climate conditions.

6.1.3 Do the two geologies age differently?

The observed disparities in the hydrological response across the geologies indicate that geological age alone cannot be utilized as a controlling factor for predicting the hydrological response in ungauged landscapes. Troch et al. (2015) introduced the concept of the 'hydrological age', aiming to enhance hydrological predictions within the context of dynamic environmental landscapes. This concept shifts the assessment of landscape age from geological ages to an age classification that depends on the activity of catchment/hillslope forming factors, including geology, climate, and tectonics. The disparity in the hydrological response between the observed system state and the initial system state is used as a measure for the (relative) hydrological age. Using this concept, it was discovered that despite the lower geological age of the oldest siliceous moraine (10 000 years), its hydrological age surpasses that of the oldest calcareous moraine (13 500 years). The hydrological response found in Chapter 5 exhibits a significant divergence between the youngest and the oldest moraine at the siliceous site, whereas at the calcareous

site, the disparities in the hydrological response between the young and old moraines are less distinct. With other driving factors nearly eliminated, differences in hydrological age are attributed to varying activity levels of the parent material driving coevolution. The activity level of the siliceous parent material is therefore higher than that of the calcareous parent material. The higher chemical weathering rates of the siliceous parent material (Musso et al., 2022) are an indicator for its higher activity level (Troch et al., 2015). However, the activity level of geology is not completely independent of the other driving factors. The occurrence of podsolization in the siliceous material is largely attributed to the cool and humid climate, which favors the accumulation of organic matter and the translocation of organic acids. Comparing both geologies in different climatic settings may lead to diverse results and activity levels of the parent material.

6.2 The role of subsurface (preferential) water flow within the hillslope feedback cycle

6.2.1 Subsurface flow processes dominate water transport in both glacier forefields

Despite a decrease in saturated hydraulic conductivity with age (Maier et al., 2020; Maier and van Meerveld, 2021a), it was found that surface runoff at both sites only occurs due to saturation excess or ex-filtration, even under high irrigation intensities. Notably, surface runoff was rarely observed at the calcareous chronosequence. This information combined with the results in Chapter 5 showed that lateral and vertical subsurface flow play the most important role in water redistribution at both geologies. Soil genetic processes such as podsolization and decalcification or transport processes are largely controlled by subsurface flow paths. Water transport in the calcareous material is predominantly vertical, whereas lateral flow was observed at the older moraines at the siliceous site (Chapter 5). Throughout the evolution of the hillslope feedback cycle, the direction and type of flow are influenced by material weathering and vegetation development, while in turn, weathering and vegetation development are affected by flow paths.

6.2.2 Interactions between subsurface flow paths, soil development, and vegetation characteristics change during coevolution

The results of the irrigation experiments with blue dye in Chapter 3 and 4 revealed a transition from homogeneous/heterogeneous matrix flow to more preferential flow with increasing moraine age at both geologies. This transition closely coevolves with pedogenic and biotic processes. The observed heterogeneous/homogeneous matrix flow at the young moraines at both geologies is characteristic for leptosols (Jarvis et al., 2012). The coarse textured soils with almost no profile layering and limited vegetation cover offer little opportunity for inhomogeneous infiltration patterns or building of preferential flow paths. At these age classes, water is transported downwards quickly and water flow paths are solely defined by the soil texture. The fast vertical water and nutrient transport influence the root system of early colonizers, which develop far-reaching root systems of fine roots to ensure rapid water and nutrient uptake (Greinwald et al., 2021a). The rapid resource acquisition is achieved by investing little energy into

the development of a stable root system and the quick development of long and thin roots. The thin and elongated roots of the pioneer vegetation have minimal impact on the flow paths as they neither block pore space nor create new pathways in the coarsely textured substrate.

For the youngest age class, the observations of the root distribution in Greinwald et al. (2021a) deviate from those presented in Chapter 3. In Chapter 3, it was observed that the root distribution was concentrated in the upper 15 cm of the soil, which contrasts with the findings in Greinwald et al. (2021a), where the presence of fine roots extending deeper into the soil was documented. While the root analysis in Greinwald et al. (2021a) is a laboratory-based assessments of core samples, encompassing both coarse and fine roots, Chapter 3 shows purely visual observations during profile excavations, primarily capturing prominent coarse roots. As fine roots in the young age class do not significantly affect flow paths, the additional information on the fine root distribution does not significantly impact the assessments made in Chapter 3.

Findings from Chapters 3 and 4 highlight that pedogenesis and vegetation development significantly influence the further evolution of flow paths with age. At the younger cambisols of the intermediate age classes (3000 years/4900 years), weathering processes created layers of fine-textured soil lying above layers of coarse-textured soil, resulting in the formation of finger-shaped flow paths at the material boundaries. Additionally, the increase in organic matter content, hydrophobicity, root length density, and above ground biomass were also identified as influencing factors in the increase in finger-like flow paths with increasing soil age (Chapter 4). Vegetation succession resulting in a heterogeneous surface cover favors the formation of finger-like flow paths at the soil surface (Chapter 3). In addition to changes in flow type, the ongoing weathering processes and organic matter accumulation improved storage properties in the topsoil (Chapter 5). This change in water redistribution feeds back to the vegetation development. The enhanced water (and nutrient) supply allows plants to invest more energy into the stability of the root system by creating stronger roots in the topsoil and thus attracts plants with a higher water demand. This effect was observed by an increase in the root mass proportion in the upper 30 cm of the soil (Greinwald et al., 2021a).

The distinct differences in (preferential) flow paths observed at the oldest moraines in Chapter 3 and 4 provide valuable insights into how water flow paths are influenced during coevolution by different components of the hillslope feedback cycle. The findings in Chapter 4 reveal that at the calcareous parent material, the primary direction of water flow remains vertical. Despite strong changes in hillslope structure, lateral subsurface runoff was not observed (Maier and van Meerveld, 2021a). The subsurface flow pattern at the oldest moraine appears similar to that of the intermediate age class and is dominated by preferential flow, mainly in the form of finger-shaped flow paths (Chapter 4). Additionally, the vegetation cover does not change distinctly between the ages of 4900 and 13 500 years. The heterogeneous distribution of water may result in a heterogeneous availability of plant nutrients. The rapid and vertical water transport, combined with insufficient nutrient availability within the calcareous parent material, might hinder the establishment or prevalence of larger vegetation in this area. However, this assumption lacks supporting data on plant nutrition.

Findings in Chapter 3 and 5 revealed that at the siliceous parent material, the fast, vertical water transport in the sandy soil facilitated a fast transport of chemical complexes from the organic top layer into the soil, initiating the podsolization process. The acidic conditions resulting from the weathering of the parent material allowed the dissolution of humic substances, aluminum and iron compounds (sesquioxides) in

the soil water, transporting them to deeper layers (podsolization). With the continued hardening of the subsoil (due to precipitation of the dissolved substances) and the accumulation of a thick organic top layer, water storage and the proportion of lateral subsurface water flow increased. The strong organic matter accumulation probably results from a feedback cycle between acidic soil conditions, vegetation in the form of acid loving and litter producing shrubs, and water storage properties of the organic top layer (Chapter 5). Lateral subsurface flow (biomat flow) and water storage in the organic top layer were identified as the dominant water transport processes (Chapter 5). Vertical water transport beyond the organic top layer was mainly restricted to macropores. However, macropore flow played only a subordinate role in water redistribution. The occurrence of macropore flow is generally not very common in podsols (Jarvis et al., 2012). Moreover, the proportion of observed roots reaching beyond the organic top layer into the solidified subsoil was minimal, with more than 90 percent of the root mass concentrated within the top 30 cm of the soil (Greinwald et al., 2021a).

The significant factors contributing to podsolization at the siliceous site include rapid vertical water transport, a cool and humid climate, the accumulation of organic matter, and acidic soil conditions. Although the first two factors are also applicable to the calcareous site, the differences in flow path evolution arise from the variations in soil pH resulting from the weathering of different parent materials. Both studies have demonstrated that the evolution of subsurface flow paths within the hillslope feedback cycle is characterized by complex interactions with pedogenic and biotic processes. The studies provide previously unavailable observations of this development. The similarity in flow path evolution within the first hundred years and the marked differences after several thousand years suggest that age becomes less important, while geology becomes a more influential factor in the evolution of flow paths as the hillslope feedback cycle evolves. To accurately project the evolution of flow paths, it is imperative to consider the boundary conditions, including the parent material, climatic conditions, and the type of vegetation prevalent under these conditions.

6.3 The identification of links between hillslope structure and hillslope response

By identifying general links between hillslope structure and hillslope hydrological response, it becomes possible to assess the hydrological response in ungauged landscapes based on easily observable structural information. Additionally, such connections enable estimations of changes in the hydrological response by observing changes in structural information resulting from external boundary conditions, such as climate change or changes in land cover and use.

The analysis in Chapter 5, linking response signatures to clusters of structural properties, highlights the challenges of identifying specific links between hillslope structure and hydrological response within the hillslope feedback cycle. The links found are often a combination of various physical and biological soil properties, as well as vegetation characteristics. However, the success of identifying a relationship between hydrological response and structure also depends on selecting appropriate structure variables and response signatures (Gnann et al., 2021). In this study, variables were deliberately chosen for their ease of measurement and common usage in environmental science studies (e.g., ecology, botany, geomorphology,

geography). While other structural variables may provide a more direct correlation between structure and hydrological response, they might not meet the study's objective of using easily measurable or common variables.

The strongest link found was that the accumulation of dead organic matter positively influenced the soils' storage properties. The accumulation of organic matter can increase the storage capacity of a soil, in that even soils with a coarser texture can have better storage properties than soils with a finer texture. The presence of a thick organic layer also appeared to correlate with lateral subsurface flow occurrence (Chapter 5). A strong organic layer gives first hints at storage properties and flow directions in ungauged landscapes. Therefore, it is important to consider the build-up or loss of soil organic matter when predicting the hillslope hydrological response under the impact of global change.

The controls on the soil susceptibility to preferential flow could only be examined regarding the steady increase in finger-like flow paths. It was observed that microtopography, texture, and root activity influenced flow path formation. As these factors act simultaneously, it is challenging to isolate a single key factor and quantitatively describe its influence. A relation between preferential flow fraction and above ground biomass (positive correlation) and specific root length (negative correlation) was also observed, but could only be verified within the context of the chronosequence study (Chapter 5). The hypothesis that a high above-ground biomass is associated with a high preferential flow fraction outside the chronosequence study appears plausible, given that larger vegetation builds a stronger root system, thereby causing preferential flow patterns. However, the general validity of this connection would still have to be evaluated. The findings from Zheng et al. (2021) already indicate the opposite. Their results indicate that with strong preferential flow patterns, the vegetation has to put more energy into the development of the roots for an adequate water and nutrient supply, which is at the expense of the above ground biomass. This illustrates the complexity of the interplay between vegetation and subsurface water flow paths, which makes the derivation of direct links between vegetation indicators and the hydrological response, especially in the form of the extent of preferential flow, extremely challenging.

Even though this study did not provide significant insights into direct links between hillslope structure and hydrological response that were not already known in the literature, the approach of assessing the hydrological response based on landscape characteristics remains crucial.

6.4 Consequences for the future assessment of hydrological systems under change

There is no question that, for future hydrological predictions under the impact of global change, the system components cannot no longer be regarded as static (Sullivan et al., 2022). According to Sivapalan (2018), catchments (including hillslopes) should be regarded as complete ecosystems, where the emphasis shifts from solely hydrological processes to encompassing all land surface processes that interact and mutually influence one another. This holistic approach is essential for a comprehensive understanding of hydrological processes and for enhancing hydrological predictions. The hydrological response thus should be seen as the result of two interconnected processes: the movement of water itself and the modifications to the surrounding environment (Sivapalan, 2018). These changes in the environment are brought about

by the coevolution of geomorphological, biological, pedological, and hydrological processes in response to the climatic and geological boundary conditions. To meet these requirements, the complexity of catchment coevolution (including the hillslope feedback cycle) must be better understood. This study, along with other studies (Schoonejans et al., 2016; Paez-Bimos et al., 2023), contributes to the discussion by elucidating the interactions among the distinct components of the ecosystem.

van der Meij et al. (2018) outlined the requirements for improving hydrologic modeling in soil landscape evolution models in order to accurately describe the coevolution of all feedback cycle components. While some challenges related to model architecture, such as integrating processes operating on various time scales, remain to be addressed, this study significantly contributes to our understanding of the evolution of soil hydraulic parameters and the soil hydrological response over time. This comparative study of two different geologies led to first insights into the coevolution of vegetation, soil, and hydrology under the given climatic conditions and geologies. The clear differences in the hillslope feedback cycle between the two geologies have demonstrated how important it is for a comprehensive gain of knowledge to carry out further studies across gradients of climate and in different geologies (Sivapalan, 2018). Only by understanding the influence of external factors, such as climate and geology on the complex network of interactions within the coevolution, can we make reliable statements about the future hydrology of landscapes under the impact of global change.

Breaking down important relationships between structure and response to a simple description of links using easily measured/observed variables would be helpful for future model-based assessments of the hydrological response in ungauged landscapes or to roughly predict changes in the hillslope hydrological response by observing changes in the hillslope structure. However, in Chapter 5, it became clear that these kinds of links are not as obvious or easy to detect, and furthermore, cannot be derived without evaluating the hillslope structure and hydrological response in their own context and spatial circumstances (Jackisch et al., 2017), e.g., their history of coevolution. This does not imply that the identified connections, such as the accumulation of biomass and enhanced storage properties or the soil susceptibility to preferential flow resulting from diverse factors, are not valuable and could not be used for the hydrological assessment of ungauged landscapes. Further comparative studies would be beneficial to assess the significance of possible links. Studies aiming to identify specific links between hydrological response and structure (Archer et al., 2013; Tian et al., 2017) contribute significantly to our understanding of individual interactions within the hillslope feedback cycle. This would also enhance our comprehension of the hydrological evolution of landscapes under change, provided that the findings are evaluated and applied within their respective contexts and spatial circumstances.

6.5 Conclusion and Outlook

The presented thesis on the coevolution of hillslope structure and hillslope response provides an improved understanding of how landscapes in the alpine region develop after exposure to glacier retreat. The studies within this thesis are the first to analyze the flow path evolution as part of the hillslope feedback cycle in detail. By comparing two contrasting geologies, it was demonstrated how the composition of the parent material affects the evolution of the hydrological response and its interaction with biotic and pedogenic processes. The siliceous parent material was found to have a higher activity level in driving the coevolution under alpine climatic conditions than calcareous parent material. Soil pH resulting from chemical weathering of the parent material was discovered as a key variable affecting soil development and hydrological response, indicating that parent material composition plays a vital role in landscape evolution under humid conditions. However, the results of the investigation in the alpine region cannot generally be transferred to other areas, as the activity of underlying geology as a landscape-forming factor can be influenced by different climatic conditions.

With advancing age development, the formation of subsurface flow paths is clearly determined by the interactions between geology, soil, and vegetation. The observed disparities in the type and direction of subsurface flow paths across the geologies indicate that age cannot be utilized as a controlling factor for predicting the hydrological response in ungauged landscapes. It was found that age becomes less important and geology gains more significance in the evolution of the flow path as the hillslope feedback cycle evolves. The interactions between biotic, pedogenic, and water transport processes are complex. Determining the order of causal relationships and interactions is extremely challenging, as the components of the hillslope feedback cycle interact within a complex and intertwined network.

In this context, deriving specific links between hillslope structure and hillslope response is valuable. Although various factors influencing the hydrological response appear to be intertwined, and it was not feasible to identify direct links, it became evident that the hydrological response coevolved with soil characteristics such as texture, structure, organic matter content, and surface characteristics such as microtopography, vegetation cover, root activities, and hydrophobicity. This not only affected the formation of preferential flow paths, but also the direction of subsurface flow paths.

The study did not cover all aspects of the hillslope feedback cycle. An important aspect that has not been addressed in this context is the evolution of nutrient availability, which results from weathering of the parent material and hydrological flow paths and affects vegetation development. Considering nutrient availability would have broadened the understanding of the mutual interactions between geology, vegetation, and water transport.

Predicting the development of the hydrological response of landscapes, catchments, or hillslopes in the face of global change is a significant challenge. It is crucial to intensify our understanding of how hydrological systems, including their structure and response, will react to changes in boundary conditions. The complexity of the hillslope feedback cycle emphasizes the importance of interdisciplinary approaches and the need to intensify studies involving multiple experts. This study makes an important contribution to closing the gap in observations of the dynamics of pedologic and hydrologic properties and processes, necessary for calibrating and validating models to predict soil-water-landscape relationships under changing conditions. Nonetheless, owing to the diverse range of climatic conditions and geologies,

this study alone is insufficient. Only through an ensemble of numerous studies, including comparative studies, chronosequence studies (like this one), and results from observatories, covering a wide range of geologies and climatic conditions, can we gain a deeper understanding of the coevolution of hydrological systems.

Bibliography

© Google Maps: Stone Glacier Map, 3863 Gadmen, CH, Google Maps, April 2020, maps.google.com. (Pictures 2020 Flotron/Perinjaquet, Maxar Technologies, Maps), last access: 12 April 2020, 2020a.

© Google Maps: Griess Firn Map, 8751 Spiringen, CH, Google Maps, January 2020, maps.google.com. (Kartendaten 2020, Maps), last access: 20 January 2020, 2020b.

Abbott, B. W., Bishop, K., Zarnetske, J. P., Minaudo, C., Chapin, F. S., Krause, S., Hannah, D. M., Conner, L., Ellison, D., Godsey, S. E., Plont, S., Marçais, J., Kolbe, T., Huebner, A., Frei, R. J., Hampton, T., Gu, S., Buhman, M., Sara Sayedi, S., Ursache, O., Chapin, M., Henderson, K. D., and Pinay, G.: Human domination of the global water cycle absent from depictions and perceptions, Nature Geoscience, 12, 533–540, https://doi.org/10.1038/s41561-019-0374-y, 2019.

Alexander, E. and Burt, R.: Soil development on moraines of Mendenhall Glacier, southeast Alaska. 1. The moraines and soil morphology, Geoderma, 72, 1–17, https://doi.org/10.1016/0016-7061(96)00021-3, 1996.

Allaire, S. E., Roulier, S., and Cessna, A. J.: Quantifying preferential flow in soils: A review of different techniques, Journal of Hydrology, 378, 179–204, https://doi.org/10.1016/j.jhydrol.2009.08.013, 2009.

Allen, R. G., Pereira, L. S., Raes, D., and M, S.: Crop evapotranspiration - Guidelines for computing crop water requirements - FAO Irrigation and drainage paper 56, Tech. rep., FAO - Food and Agriculture Organization of the United Nations, http://www.fao.org/3/x0490e/x0490e00.htm, 1998.

Šamonil, P., Daněk, P., Lutz, J. A., Anderson-Teixeira, K. J., Jaroš, J., Phillips, J. D., Rousová, A., Adam, D., Larson, A. J., Kašpar, J., Janik, D., Vašíčková, I., Gonzalez-Akre, E., and Egli, M.: Tree Mortality may Drive Landscape Formation: Comparative Study from Ten Temperate Forests, Ecosystems, 26, 257–276, https://doi.org/10.1007/s10021-022-00755-8, 2022.

Amundson, R., Berhe, A. A., Hopmans, J. W., Olson, C., Sztein, A. E., and Sparks, D. L.: Soil and human security in the 21st century, Science, 348, 1261 071, https://doi.org/10.1126/science.1261071, 2015.

Angermann, L., Jackisch, C., Allroggen, N., Sprenger, M., Zehe, E., Tronicke, J., Weiler, M., and Blume, T.: Form and function in hillslope hydrology: characterization of subsurface flow based on response observations, Hydrology and Earth System Sciences, 21, 3727–3748, https://doi.org/10.5194/hess-21-3727-2017, 2017.

Archer, N., Bonell, M., Coles, N., MacDonald, A., Auton, C., and Stevenson, R.: Soil characteristics and landcover relationships on soil hydraulic conductivity at a hillslope scale: A view towards local flood management, Journal of Hydrology, 497, 208–222, https://doi.org/10.1016/j.jhydrol.2013.05.043, 2013.

Armenise, E., Simmons, R. W., Ahn, S., Garbout, A., Doerr, S. H., Mooney, S. J., Sturrock, C. J., and Ritz, K.: Soil seal development under simulated rainfall: Structural, physical and hydrological dynamics, Journal of Hydrology, 556, 211–219, https://doi.org/10.1016/j.jhydrol.2017.10.073, 2018.

Arvidsson, J.: Influence of soil texture and organic matter content on bulk density, air content, compression index and crop yield in field and laboratory compression experiments, Soil and Tillage Research, 49, 159 –170, https://doi.org/10.1016/S0167-1987(98)00164-0, 1998.

Assouline, S.: Rainfall-induced soil surface sealing: A critical review of observations, conceptual models, and solutions, Vadose Zone Journal, 3, 570–591, https://doi.org/10.2113/3.2.570, 2004.

Bachmair, S. and Weiler, M.: Hillslope characteristics as controls of subsurface flow variability, Hydrology and Earth System Sciences, 16, 3699–3715, https://doi.org/10.5194/hess-16-3699-2012, 2012.

Bachmair, S., Weiler, M., and Nützmann, G.: Controls of land use and soil structure on water movement: Lessons for pollutant transfer through the unsaturated zone, Journal of Hydrology, 369, 241–252, https://doi.org/10.1016/j.jhydrol.2009.02.031, 2009.

Bearup, L. A., Maxwell, R. M., Clow, D. W., and McCray, J. E.: Hydrological effects of forest transpiration loss in bark beetle-impacted watersheds, Nature Climate Change, 4, 481–486, https://doi.org/10.1038/nclimate2198, 2014.

Bearup, L. A., Maxwell, R. M., and McCray, J. E.: Hillslope response to insect-induced land-cover change: an integrated model of end-member mixing, Ecohydrology, 9, 195–203, https://doi.org/10.1002/eco.1729, 2016.

Beckwith, C. W., Baird, A. J., and Heathwaite, A. L.: Anisotropy and depth-related heterogeneity of hydraulic conductivity in a bog peat. I: laboratory measurements, Hydrological Processes, 17, 89–101, https://doi.org/10.1002/hyp.1116, 2003.

Beerten, K., Deforce, K., and Mallants, D.: Landscape evolution and changes in soil hydraulic properties at the decadal, centennial and millennial scale: A case study from the Campine area, northern Belgium, CATENA, 95, 73–84, https://doi.org/10.1016/j.catena.2012.03.005, 2012.

Beiter, D., Weiler, M., and Blume, T.: Characterising hillslope–stream connectivity with a joint event analysis of stream and groundwater levels, Hydrology and Earth System Sciences, 24, 5713–5744, https://doi.org/10.5194/hess-24-5713-2020, 2020.

Beven, K.: How far can we go in distributed hydrological modelling?, Hydrology and Earth System Sciences, 5, 1–12, https://doi.org/10.5194/hess-5-1-2001, 2001.

Beven, K. and Germann, P.: Macropores and water flow in soils revisited, Water Resources Research, 49, 3071–3092, https://doi.org/10.1002/wrcr.20156, 2013.

Bevington, J., Piragnolo, D., Teatini, P., Vellidis, G., and Morari, F.: On the spatial variability of soil hydraulic properties in a Holocene coastal farmland, Geoderma, 262, 294–305, https://doi.org/10.1016/j.geoderma.2015.08.025, 2016.

Biavati, G., Godt, J. W., and McKenna, J. P.: Drainage effects on the transient, near-surface hydrologic response of a steep hillslope to rainfall: implications for slope stability, Edmonds, Washington, USA,

Natural Hazards and Earth System Sciences, 6, 343–355, https://doi.org/10.5194/nhess-6-343-2006, 2006.

Birse, E. L.: Suggested amendments to the world soil classification to accomodate scottish mountain and aeolian soils, Journal of Soil Science, 31, 117–124, https://doi.org/10.1111/j.1365-2389.1980.tb02069.x, 1980.

Blass, A., Anselmetti, F. S., and Ariztegui, D.: 60 years of glaciolacustrine sedimentation in Steinsee (Sustenpass, Switzerland) compared with historic events and instrumental meteorological data, Eclogae Geol. Helv. 96 (Supplement1), pp. 59–71, https://doi.org/10.1007/978-3-0348-7992-7_8, 2003.

Blöschl, G.: Predictions in ungauged basins – where do we stand?, Proceedings of the International Association of Hydrological Sciences, 373, 57–60, https://doi.org/10.5194/piahs-373-57-2016, 2016.

Blume, T., Zehe, E., and Bronstert, A.: Investigation of runoff generation in a pristine, poorly gauged catchment in the Chilean Andes II: Qualitative and quantitative use of tracers at three spatial scales, Hydrol. Process., 22, 3676–3688, https://doi.org/10.1002/hyp.6970, 2008.

Blume, T., Zehe, E., and Bronstert, A.: Use of soil moisture dynamics and patterns at different spatio-temporal scales for the investigation of subsurface flow processes, Hydrology and Earth System Sciences, 13, 1215–1233, https://doi.org/10.5194/hess-13-1215-2009, 2009.

Bogner, C., Wolf, B., Schlather, M., and Huwe, B.: Analysing flow patterns from dye tracer experiments in a forest soil using extreme value statistics, European Journal of Soil Science, 59, 103–113, https://doi.org/10.1111/j.1365-2389.2007.00974.x, 2008.

Bogner, C., Bauer, F., y Widemann, B. T., Viñan, P., Balcazar, L., and Huwe, B.: Quantifying the morphology of flow patterns in landslide-affected and unaffected soils, Journal of Hydrology, 511, 460 – 473, https://doi.org/10.1016/j.jhydrol.2014.01.063, 2014.

Bonetti, S., Wei, Z., and Or, D.: A framework for quantifying hydrologic effects of soil structure across scales, Communications Earth & Environment, 2, 1–10, https://doi.org/10.1038/s43247-021-00180-0, 2021.

Bourgeois, O. L., Bouvier, C., Brunet, P., and Ayral, P.-A.: Inverse modeling of soil water content to estimate the hydraulic properties of a shallow soil and the associated weathered bedrock, Journal of Hydrology, 541, 116 –126, https://doi.org/10.1016/j.jhydrol.2016.01.067, flash floods, hydro-geomorphic response and risk management, 2016.

Branger, F. and McMillan, H. K.: Deriving hydrological signatures from soil moisture data, Hydrological Processes, 34, 1410–1427, https://doi.org/10.1002/hyp.13645, 2020.

Brocca, L., Morbidelli, R., Melone, F., and Moramarco, T.: Soil moisture spatial variability in experimental areas of central Italy, Journal of Hydrology, 333, 356–373, https://doi.org/10.1016/j.jhydrol.2006.09.004, 2007.

Bronstert, A., Niehoff, D., and Bürger, G.: Effects of climate and land-use change on storm runoff generation: present knowledge and modelling capabilities, Hydrological Processes, 16, 509–529, https://doi.org/10.1002/hyp.326, 2002.

Brooks, S. M. and Richards, K. S.: Establishing the role of pedogenesis in changing soil hydraulic properties, Earth Surface Processes and Landforms, 18, 573–578, https://doi.org/10.1002/esp.3290180609, 1993.

Bundt, M., Albrecht, A., Froidevaux, P., Blaser, P., and Flühler, H.: Impact of Preferential Flow on Radionuclide Distribution in Soil, Environ. Sci. Technol., 34, 3895–3899, https://doi.org/10.1021/es9913636, 2000.

Burga, C. A., Krüsi, B., Egli, M., Wernli, M., Elsener, S., Ziefle, M., Fischer, T., and Mavris, C.: Plant succession and soil development on the foreland of the Morteratsch glacier (Pontresina, Switzerland): Straight forward or chaotic?, Flora - Morphology, Distribution, Functional Ecology of Plants, 205, 561–576, https://doi.org/10.1016/j.flora.2009.10.001, 2010.

Cammeraat, E. L. H. and Kooijman, A. M.: Biological control of pedological and hydrogeomorphological processes in a deciduous forest ecosystem, Biologia, 64, 428–432, https://doi.org/10.2478/s11756-009-0075-x, 2009.

Carey, S. K., Quinton, W. L., and Goeller, N. T.: Field and laboratory estimates of pore size properties and hydraulic characteristics for subarctic organic soils, Hydrol. Process., 21, 2560–2571, https://doi.org/10.1002/hyp.6795, 2007.

Casagrande, A.: Die Aräometer-Methode zur Bestimmung der Kornverteilung von Böden und anderen Materialien, Springer Berlin Heidelberg, 1934.

Chason, D. B. and Siegel, D. I.: Hydraulic conductivity and related properties of peat, lost river peatland, Northern Minnesota, Soil Science, 142, 91–99, https://doi.org/10.1097/00010694-198608000-00005, 1986.

Chen, H., Zhang, X., Abla, M., Lü, D., Yan, R., Ren, Q., Ren, Z., Yang, Y., Zhao, W., Lin, P., Liu, B., and Yang, X.: Effects of vegetation and rainfall types on surface runoff and soil erosion on steep slopes on the Loess Plateau, China, CATENA, 170, 141–149, https://doi.org/10.1016/j.catena.2018.06.006, 2018.

Cheng, J., Wu, J., Chen, Y., and Zhang, H.: Characteristics of preferential flow paths and their effects on soil properties, The Forestry Chronicle, 90, 192–196, https://doi.org/10.5558/tfc2014-037, 2014.

Cheng, Y., Ogden, F. L., and Zhu, J.: Earthworms and tree roots: A model study of the effect of preferential flow paths on runoff generation and groundwater recharge in steep, saprolitic, tropical lowland catchments, Water Resources Research, 53, 5400–5419, https://doi.org/10.1002/2016WR020258, 2017.

Cichota, R., Kelliher, F., Thomas, S., Clemens, G., Fraser, P., and Carrick, S.: Effects of irrigation intensity on preferential solute transport in a stony soil, New Zealand Journal of Agricultural Research, 59, 141–155, https://doi.org/10.1080/00288233.2016.1155631, 2016.

Clark, E. V. and Zipper, C. E.: Vegetation influences near-surface hydrological characteristics on a surface coal mine in eastern USA, CATENA, 139, 241–249, https://doi.org/10.1016/j.catena.2016.01.004, 2016.

Clothier, B. E., Green, S. R., and Deurer, M.: Preferential flow and transport in soil: progress and prognosis, European Journal of Soil Science, 59, 2–13, https://doi.org/10.1111/j.1365-2389.2007.00991.x, 2008.

Costantini, E. A. and Dazzi, C., eds.: The Soils of Italy, World Soils Book Series, Springer, Dordrecht, Springer Science+Business Media Dordrecht 2013, 1 edn., https://doi.org/10.1007/978-94-007-5642-7, 354, 2013.

Cremer, C., Schuetz, C., Neuweiler, I., Lehmann, P., and Lehmann, E.: Unstable Infiltration Experiments in Dry Porous Media, Vadose Zone Journal, 16, 1–13, https://doi.org/10.2136/vzj2016.10.0092, 2017.

Crocker, R. L. and Dickson, B. A.: Soil Development on the Recessional Moraines of the Herbert and Mendenhall Glaciers, South-Eastern Alaska, Journal of Ecology, 45, 169–185, https://doi.org/10.2307/2257083, 1957.

Crocker, R. L. and Major, J.: Soil Development in Relation to Vegetation and Surface Age at Glacier Bay, Alaska, Journal of Ecology, 43, 427–448, https://doi.org/10.2307/2257005, 1955.

Cui, L., Li, G., Chen, Y., and Li, L.: Response of Landscape Evolution to Human Disturbances in the Coastal Wetlands in Northern Jiangsu Province, China, Remote Sensing, 13, 2030, https://doi.org/10.3390/rs13112030, 2021.

D'Amico, M. E., Freppaz, M., Filippa, G., and Zanini, E.: Vegetation influence on soil formation rate in a proglacial chronosequence (Lys Glacier, NW Italian Alps), CATENA, 113, 122–137, https://doi.org/10.1016/j.catena.2013.10.001, 2014.

de Jonge, L. W., Moldrup, P., and Schjønning, P.: Soil Infrastructure, Interfaces & Translocation Processes in Inner Space ("Soil-it-is"): towards a road map for the constraints and crossroads of soil architecture and biophysical processes, Hydrology and Earth System Sciences, 13, 1485–1502, https://doi.org/10.5194/hess-13-1485-2009, 2009.

DeBano, L. F.: Water Repellent Soils: A state-of-the-art, NASA STI/Recon Technical Report N, 1981.

Dekker, L. and Ritsema, C.: Wetting patterns and moisture variability in water repellent Dutch soils, Journal of Hydrology, 231-232, 148–164, https://doi.org/10.1016/S0022-1694(00)00191-8, 2000.

Demand, D., Blume, T., and Weiler, M.: Spatio-temporal relevance and controls of preferential flow at the landscape scale, Hydrology and Earth System Sciences, 23, 4869–4889, https://doi.org/10.5194/hess-23-4869-2019, 2019.

Demir, Y. and Doğan Demir, A.: The effect of organic matter applications on the saturated hydraulic conductivity and available water-holding capacity of sandy soils, Applied Ecology and Environmental Research, 17, 3137–3146, https://doi.org/10.15666/aeer/1702_31373146, 2019.

Deuchars, S., Townend, J., Aitkenhead, M. J., and FitzPatrick, E.: Changes in soil structure and hydraulic properties in regenerating rain forest, Soil Use and Management, 15, 183–187, https://doi.org/10.1111/j.1475-2743.1999.tb00086.x, 1999.

Dümig, A., Smittenberg, R., and Kögel-Knabner, I.: Concurrent evolution of organic and mineral components during initial soil development after retreat of the Damma glacier, Switzerland, Geoderma, 163, 83–94, https://doi.org/10.1016/j.geoderma.2011.04.006, 2011.

Doerr, S., Shakesby, R., and P.D. Walsh, R.: Spatial Variability of Soil Hydrophobicity in Fire-Prone Eucalyptus and Pine Forests, Portugal, Soil Science, 163, 313–324, https://doi.org/10.1097/00010694-199804000-00006, 1998.

Doerr, S., Shakesby, R., and Walsh, R.: Soil water repellency: its causes, characteristics and hydro-geomorphological significance, Earth-Science Reviews, 51, 33–65, https://doi.org/10.1016/S0012-8252(00)00011-8, 2000.

Douglass, D. C. and Bockheim, J. G.: Soil-forming rates and processes on Quaternary moraines near Lago Buenos Aires, Argentina, Quaternary Research, 65, 293–307, https://doi.org/10.1016/j.yqres.2005.08.027, 2006.

Dunne, T.: Hillslope Hydrology, chap. Field studies of hillslope flow processes, pp. 227–293, John Wiley and Sons, Ed.: M.J. Kirkby, 1978.

Egli, M., Fitze, P., and Mirabella, A.: Weathering and evolution of soils formed on granitic, glacial deposits: results from chronosequences of Swiss alpine environments, CATENA, 45, 19–47, https://doi.org/10.1016/S0341-8162(01)00138-2, 2001.

Egli, M., Wernli, M., Kneisel, C., and Haeberli, W.: Melting Glaciers and Soil Development in the Proglacial Area Morteratsch (Swiss Alps): I. Soil Type Chronosequence, Arctic Antarctic and Alpine Research - ARCT ANTARCT ALP RES, 38, 499–509, https://doi.org/10.1657/1523-0430(2006)38[499:MGASDI]2.0.CO;2, 2006.

Egli, M., Mirabella, A., and Sartori, G.: The role of climate and vegetation in weathering and clay mineral formation in late Quaternary soils of the Swiss and Italian Alps, Geomorphology, 102, 307–324, https://doi.org/10.1016/j.geomorph.2008.04.001, 2008.

Egli, M., Mavris, C., Mirabella, A., and Giaccai, D.: Soil organic matter formation along a chronosequence in the Morteratsch proglacial area (Upper Engadine, Switzerland), CATENA, 82, 61–69, https://doi.org/10.1016/j.catena.2010.05.001, 2010.

Egli, M., Filip, D., Mavris, C., Fischer, B., Götze, J., Raimondi, S., and Seibert, J.: Rapid transformation of inorganic to organic and plant-available phosphorous in soils of a glacier forefield, Geoderma, 189-190, 215–226, https://doi.org/10.1016/j.geoderma.2012.06.033, 2012.

Ehret, U., Gupta, H. V., Sivapalan, M., Weijs, S. V., Schymanski, S. J., Blöschl, G., Gelfan, A. N., Harman, C., Kleidon, A., Bogaard, T. A., Wang, D., Wagener, T., Scherer, U., Zehe, E., Bierkens, M. F. P.,

Di Baldassarre, G., Parajka, J., van Beek, L. P. H., van Griensven, A., Westhoff, M. C., and Winsemius, H. C.: Advancing catchment hydrology to deal with predictions under change, Hydrology and Earth System Sciences, 18, 649–671, https://doi.org/10.5194/hess-18-649-2014, 2014.

Ehrlich, W., Rice, H., and Ellis, J.: Influence of the Composition of Parent Materials on Soil Formation in Manitoba, Canadian Journal of Agricultural Science, 35, 407–421, https://doi.org/10.4141/agsci-1955-0053, 1955.

Ellenberg, H. H.: Vegetation Ecology of Central Europe, Cambridge University Press, 756 pp, 1988.

Ellis, S.: Weathering, soils and paleosols edited by I. P. Martini and W. Chesworth, Elsevier, Amsterdam and New York, Earth Surface Processes and Landforms, 18, 469–469, https://doi.org/10.1002/esp.3290180508, 1992.

Fan, B., Liu, X., Zhu, Q., Qin, G., Li, J., Lin, H., and Guo, L.: Exploring the interplay between infiltration dynamics and Critical Zone structures with multiscale geophysical imaging: A review, Geoderma, 374, 114 431, https://doi.org/10.1016/j.geoderma.2020.114431, 2020.

Fan, Y., Clark, M., Lawrence, D. M., Swenson, S., Band, L. E., Brantley, S. L., Brooks, P. D., Dietrich, W. E., Flores, A., Grant, G., Kirchner, J. W., Mackay, D. S., McDonnell, J. J., Milly, P. C. D., Sullivan, P. L., Tague, C., Ajami, H., Chaney, N., Hartmann, A., Hazenberg, P., McNamara, J., Pelletier, J., Perket, J., Rouholahnejad-Freund, E., Wagener, T., Zeng, X., Beighley, E., Buzan, J., Huang, M., Livneh, B., Mohanty, B. P., Nijssen, B., Safeeq, M., Shen, C., van Verseveld, W., Volk, J., and Yamazaki, D.: Hillslope Hydrology in Global Change Research and Earth System Modeling, Water Resources Research, 55, 1737–1772, https://doi.org/10.1029/2018WR023903, 2019.

FAO: Global Forest Resources Assessment 2020: Main report. Rome, Tech. rep., Food and Agriculture Organization of the United Nations, https://doi.org/10.4060/ca9825en, 2020.

Frey, F.: Geologie der östlichen Claridenkette, Ph.D. thesis, ETH Zurich, Zürich, https://doi.org/10.3929/ethz-a-000088454, sA aus: Vierteljahrsschrift der Naturforschenden Gesellschaft in Zürich, Jg.110, Heft 1, S.1-287. Diss. Naturwiss. ETH Zürich, Nr. 3590, 0000. Ref.: Trümpy, R. ; Korref.: Gansser, A., 1965.

Fujimoto, M., Ohte, N., and Tani, M.: Effects of hillslope topography on hydrological responses in a weathered granite mountain, Japan: comparison of the runoff response between the valley-head and the side slope, Hydrological Processes, 22, 2581–2594, https://doi.org/10.1002/hyp.6857, 2008.

Fukutome, S., Schindler, A., and Capobianco, A.: MeteoSwiss extreme value analyses: User manual and documentation, Technical Report MeteoSwiss, 255, 2 edn., URL `https://www.meteoswiss.admin.ch/services-and-publications/publications/reports-and-bulletins/en/2015/meteoswiss-extreme-value-analyses-user-manual-and-documentation.html`, last date of access: 28.06.2023, 2017.

Germer, S., Neill, C., Krusche, A. V., and Elsenbeer, H.: Influence of land-use change on near-surface hydrological processes: Undisturbed forest to pasture, Journal of Hydrology, 380, 473–480, https://doi.org/10.1016/j.jhydrol.2009.11.022, 2010.

Ghestem, M., Sidle, R. C., and Stokes, A.: The Influence of Plant Root Systems on Subsurface Flow: Implications for Slope Stability, BioScience, 61, 869–879, https://doi.org/10.1525/bio.2011.61.11.6, 2011.

Gimbel, K. F., Puhlmann, H., and Weiler, M.: Does drought alter hydrological functions in forest soils?, Hydrology and Earth System Sciences, 20, 1301–1317, https://doi.org/10.5194/hess-20-1301-2016, 2016.

Glass, R., Parlange, J.-Y., and Steenhuis, T.: Wetting front instability I: Theoretical discussion and dimensional analysis, Water Resources Research, 25, 1187–1194, https://doi.org/10.1029/WR025i006p01187, 1989.

Gnann, S. J., McMillan, H. K., Woods, R. A., and Howden, N. J. K.: Including Regional Knowledge Improves Baseflow Signature Predictions in Large Sample Hydrology, Water Resources Research, 57, e2020WR028 354, https://doi.org/10.1029/2020WR028354, 2021.

Godsey, S. and Elsenbeer, H.: The soil hydrologic response to forest regrowth: A case study from Southwestern Amazonia, Hydrological Processes, 16, 1519 –1522, https://doi.org/10.1002/hyp.605, 2002.

Goeking, S. A. and Tarboton, D. G.: Forests and Water Yield: A Synthesis of Disturbance Effects on Streamflow and Snowpack in Western Coniferous Forests, Journal of Forestry, 118, 172–192, https://doi.org/10.1093/jofore/fvz069, 2020.

Gralher, B., Herbstritt, B., Weiler, M., Wassenaar, L. I., and Stumpp, C.: Correcting Laser-Based Water Stable Isotope Readings Biased by Carrier Gas Changes, Environmental Science and Technology, 50, 7074–7081, https://doi.org/10.1021/acs.est.6b01124, pMID: 27291718, 2016.

Greinwald, K., Dieckmann, L. A., Schipplick, C., Hartmann, A., Scherer-Lorenzen, M., and Gebauer, T.: Vertical root distribution and biomass allocation along proglacial chronosequences in Central Switzerland, Arctic, Antarctic, and Alpine Research, 53, 20–34, https://doi.org/10.1080/15230430.2020.1859720, 2021a.

Greinwald, K., Gebauer, T., Musso, A., and Scherer-Lorenzen, M.: Similar successional development of functional community structure in glacier forelands despite contrasting bedrocks, Journal of Vegetation Science, 32, e12 993, https://doi.org/10.1111/jvs.12993, 2021b.

Greinwald, K., Gebauer, T., Treuter, L., Kolodziej, V., Musso, A., Maier, F., Lustenberger, F., and Scherer-Lorenzen, M.: Root density drives aggregate stability of soils of different moraine ages in the Swiss Alps, Plant and Soil, 468, 439–457, https://doi.org/10.1007/s11104-021-05111-8, 2021c.

Haeberli, W.: Integrative modelling and managing new landscapes and environments in de-glaciating mountain ranges: An emerging trans-disciplinary research field, Forestry Research and Engineering: International Journal, 1, 00 005, https://doi.org/10.15406/freij.2017.01.00005, 2017.

Haeberli, W., Oerlemans, J., and Zemp, M.: The Future of Alpine Glaciers and Beyond, https://doi.org/10.1093/acrefore/9780190228620.013.769, 2019.

Hahm, W. J., Riebe, C. S., Lukens, C. E., and Araki, S.: Bedrock composition regulates mountain ecosystems and landscape evolution, Proceedings of the National Academy of Sciences, 111, 3338–3343, https://doi.org/10.1073/pnas.1315667111, 2014.

Hallema, D. W., Moussa, R., Sun, G., and McNulty, S. G.: Surface storm flow prediction on hillslopes based on topography and hydrologic connectivity, Ecological Processes, 5, 13, https://doi.org/10.1186/s13717-016-0057-1, 2016.

Hamilton, N. and Ferry, M.: ggtern: Ternary Diagrams Using ggplot2, Journal of Statistical Software, 87, 1–17, https://doi.org/10.18637/jss.v087.c03, code Snippet 3, 2018.

Hardie, M. A., Cotching, W. E., Doyle, R. B., Holz, G., Lisson, S., and Mattern, K.: Effect of antecedent soil moisture on preferential flow in a texture-contrast soil, Journal of Hydrology, 398, 191–201, https://doi.org/10.1016/j.jhydrol.2010.12.008, 2011.

Hartmann, A., Semenova, E., Weiler, M., and Blume, T.: Field observations of soil hydrological flow path evolution over 10 millennia, Hydrology and Earth System Sciences, 24, 3271–3288, https://doi.org/10.5194/hess-24-3271-2020, 2020a.

Hartmann, A., Weiler, M., and Blume, T.: The impact of landscape evolution on soil physics: evolution of soil physical and hydraulic properties along two chronosequences of proglacial moraines, Earth System Science Data, 12, 3189–3204, https://doi.org/10.5194/essd-12-3189-2020, 2020b.

Hartmann, A., Weiler, M., and Blume, T.: Soil physical and hydraulic properties along two chronosequences of proglacial moraines, GFZ Data Services, https://doi.org/10.5880/GFZ.4.4.2020.004, 2020c.

Hartmann, A., Weiler, M., Greinwald, K., and Blume, T.: Subsurface flow paths in a chronosequence of calcareous soils: impact of soil age and rainfall intensities on preferential flow occurrence, Hydrology and Earth System Sciences, 26, 4953–4974, https://doi.org/10.5194/hess-26-4953-2022, 2022.

Hassler, S. K., Zimmermann, B., van Breugel, M., Hall, J. S., and Elsenbeer, H.: Recovery of saturated hydraulic conductivity under secondary succession on former pasture in the humid tropics, Forest Ecology and Management, 261, 1634–1642, https://doi.org/10.1016/j.foreco.2010.06.031, 2011.

Hatfield, L. J., Sauer, T., and M. Cruse, R.: Soil: The Forgotten Piece of the Water, Food, Energy Nexus, Advances in Agronomy, 143, 1–46, https://doi.org/10.1016/bs.agron.2017.02.001, 2017.

He, L. and Tang, Y.: Soil development along primary succession sequences on moraines of Hailuogou Glacier, Gongga Mountain, Sichuan, China, CATENA, 72, 259–269, https://doi.org/10.1016/j.catena.2007.05.010, 2008.

Heikkinen, O. and Fogelberg, P.: Bodenentwicklung im Hochgebirge: Ein Beispiel am Vorfeld des Steingletschers in der Schweiz, Geographica Helvicta, 3, 107–112, https://doi.org/10.5194/gh-35-107-1980, 1980.

Hendrickx, J. M. H. and Flury, M.: Uniform and Preferential Flow Mechanisms in the Vadose Zone, In: Conceptual Models of Flow and Transport in the Fractured Vadose Zone, pp. 149–187, National Research Council, National Academy Press, Washington, DC, 2001.

Hervé, M.: RVAideMemoire: testing and plotting procedures for biostatistics, R package version 0.9-69, 3, 2018.

Hopkins, B. and Ellsworth, J.: Phosphorus availability with alkaline/calcareous soil Western Nutrient Salt, Proceeding of 6th Western Nutrient Management Conference, Lake City, UT, March 3-4, 88–93, 2005.

Hopp, L. and McDonnell, J.: Connectivity at the hillslope scale: Identifying interactions between storm size, bedrock permeability, slope angle and soil depth, Journal of Hydrology, 376, 378–391, https://doi.org/10.1016/j.jhydrol.2009.07.047, 2009.

Hou, J., Fu, B., Liu, Y., Lu, N., Gao, G., and Zhou, J.: Ecological and hydrological response of farmlands abandoned for different lengths of time: Evidence from the Loess Hill Slope of China, Global and Planetary Change, 113, 59–67, https://doi.org/10.1016/j.gloplacha.2013.12.008, 2014.

Öhrström, P., Persson, M., Albergel, J., Zante, P., Nasri, S., Berndtsson, R., and Olsson, J.: Field-scale variation of preferential flow as indicated from dye coverage, Journal of Hydrology, 257, 164 –173, https://doi.org/10.1016/S0022-1694(01)00537-6, 2002.

Hu, W., Shao, M. A., Wang, Q. J., Fan, J., and Reichardt, K.: Spatial variability of soil hydraulic properties on a steep slope in the loess plateau of China, Scientia Agricola, 65, 268–276, 2008.

Hübner, R., Günther, T., Heller, K., Noell, U., and Kleber, A.: Impacts of a capillary barrier on infiltration and subsurface stormflow in layered slope deposits monitored with 3-D ERT and hydrometric measurements, Hydrology and Earth System Sciences, 21, 5181–5199, https://doi.org/10.5194/hess-21-5181-2017, 2017.

Hudek, C., Stanchi, S., D'Amico, M., and Freppaz, M.: Quantifying the contribution of the root system of alpine vegetation in the soil aggregate stability of moraine, International Soil and Water Conservation Research, 5, 36 – 42, https://doi.org/10.1016/j.iswcr.2017.02.001, 2017.

Hunt, A., Egli, M., and Faybishenko, B.: Where Are We and Where Are We Going? Pedogenesis Through Chemical Weathering, Hydrologic Fluxes, and Bioturbation, chap. 14, pp. 253–269, American Geophysical Union (AGU), https://doi.org/10.1002/9781119563952.ch14, 2021.

Hupet, F., Lambot, S., Javaux, M., and Vanclooster, M.: On the identification of macroscopic root water uptake parameters from soil water content observations, Water Resources Research, 38, 1300, https://doi.org/10.1029/2002WR001556, 2002.

Huss, M., Farinotti, D., Bauder, A., and Funk, M.: Modelling runoff from highly glacierized alpine drainage basins in a changing climate, Hydrological Processes, 22, 3888–3902, https://doi.org/10.1002/hyp.7055, 2008.

IAEA/WMO: Global Network of Isotopes in Precipitation., Tech. rep., The GNIP Database. Accessible at: http://www.iaea.org/water, last access at 15. February 2022, 2021.

Šimůnek, J., van Genuchten, M. T., and Šejna, M.: Recent Developments and Applications of the HYDRUS Computer Software Packages, Vadose Zone Journal, 15, vzj2016.04.0033, https://doi.org/10.2136/vzj2016.04.0033, 2016.

IUSS Working Group WRB: World Reference Base for Soil Resources, Rome: World Soil Resources Reports, 2014.

Jackisch, C., Angermann, L., Allroggen, N., Sprenger, M., Blume, T., Tronicke, J., and Zehe, E.: Form and function in hillslope hydrology: in situ imaging and characterization of flow-relevant structures, Hydrology and Earth System Sciences, 21, 3749–3775, https://doi.org/10.5194/hess-21-3749-2017, 2017.

Janssen, M. and Lennartz, B.: Horizontal and vertical water and solute fluxes in paddy rice fields, Soil and Tillage Research, 94, 133–141, https://doi.org/10.1016/j.still.2006.07.010, 2007.

Janzen, D. and McDonnell, J. J.: A stochastic approach to modelling and understanding hillslope runoff connectivity dynamics, Ecological Modelling, 298, 64–74, https://doi.org/10.1016/j.ecolmodel.2014.06.024, complexity of Soils and Hydrology in Ecosystems, 2015.

Jarvis, N., Moeys, J., Hollis, J., Reichenberger, S., Lindahl, A., and Dubus, I.: A Conceptual Model of Soil Susceptibility to Macropore Flow, Vadose Zone Journal - VADOSE ZONE J, 8, 902–910, https://doi.org/10.2136/vzj2008.0137, 2009.

Jarvis, N., Moeys, J., Koestel, J., and Hollis, J.: Preferential flow in a pedological perspective. In: Hydropedology: synergistic integration of soil science and hydrology (ed. H. Lin), Academic Press, Elsevier B.V., pp.75-120, 2012.

Jarvis, N., Koestel, J., Messing, I., Moeys, J., and Lindahl, A.: Influence of soil, land use and climatic factors on the hydraulic conductivity of soil, Hydrology and Earth System Sciences, 17, 5185–5195, https://doi.org/10.5194/hess-17-5185-2013, 2013.

Jarvis, N., Koestel, J., and Larsbo, M.: Understanding Preferential Flow in the Vadose Zone: Recent Advances and Future Prospects, Vadose Zone Journal, 15, 1–11, https://doi.org/10.2136/vzj2016.09.0075, 2016.

Jarvis, N. J.: A review of non-equilibrium water flow and solute transport in soil macropores: principles, controlling factors and consequences for water quality, European Journal of Soil Science, 58, 523–546, https://doi.org/10.1111/j.1365-2389.2007.00915.x, 2007.

Jefferson, A., Grant, G., Lewis, S., and Lancaster, S.: Coevolution of hydrology and topography on a basalt landscape in the Oregon Cascade Range, USA, Earth Surface Processes and Landforms, 35, 803 – 816, https://doi.org/10.1002/esp.1976, 2010.

Jenny, H.: Factors of soil formation. A system of quantitative pedology, McGraw-Hill, New York, dover publications edn., 1941.

Jin, L. and Brantley, S. L.: Soil chemistry and shale weathering on a hillslope influenced by convergent hydrologic flow regime at the Susquehanna/Shale Hills Critical Zone Observatory, Applied Geochemistry, Ninth International Symposium on the Geochemistry of the Earth's Surface (GES-9), 26, S51 – S56, https://doi.org/10.1016/j.apgeochem.2011.03.027, 2011.

Jin, Z., Zhao, Q., Qin, X., Zhang, J., Zhang, H., Qin, J., Qin, Y., Li, H., Chen, J., Liu, Y., Li, Y., and Wang, L.: Quantifying the impact of landscape changes on hydrological variables in the alpine and cold region using hydrological model and remote sensing data, Hydrological Processes, 35, e14 392, https://doi.org/10.1002/hyp.14392, 2021.

Keith, A., Henrys, P., Rowe, R., and Mcnamara, N.: Technical note: A bootstrapped LOESS regression approach for comparing soil depth profiles, Biogeosciences, 13, 3863–3868, https://doi.org/10.5194/bg-13-3863-2016, 2016.

Khaleel, R., Reddy, K. R., and Overcash, M. R.: Changes in Soil Physical Properties Due to Organic Waste Applications: A Review, Journal of Environmental Quality, 10, 133–141, https://doi.org/10.2134/jeq1981.00472425001000020002x, 1981.

Khan, M. R., Koneshloo, M., Knappett, P. S. K., Ahmed, K. M., Bostick, B. C., Mailloux, B. J., Mozumder, R. H., Zahid, A., Harvey, C. F., van Geen, A., and Michael, H. A.: Megacity pumping and preferential flow threaten groundwater quality, Nature Communications, 7, 12 833, https://doi.org/10.1038/ncomms12833, 2016.

Khlosi, M., Cornelis, W. M., Douaik, A., Hazzouri, A., Habib, H., and Gabriels, D.: Exploration of the Interaction between Hydraulic and Physicochemical Properties of Syrian Soils, Vadose Zone Journal, 12, vzj2012.0209, https://doi.org/10.2136/vzj2012.0209, 2013.

Kim, S.: Characterization of soil moisture responses on a hillslope to sequential rainfall events during late autumn and spring, Water Resources Research, 45, W09 425, https://doi.org/10.1029/2008WR007239, 2009.

Kirkby, M.: Hillslope runoff processes and models, Journal of Hydrology, 100, 315–339, https://doi.org/10.1016/0022-1694(88)90190-4, 1988.

Koestel, J. and Jorda, H.: What determines the strength of preferential transport in undisturbed soil under steady-state flow?, Geoderma, 217-218, 144–160, https://doi.org/10.1016/j.geoderma.2013.11.009, 2014.

Laine-Kaulio, H., Backnäs, S., Koivusalo, H., and Laurén, A.: Dye tracer visualization of flow patterns and pathways in glacial sandy till at a boreal forest hillslope, Geoderma, 259-260, 23–34, https://doi.org/10.1016/j.geoderma.2015.05.004, 2015.

Laurent, L., Buoncristiani, J.-F., Pohl, B., Zekollari, H., Farinotti, D., Huss, M., Mugnier, J.-L., and Pergaud, J.: The impact of climate change and glacier mass loss on the hydrology in the Mont-Blanc massif, Scientific Reports, 10, 10 420, https://doi.org/10.1038/s41598-020-67379-7, 2020.

Leimer, S., Berner, D., Birkhofer, K., Boeddinghaus, R. S., Fischer, M., Kandeler, E., Kuka, K., Marhan, S., Prati, D., Schäfer, D., Schöning, I., Solly, E. F., Wolters, V., and Wilcke, W.: Land-use intensity and biodiversity effects on infiltration capacity and hydraulic conductivity of grassland soils in southern Germany, Ecohydrology, 14, e2301, https://doi.org/10.1002/eco.2301, 2021.

Li, Z., Zhong, J., Li, S.-L., Lang, Y.-C., Zhu, X., and Chen, S.: The effects of hydrological variations on chemical weathering: Evidences from temporal water chemistry, stable carbon and sulfur isotopes, CATENA, 214, 106 301, https://doi.org/10.1016/j.catena.2022.106301, 2022.

Lin, H.: Hydropedology: Bridging Disciplines, Scales, and Data, Vadose Zone J., 2, 1–11, https://doi.org/10.2113/2.1.1, 2003.

Lin, H. and Zhou, X.: Evidence of subsurface preferential flow using soil hydrologic monitoring in the Shale Hills catchment, European Journal of Soil Science, 59, 34–49, https://doi.org/10.1111/j.1365-2389.2007.00988.x, 2008.

Lin, H., Bouma, J., Pachepsky, Y., Western, A., Thompson, J., van Genuchten, R., Vogel, H.-J., and Lilly, A.: Hydropedology: Synergistic integration of pedology and hydrology, Water Resources Research, 42, W05 301, https://doi.org/10.1029/2005WR004085, 2006.

Lohse, K. A. and Dietrich, W. E.: Contrasting effects of soil development on hydrological properties and flow paths, Water Resources Research, 41, W12 419, https://doi.org/10.1029/2004WR003403, 2005.

Lv, X., Zuo, Z., Ni, Y., Sun, J., and Wang, H.: The effects of climate and catchment characteristic change on streamflow in a typical tributary of the Yellow River, Scientific Reports, 9, 14 535, https://doi.org/10.1038/s41598-019-51115-x, 2019.

Ma, K.-C., Tan, Y.-C., and Chen, C.-H.: Effect of hysteresis and rainfall intensity on finger dynamics, Irrigation and Drainage, 57, 585–602, https://doi.org/10.1002/ird.388, 2008.

Ma, Y., Li, X., Guo, L., and Lin, H.: Hydropedology: Interactions between pedologic and hydrologic processes across spatiotemporal scales, Earth-Science Reviews, 171, 181–195, https://doi.org/10.1016/j.earscirev.2017.05.014, 2017.

Maeda, K., Tanaka, T., Park, H., and Hattori, S.: Spatial distribution of soil structure in a suburban forest catchment and its effect on spatio-temporal soil moisture and runoff fluctuations, Journal of Hydrology, 321, 232–256, https://doi.org/10.1016/j.jhydrol.2005.08.003, 2006.

Maier, F. and van Meerveld, I.: Long-Term Changes in Runoff Generation Mechanisms for Two Proglacial Areas in the Swiss Alps I: Overland Flow, Water Resources Research, 57, e2021WR030 221, https://doi.org/10.1029/2021WR030221, 2021a.

Maier, F. and van Meerveld, I.: HILLSCAPE Project - Data on moraine soil properties and on overland flow and subsurface flow characteristics, https://doi.org/10.5880/fidgeo.2021.011, 2021b.

Maier, F., van Meerveld, I., Greinwald, K., Gebauer, T., Lustenberger, F., Hartmann, A., and Musso, A.: Effects of soil and vegetation development on surface hydrological properties of moraines in the Swiss Alps, CATENA, 187, 104 353, https://doi.org/10.1016/j.catena.2019.104353, 2020.

Maier, F., van Meerveld, I., and Weiler, M.: Long-Term Changes in Runoff Generation Mechanisms for Two Proglacial Areas in the Swiss Alps II: Subsurface Flow, Water Resources Research, 57, e2021 WR030 223, https://doi.org/10.1029/2021WR030223, 2021.

Mainwaring, K. A., Morley, C. P., Doerr, S. H., Douglas, P., Llewellyn, C. T., Llewellyn, G., Matthews, I., and Stein, B. K.: Role of heavy polar organic compounds for water repellency of sandy soils, Environmental Chemistry Letters, 2, 35–39, https://doi.org/10.1007/s10311-004-0064-9, 2004.

Mancosu, N., Snyder, R. L., Kyriakakis, G., and Spano, D.: Water Scarcity and Future Challenges for Food Production, Water, 7, 975–992, https://doi.org/10.3390/w7030975, 2015.

Mangiafico, S. S.: Summary and analysis of extension program evaluation in R, Rutgers Cooperative Extension: New Brunswick, NJ, USA, 125, 16–22, 2016.

Marshall, M. R., Francis, O. J., Frogbrook, Z. L., Jackson, B. M., McIntyre, N., Reynolds, B., Solloway, I., Wheater, H. S., and Chell, J.: The impact of upland land management on flooding: results from an improved pasture hillslope, Hydrological Processes, 23, 464–475, https://doi.org/10.1002/hyp.7157, 2009.

Marzeion, B., Cogley, J. G., Richter, K., and Parkes, D.: Attribution of global glacier mass loss to anthropogenic and natural causes, Science, 345, 919–921, https://doi.org/10.1126/science.1254702, 2014.

Mataix-Solera, J. and Doerr, S.: Hydrophobicity and aggregate stability in calcareous topsoils from fire-affected pine forests in southeastern Spain, Geoderma, 118, 77–88, https://doi.org/10.1016/S0016-7061(03)00185-X, 2004.

Maus, V., Giljum, S., Gutschlhofer, J., da Silva, D. M., Probst, M., Gass, S. L. B., Luckeneder, S., Lieber, M., and McCallum, I.: A global-scale data set of mining areas, Scientific Data, 7, 289, https://doi.org/10.1038/s41597-020-00624-w, 2020.

Meerveld, H. J. T. and McDonnell, J. J.: Threshold relations in subsurface stormflow: 2. The fill and spill hypothesis, Water Resources Research, 42, W02 411, https://doi.org/10.1029/2004WR003800, 2006.

MeteoSwiss: Climate normals Grimsel Hospiz Reference period 1981-2010, Federal Office of Meteorology and Climatology MeteoSwiss, URL `https:`

//www.meteoswiss.admin.ch/product/output/climate-data/climate-diagrams-normal-values-station-processing/GRH/climsheet_GRH_np8110_e.pdf, last access: 8 July 2021, 2020a.

MeteoSwiss: Climate normals Pilatus 1981-2010, Referene period 1981-2010, Federal Office of Meteorology and Climatology MeteoSwiss, URL https://www.meteoswiss.admin.ch/product/output/climate-data/climate-diagrams-normal-values-station-processing/PIL/climsheet_PIL_np8110_e.pdf, last access 8 July 2021, 2020b.

Michalet, R., Gandoy, C., Joud, D., Pagès, J.-P., and Choler, P.: Plant Community Composition and Biomass on Calcareous and Siliceous Substrates in the Northern French Alps: Comparative Effects of Soil Chemistry and Water Status, Arctic, Antarctic, and Alpine Research, 34, 102–113, https://doi.org/10.1080/15230430.2002.12003474, 2002.

Müller, M. H., Alaoui, A., Kuells, C., Leistert, H., Meusburger, K., Stumpp, C., Weiler, M., and Alewell, C.: Tracking water pathways in steep hillslopes by δ^{18}O depth profiles of soil water, Journal of Hydrology, 519, 340–352, https://doi.org/10.1016/j.jhydrol.2014.07.031, 2014.

Montagne, D. and Cornu, S.: Do we need to include soil evolution module in models for prediction of future climate change?, Climatic Change, 98, 75–86, https://doi.org/10.1007/s10584-009-9666-3, 2010.

Mooney, S. J. and Morris, C.: A morphological approach to understanding preferential flow using image analysis with dye tracers and X-ray Computed Tomography, CATENA, 73, 204–211, https://doi.org/10.1016/j.catena.2007.09.003, hydropedology: Fundamental Issues and Practical Applications, 2008.

Morales, V. L., Parlange, J.-Y., and Steenhuis, T. S.: Are preferential flow paths perpetuated by microbial activity in the soil matrix? A review, Journal of Hydrology, 393, 29–36, https://doi.org/10.1016/j.jhydrol.2009.12.048, 2010.

Musielok, u., Drewnik, M., Szymański, W., Stolarczyk, M., Gus-Stolarczyk, M., and Skiba, M.: Conditions favoring local podzolization in soils developed from flysch regolith – A case study from the Bieszczady Mountains in southeastern Poland, Geoderma, 381, 114 667, https://doi.org/10.1016/j.geoderma.2020.114667, 2021.

Musso, A., Lamorski, K., Sławiński, C., Geitner, C., Hunt, A., Greinwald, K., and Egli, M.: Evolution of soil pores and their characteristics in a siliceous and calcareous proglacial area, CATENA, 182, 104 154, https://doi.org/10.1016/j.catena.2019.104154, 2019.

Musso, A., Ketterer, M. E., Greinwald, K., Geitner, C., and Egli, M.: Rapid decrease of soil erosion rates with soil formation and vegetation development in periglacial areas, Earth Surface Processes and Landforms, 45, 2824–2839, https://doi.org/10.1002/esp.4932, 2020.

Musso, A., Tikhomirov, D., Plötze, M. L., Greinwald, K., Hartmann, A., Geitner, C., Maier, F., Petibon, F., and Egli, M.: Soil chemical and mineralogical data from moraine chronosequences of the proglacial

areas of Stein glacier (Sustenpass) and Griess glacier (Klausenpass) in the Swiss Alps, https://doi.org/10.1594/PANGAEA.949699, 2022.

Musso, A., Tikhomirov, D., Plötze, M. L., Greinwald, K., Hartmann, A., Geitner, C., Maier, F., Petibon, F., and Egli, M.: Soil Formation and Mass Redistribution during the Holocene Using Meteoric 10Be, Soil Chemistry and Mineralogy, Geosciences, 12, 99, https://doi.org/10.3390/geosciences12020099, 2022.

Nahar, N., Govindaraju, R., Corradini, C., and Morbidelli, R.: Role of run-on for describing field-scale infiltration and overland flow over spatially variable soils, Journal of Hydrology, 286, 36–51, https://doi.org/10.1016/j.jhydrol.2003.09.011, 2004.

Neris, J., Jiménez, C., Fuentes, J., Morillas, G., and Tejedor, M.: Vegetation and land-use effects on soil properties and water infiltration of Andisols in Tenerife (Canary Islands, Spain), CATENA, 98, 55–62, https://doi.org/10.1016/j.catena.2012.06.006, 2012.

Newman, S., Osborne, T. Z., Hagerthey, S. E., Saunders, C., Rutchey, K., Schall, T., and Reddy, K. R.: Drivers of landscape evolution: multiple regimes and their influence on carbon sequestration in a sub-tropical peatland, Ecological Monographs, 87, 578–599, https://doi.org/10.1002/ecm.1269, 2017.

Nimmo, J.: Vadose Water, in: Encyclopedia of Inland Waters, edited by Likens, G. E., pp. 766–777, Academic Press, Oxford, https://doi.org/10.1016/B978-012370626-3.00014-4, 2009.

Nimmo, J. R.: The processes of preferential flow in the unsaturated zone, Soil Science Society of America Journal, 85, 1–27, https://doi.org/10.1002/saj2.20143, 2021.

Nimmo, J. R., Perkins, K. S., Schmidt, K. M., Miller, D. M., Stock, J. D., and Singha, K.: Hydrologic Characterization of Desert Soils with Varying Degrees of Pedogenesis: 1. Field Experiments Evaluating Plant-Relevant Soil Water Behavior, Vadose Zone Journal, 8, 480–495, https://doi.org/10.2136/vzj2008.0052, 2009.

Nippgen, F., McGlynn, B. L., Emanuel, R. E., and Vose, J. M.: Watershed memory at the Coweeta Hydrologic Laboratory: The effect of past precipitation and storage on hydrologic response, Water Resources Research, 52, 1673–1695, https://doi.org/10.1002/2015WR018196, 2016.

Nyberg, L.: Water flow path interactions with soil hydraulic properties in till soil at Gårdsjön, Sweden, Journal of Hydrology, 170, 255–275, https://doi.org/10.1016/0022-1694(94)02667-Z, 1995.

Pachepsky, Y. and Van Genuchten, M.: Encyclopedia of Agrophysics, chap. Pedotransfer Functions, pp. 556–561, Springer, Editor: J. Glinski and J. Horabik and J. Lipiec, https://doi.org/10.1007/978-90-481-3585-1_109, 2011.

Paez-Bimos, S., Molina, A., Calispa, M., Delmelle, P., Lahuatte, B., Villacis, M., Munoz, T., and Vanacker, V.: Soil–vegetation–water interactions controlling solute flow and chemical weathering in volcanic ash soils of the high Andes, Hydrology and Earth System Sciences, 27, 507–1529, https://doi.org/10.5194/hess-27-1507-2023, 2023.

Parlange, J. Y. and Hill, D. E.: Theoretical analysis of wetting front instability in soils, Soil Science, 122, 236–239, https://doi.org/10.1097/00010694-197610000-00008, 1976.

Pertassek, T., Peters, A., and Durner, W.: HYPROP-FIT software user's manual, V. 3.0, UMS GmbH, Munich, Germany, 2015.

Peters, A. and Durner, W.: Simplified evaporation method for determining soil hydraulic properties, Journal of Hydrology, 356, 147–162, https://doi.org/10.1016/j.jhydrol.2008.04.016, 2008.

Peterson, B. S.: Form determines function: new methods for identifying the neuroanatomical loci of circuit-based disturbances in childhood disorders., in: Journal of the American Academy of Child and Adolescent Psychiatry, vol. 49, pp. 533–8, United States, https://doi.org/10.1016/j.jaac.2010.03.010, 2010.

Pfister, L., Martínez-Carreras, N., Hissler, C., Klaus, J., Carrer, G. E., Stewart, M. K., and McDonnell, J. J.: Bedrock geology controls on catchment storage, mixing, and release: A comparative analysis of 16 nested catchments, Hydrological Processes, 31, 1828–1845, https://doi.org/10.1002/hyp.11134, 2017.

Phillips, J. D.: The robustness of chronosequences, Ecological Modelling, 298, 16–23, https://doi.org/10.1016/j.ecolmodel.2013.12.018, 2015.

Phillips, J. D.: Store and pour: Evolution of flow systems in landscapes, CATENA, 216, 106 357, https://doi.org/10.1016/j.catena.2022.106357, 2022.

Pornon, A. and Doche, B.: Age structure and dynamics of Rhododendron ferrugineum L. populations in the northwestern French Alps, Journal of Vegetation Science, 7, 265–272, https://doi.org/10.2307/3236327, 1996.

Quisenberry, V., Smith, B., Phillips, R., Scott, H., and Nortcliff, S.: A Soil Classification System for Describing Water and Chemical Transport, Soil Science, 156, 306–315, https://doi.org/10.1097/00010694-199311000-00003, 1993.

R Core Team: R: A Language and Environment for Statistical Computing, R Foundation for Statistical Computing, Vienna, Austria, URL `https://www.R-project.org/`, 2017.

Ramírez, B. H., van der Ploeg, M., Teuling, A. J., Ganzeveld, L., and Leemans, R.: Tropical Montane Cloud Forests in the Orinoco river basin: The role of soil organic layers in water storage and release, Geoderma, 298, 14–26, https://doi.org/10.1016/j.geoderma.2017.03.007, 2017.

Rawls, W., Pachepsky, Y., Ritchie, J., Sobecki, T., and Bloodworth, H.: Effect of soil organic carbon on soil water retention, Geoderma, 116, 61–76, https://doi.org/10.1016/S0016-7061(03)00094-6, 2003.

Reeder, C. J. and Jurgensen, M.: Fire-induced water repellency in forest soils of upper Michigan, Canadian Journal of Forest Research, 9, 369–373, https://doi.org/10.1139/x79-062, 1979.

Retzer, J. L.: Soil Development in the Rocky Mountains, Soil Science Society of America Journal, 13, 446–448, https://doi.org/10.2136/sssaj1949.036159950013000C0080x, 1949.

Reynolds, D., Bowman, B., Drury, C., Tan, C., and Lu, X.: Indicators of good soil physical quality: Density and storage parameters, Geoderma, 110, 131–146, https://doi.org/10.1016/S0016-7061(02)00228-8, 2002.

Richter, D. d. and Mobley, M. L.: Monitoring Earth's Critical Zone, Science, 326, 1067–1068, https://doi.org/10.1126/science.1179117, 2009.

Ritsema, C. J. and Dekker, L. W.: How water moves in a water repellent sandy soil: 2. Dynamics of fingered flow, Water Resour. Res., 30, 2519–2531, https://doi.org/10.1029/94wr00750, 1994.

Roe, G., Baker, M., and Herla, F.: Centennial glacier retreat as categorical evidence of regional climate change, Nature Geoscience, 10, 95–99, https://doi.org/10.1038/ngeo2863, 2017.

Ross, M. R. V., Nippgen, F., McGlynn, B. L., Thomas, C. J., Brooks, A. C., Shriver, R. K., Moore, E. M., and Bernhardt, E. S.: Mountaintop mining legacies constrain ecological, hydrological and biogeochemical recovery trajectories, Environmental Research Letters, 16, 075 004, https://doi.org/10.1088/1748-9326/ac09ac, 2021.

Rye, C. and Smettem, K.: The effect of water repellent soil surface layers on preferential flow and bare soil evaporation, Geoderma, 289, 142–149, https://doi.org/10.1016/j.geoderma.2016.11.032, 2017.

Sajikumar, N. and Remya, R.: Impact of land cover and land use change on runoff characteristics, Journal of Environmental Management, 161, 460–468, https://doi.org/10.1016/j.jenvman.2014.12.041, 2015.

Samouëlian, A., Finke, P., Goddéris, Y., and Cornu, S.: Hydropedology: Synergistic Integration of Soil Science and Hydrology, chap. Hydrologic information in pedologic models, pp. 595–636, Academic Press, Elsevier B.V., Lin, H. (Editor), iSBN 9780123869418, 2012.

Sauer, D., Finke, P., Sørensen, R., Sperstad, R., Schülli-Maurer, I., Høeg, H., and Stahr, K.: Testing a soil development model against southern Norway soil chronosequences, Quaternary International, 265, 18–31, https://doi.org/10.1016/j.quaint.2011.12.018, 2012.

Sauer, D., Schülli-Maurer, I., Wagner, S., Scarciglia, F., Sperstad, R., Svendgård-Stokke, S., Sørensen, R., and Schellmann, G.: Soil development over millennial timescales - A comparison of soil chronosequences of different climates and lithologies, IOP Conference Series: Earth and Environmental Science, 25, 012 009, https://doi.org/10.1088/1755-1315/25/1/012009, 2015.

Schaap, M. G., Leij, F. J., and van Genuchten, M. T.: rosetta: a computer program for estimating soil hydraulic parameters with hierarchical pedotransfer functions, Journal of Hydrology, 251, 163–176, https://doi.org/10.1016/S0022-1694(01)00466-8, 2001.

Schaetzl, R. J.: A Spodosol-Entisol Transition in Northern Michigan, Soil Science Society of America Journal, 66, 1272–1284, https://doi.org/10.2136/sssaj2002.1272, 2002.

Scherrer, P. and Pickering, C. M.: Recovery of Alpine Vegetation from Grazing and Drought: Data from Long-term Photoquadrats in Kosciuszko National Park, Australia, Arctic, Antarctic, and Alpine Research, 37, 574–584, https://doi.org/10.1657/1523-0430(2005)037[0574:ROAVFG]2.0.CO;2, 2005.

Scherrer, S., Naef, F., Faeh, A. O., and Cordery, I.: Formation of runoff at the hillslope scale during intense precipitation, Hydrology and Earth System Sciences, 11, 907–922, https://doi.org/10.5194/hess-11-907-2007, 2007.

Schimmelpfennig, I., Schaefer, J. M., Akçar, N., Koffman, T., Ivy-Ochs, S., Schwartz, R., Finkel, R. C., Zimmerman, S., and Schlüchter, C.: A chronology of Holocene and Little Ice Age glacier culminations of the Steingletscher, Central Alps, Switzerland, based on high-sensitivity beryllium-10 moraine dating, Earth and Planetary Science Letters, 393, 220–230, https://doi.org/10.1016/j.epsl.2014.02.046, 2014.

Schindler, U.: Ein Schnellverfahren zur Messung der Wasserleitfähigkeit im teilgesättigten Boden an Stechzylinderproben, Arch. Acker- u. Pflanzenbau u. Bodenkd. Berlin, 24, 1–7, 1980.

Schindler, U. and Müller, L.: Simplifying the evaporation method for quantifying soil hydraulic properties, Journal of Plant Nutrition and Soil Science, 169, 623–629, https://doi.org/10.1002/jpln.200521895, 2006.

Schoonejans, J., Vanacker, V., Opfergelt, S., Ameijeiras-Mariño, Y., and Christl, M.: Kinetically limited weathering at low denudation rates in semiarid climatic conditions, Journal of Geophysical Research: Earth Surface, 121, 336–350, https://doi.org/10.1002/2015JF003626, 2016.

Schwen, A., Zimmermann, M., and Bodner, G.: Vertical variations of soil hydraulic properties within two soil profiles and its relevance for soil water simulations, Journal of Hydrology, 516, 169–181, https://doi.org/10.1016/j.jhydrol.2014.01.042, 2014.

Shang, J., Zhu, Q., and Zhang, W.: Advancing Soil Physics for Securing Food, Water, Soil and Ecosystem Services, Vadose Zone Journal, 17, 180 207, https://doi.org/10.2136/vzj2018.11.0207, 2018.

Sililo, O. T. and Tellam, J. H.: Fingering in Unsaturated Zone Flow: A Qualitative Review with Laboratory Experiments on Heterogeneous Systems, Groundwater, 38, 864–871, https://doi.org/10.1111/j.1745-6584.2000.tb00685.x, 2000.

Singh, N. K., Emanuel, R. E., McGlynn, B. L., and Miniat, C. F.: Soil Moisture Responses to Rainfall: Implications for Runoff Generation, Water Resources Research, 57, e2020WR028 827, https://doi.org/10.1029/2020WR028827, 2021.

Sivapalan, M.: Pattern, Process and Function: Elements of a Unified Theory of Hydrology at the Catchment Scale, chap. 13, John Wiley & Sons, Ltd, https://doi.org/10.1002/0470848944.hsa012, 2006.

Sivapalan, M.: From engineering hydrology to Earth system science: milestones in the transformation of hydrologic science, Hydrology and Earth System Sciences, 22, 1665–1693, https://doi.org/10.5194/hess-22-1665-2018, 2018.

Starr, J. L., DeRoo, H. C., Frink, C. R., and Parlange, J.-Y.: Leaching Characteristics of a Layered Field Soil, Soil Science Society of America Journal, 42, 386–391, https://doi.org/10.2136/sssaj1978.03615995004200030002x, 1978.

Stumpp, C., Stichler, W., Kandolf, M., and Šimůnek, J.: Effects of Land Cover and Fertilization Method on Water Flow and Solute Transport in Five Lysimeters: A Long-Term Study Using Stable Water Isotopes, Vadose Zone Journal, 11, vzj2011.0075, https://doi.org/10.2136/vzj2011.0075, 2012.

Sullivan, P., Billings, S., Hirmas, D., Li, L., Zhang, X., Ziegler, S., Murenbeeld, K., Ajami, H., Guthrie, A., Singha, K., Giménez, D., Duro, A., Moreno, V., Flores, A., Cueva, A., Koop, Aronson, E., Barnard, H., Banwart, S., Keen, R., Nemes, A., Nikolaidis, N., Nippert, J., Richter, D., Robinson, D., Sadayappan, K., de Souza, L., Unruh, M., and Wen, H.: Embracing the dynamic nature of soil structure: A paradigm illuminating the role of life in critical zones of the Anthropocene, Earth-Science Reviews, 225, 103 873, https://doi.org/10.1016/j.earscirev.2021.103873, 2022.

Taalab, A., Ageeb, G., Siam, H. S., and Mahmoud, S. A.: Some Characteristics of Calcareous soils. A review, Middle East Journal of Agriculture Research, 8, 96–105, 2019.

Tao, Z., Li, H., Neil, E., and Si, B.: Groundwater recharge in hillslopes on the Chinese Loess Plateau, Journal of Hydrology: Regional Studies, 36, 100 840, https://doi.org/10.1016/j.ejrh.2021.100840, 2021.

Tian, J., Zhang, B., He, C., and Yang, L.: Variability In Soil Hydraulic Conductivity And Soil Hydrological Response Under Different Land Covers In The Mountainous Area Of The Heihe River Watershed, Northwest China, Land Degradation and Development, 28, 1437–1449, https://doi.org/10.1002/ldr.2665, 2017.

Tillman, R. W., Scotter, D. R., Wallis, M. G., and Clothier, B. E.: Water repellency and its measurement by using intrinsic sorptivity, Soil Res., 27, 637–644, https://doi.org/10.1071/SR9890637, 1989.

Treter, U., Ramsbeck-Ullmann, M., Böhmer, H. J., and Bösche, H.: Vegetationsdynamik im Vorfeld des Lysgletschers (Valle di Gressoney/ Region Aosta/ Italien) seit 1821, Erdkunde, 56, 2563–267, 2002.

Troch, P. A., Lahmers, T., Meira, A., Mukherjee, R., Pedersen, J. W., Roy, T., and Valdés-Pineda, R.: Catchment coevolution: A useful framework for improving predictions of hydrological change?, Water Resources Research, 51, 4903–4922, https://doi.org/10.1002/2015WR017032, 2015.

Truong, N. C. Q., Khoi, D. N., Nguyen, H. Q., and Kondoh, A.: Impact of Forest Conversion to Agriculture on Hydrologic Regime in the Large Basin in Vietnam, Water, 14, 854, https://doi.org/10.3390/w14060854, 2022.

van der Heijden, G., Legout, A., Pollier, B., Bréchet, C., Ranger, J., and Dambrine, E.: Tracing and modeling preferential flow in a forest soil — Potential impact on nutrient leaching, Geoderma, 195-196, 12–22, https://doi.org/10.1016/j.geoderma.2012.11.004, 2013.

van der Meij, W., Temme, A., Lin, H., Gerke, H., and Sommer, M.: On the role of hydrologic processes in soil and landscape evolution modeling: concepts, complications and partial solutions, Earth-Science Reviews, 185, 1088–1106, https://doi.org/10.1016/j.earscirev.2018.09.001, 2018.

Van Genuchten, M.: A Closed-form Equation for Predicting the Hydraulic Conductivity of Unsaturated Soils, Soil Science Society of America Journal, 44, 892–898, https://doi.org/10.2136/sssaj1980.03615995004400050002x, 1980.

van Schaik, N.: Spatial variability of infiltration patterns related to site characteristics in a semi-arid watershed, CATENA, 78, 36–47, https://doi.org/10.1016/j.catena.2009.02.017, 2009.

Vereecken, H., Weynants, M., Javaux, M., Pachepsky, Y., Schaap, M. G., and Genuchten, M. v.: Using Pedotransfer Functions to Estimate the van Genuchten–Mualem Soil Hydraulic Properties: A Review, Vadose Zone Journal, 9, 795–820, https://doi.org/10.2136/vzj2010.0045, 2010.

Vilmundardóttir, O. K., Gísladóttir, G., and Lal, R.: Early stage development of selected soil properties along the proglacial moraines of Skaftafellsjökull glacier, SE-Iceland, CATENA, 121, 142–150, https://doi.org/10.1016/j.catena.2014.04.020, 2014.

Volkmann, T., Sengupta, A., Meredith, L., Dontsova, K., and Cueva, A.: Controlled experiments of hillslope coevolution at the Biosphere 2 Landscape Evolution Observatory: Toward prediction of coupled hydrological, biogeochemical, and ecological change, in: Hydrology of Artificial and Controlled Experiments, pp. 25–74, edited by Jiu-Fu Liu and Wei-Zu Gu, https://doi.org/10.5772/intechopen.72325, 2018.

Wallach, R. and Jortzick, C.: Unstable finger-like flow in water-repellent soils during wetting and drainage—The case of a point water source, Journal of Hydrology, 351, 26–41, https://doi.org/10.1016/j.jhydrol.2007.11.032, 2008.

Wang, T., Zlotnik, V. A., Šimunek, J., and Schaap, M. G.: Using pedotransfer functions in vadose zone models for estimating groundwater recharge in semiarid regions, Water Resources Research, 45, W04 412, https://doi.org/10.1029/2008WR006903, 2009.

Wang, Y. and Zhang, B.: Chapter Four - Interception of Subsurface Lateral Flow Through Enhanced Vertical Preferential Flow in an Agroforestry System Observed Using Dye-Tracing and Rainfall Simulation Experiments, in: Quantifying and Managing Soil Functions in Earth's Critical Zone, edited by Banwart, S. A. and Sparks, D. L., vol. 142 of *Advances in Agronomy*, pp. 99–118, Academic Press, https://doi.org/10.1016/bs.agron.2016.10.014, 2017.

Wang, Y., Li, Y., Wang, X., and Chau, H. W.: Finger Flow Development in Layered Water-Repellent Soils, Vadose Zone Journal, 17, 170 171, https://doi.org/10.2136/vzj2017.09.0171, 2018.

Wassenaar, L., Hendry, M., Chostner, V., and Lis, G.: High Resolution Pore Water d2H and d18O Measurements by H2O(liquid)-H2O(vapor) Equilibration Laser Spectroscopy, Environmental Science and Technology, 42, 9262–9267, https://doi.org/10.1021/es802065s, pMID: 19174902, 2008.

Weibel, E. R.: In: Stereological Methods, Vol. 1:, Practical Methods for Biological Morphometry. Academic Press, London, 21, 630–630, https://doi.org/10.1002/jobm.19810210824, 1979.

Weiler, M.: Mechanisms controlling macropore flow during infiltration dye tracer experiments and simulations, Ph.D. thesis, Swiss Federal Institute of Technology Zurich, https://doi.org/10.3929/ethz-a-004180115, 2001.

Weiler, M. and Flühler, H.: Inferring flow types from dye patterns in macroporous soils, Geoderma, 120, 137–153, https://doi.org/10.1016/j.geoderma.2003.08.014, 2004.

Weiler, M. and McDonnell, J. J.: Conceptualizing lateral preferential flow and flow networks and simulating the effects on gauged and ungauged hillslopes, Water Resources Research, 43, W03 403, https://doi.org/10.1029/2006WR004867, 2007.

Weiler, M. and Naef, F.: An experimental tracer study of the role of macropores in infiltration in grassland soils, Hydrological Processes, 17, 477–493, https://doi.org/10.1002/hyp.1136, 2003.

Weiss, T., Siegesmund, S., Kirchner, D., and Sippel, J.: Insolation weathering and hygric dilatation: two competitive factors in stone degradation, Environmental Geology, 46, 402–413, https://doi.org/10.1007/s00254-004-1041-0, 2004.

White, A. F. and Blum, A. E.: Effects of climate on chemical weathering in watersheds, Geochimica et Cosmochimica Acta, 59, 1729–1747, https://doi.org/10.1016/0016-7037(95)00078-E, 1995.

White, I., Colombera, P. M., and Philip, J. R.: Experimental Study of Wetting Front Instability Induced by Sudden Change of Pressure Gradient, Soil Science Society of America Journal, 40, 824–829, https://doi.org/10.2136/sssaj1976.03615995004000060012x, 1976.

Wickham, H.: ggplot2: Elegant Graphics for Data Analysis, Springer-Verlag New York, URL `https://ggplot2.tidyverse.org`, 2016.

Wiekenkamp, I., Huisman, J., Bogena, H., Lin, H., and Vereecken, H.: Spatial and temporal occurrence of preferential flow in a forested headwater catchment, Journal of Hydrology, 534, 139–149, https://doi.org/10.1016/j.jhydrol.2015.12.050, 2016.

Williams, D. W. and Liebhold, A. M.: Climate change and the outbreak ranges of two North American bark beetles, Agricultural and Forest Entomology, 4, 87–99, https://doi.org/10.1046/j.1461-9563.2002.00124.x, 2002.

Wilson, D. J., Western, A. W., and Grayson, R. B.: Identifying and quantifying sources of variability in temporal and spatial soil moisture observations, Water Resources Research, 40, W02 507, https://doi.org/10.1029/2003WR002306, 2004.

Wlostowski, A. N., Molotch, N., Anderson, S. P., Brantley, S. L., Chorover, J., Dralle, D., Kumar, P., Li, L., Lohse, K. A., Mallard, J. M., McIntosh, J. C., Murphy, S. F., Parrish, E., Safeeq, M., Seyfried, M., Shi, Y., and Harman, C.: Signatures of Hydrologic Function Across the Critical Zone Observatory Network, Water Resources Research, 57, e2019WR026 635, https://doi.org/10.1029/2019WR026635, 2021.

Wojcik, R., Eichel, J., Bradley, J. A., and Benning, L. G.: How allogenic factors affect succession in glacier forefields, Earth-Science Reviews, 218, 103 642, https://doi.org/10.1016/j.earscirev.2021.103642, 2021.

Wojkowski, J., Wałęga, A., Radecki-Pawlik, A., Młyński, D., and Lepeška, T.: The influence of land cover changes on landscape hydric potential and river flows: Upper Vistula, Western Carpathians, CATENA, 210, 105 878, https://doi.org/10.1016/j.catena.2021.105878, 2022.

Wu, Q., Liu, C., Lin, W., Zhang, M., Wang, G., and Zhang, F.: Quantifying the preferential flow by dye tracer in the North China Plain, Journal of Earth Science, 26, 435–444, https://doi.org/10.1007/s12583-014-0489-4, 2015.

Yang, F., Zhang, G.-L., Yang, J.-L., Li, D.-C., Zhao, Y.-G., Liu, F., Yang, R.-M., and Yang, F.: Organic matter controls of soil water retention in an alpine grassland and its significance for hydrological processes, Journal of Hydrology, 519, 3086–3093, https://doi.org/10.1016/j.jhydrol.2014.10.054, 2014.

Yang, Y., Fang, J., Ji, C., and Han, W.: Above- and belowground biomass allocation in Tibetan grasslands, Journal of Vegetation Science, 20, 177–184, https://doi.org/10.1111/j.1654-1103.2009.05566.x, 2009.

Yang, Y., Xiao, H., Wei, Y., Zhao, L., Zou, S., Yang, Q., and Yin, Z.: Hydrological processes in the different landscape zones of alpine cold regions in the wet season, combining isotopic and hydrochemical tracers, Hydrological Processes, 26, 1457–1466, https://doi.org/10.1002/hyp.8275, 2012.

Yoshida, T. and Troch, P. A.: Coevolution of volcanic catchments in Japan, Hydrology and Earth System Sciences, 20, 1133–1150, https://doi.org/10.5194/hess-20-1133-2016, 2016.

Zehe, E. and Flühler, H.: Slope scale variation of flow patterns in soil profiles, Journal of Hydrology, 247, 116 –132, https://doi.org/10.1016/S0022-1694(01)00371-7, 2001.

Zeng, C., Zhang, F., Wang, Q., Chen, Y., and Joswiak, D. R.: Impact of alpine meadow degradation on soil hydraulic properties over the Qinghai-Tibetan Plateau, Journal of Hydrology, 478, 148–156, https://doi.org/10.1016/j.jhydrol.2012.11.058, 2013.

Zhang, J., Duan, L., Liu, T., Chen, Z., Wang, Y., Li, M., and Zhou, Y.: Experimental analysis of soil moisture response to rainfall in a typical grassland hillslope under different vegetation treatments, Environmental Research, 213, 113 608, https://doi.org/10.1016/j.envres.2022.113608, 2022.

Zhang, Y., Niu, J., Yu, X., Zhu, W., and Du, X.: Effects of fine root length density and root biomass on soil preferential flow in forest ecosystems, Forest Systems, 24, e012, https://doi.org/10.5424/fs/2015241-06048, 2015.

Zheng, Y., Chen, N., Zhang, C.-k., Dong, X.-x., and Zhao, C.-m.: Soil Macropores Affect the Plant Biomass of Alpine Grassland on the Northeastern Tibetan Plateau, Frontiers in Ecology and Evolution, 9, 678 186, https://doi.org/10.3389/fevo.2021.678186, 2021.

Zimmermann, B., Elsenbeer, H., and De Moraes, J. M.: The influence of land-use changes on soil hydraulic properties: Implications for runoff generation, Forest Ecology and Management, 222, 29–38, https://doi.org/10.1016/j.foreco.2005.10.070, 2006.

Zimmermann, B., Papritz, A., and Elsenbeer, H.: Asymmetric response to disturbance and recovery: Changes of soil permeability under forest–pasture–forest transitions, Geoderma, 159, 209–215, https://doi.org/10.1016/j.geoderma.2010.07.013, 2010.

Declaration On Honor

I hereby confirm that I have personally prepared this dissertation without any unlawful assistance. I also affirm that I have solely utilized the declared resources and have appropriately cited any verbatim or substantially similar formulations and concepts derived from printed, unpublished, or online sources, following the stipulated guidelines for academic work.
This dissertation has not been previously submitted for evaluation at any other university, either in Germany or any other country. The work is being submitted both in printed and electronic formats. I further verify that the content of the digital version is entirely identical to that of the printed copy.

Anne Hartmann

Acknowledgment

To begin, I wish to extend my heartfelt gratitude to my direct supervisor, Dr. Theresa Blume. Her unwavering guidance, invaluable advice, unending support, enriching discussions, and boundless patience throughout these past years have been essential to the success of this thesis.
This thesis received funding from the German Research Foundation and the Swiss National Science Foundation (SNF) as part of the DFG-SNF project Hillscape (Hillslope Chronosequence and Process Evolution, BL 1184/4-1). I am deeply thankful to my Hillscape colleagues – Fabian Maier, Konrad Greinwald, and Alessandra Musso – whose individual scientific work contributed significantly to the success of this interdisciplinary endeavor.
My sincere appreciation goes to Britta Kattenstroth and Jonas Zimmermann for their technical guidance, indispensable assistance, and pivotal roles in executing the field campaigns.
I would also like to acknowledge the invaluable contributions of our student helpers: Moritz Lesche, Jonas Freymüller, Franziska Röpke, Nina Zahn, Wibke Richter, Louisa Kanis, Peter Grosse, and Carlo Seehaus. Their unwavering dedication in the field was indispensable.
I am deeply grateful for the unwavering support of my GFZ colleagues – Markus Morgner, Stephan Schröder, Jörg Wummel, Astrid Krahn, Heiko Thoss, and Knut Günther – whose presence and help significantly eased my work life at GFZ.
A special note of gratitude goes to my dear friend, Daniel Rasche. Our discussions (both scientifically and personally), leisurely afternoons by the Havel, shared lunch breaks, and countless more moments have been one of the enriching aspects of my doctoral life during the past years.
As always, I remain profoundly thankful for my family. I extend special thanks to Jan Gieseler, who consistently provided me with fresh perspectives on science when needed.
Lastly, I am genuinely appreciative of the companionship of my beloved (now late) dog during the six months of field campaigns. Her presence provided comfort and motivation in equal measure.